UCL SCHOOL OF PHARMACY
BRUNSWICK SQUARE

Nanoparticle based strategies for the treatment of Glioblastoma

Funmilola AdesodunFisusi

Thesis submitted in accordance with the requirements of UCL School of Pharmacy for the degree of Doctor of Philosophy

2014

UCL SCHOOL OF PHARMACY

29 – 39 Brunswick Square,

London, WC1N 1AX

Declaration

I, Funmilola Adesodun Fisusi confirm that the work presented in this thesis is my own. Where information has been derived from other sources, I confirm that this has been indicated in the thesis.

Signature:

Date:

Abstract

Glioblastoma is the most common and most biologically aggressive primary brain tumour in adults. In spite of tremendous investment into research which has led to the development and application of novel diagnostic and therapeutic measures in the management of glioblastoma, the prognosis is still dismal with median survival time of about 12 – 15 months. Also, the success of most cytotoxic drugs clinically employed in the treatment of glioblastoma is greatly limited by their dose-limiting toxicity which typically manifests as clinically significant reduction in blood cell counts. The aim of this study is to demonstrate that a high dose nanoparticle formulation of the cytotoxic drug lomustine using a self-assembling chitosan amphiphile, quaternary ammonium palmitoyl glycol chitosan would lead to improved survival outcomes without a commensurate increase in toxic effects.

The novel nanoparticle based lomustine formulation employed in this study enabled the administration of a lomustine dose (13 mg kg^{-1}) 10 times higher than the dose (1.2 mg kg^{-1}) achievable with an ethanolic formulation of lomustine. Human glioblastoma tumour bearing mice treated with the high dose formulation had a mean survival time of 33.1 days while the mice treated with the low dose formulation had a mean survival time of 22.5 days after intravenous administration of the drug once daily for 10 consecutive days. The increased (1.5 times longer) survival time resulting from treatment with the nanoparticle based high dose formulation was not accompanied by an increase in gross toxic effects. Thus, the nanoparticle based formulation afforded the administration of lomustine in a continuous high dose schedule which led to beneficial therapeutic outcomes.

In addition, three self-assembling peptide amphiphiles were synthesised and characterised for potential application in the transport and delivery of therapeutic molecules to the brain for the treatment of intracranial tumours.

Acknowledgements

Firstly, I would like to thank my supervisors, Prof. Ijeoma Uchegbu and Prof. Andreas Schätzlein for the tremendous support they gave me since I started this project and all through the various stages of the project. I appreciate very much their patience, advice, guidance, understanding and encouragement all through the project. I could not have completed the project without such support.

Next, I would like to thank Dr. Aikaterini Lalatsa for "starting me off" in the lab and for always being there to answer my questions and offer assistance whenever needed. I also want to thank Dr. Vicky Lozano for patiently guiding me through the initial and crucial stages of my in vivo experiments. Also, I would like to thank Dr. John Malkinson for all his help, for granting me free access to the facilities in his lab and also providing necessary support, guidance and advice. I also want to thank the members of his group: Dr. Gary Kemp for his help and advice in the lab; Francesca and Zuhaira for being ever so helpful.

Also, I would like to thank Dr. John Turton for helping me to get on with the toxicity studies. I also want to thank Dr. Adeline Siew for sharing her experience on the toxicity studies which was very helpful. I want to thank Dr. Mariarosa Mazza for "taking care of me" when I started PhD newly. I want to thank Dr. Andrew Lawrie and UCL Haemostasis Research Unit for provision of facilities for haematologic analysis and kind assistance in carrying out the analyses. I thank Mr. David McCarthy for electron microscopy services. I also like to thank Dr. Dave Gathercole for his help with confocal microscopy analysis. I thank Mr. Emmanuel Samuel and Structural Chemistry Unit within the School of Pharmacy for help with mass spectrometry analysis. I also thank Dr. Kersti Karu and UCL Department of Chemistry for additional mass spectrometry analysis. I also would like to thank Mr. Steve Coppard and all staff of the Biological Services Unit for their help during the conduct of my in vivo experiments. I also like to acknowledge Mr. Owen Sheppard, Ms Isabel Gonçalves, Mrs Kate Keen and all technical staff of the Department of Pharmaceutics.

Also, I want to thank the Biomedical group, School of Physics, University of Exeter: Ahmed, Malek, Dr. Ian Summers, and Dr. Julian Morger for MR imaging facilities and for painstakingly imaging all my tumour samples. I also want to thank Dr. Rebecca Notman and Louise Granger of Warwick University for simulation (molecular dynamics) studies. I also want to thank Dr. Jose Prieto-Garcia for the use of HPLC facilities in his lab and for his advice. I also thank members of his group: Mukrish and Amaka for their assistance.

I want to thank the Postdocs in our group (past and present): Dr. KarWai Chooi, Dr. Manuel Santander-Ortega, Dr. Lisa Godfrey, Dr. Antonio Ianitelli, Dr. Jay Freemen, Dr. Lorenzo Capretto, Dr. George Wang and Dr. Fionn O'Brien; for their assistance at various times. I would like to thank all my "colleagues" in the group: Dr. Jayanat Iemsam-arng (my first "friend" in the lab); Margarida; Ramesh for all the "rescue missions"; Preethi for all the encouragement and friendly support; Abdullah; Sunish; Nick; Era; Clemens; Xian; and Kawsar, for a great working environment. I want to thank Loli (Dr. Doleres Serrano) for being such a great friend and always encouraging me to focus on "the light at the end of the tunnel". I also want to acknowledge all my "roommates" in Room 416 (PhD study area): Dr. Fouad Helal for "more error bars options"; Dr. Haydar Abdalghafor for being so supportive; Mansa, Sahar and Mustapha for friendly support; Jip, Rin, Honey, Sheiliza, and indeed everyone for being so nice and making Room 416 such a great "room to live in".

Also, I want to greatly appreciate my family for always being there for me. I want to express profound gratitude to my parents Mr. and Mrs. R. Z. Fisusi for being the best parents in the world, always giving me so much support, encouraging me, always giving their best and looking out for me at all times. I want to thank my "big" sister Dolapo, her husband, Temitope (my able editors) and company: Toluwanimi, Olawolemi, and Ola-Precious for their support and encouragement. I want to thank my brother "Mr. Bimbọ" for been there for me at all times, and for all the encouragement and moral support.

I thank my younger sisters Olabisi (plus Babawale) and Opeyemi (plus Gbenga, David and Daniel), also Dare and IniOluwa Sanni for moral support at all times. I also like to appreciate my "London family" Mr and Mrs Olusola Ola along with Feranmi, Nifemi and Tifemi for been very supportive. I also acknowledge my dear sister Dr. Bola Fisusi Sanni (God rest her soul) for all the times we had together, who very sadly is not here to share this very great time. I dedicate this thesis to her memory.

I want to express profound gratitude to my sponsors, Education Trust Fund, Abuja, Nigeria and Obafemi Awolowo University, Ile – Ife, Nigeria for funding my PhD. I would not have had the opportunity to work on this exciting project without their sponsorship.

Finally and most importantly, for life and strength to work on this project and complete it, I give thanks and praise from the depth of my heart unto the Almighty God.……..."Now unto the King eternal, immortal, invisible, the only wise God, be honour and glory forever and ever. Amen."

Table of contents

List of tables

List of figures

List of Abbreviations

%	Percent
≈	Approximately
µL	Microlitre
µm	Micrometre
^{1}HNMR	Proton nuclear magnetic resonance
ABC	ATP-binding cassette
ADC	Apparent diffusion coefficient
AGAT	O^{6}-alkylguanine-DNA alkyltransferase
AMT	Adsorptive mediated transcytosis
APCI	Atmospheric pressure chemical ionisation
Arg/ R	Arginine
BBB	Blood brain barrier
BCNU	N,N'-Bis(2-chloroethyl)-N-nitrosourea (Carmustine)
BCRP	Breast cancer resistance protein
BCSFB	Blood cerebrospinal fluid barrier
bFGF	Basic fibroblast growth factor

BG	O^6-Benzylguanine
Boc	Butyloxycarbonyl
BSU	Biological Services Unit
BTB	Blood-tumour barrier
Bzl	Benzyl
CBTRUS	Central Brain Tumour Registry of the United States
CCNU	3-(2-chloroethyl)-1-cyclohexyl-3-nitrosourea (Lomustine)
CDKN2A	Cyclin-dependent kinase inhibitor 2A
CG	Coarse-grained
CI	Chemical ionisation
CMT	Carrier-mediated transport
CMT	Critical micelle temperature
CNS	Central nervous system
CNT2	Concentrative nucleoside transporter type 2
CPP	Cell penetrating peptides
CSF	Cerebrospinal fluid
CT	Computed tomography
CVOs	Circumventricular Organs

CW	Continuous wave
DCM	Dichloromethane
DIEA	N,N-Diisopropylethylamine
DLS	Dynamic light scattering
DMF	Dimethylformamide
DMSO	Dimethylsulfoxide
DNA	Deoxyribonucleic acid
DSC	Dynamic susceptibility-weighted contrast-enhanced
DW	Diffusion-weighted
DW-MRI	Diffusion-weighted magnetic resonance imaging
ECM	Extracellular matrix
EDTA	Ethylenediaminetetraacetic acid
EGFR	Epidermal growth factor receptor
EI	Electron ionisation
EORTC	European Organisation for Research and Treatment of Cancer
EPR	Enhanced permeability and retention
ESI	Electrospray ionisation
FACS	Fluorescence activated cell sorting

FDA	Food and Drug Administration
FID	Free induction decay
Fmoc	9-Fluorenylmethoxycarbonyl
fMRI	Functional magnetic resonance imaging
FT	Fourier transform
GB	Great Britain
GCPQ	Quaternary ammonium palmitoyl glycol chitosan
GLUT1	Glucose transporter
Gly/ G	Glycine
GPC/ MALLS	Multi-angle laser light scattering and gel permeation chromatography
Gy	Gray
H_2O	Water
HBTU	2-(1 H- Benzotriazole- 1- yl)- 1,1,3,3- tetramethyluronium hexafluorophosphate
HER2	Human epidermal growth factor receptor 2
HF	Hydrogen fluoride
HPLC	High performance liquid chromatography

HSC	Haematopoietic stem cells
IDH1	Isocitrate dehydrogenase 1
IR	Infrared
ISF	Interstitial fluid
Kg	Kilogram
KPS	Karnofsky performance scale
LAT1	Large neutral amino acid transporter
Leu/ L	Leucine
LOH	Loss of heterozygosity
LOM-ETOH	Ethanolic lomustine
MALDI	Matrix assisted laser desorption ionisation
MD	Molecular dynamics
MDM2	Murine double minute 2
MDR	Multidrug resistance
MeCN	Acetonitrile
MEM	Minimum Essential Medium
Met/ M	Methionine
mg	Milligram

MGMT	O^6-methylguanine-DNA-methyltransferase
mL	Millilitre
mM	Millimolar
mmol	Millimole
MR	Magnetic resonance
MRI	Magnetic resonance imaging
MRP	Multidrug resistance protein
MS	Mass spectrometry
MTD	Maximal tolerated dose
Mwt	Molecular weight
NCIC	National Cancer Institute of Canada Clinical Trials Group
NEFL	Neurofilament light polypeptide
NF1	Neurofibromin1
NF-kB	Nuclear factor- B
nm	Nanometre
nM	Nanomolar
NMR	Nuclear magnetic resonance
NR	Nile red

OLIG2	Oligodendrocyte lineage transcription factor
O-Palm	O-Palmitoyl
PA	Peptide amphiphile
PBPC	Peripheral blood progenitor cells
PBS	Phosphate buffered saline
PCV	Procarbazine, lomustine, and vincristine
PDGF	Platelet-derived growth factor
PDGFRA	Platelet-derived growth factor receptor-A
PEG	Poly ethylene glycol
PFS	Progression free survival
P-gp	P-glycoprotein
Phe/ F	Phenylalanine
PLA	Poly lactic acid
PMR	Perfusion-weighted magnetic resonance imaging
PTEN	Phosphatase and tensin homolog
Q-ETOP	GCPQ–etoposide
Q-LOM	GCPQ-lomustine
rCBV	Relative cerebral blood volume

RDF	Radial distribution function
RMT	Receptor mediated transcytosis
RNA	Ribonucleic acid
ROI	Regions of interest
RP	Reversed phase
siRNA	Small interfering ribonucleic acid
SPPS	Solid phase peptide synthesis
SRP	Subcutaneous reservoir and pump
sVEGFR2	Soluble vascular endothelial growth factor receptor 2
tBu	Tert-butyl
TEM	Transmission light microscopy
TFA	Trifluoroacetic acid
TIS	Triisopropylsilane
TKI	Tyrosine kinase inhibitor
TNF	Tumour necrosis factor
TP53	Cellular tumour antigen p53 (Tumour protein p53)
Tyr/ Y	Tyrosine
UK	United Kingdom

USA	United States of America
UV	Ultraviolet
v/v	Volume per volume
VEGF	Vascular endothelial growth factor
w/v	Weight per volume
WHO	World Health Organisation

Chapter 1 Introduction

1.1 Glioblastoma

Glioblastoma, previously named glioblastoma multiforme is a highly malignant glial tumour of astrocytic origin, occurring most commonly in the cerebral hemispheres, although glioblastoma may involve any neuroanatomical structure. Glioblastoma is a Grade IV astrocytoma (DeAngelis 2001; Furnari et al. 2007; Khasraw and Lassman 2010; Allard et al. 2009; Kesari 2011; Lima et al. 2012) and is still classified as such in the current World Health Organisation (WHO) classification of tumours of the central nervous system (CNS) (Louis et al. 2007).

Glioblastoma is the most frequently occurring (constituting at least 50 % of malignant gliomas) primary brain tumour in adults, and is the most biologically aggressive malignancy of the CNS (Furnari et al. 2007; Stark et al. 2005; Louis et al. 2007 Olar and Adalpe 2014). Glioblastoma is a leading cause of morbidity and mortality (Fine 1994; Yust-Katz et al. 2013) and together with other astrocytomas accounts for most of the deaths due to primary tumours (Fine 1994). At least 3 new cases of the disease are diagnosed per 100,000 people per year (Laperriere et al. 2002; Ohgaki and Kleihues 2005; Dolecek et al. 2012).

The current Central Brain Tumour Registry of the United States (CBTRUS) statistical reports of primary brain and CNS tumours diagnosed in the United States in the period 2005 – 2009 revealed that glioblastoma is uncommon in children but more common in older adults with peak incidence in the 75 – 84 years age range. The results showed that incidence was higher in white males compared to other races like African Americans, American Indian / Alaskan Natives and Asian Pacific Islanders (Dolecek et al. 2012).

The results also showed that to some extent, five year survival rates were better in children of less than 20 years of age (12 %) compared to those in adults (5 %). In most glioblastoma cases, tumours occur without pre-existing genetic predisposition and there is no clear-cut association of tumour occurrence with identifiable underlying causes or risk factors (Krex et al. 2007; Wen and Kesari 2008).

1.1.1 **Characteristics of Glioblastoma**

Glioblastoma, like most other neoplasia is characterised by unrestrained cell proliferation, vigorous angiogenesis, a tendency for necrosis, profound resistance to apoptosis, a high degree of genomic instability and diffuse invasion of surrounding healthy tissue (Furnari et al. 2007; Bokstein et al. 2008; Allard et al. 2009; Agarwal et al. 2011a; Florio and Barbieri 2012; Agarwal et al. 2013; Juratli et al. 2013; Olar and Aldape 2014) [Figure 1-1].

Also, in glioblastoma there is significant tumour heterogeneity such that cytogenetically similar and dissimilar clones could occur in different portions of the same glioblastoma tumour sample. This poses a challenge in understanding and treatment of the disease (Burger and Green 1987; Harada et al. 1998; Walker et al. 2003; Zhou et al. 2003; Furnari et al. 2007; Huse et al. 2011; Kesari 2011; Florio and Barbieri 2012; Jafri et al. 2013; Olar and Aldape 2014). The term multiforme used in the previous nomenclature of the disease is a reflection of the heterogenous nature of the tumours (Furnari et al. 2007; Agarwal et al. 2011a).

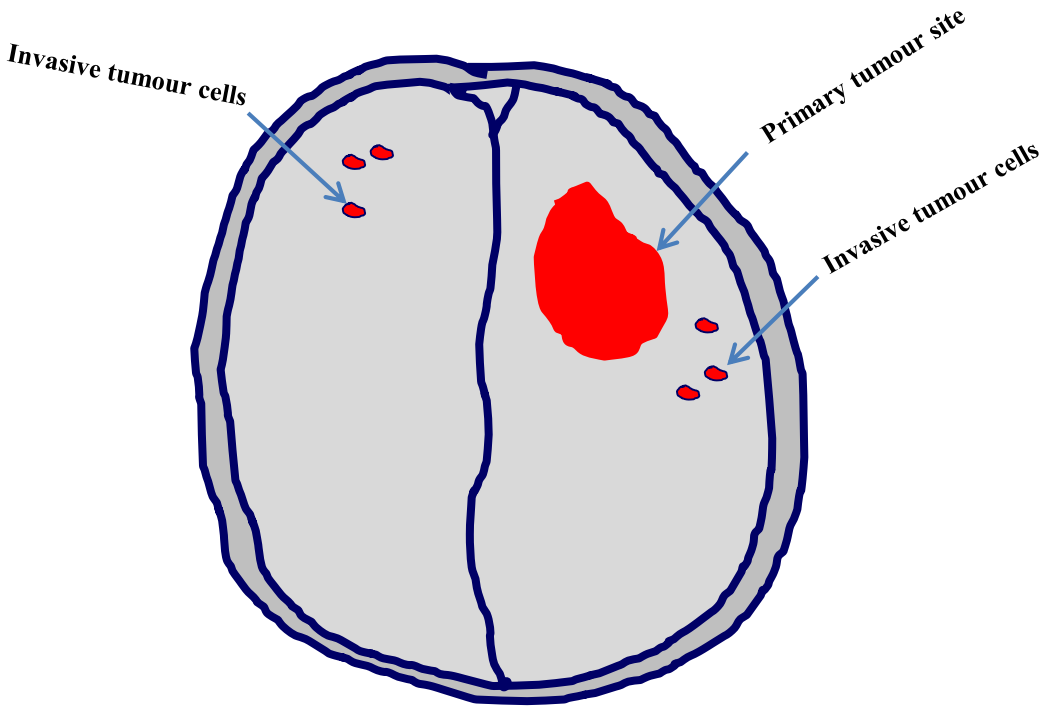

Figure 1-1: Schematic depicting glioblastoma a diffusely infiltrating disease

1.2 Diagnosis of Glioblastoma

Glioblastoma diagnosis is made only at clinical presentation as there is currently no other means of detecting or screening for the disease (Kesari 2011). Tomographic techniques are used for diagnosis because they provide high spatial resolution and techniques such as computed tomography (CT) can be used in initial diagnosis (Jarzabek et al. 2013). However, magnetic resonance imaging (MRI), which is the only test required for a brain tumour diagnosis (DeAngelis 2001), remains the gold standard for establishing diagnosis (DeAngelis 2001; Jenkinson et al. 2007; Kesari 2011). High resolution brain images generated by conventional MRI yield information to determine tumour size, location, and the presence and extent of necrosis and associated oedema. However, such images provide limited information on the physiological characteristics of the tumour (Jenkinson et al. 2007).

Recent advances in MRI have led to the development of newer MR techniques such as diffusion-weighted MRI (DW-MRI), perfusion-weighted MRI (PMR), functional MRI (fMRI), and proton magnetic resonance (proton MR) spectroscopy, which can be used for monitoring tumour vasculature, study tumour drug response and also distinguish high-grade gliomas from brain metastasis, thus providing more pertinent information (Law et al. 2002; Young 2007; Jenkinson et al. 2007; Server et al. 2010). Conventional MRI and clinical history can be used to differentiate between brain metastasis and high-grade gliomas in many cases (Law et al. 2002; Cha 2004). However, in some other cases especially those in which the lesion is solitary and the clinical data are non-contributory, conventional MRI has limited capacity to differentiate brain metastasis and high-grade gliomas as their neuroimaging appearance is frequently similar and may be ambiguous or indistinguishable (Law et al. 2002; Cha 2004; Server et al. 2010).

Proton MR spectroscopy (spectroscopic MR imaging) which permits simultaneous spectra acquisition from the enhancing portion, the peritumoural region, and normal contralateral brain tissue, and perfusion-weighted MRI (PMR) measurements in the peritumoural region have been shown to be useful in revealing the differences in solitary brain metastasis and high-grade gliomas (Law et al. 2002; Cha et al. 2007; Server et al. 2010). These two different types of intracranial lesions can be differentiated based on the metabolic and physiologic information obtained from the advanced MRI techniques which complement the anatomic images furnished by conventional MRI (Law et al. 2002). Moreover, tumour types have been shown to exhibit distinctive metabolic patterns (Meyerand et al. 1999) characteristic of each tumour type with histologically similar tumours exhibiting similar spectra patterns while histologically dissimilar tumours exhibit different spectral patterns (Bruhn et al. 1989).

The metabolites usually monitored by MR spectroscopy for distinguishing brain lesions include: choline, creatinine and N-acetyl-aspartate. Increased choline levels are associated with processes where there is increased cell proliferation or growth stimulation such as in tumours (Go et al. 1995; Herminghaus et al. 2002). The choline signal also yields information about the malignancy of tumours which is useful in the grading of gliomas (Möller-Hartmann et al. 2002). Creatinine is taken to be indicative of energy metabolism and is frequently employed as the internal standard (denominator) for semi-quantitative assessment of other brain metabolites since creatinine is assumed to be constant in a variety of metabolic conditions (Möller-Hartmann et al. 2002; Hattingen et al. 2008). N-acetyl-aspartate is commonly identified as a neuronal marker and the level is greatly reduced anytime brain tissue is damaged or replaced by any destructive, degenerative or infiltrative process (Möller-Hartmann et al. 2002).

In addition, lactate and lipid levels are also assessed in MR spectroscopy of brain lesions (Server et al. 2010). Some studies have employed MR spectroscopy in differentiation of brain lesions by comparing the ratios of the different metabolites (usually with creatinine as denominator) obtained for the different lesions evaluated. The spectra information obtained for the ratios of the different metabolites has permitted the differentiation of different brain lesions including the differentiation of brain metastasis of systemic tumours from high-grade gliomas (Law et al. 2002; Möller-Hartmann et al. 2002; Server et al. 2010).

Furthermore, PMR may provide a means of differentiating solitary brain metastasis from primary gliomas on the basis of the differences in peritumoural relative cerebral blood volume (rCBV) (Law et al. 2002), as well as the peak height of the non-enhancing T2 region and the percentage of signal intensity recovery of the contrast-enhancing region derived from dynamic susceptibility-weighted contrast-enhanced (DSC) PMR (Cha et al. 2007). These studies demonstrated markedly increased rCBV and the peak height of the non-enhancing T2 region as well as the percentage of signal intensity recovery of the contrast-enhancing region in glioblastoma (a high-grade glioma) compared to solitary brain metastasis (Law et al. 2002; Cha et al. 2007). Pathologic examination of peritumoural abnormality shows that there is a tumour induced increase in interstitial water due to alterations in capillary permeability and blood-brain barrier breakdown. In high-grade gliomas, the peritumoural areas manifest altered capillary morphologic findings and interstitial water as well as scattered tumour cells infiltrating along newly formed or pre-existing but dilated vascular channels. The enhancing portion of the tumour shows breakdown of the blood brain barrier, whereas the neural vasculature remains relatively impervious in the peritumoural region and the T2 hyper-intensity in the peritumoural region is partly the result of tumour infiltration.

Contrariwise, in solitary brain metastasis, the capillary endothelium of the metastatic tumour demonstrates increased permeability (Long 1979; Bertossi et al. 1997; Law et al. 2002). Moreover, the capillaries of solitary brain metastases typically resemble capillaries from the tissue of origin and do not possess the characteristics of brain capillaries (Long 1979). Thus, the increased rCBV, peak height of the non-enhancing T2 region and the percentage of signal intensity recovery of the contrast-enhancing region in glioblastoma compared to solitary brain metastasis shows that for metastatic tumors the peritumoural oedema observed represents pure vasogenic oedema resulting from increased interstitial water due to leaky capillaries, that is there is no histologic evidence of tumour beyond the outer contrast-enhancing margin of the tumour. In high-grade glioma, on the other hand, the peritumoural region depicts a variable combination of vasogenic oedema and infiltrating tumour cells (Long 1979; Bertossi et al. 1997; Law et al. 2002; Cha et al. 2007). Taken together, the spectra information obtained made it possible to differentiate brain metastasis from high-grade glioma (Law et al. 2002; Cha et al. 2007).

1.3 Prognosis for Glioblastoma

Glioblastoma continues to have a poor prognosis in spite of recent advances in diagnosis and therapeutic management of the disease. The mean survival time is about 12 – 15 months, 5 year survival rate is less than 5% and 75 % of patients die within 18 months of diagnosis (Stark et al. 2005; Mineo et al. 2007; Wen and Kesari 2008; Brandes et al. 2008; Mangiola et al. 2010; Chamberlain 2010; Dolecek 2012; Jafri et al. 2013) or within shorter periods as demonstrated in population based studies (Ohgaki et al. 2004). Although a small number of patients, called long-term survivors, survive for more than 3 years (Simpson et al. 1993; Krex et al. 2007; Bokstein et al. 2008; Dolecek 2012), the disease is consistently fatal (Rainov et al. 1997; Verhaak et al. 2010; Olar and Aldape 2014).

Some variables have been considered in determining prognosis in glioblastoma. These include treatment independent variables such as patient age, Karnofsky performance scale (KPS) score, tumour histology at diagnosis and treatment related variables such as the extent of surgery (Curran et al. 1993; Wong et al. 1999) [Figure 1-2; Table 1-1].

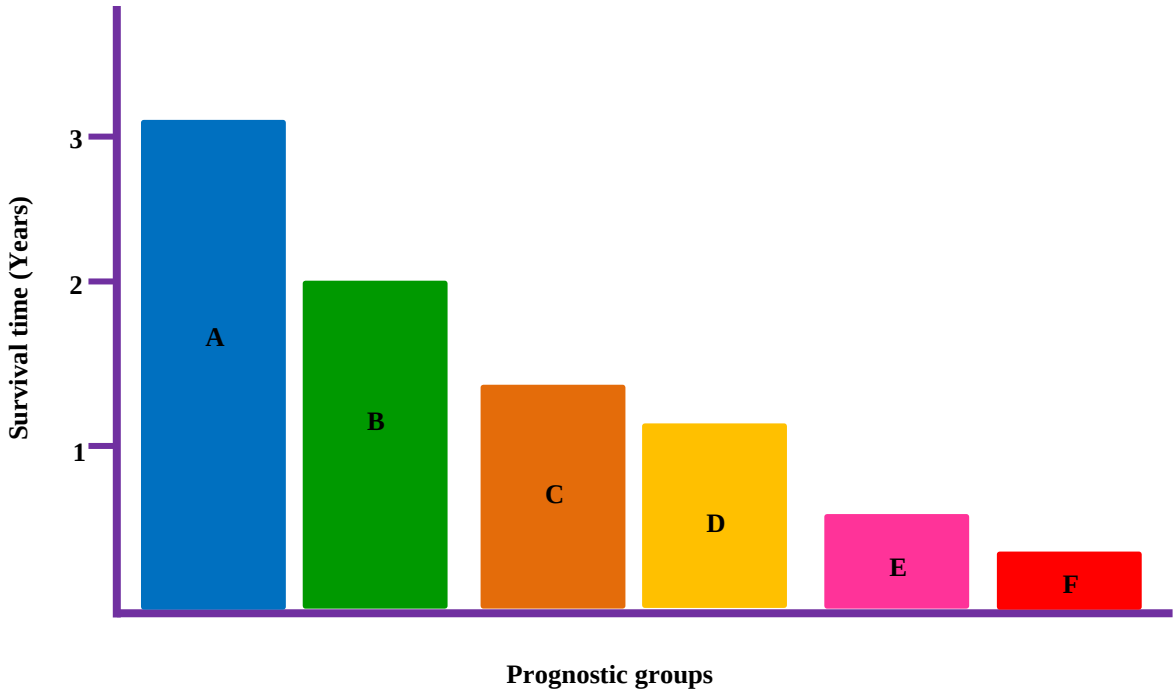

Figure 1-2: Schematic representation of survival with glioblastoma

Group	Prognostic factors
A	Long-term survivors: clinical and molecular factors largely unknown (Krex et al. 2007); favourable clinical factors such as younger patient age, high KPS.
B	Younger patient age at diagnosis, high KPS, absence of necrosis, maximal surgical resection (≥ 98 %), combined post-surgical radiotherapy plus concomitant chemotherapy, followed by adjuvant chemotherapy
C	Surgery plus post-surgical radiotherapy with adjuvant chemotherapy
D	Surgery plus post-surgical radiotherapy
E	Surgery alone
F	Older age at diagnosis, low KPS, no surgery, best supportive care

Table 1-1: Genenral survival trends in glioblastoma patients

Younger patient age at diagnosis, better KPS score at diagnosis (Burger and Green 1987; Franklin 1992; Lacroix et al. 2001; Filippini et al. 2008) as well as maximal surgical resection with minimal residual disease (Wood et al. 1988; Simpson et al. 1993; Wong et al. 1999; Lacroix et al. 2001) are favourable prognostic variables that lead to better survival outcomes.

Tumour histology also impacts significantly on survival as the presence of necrosis negatively impacts on survival as it is associated with unfavourable outcomes (Burger and Green 1987; Hammoud et al. 1996; Lacroix et al. 2001) as well as increased enhancement on preoperative MRI (Hammoud et al. 1996; Lacroix et al. 2001). More recently, information obtained from more advanced MR imaging techniques such as diffusion weighted (DW) MRI (DW-MRI) about the apparent diffusion coefficient (ADC) is also predictive of survival. Areas with minimum ADCs within heterogeneous tumours (such as glioblastoma) correspond to areas of highest cellularity and aggressiveness. Therefore patients with tumours showing low minimum ADC on pre-treatment DWMRI would likely have a poor outcome with post-surgical radio-chemotherapy (Yamasaki et al. 2010; Nakamura et al. 2013).

Furthermore, the use of post-surgical radio and chemotherapy has been shown to significantly impact survival, with patients treated with regimens containing a combination of post-surgical radiotherapy with chemotherapy showing significantly pronounced survival times (Stupp et al. 2005; Filippini et al. 2008).

1.4 Subtypes of Glioblastoma

Glioblastoma may be subdivided into two subtypes; namely primary and secondary glioblastomas, a concept first advanced by Hans-Joachim Scherer, a German neuropathologist (Scherer 1940). Primary and secondary glioblastomas are morphologically and clinically alike, and they have equally poor prognosis when adjustment is made for patient age (Newcomb et al. 1998; Furnari et al. 2007). Nevertheless, these two glioblastoma subtypes possess different clinical histories and show distinct patterns of gene expression or aberrations.

Primary glioblastoma is the most frequently occurring subtype comprising about 90 % of all cases. It develops acutely de novo, with a short clinical history without evidence of pre-existing lower grade precursor lesions and is more common in older adults (older than 50 years). Secondary glioblastoma on the other hand is less common and occurs in younger patients (younger than 45 years). It develops more slowly as a result of progression from a lower grade diffuse astrocytoma (WHO grade II) or anaplastic astrocytoma (WHO grade III) to glioblastoma (WHO grade IV) (Furnari et al. 2007; Ohgaki and Kleihues 2007). Usually, the time to progression from anaplastic astrocytoma to glioblastoma is shorter (about 2 years) than time to progression from low grade diffuse astrocytoma (about 5 years) to glioblastoma (Ohgaki and Kleihues 2005). However, this is not always the case as there have been cases of very rapid progression from anaplastic astrocytoma to glioblastoma in less than 1 year (Olar et al. 2012).

1.4.1 **Primary and secondary Glioblastomas**

Primary glioblastoma is usually characterised by epidermal growth factor receptor (EGFR) amplification/overexpression, cyclin-dependent kinase inhibitor 2A (CDKN2A / p16) deletion, phosphatase and tensin homolog (PTEN) gene mutations and occasionally murine double minute 2 (MDM2) amplification (Reifenberger et al. 1993; Watanabe et al. 1996; Tohma et al. 1998; Ohgaki et al. 2004) Secondary glioblastoma on the other hand is characterised by cellular tumour antigen p53 (TP53) gene mutations or accumulation (with LOH at chromosome 17p) which are known to occur in grade II and grade III astrocytomas and in the majority of cases already existed in the initial biopsies of patient tumours (James et al. 1989; von Deimling et al. 1992; von Deimling et al. 1993; Kleihues and Ohgaki 2000; Ohgaki et al. 2004). These genetic alterations distinguishing primary and secondary glioblastomas were found to be exclusive events in the evolution of these glioblastomas. This has been shown to be the case particularly when tumours for genetic analysis have been carefully selected from patients with confirmed diagnosis for either primary or secondary glioblastoma. That is, patients for primary glioblastoma had a short clinical history (less than 3 months) and presented with tumours that had histopathologic characteristics of glioblastoma at the first biopsy. Patients for secondary glioblastoma on the other hand were selected based on at least two previous biopsies taken at different time periods (6 months interval) for which clinical and histopathologic features had confirmed progression from a low grade glioma or anaplastic astrocytoma (Watanabe et al. 1996; Tohma et al. 1998; Kleihues and Ohgaki 2000).

In addition, a further subgroup of glioblastoma was identified which contain foci similar to oligodendroglioma and have been classified in the recent WHO classification of tumours of the CNS as glioblastoma with an oligodendroglial component (Louis et al. 2007). Some studies have reported that glioblastoma with oligodendroglial component (at least focally) make up a proportion (in the range of 20 %) of glioblastoma tumours analysed (He et al. 2001; Homma et al. 2006; Laxton et al. 2013). This subgroup of glioblastoma has been reported to be associated with increased survival which was attributed to younger patient age (Homma et al. 2006; Wang et al. 2012; Laxton et al. 2013). However, Homma and co-workers reported that in their study, the predictive value for longer survival associated with the oligodendroglial component in glioblastoma was lost when they made adjustment for age and gender in their multivariate analyses (Homma et al. 2006). On the whole, for glioblastoma with oligodendroglial component, the terminology, diagnostic criteria and outcome are still ambiguous, also their identity as a specific subgroup of glioblastoma has yet to be determined (Laxton et al. 2013).

Albeit none of the identified genetic alterations have not been able to provide a clear-cut distinction between primary and secondary glioblastomas. Moreover, there are some tumours that had genetic alterations that did not quite fit in to either primary or secondary subtypes, thus suggesting the existence of other subtypes of the disease (Tohma et al. 1998; Kleihues and Ohgaki 2000; Parsons et al. 2008; Ohgaki and Kleihues 2013).

1.4.2 **Molecular classification of Glioblastomas**

More recently, further subtypes of glioblastoma have been identified through molecular classification. In one study, three subtypes were identified as follows: Proneural subtype characterised by expression of genes associated with neurogenesis and the normal brain; Mesenchymal subtype which show activation of gene expression pathways characteristic of angiogenesis; and the Proliferative subtype with gene expressions indicating cell proliferation (Phillips et al. 2006). In a more recent study, four different subtypes of the disease were defined based on the most pronounced gene expression alteration and associated mutations determined by genomic profiling of glioblastoma (Table 1-2).

Subtype	Characteristics
Classical	EGFR amplification/overexpression and CDNK2A loss.
Proneural	Focal amplification along with high levels of platelet-derived growth factor receptor-A (PDGFRA) gene expression, high expression of oligodendrocyte lineage transcription factor (OLIG2), isocitrate dehydrogenase 1 (IDH1) mutation and TP53 mutations and loss of heterozygosity.
Neural	Expression of neuron markers such as neurofilament light polypeptide (NEFL).
Mesenchymal	NF1 loss, PTEN mutation and activation of tumour necrosis factor (TNF) and nuclear factor- B (NF-kB) pathways.

Table 1-2: Subtypes of glioblastoma based on major characteristic features

Most of the tumours previously diagnosed as secondary glioblastomas were classified as the proneural subtype in this study (Verhaak et al. 2010). The Proneural subtype has also been linked with younger patient age and genetic profiles such as PDGFRA abnormalities, TP53 and IDH1 mutations which had formerly been linked to secondary glioblastoma (Watanabe et al. 1996; Tohma et al. 1998; Kleihues and Ohgaki, 1999; Ohgaki et al. 2004; Yan et al. 2009). Furthermore, Proneural subtype glioblastomas were found to present with better prognosis than other subtypes as median survival for this subtype has been found to be remarkably longer than the other subtypes (Phillips et al. 2006; Verhaak et al. 2010). Also, although a distinct effect of treatment was demonstrated in other subtypes such as the Classical and Mesenchymal subtypes, the Proneural subtype did not show any survival benefit from aggressive treatment regimens (Verhaak et al. 2010).

Also, IDH1 mutations have been found to be associated with longer survival. It has been shown in separate analyses of glioblastoma patients treated with surgery and radiotherapy or radio- and chemotherapy that patients with IDH1 mutant ($IDH1^{mut}$) glioblastomas had mean overall survival more than twice as long as that of patients with wild type IDH1 ($IDH1^{wt}$) glioblastomas (Nobusawa et al. 2009; Yan et al. 2009). Likewise, a population – based study (Ohgaki et al. 2004) showed a significantly ($p = 0.003$) longer median overall survival for patients clinically diagnosed with secondary glioblastoma (7.8 months) compared to primary glioblastoma patients (4.7 months).

Furthermore, identification of these subtypes and their markers has also made it possible to make a clearer distinction between different subtypes of glioblastoma. For instance, IDH1 mutations are now recognised as a specific molecular diagnostic marker for secondary glioblastomas as they are found to occur in the majority (greater than 80 %) of secondary glioblastoma cases but rarely occur (less than 5 %) in primary glioblastomas.

This mutation was also found to occur with high frequency in WHO grade II (diffuse astrocytoma), WHO grade III (anaplastic astrocytoma) from which secondary glioblastomas evolve and in oligodendroglial tumors, suggesting this mutation occurs early on and may have a key function in the tumour evolution process (Balss et al. 2008; Watanabe et al. 2009; Yan et al. 2009; Nobusawa et al. 2009; Ichimura et al. 2009).

Some studies showed that for some glioblastomas which had IDH1 mutations that had been clinically diagnosed as primary glioblastomas, the patients were younger (10 – 27 years younger) than the mean age for primary glioblastoma (Nobusawa et al. 2009; Yan et al. 2009; Toedt et al. 2011), the tumours had genetic profiles (absence of EGFR amplification and TP53 mutations) identical to secondary glioblastomas with IDH1 mutation (Nobusawa et al. 2009; Toedt et al. 2011), and they had a longer (28.8 months compared to 3.8 months) clinical history than tumours without IDH1 mutations (Nobusawa et al. 2009). These findings suggest that these tumours with IDH1 mutations may actually be cases of secondary glioblastoma in which there had been very rapid progression from lower grade tumours which had not been previously diagnosed or tumours arising from lower grade lesions which had been clinically quiescent, leading to their erroneous classification as primary glioblastomas (Verhaak et al. 2010; Toedt et al. 2011; Ohgaki and Kleihues 2013). On the other hand, in some glioblastomas without IDH1 mutations that had been clinically diagnosed as secondary glioblastoma, the tumours showed less frequent TP53 mutations and more frequent p16 deletion than those with IDH1 mutations. More than 80 % of these tumours had progressed from anaplastic astrocytoma (WHO grade III) whereas most secondary glioblastomas with IDH1 mutations develop from diffuse (WHO grade II) gliomas (Nobusawa et al. 2009).

These may also represent cases in which the tumours had been diagnosed as anaplastic astrocytoma when they were really primary glioblastomas that were incorrectly diagnosed as a result of errors in sampling (Nobusawa et al. 2009; Toedt et al. 2011; Ohgaki and Kleihues 2013). Thus, IDH1 mutation is now considered to be a more unequivocal bench mark for diagnosis of secondary glioblastoma than conventional clinical and/or pathologic markers (Ohgaki and Kleihues 2013).

These finding could be potentially useful in determining treatment courses for glioblastoma patients such that dose escalation could be applied for patients (Classical and Mesenchymal subtypes) who would benefit from such regimens. For secondary glioblastoma patients on the other hand, dose escalation may not be necessary since most secondary glioblastomas have been classified as the Proneural subtype for which aggressive treatment did not yield survival benefit unlike the Classical and Mesenchymal subtypes which benefited from dose escalation (Verhaak et al. 2010; Ohgaki and Kleihues 2013).

1.5 Treatment of Glioblastoma

Presently, standard therapeutic management of newly diagnosed glioblastoma is based on an integrative approach comprising surgery followed by concurrent radio–chemotherapy and then adjuvant chemotherapy (Figure 1-3). This treatment strategy was adopted following the publication of the results of the 2004 European Organisation for Research and Treatment of Cancer (EORTC) 26981-22981/National Cancer Institute of Canada Clinical Trials Group (NCIC) CE3 randomised phase III trial (Stupp et al. 2005) which demonstrated an improvement in the median survival as well as 2-year survival rates of glioblastoma patients with post-surgical concomitant and adjuvant temozolomide (the Stupp regimen) compared to post-surgical radiotherapy alone (Stupp et al. 2009; Grossman et al. 2010; Khasraw and Lassman 2010; Niyazi et al. 2011; Juratli et al. 2013; Hong et al. 2013; Jarzabek et al. 2013; Olar and Aldape 2014).

However, there is no standardised treatment modality for the management of recurrent glioblastoma. Therapeutic options for patients with recurrent disease are limited so patients usually receive investigational agents in clinical trials (Wong et al. 1999; Florio and Barbieri 2012; Hong et al. 2013; Juratli et al. 2013).

For optimal management of glioblastoma, pathological diagnosis must first be established, usually by surgical biopsy before commencing radio- or chemotherapy, unless craniotomy is not possible, as in exceptional cases where surgery is contraindicated due to a great risk for the patient. In such cases, a stereotactic biopsy should be carried out for histological confirmation of diagnosis (Nieder et al. 2006; Chamberlain 2010; Lonardi et al. 2005).

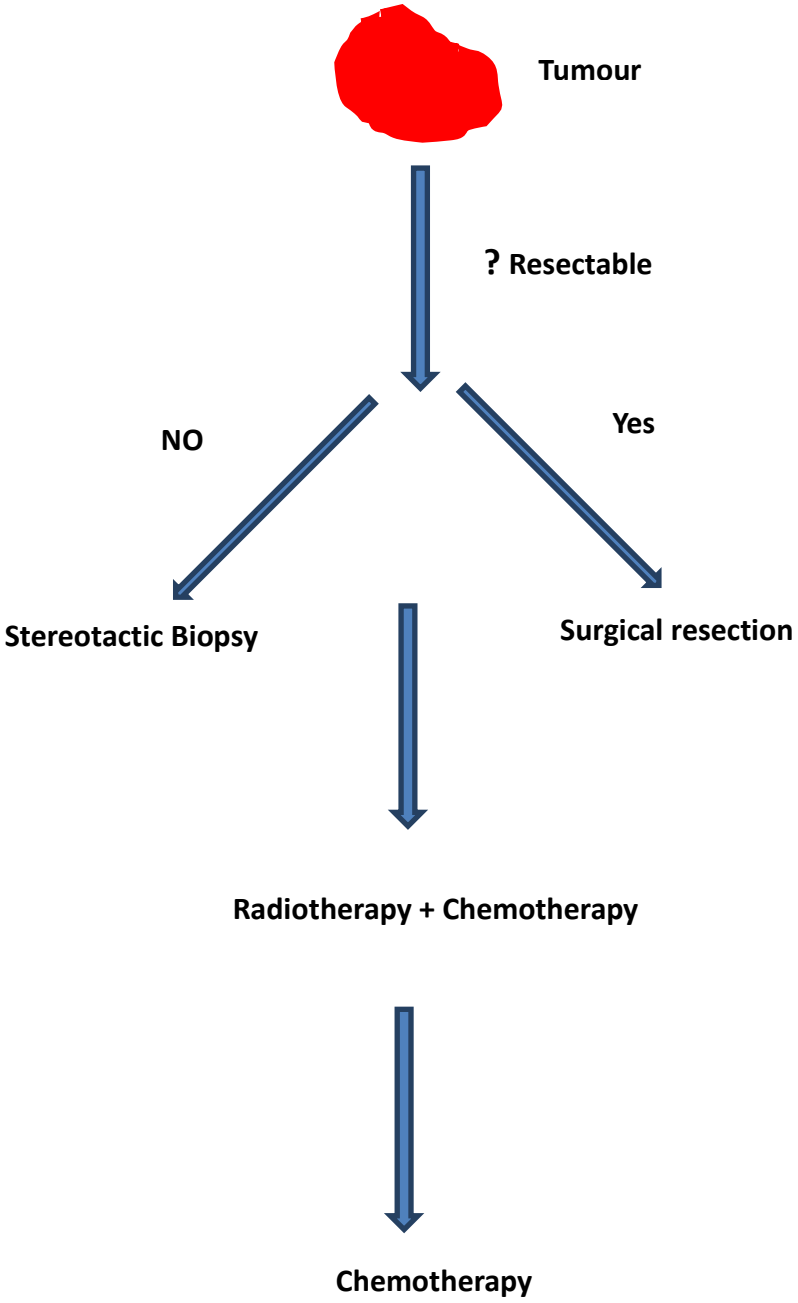

Figure 1-3: Treatment modalities for glioblastoma

1.5.1 **The role of surgery in the treatment of Glioblastoma**

Surgical resection is the first treatment strategy in the management of glioblastomas (Lonardi et al. 2005; Neider et al. 2006). The ultimate aim of surgery in high grade gliomas such as glioblastoma should ideally be to perform a total tumour resection which would have produced a cure (Lonardi et al. 2005). However, this is practically unfeasible owing to the highly infiltrative nature of the tumour cells which are sometimes located at or close to sites of vital brain function and may also involve recruitment of cells adjacent to the lateral ventricles. An attempt at total surgical resection would therefore pose a risk of functional loss. This restriction in the extent of tumour resection makes tumour recurrence imminent (Halperin et al. 1988; Fine 1994; Sanai and Berger 2009; Raizer 2011; Florio and Barbieri 2012; Agarwal et al. 2013; Hong et al. 2013; Juratli et al. 2013) and repeated surgeries may not always be feasible due to invasion of tumour cells into vital areas of the brain and even where it may be carried out, the benefits are limited unless combined with other salvage therapies (Wong et al. 1999; Mandl et al. 2008).

Therefore, the alternative strategy is to perform surgical resection to the greatest feasible extent for tumour debulking with the aim of brain decompression and reduction of symptoms such as intracranial pressure and other neurological symptoms; and improving the patients' quality of life and survival (Chamberlain 2010; Lonardi et al. 2005; Sanai and Berger 2009). Maximal surgical resection has been shown to lead to better overall outcomes (Simpson et al. 1993; Keles et al. 1999; Stummer et al. 2006; Stummer et al. 2008; Kreth et al. 2013), and leads to an improvement in the efficacy of adjuvant therapy (Stummer et al. 2006) even in recurrent disease where there is an indication of a better response to chemotherapy and outcome in patients with smaller volume of residual disease (Keles et al. 2004). This may be due to a greater permeability of the tumour vasculature leading to higher penetration of therapeutic agents.

Extent of surgical resection has been identified as an important predictor of survival outcome in glioblastoma although some studies did not demonstrate a clear association between the extent of surgery and survival (Franklin 1992; Hess 1999). Various studies have demonstrated that patients who have maximal resection with minimal residual disease have significantly increased survival compared with patients who have partial resection (Wood et al. 1988; Simpson et al. 1993; Wong et al. 1999; Lacroix et al. 2001).

1.5.2 **Radiotherapy in the treatment of Glioblastoma**

Radiotherapy with external beam irradiation has long been considered to be important in the treatment of high grade gliomas such as glioblastoma, as it was shown to produce improved survival compared to surgery alone or with best supportive care (Andersen 1978; Walker et al. 1978).

A post-surgical radiation dose of 60 Gy has been found to be optimal following studies that showed that this dose produced superior survival compared to lower doses (Walker et al. 1979; Chang et al. 1983; Bleehen et al. 1991), with demonstration of a clear trend of increased survival when the dose is increased from 45 – 55 Gy up to 60 Gy (Walker et al. 1979). Further increases in radiation dose up to 70 Gy did not produce superior results (Chang et al. 1983). In current standard clinical practice, radiation doses of 58 – 60 Gy are administered in 30 – 35 fractional doses of 1.8 – 2 Gy each, five days per week (Lonardi et al. 2005; Florio and Barbieri 2012; Juratli et al. 2013). The most popularly adopted dosing design involves the application of a focal dose up to 50 Gy to the tumour mass and surrounding oedema, with a further boost dose (total dose of 60 Gy) applied to the contrast enhancing tumour up to a 2 – 3 cm margin in order to reach most (up 80 %) of the tumour cells including those that might have infiltrated surrounding areas (Halperin et al. 1988; Halperin et al. 1989; Bokstein et al. 2008; Juratli et al. 2013).

In spite of improvements in survival with post-surgical radiotherapy, most tumour cells appear to be resistant to the therapy indicating the imminence of recurrence even after application of the optimal dose (Halperin et al. 1989; Baumann et al. 1992; Juratli et al. 2013).

Conventional post-surgical treatment for glioblastoma in the past comprised radiotherapy alone (Stupp et al. 2009; Raizer 2011). However the survival benefit was minimal (Stupp et al. 2005; Stupp et al. 2009; Brada et al. 2010) as it did not produce a significant improvement in overall survival and long term survivors were rare (Stupp et al. 2009). In current times, radiotherapy is combined with concurrent and adjuvant chemotherapy (Stupp et al. 2005) as the addition of chemotherapy has previously been shown to improve survival compared to post-surgical radiotherapy alone (Walker et al. 1978; Fine et al. 1993; Stewart 2002).

1.5.3 **Chemotherapy in the treatment of Glioblastoma**

The place of chemotherapy in the management of glioblastoma has become established in spite of initial controversy and uncertainty about the value of inclusion of chemotherapy in treatment protocols owing to failure of initial clinical trials to clearly demonstrate improved survival outcomes (Fine et al. 1993; Fine 1994; Gundersen 1998; Grossman 2003; Khasraw and Lassman 2010). Post-surgical chemotherapy may be administered as neoadjuvant (before radiotherapy), concomitant (simultaneously with radiotherapy) or as adjuvant (immediately after radiotherapy) chemotherapy (Lonardi et al. 2005; Chamberlain 2010).

The nitrosoureas had previously been recognised as the mainstay of chemotherapy for high grade gliomas (Jakacki et al. 1998; Weller et al. 2013) and have been employed, and continue to have a place as single agents (Hoogstraten et al. 1973; Walker et al. 1978; Cianfriglia et al. 1980; Rosenthal et al. 2004; Brandes et al. 2004; Reithmeier et al. 2010; Wick et al. 2010) and in combination with other agents (Kappelle et al. 2001; Stewart 2002; Brada et al. 2010; Weller et al. 2013; Yi et al. 2014) in glioblastoma therapy.

The major factor undermining the therapeutic success of these agents is dose limiting myelosuppression mainly neutropenia and thrombocytopenia associated with their use, which often necessitates dose delay and reductions thus compromising the tumour response to therapy (Cianfriglia et al. 1980; Kriegler et al. 1994; van den Bent et al. 1998; Jakacki et al. 1998; Gerber et al. 2007; Chamberlain 2010).

Temozolomide is the current drug of choice as first line chemotherapy for glioblastoma (Stupp et al. 2005; Gerber et al. 2007; Stupp et al. 2009; Brada et al. 2010; Grossman et al. 2010; Khasraw and Lassman 2010; Agarwal et al. 2011a; Raizer 2011; Yust-Katz et al. 2013; Juratli et al. 2013; Olar and Adalpe 2014). Temozolomide, an orally active imidazotetrazine derivative of dacarbazine is a second generation alkylating agent developed in the 1980s and introduced for chemotherapy of primary brain tumours in the 1990s (Newlands et al. 1992; Newlands et al. 1997; Juratli et al. 2013).

Temozolomide replaced nitrosoureas as first line chemotherapy for glioblastoma following the demonstration of significant benefits from concomitant and adjuvant temozolomide chemotherapy with radiotherapy in the EORTC-NCIC trial. In this trial involving 573 patients, this combination regimen produced median survival (at 28 months follow up) of 14.6 months compared to 12.1 months for radiotherapy alone and 2 year survival rate of 26.5 % compared to 10.4 % for radiotherapy alone, representing more than 2.5 times longer survival in the combination therapy group (Stupp et al. 2005). This survival advantage was an improvement on what had previously been demonstrated in a meta–analysis of 12 randomised trials of adjuvant nitrosourea chemotherapy which revealed a modest improvement (6 %) in survival with the addition of nitrosourea compared to radiotherapy alone (Stewart 2002).

Temozolomide is reportedly less toxic than most other alkylating agents and therapy is associated with improved quality of life (Newlands et al. 1992; Yung et al. 2000; Stupp et al. 2005; Combs et al. 2008; Chamberlain 2010;). However, therapy with this agent is also associated with dose limiting myelosuppressive effects, mainly thrombocytopenia, neutropenia and some other effects such as lymphopenia and induction of myelodysplastic syndrome which may necessitate discontinuation of therapy (Newlands et al. 1992; Gerber et al. 2007; Su et al. 2005; Tosoni et al. 2006; Chamberlain and Raizer 2009; Chamberlain 2010). Moreover in some studies, there was no distinct survival benefit of temozolomide compared to a standard procarbazine, lomustine, and vincristine (PCV) combination regimen (Brada et al. 2010) in a large (447 patients) randomised trial in chemotherapy-naïve patients with recurrent high grade gliomas. Also, in a study of 47 patients with newly diagnosed or recurrent glioblastoma treated with carmustine wafers, patients who received radio-chemotherapy with temozolomide and local carmustine delivery (wafers) did not have a significant survival advantage compared to patients who had received local carmustine alone and there was increased toxicity in the combination group (Gutenberg et al. 2013).

1.5.4 **Anti-angiogenic agents for Glioblastoma therapy**

Due to the importance of angiogenesis in tumour development and sustenance processes, angiogenic factors such as vascular endothelial growth factor (VEGF) and pathways are potential targets for the treatment of glioblastoma (Jarzabek et al. 2013), a highly vascularised tumour which possesses irregular blood vessels, high level of vascular proliferation and elevated expression of angiogenic factors particularly VEGF (Brem et al. 1972; Leon et al. 1996; Salmaggi et al. 2003; Grossman et al. 2014). Moreover, the degrees of vasculature density and VEGF expression have been found to correlate to tumour necrosis, hypoxia, grade and biological aggressiveness of the tumour and the overall clinical outcome (Shweiki et al. 1992; Leon et al. 1996; Zhou et al. 2003).

Bevacizumab, a humanized monoclonal antibody inhibitor of VEGF is the first anti - angiogenic agent approved for cancer therapy and is currently the only anti - angiogenic agent licensed by the FDA for treatment of recurrent glioblastoma (Friedman et al. 2009; Jarzabek et al. 2013; Grossman et al. 2014). The approval was based on the success of this agent in two phase II clinical trials (Friedman et al. 2009; Kreisl et al. 2009).

The first trial, was a prospective single institution trial of bevacizumab in combination with irinotecan (a topoisomerase I inhibitor frequently used in disease relapse, though with limited success) for the treatment of recurrent glioblastoma patients. The results of this trial showed 6 – month progression free survival rates of 42.6 % and 50.3 %, and median overall survival times of 9.2 months and 8.7 months for bevacizumab alone and in combination with irinotecan respectively (Friedman et al. 2009). The second trial, a single institution trial of bevacizumab as a single agent therapy in 48 patients with recurrent glioblastoma, the 6 – month overall survival was 57 %, median overall survival was 31 weeks and 6 – month progression free survival was 29 %. Also, radiographic response was achieved in 71 % (Levin criteria) and 35 % (MacDonald criteria) of the patients (Kreisl et al. 2009).

Efficacy and safety of bevacizumab with radiotherapy has also been investigated and a study demonstrated 50 % overall response rate, mean overall survival of 12.5 months, 1 – year survival of 54 % and 6 – month progression free survival rate of 65 % (Gutin et al. 2009). Therapy with bevacizumab is associated with some toxic effects such as intracranial haemorrhage, hypertension, proteinuria and reduced wound healing (Vredenburgh et al. 2007; Friedman et al. 2009; Kreisl et al. 2009), which are apparently related to the anti - angiogenic effects and depict VEGF blockade in healthy tissue (Chamberlain 2011).

The incidence of more serious toxic effects such as gastrointestinal perforation, cardiac failure and wound healing complications is low (usually less than 2 %) in glioblastoma patients (Friedman et al. 2009; Vredenburgh et al. 2007; Norden et al. 2008; Gutin et al. 2009). Also, tumour recurrence following bevacizumab result in more infiltrative tumours and resistance to therapy (Norden et al. 2008; de Groot et al. 2010; Scott et al. 2010).

Other antiangiogenic agents, namely sunitinib and sorafenib have demonstrated the preclinical potential for glioblastoma therapy (Yang et al. 2010; Grossman et al. 2014), however available clinical data do not compellingly demonstrate their benefit in glioblastoma therapy (Neyns et al. 2011; Hainsworth et al. 2010).

In addition, cediranib an orally available tyrosine kinase inhibitor (TKI) of VEGFR2, platelet-derived growth factor (PDGF) receptor-α and –β and stem cell growth factor receptor has been evaluated in phase III randomised trials as monotherapy, in combination with and compared to lomustine in recurrent glioblastoma. In the study, plasma samples were obtained at baseline and in the course of the study in order to determine the levels of the soluble biomarkers VEGF, sVEGFR2, as well as basic fibroblast growth factor (bFGF) and to calculate changes from baseline levels during the study. They recorded an increase in median VEGF levels in the cediranib monotherapy (30 mg) arm of 89 %, 108 %, and 106 % above baseline levels at days 42, 84, and 126, respectively. Similarly, an increase in VEGF levels was recorded at each time point in the cediranib (20 mg) plus lomustine arm (day 42, 46%; day 84, 41%; day 126, 61%). However, these median increases were lower than those for the cediranib monotherapy (30 mg) arm. In the lomustine arm on the other hand, median VEGF levels at day 42 were similar to those at baseline and decreased by 21% at day 84.

Median baseline levels of sVEGFR2 recorded were similar in the three arms. At day 42, decreases in median sVEGFR2 levels from baseline of 27% and 22% were recorded for the cediranib monotherapy (30 mg) and cediranib 20 mg plus lomustine arms, respectively; which were maintained in both arms at days 84 and 126. There was no change in median sVEGFR2 levels in the lomustine arm as the levels remained similar to baseline levels throughout the trial. There were no consistent changes in bFGF levels from baseline levels in any of the three arms. In the study, subgroup analyses showed that the baseline VEGF levels had no significant effect on either PFS or the overall survival outcome. Overall, the agent did not demonstrate an advantage of prolonging progression free survival (Batchelor et al. 2013).

From the foregoing, it is clear that there is still a great need for the development and application of safer and more effective therapeutic modalities for optimal management of glioblastoma, with the aim of increasing progression free and overall survival outcomes, as well as providing patients with a good quality of life (Chamberlain 2010; Agarwal et al. 2011a; Raizer 2011; Malmström et al. 2012).

1.6 Challenges of successful Glioblastoma treatment

The challenges of effective treatment of glioblastoma include: dose limiting toxicity of clinically used cytotoxic agents; development of tumour resistance to currently employed therapeutics; and limitation in the number of drug candidates due to the blood brain barrier (BBB) which restricts the entry of molecules to the brain.

1.6.1 **Toxicity**

The most important toxic effect of cytotoxic chemotherapy is their myelosuppressive effects (Lyman et al. 1998) due to their toxic effects on the cells of the bone marrow (Maxwell and Maher 1992; Kriegler et al. 1994; Raizer 2011). Myelosuppression resulting from cytotoxic chemotherapy represents the most frequent cause of combined reduction in peripheral blood cell counts in the developed world (Carey 2003).

Chemotherapy induced myelosuppression manifests mainly as neutropenia which carries the risk for life threatening infections (Peters et al. 1993; Lyman et al. 1998; Crawford et al. 2004; Dale 2002) and thrombocytopenia which predisposes patients to bleeding complications (Morstyn et al. 1988; Elting et al. 2001; Gerber et al. 2007; Hitron et al. 2011). Chemotherapy dose intensity is greatly restrained by myelosuppressive effects of clinically employed cytotoxic agents (Cianfriglia et al. 1980; Peters et al. 1993; Cairncross et al. 1994; Chamberlain and Raizer 2009; Chamberlain 2010). This frequently leads to the necessity for dosing delays, reductions or outright discontinuation (Intile et al. 2009; van den Bent et al. 2006; Hitron et al. 2011).

These toxic effects may lead to a need for hospitalisations, additional costs for rescue therapy and a poor quality of life for patients (Intile et al. 2009; Hitron et al. 2011). Also, it may compromise tumour response and overall survival time as a result of the attendant dose reductions and treatment delays (Hitron et al. 2011).

1.6.2 **Chemotherapy resistance in Glioblastoma**

Tumour resistance to alkylating agents employed in chemotherapy is mainly mediated by the overexpression of O^6-alkylguanine-DNA alkyltransferase (AGAT), a ubiquitous protein encoded by the O^6-methylguanine-DNA-methyltransferase (MGMT) gene. AGAT is a DNA repair enzyme that functions alone to remove damages in DNA by removing alkyl groups from the O^6 position of guanine and O^4 position of thymine by transferring the alkyl group to a cysteine acceptor residue in its own amino acid sequence in a stoichiometric manner, thereby reversing the alkylation reaction and restoring DNA structure (Dumenco et al. 1989; Pegg 1990; Tano et al. 1990; Gerson 2004). As these (O^6 position of guanine and O^4 position of thymine) are important alkylation sites for alkylating agents commonly employed in cancer chemotherapy, high levels of DNA repair activity of AGAT render tumour cells resistant to these agents (Dumenco et al. 1989; Schold et al. 1989; Tano et al. 1990; Gerson 2004). However, if the toxic (mutagenic) lesions produced by DNA alkylation are not repaired, the process of cytotoxicity and apoptosis will be activated in the tumour cells leading eventually to cell death (Ochs and Kaina 2000; Gerson 2004). Upon alkylation of AGAT, the alkylated protein is permanently inactivated, thus the protein can act only once and new AGAT protein has to be synthesised in order to "replenish the stock" and restore cellular function of this protein (Pegg, 1990; Tano et al. 1990).

Studies have suggested that the majority of gliomas express the AGAT protein which makes it of clinical significance as it is an important predictor of chemo sensitivity or resistance (Hegi et al. 2005; Chamberlain 2010). Activity of the protein is turned off by methylation (hypermethylation) through epigenetic silencing of the promoter for the gene which leads to decreased levels of the protein (AGAT) resulting in better response to chemotherapy (Gerson 2004; Weller et al. 2010).

The clinical significance of the promoter methylation status has been demonstrated in studies which have shown an increased response to chemotherapy with alkylating agents and survival benefits in patients with a hypermethylated promoter (Hegi et al. 2004; Hegi et al. 2005).

Since AGAT is consumed in the process of alkylation damage repair, administration of alkylating agents in regimens that produce cumulative and continued consumption and inactivation of the protein, leading to increased chemosensitivity may lead to improved therapeutic efficacy (Dolan et al. 1990). This approach has been evaluated by administering protracted doses of temozolomide which has been found to produce considerable inactivation of AGAT (Tolcher et al. 2003), and some studies have demonstrated survival benefits (Brandes et al. 2006; Wick et al. 2007) for such an approach. However, it is not clear if accruing benefits of such regimen can be attributed to AGAT depletion since repeated brain biopsy is impracticable (Weller et al. 2010). Moreover, some clinical studies have shown that the survival benefit with such a dosing regimen is produced in patients with a methylated promoter (Herrlinger et al. 2006; Glas et al. 2009; Weiler et al. 2010).

Furthermore, an alternative approach to increase sensitivity of chemotherapeutic agents would be to administer a pseudosubstrate for AGAT before the therapeutic agent such that the protein is inactivated and would need to be synthesised again by cells (Schold et al. 2004). This approach has been evaluated in a Phase II clinical trial in which O^6-benzylguanine was administered to patients just before administration of temozolomide. Although there was restoration of temozolomide sensitivity in temozolomide-resistant anaplastic glioma patients, no significant restoration of temozolomide sensitivity was observed in patients with temozolomide-resistant glioblastoma (Quinn et al. 2009).

Due to the key role the AGAT gene promoter methylation status plays in determining tumour response to chemotherapy and by extension overall clinical outcomes in patients receiving chemotherapy, it is now considered as the most important prognostic factor in malignant gliomas such as glioblastoma and is used in clinical trials for stratification of patients (Stupp et al. 2009; Weller et al. 2010; Kreth et al. 2013).

1.6.3 **The Blood brain barrier (BBB)**

The BBB is a system of vascular cellular structures, characterized by continuous physical barriers such as tight junctions (which prevent blood- borne substances from seeping into the brain parenchyma) between adjacent endothelial cells; a lack of fenestrations, very low pinocytotic activity, and metabolic barriers such as enzymes, receptors, transporters, and efflux pumps of the multidrug resistance (MDR) pathways that regulate the access of molecules to the brain. This is a barrier formed in humans and other mammals by the endothelial cells lining the walls of the capillaries of the brain and spinal cord (Kniesel and Wolburg 2000; Brightman and Reese 1969; Bhaskar et al. 2010; Juillerat- Jeanneret 2008; Stamatovic et al. 2008). The BBB is exhibited by all organisms with a well-developed CNS (Abbott 2005).

Along with the BBB, there are other CNS barriers such as the blood cerebrospinal fluid barrier (BCSFB) and the avascular arachnoid epithelium which completely encloses the CNS, thus completing the seal between the CNS extracellular fluids and the general circulation (Pardridge 1995; Abbott 2004; Begley 2004; Abbott et al. 2006). At these interfaces, a combination of the different components, that is the physical (tight junctions between cells blocking the intercellular or paracellular pathway), transport (specific transport mechanisms mediating solute flux), and metabolic (enzymes metabolizing molecules in transit) barriers mediate the barrier function of the BBB (Abbott et al. 2006).

Nevertheless, the BBB is considered the main regulatory site for uptake and delivery of drug molecules into the brain parenchyma owing to its large surface area (12- 20 m^2 /1.3 kg brain) and short diffusion distance (10- 15 μm) from the capillaries to the neurons (Pardridge 1991; Abbott 2004; Schlageter et al. 1999; Abbott 2005; Begley 2003).

The presence of the BBB places considerable restriction on the number and type of molecules that can access the brain. Only a very restricted number of small (Mwt usually < 400-600 Da), lipid soluble molecules can cross the BBB by passive diffusion, all other molecules including potentially beneficial therapeutic agents can enter the brain only by receptor mediated transcytosis, or by specific carrier systems, making the treatment of CNS pathologies such as glioblastoma particularly challenging (Misra et al. 2003, Deeken and Wolfgang 2007; Juillerat-Jeanneret 2008; Raizer 2011).

1.6.3.1 Structure of the Blood brain barrier (BBB)

The brain endothelial cells in close association with other cellular structures such as the pericytes, glial cells (astrocytes), microglia, neuronal processes and the basal lamina which ensheath the cerebral blood vessels establish and maintain the BBB. The interactions between these different cell types contribute to the properties of the BBB (Iadecola 2004; Abbott 2005; Abbott et al. 2006).

1.6.3.2 Functions of the BBB

The BBB acts as a physical and metabolic barrier between the CNS and the general circulation (Calabria and Shusta 2006). In conjunction with the BCSFB, the BBB maintains brain homeostasis and protects the brain from potential damage that could arise from neuroactive and other toxic compounds, which may be endogenous metabolites or proteins; or diet ingested or environmentally acquired xenobiotics, circulating in the plasma. Neurotoxins are actively pumped out of the brain by energy- dependent ABC efflux transporters (ATP-binding cassette transporters) present in the BBB (Abbott et al. 2010; Calabria and Shusta 2006; Abbott and Romero 1996).

The BBB also provides a stable environment for neural function and maintains optimal ionic composition for synaptic signalling by a combination of specific ion channels and transporters. As a result, the concentration of potassium in cerebrospinal fluid (CSF) and brain interstitial fluid (ISF) is maintained at a defined range (≈ 2.5 mM – 2.9 mM), despite changes in the plasma after meals or exercise, experimental manipulations or pathological conditions (Bradbury and Davson 1965; Hansen 1985.) Active regulation of calcium and magnesium ions, as well as pH also occurs at the BBB (Jeong et al. 2006; Nischwitz et al. 2008; Abbott et al. 2010).

Furthermore, the BBB also helps to prevent uncontrolled release of neuroexcitatory amino acid glutamate (present in blood plasma at high levels) into the brain ISF. This protects the neural tissue from permanent neurotoxic/neuroexcitatory damage. The BBB also helps to separate between peripheral and central transmitter pools and minimizes exchange between the two (Abbott et al. 2006; Bernacki et al. 2008).

In addition, the BBB prevents the entry of many macromolecules including plasma proteins (such as albumin, pro- thrombin and plasminogen), which can cause brain tissue damage in the brain (Nadal et al. 1995; Gingrich and Traynelis, 2000; Gingrich et al. 2000).

Adequate nutritional and metabolic requirements of the BBB are maintained by specific transport systems expressed in the BBB which ensure an adequate supply of many essential water soluble nutrients and metabolites (with low BBB permeability) required by nervous tissue (Abbott et al. 2010).

1.6.3.3 Circumventricular Organs (CVOs)

The CVOs refer to those areas of the CNS where the classical BBB capillary endothelial cells (thus lacking tight junctions) are not expressed. They have micro-vessels similar to those of the periphery, thus permitting the diffusion of large molecules. These areas include the organum vasculosum of the lamina terminalis, the subfornical organ, the median eminence and the area postrema. The exchange between the specialised neurons and the blood need to be maintained in the CVOs for neuropeptide secretion into the blood and for chemosensitivity (to enable the brain to monitor blood composition). However, these regions do not form a leak across the BBB due to the presence of tight junctions between specialised ependymal cells in CVOs, and between the processes of tanycytes and astrocytic glia that isolate the CVOs from the brain parenchyma (Brightman 1977; Schlageter et al. 1999; Ganong 2000; Abbott et al. 2006).

Moreover, active drug-efflux-transporter proteins such as P-glycoprotein (P-gp), multidrug resistance protein, breast cancer resistance protein and other transporters which abound in the luminal membranes of the CNS also actively remove a wide range of structurally and functionally unrelated molecules from the brain (Dallas et al. 2006 ; Tamai and Tsuji 2000). Also, the surface area of the tight BBB capillaries is much greater (5000 times) than that of the permeable fenestrated capillaries of the CVOs. Thus, these higher permeability areas do not create a practical route of entry (drug delivery) into the brain (Begley 1996).

1.6.3.4 The Blood-Tumour Barrier (BTB)

Apart from the physiologically established CNS barriers which prevent access of most molecules to the brain parenchyma, the BTB is another barrier thought to restrict access of systemically administered chemotherapeutic agents to tumour cells thus protecting them from such agents (Cloughesy and Black 1995; Black and Ningaraj 2004; Raizer 2011 Agarwal et al. 2011a). Transport of nutrients, growth factors, therapeutics and other molecules is regulated by the tumour cell membrane which constitutes the barrier. This barrier function by the tumour cells is mediated by the expression of drug efflux pumps of the ATP-binding cassette (ABC) gene family (similar to those of the BBB) such as P-gp and multidrug resistance protein (MRP) expressed by these cells, (Nabors et al. 1991; Demeule et al. 2001; Spiegl-Kreinecker et al. 2002; Decleves et al. 2002; Fattori et al. 2007; Agarwal et al. 2011a) and their vasculature (Nabors et al. 1991; Tóth et al. 1996). The P-gp efflux pumps have been the focus of most studies on this subject, but there have been controversy about the expression and role of P-gp efflux pumps in mediating chemo resistance in glioblastoma tumours (Agarwal et al. 2011a).

Some studies have reported the expression of this drug efflux mechanism in gliomas cells (Nabors et al. 1991; Demeule et al. 2001; Fattori et al. 2007) although others have reported either the absence (Decleves et al. 2002) or infrequent (Spiegl-Kreinecker et al. 2002) expression of the efflux mechanism. However, the conflicting reports of the various studies might be due in part to inadequacies of the assay methods employed, as it has been shown that many antibodies thought to be specific for P-gp demonstrated poor specificities (Ashmore et al. 1999). In spite of the conflicting reports about the expression of P-gp efflux pumps in glioma cells, it is agreed that there is expression of MRPs in glioma cells which reduce tumour accumulation of therapeutic agents (Decleves et al. 2002; Spiegl-Kreinecker et al. 2002). From the foregoing, it is apparent that tumour cells exhibit an additional barrier (BTB) mechanism which constitutes another hurdle (in addition to the BBB) to be crossed for effective delivery of therapeutic agents for successful treatment of brain tumours (Black and Ningaraj 2004; Agarwal et al. 2011a).

1.6.3.5 Status or integrity of the BBB in glioblastoma

The BBB is reportedly altered in brain tumours such as glioblastomas which render the BBB less intact than in normal healthy brain vasculature (Nieder et al. 2006; Jain et al. 2007; Deeken and Wolfgang 2007). Analysis of glioblastoma tumour samples revealed molecular alteration in the microvessels which was demonstrated by changes in expression of the junctional proteins. These samples also showed intermittent rather than continuous endothelial and morphologically altered pericytes. (Liebner et al. 2000). However, this BBB disruption does not occur uniformly throughout the tumour. Loss of BBB integrity occurs mostly at the contrast enhancing tumour regions (tumour core) which is highly angiogenic with new and "leaky" blood vessels, while it remains intact in tumours that lack contrast enhancement.

Since glioblastomas are highly infiltrating tumours, smaller lesions located in adjacent areas of the brain will also possess intact BBB/BTB (Deeken and Wolfgang 2007; Raizer 2010; Agarwal et al. 2011a). Therefore, although high drug concentrations may be achieved at the tumour core, this does not reflect the effective drug concentration achievable for chemotherapy since this contrast enhancing tumour area is usually removed by surgery (Agarwal et al. 2011a). Thus, the challenge remains the efficient delivery of therapeutic agents to the tumour cells not located at the tumour core and diffusely infiltrating tumour cells that may have penetrated distant parts of the brain (Raizer 2010; Agarwal et al. 2011a).

1.6.4 **Drug delivery to intracranial tumours**

Although there is evidence of BBB disruption at the core tumour bed harbouring the larger lesions and evidence that this may greatly facilitate delivery of therapeutic agents to such sites, this may not yield treatment benefits because such lesions are usually removed by surgical resection (Agarwal et al. 2011a). This leaves the diffusely infiltrating tumour cells which may be located in seemingly healthy adjacent brain areas; successful treatment thus requires delivery of therapeutics to these infiltrating tumour cells, which still possess a functionally intact BBB, in sufficient and therapeutically effective concentration (Nieder et al. 2006; Allard et al. 2009; Raizer 2011; Agarwal et al. 2011a).

A number of strategies can be employed for effective delivery of therapeutics to glioglastomas and other CNS pathologies. These strategies can be classified into invasive and non-invasive strategies.

1.6.4.1 Invasive strategies for drug delivery to CNS tumours

1.6.4.1.1 Disruption of the BBB

This involves temporary disruption of the BBB by intra-arterial administration of hypertonic solutions such as mannitol, urea or saline, with mannitol (approved for human use) been the most frequently used (Kroll and Neuwelt 1998) hypertonic solution. This has been shown to increase drug (methotrexate) concentration in the CSF (Zylber-Katz et al. 2000) and in clinical studies has been shown to lead to improved survival outcomes in patients with primary CNS lymphoma (McAllister et al. 2000). This strategy has also been employed in the administration of bevacizumab in patients with recurrent malignant glioma (Boockvar et al. 2011) and also in the chemotherapy of pontine diffuse gliomas (Hall et al. 2006) with improved therapeutic outcomes. BBB disruption can also be effected by intracarotid infusion of bradykinin and has been shown to increase brain permeability (Nomura et al. 1994; Sarker et al. 2000). However, this strategy may not be applicable for long term use and the procedures are potentially risky and may produce toxic effects (Agarwal et al. 2011a).

1.6.4.1.2 Direct administration of chemotherapeutics into the CNS

This strategy involves direct application of the therapeutic agents into the CNS thereby by-passing the BBB. This may be achieved by techniques such as administration through the intracerebroventricular/intrathecal route, direct application of drug impregnated polymer delivery system at the site of action, or convection-enhanced delivery (Bobo et al. 1994; Petri et al. 2007).

1.6.4.1.2.1 Intraventricular/Intrathecal administration

This strategy involves direct intralumbar injection or intraventricular infusion of drugs directly into the CSF using a ventricular (Ommaya) reservoir. The Ommaya reservoir was introduced as a subcutaneous reservoir and pump (SRP) in 1963 (Ommaya 1963). The device was designed to overcome the challenges posed by the need for repeated sampling or repeated introduction of drugs into the CSF (Ommaya 1963). The SRP was initially introduced for access to ventricular and spinal CSF mainly for the administration of antifungal agents in the treatment of fungal meningitis, it has since been applied in the therapy of many other conditions especially in various CNS tumours (Ommaya 1984; Chamberlain et al. 1997; Sandberg et al. 2000; DeAngelis and Boutros 2005). The Ommaya [originally made of self-sealing (if needles of small gauge < no 20 are used) silicone rubber] reservoir is subcutaneously implanted in the scalp and connected to the brain ventricles through a catheter. Drug solutions can be subcutaneously injected into the implanted reservoir and delivered to the ventricles by manual compression of the reservoir through the scalp (Ommaya 1984; Misra et al. 2003). Limitations of this method include a slow rate of drug distribution within the CSF, increase in intracranial pressure, high clinical incidence of hemorrhage, CSF leaks, neurotoxicity and CNS infections. (Chamberlain et al. 1997; Misra et al. 2003).

1.6.4.1.2.2 Application of drug-impregnated polymer delivery system

This strategy for local administration of adjuvant chemotherapy to surgical tumour resection cavity in the treatment of malignant gliomas was developed in the 1990s (Juratli et al. 2013). The only agent approved by the FDA for use as adjuvant chemotherapy is Gliadel® wafer. This is a sterile wafer implant composed of the biodegradable polymer, polifeprosan 20 {Decanoic acid-4,4'-[1,3-propanediylbis (oxy)] bis (benzoic acid) copolymer)} impregnated with carmustine which is released slowly (controlled release) at the surgical cavity (Agarwal et al. 2011a; Juratli et al. 2013). Application of such locally implanted wafers leads to longer and higher local drug concentration compared to systemic (bolus) administration with the potential to reduce systemic toxicity of carmustine (Juratli et al. 2013).

Evaluation of these implants in clinical trials demonstrated survival benefits for patients who receive carmustine impregnated wafers as part of their post-surgical therapy (Westphal et al. 2003; Attenello et al. 2008). From a surgical point of view, local intracerebral chemotherapy with carmustine wafers is uncomplicated and is not associated with systemic toxicities. Nevertheless, a number of complications have been linked with implantation of the wafers including healing abnormalities, intracranial infections, cerebral edema, CSF leaks, seizures and cyst formation. Also, combination of the intracerebral carmustine with concomitant radiochemotherapy may be associated with the risk of increased toxicity (Bock et al. 2010).

1.6.4.1.2.3 Convection-enhanced delivery

Convection-enhanced delivery, a concept described by Bobo and co-workers in 1994 is another strategy for by passing the BBB by direct delivery of therapeutics to the CNS. They developed this strategy based on the hypothesis that fluid convection (or bulk flow) created within the brain by interstitial infusion at a pressure gradient can be employed to augment diffusion and consequently enhance the distribution of molecules including high molecular weight proteins in the brain (Bobo et al. 1994). This technique involves the stereotactic application of catheters directly to brain tumour or tissue through cranial burr holes. Fluid convection which can deliver desired agents at constant concentrations over a relatively large intercerebral volume is generated to the catheters by a connected motor-driven pumping device (Juratli et al. 2013). This facilitates the direct infusion of therapeutic agent to target tissue, which may be the enhancing tumour or non-enhancing infiltrating surrounding areas (Agarwal et al. 2011a; Juratli et al. 2013) at predetermined rate and concentration for the desired duration (Juratli et al. 2013). This technique has been employed in some clinical trials in delivery of therapeutic agents for recurrent gliomas with some limited success as well as some reports of treatment related complications (Lidar et al. 2004; Kunwar et al. 2010; Bernal et al. 2014).

1.6.4.2 Non-invasive strategies for drug delivery to CNS tumours

Non-invasive techniques for delivery include inhibition of BBB transporters, and nanoparticle based delivery systems.

1.6.4.2.1 Inhibition of BBB transporters

The drug transport proteins (efflux pumps) at the BBB actively remove molecules from the brain thereby restraining the access of some therapeutics which could be potentially useful for treatment of some CNS pathologies (Kniesel and Wolburg 2000; Abbott 2004; Stamatovic et al. 2008; Bhaskar et al. 2010; Agarwal et al. 2011a). Thus the inhibition of this efflux mechanism could potentially lead to an increased concentration of such therapeutics in the brain (Agarwal et al. 2011a). Several studies have shown increased brain concentrations of the therapeutic agents after administration of efflux pumps inhibitors such as P-gp or BCRP inhibitors such as elacridar (GF120918) and zosuquidar (LY335979) (Lagas et al. 2009; Chen et al. 2009; Agarwal et al. 2011b).

1.6.4.2.2 Nanoparticle-based delivery systems

Drug-carrier nanoparticles are submicroscopic colloidal systems that may act as drug vehicles, either as nanospheres or nanocapsules depending on the method of preparation (Juillerat-Jeanneret 2008; Soppimath et al. 2000). A therapeutic nanoparticle system usually comprises the therapeutic agent of interest (small molecule, peptide, protein or nucleic acid) and the components (such as lipids or polymers) that would assemble with the therapeutic agent into nanoparticles (Davis et al. 2008). These systems can increase the solubility of incorporated drug and provide a controlled release function at the site of action (Chen et al. 2008).

Nanoparticle-based systems represent a promising platform for delivery of therapeutics to cross the BBB due to their high specificity, and they tend to accumulate at higher concentrations at the site of action than drugs in solution (Chen et al. 2008; Davis et al. 2008; Bhaskar et al. 2010). Preferential accumulation of nanoparticles at sites of action such as tumour site, inflammatory site and so on, occurs as a result of the enhanced permeability and retention (EPR) effect of the vasculature (Davis et al. 2008; Singh and Lillard 2009). Subsequently, hydrophobic biodegradable polymeric nanoparticles can act as local depot (if so designed) for loaded drug, thus providing continuous supply (sustained release) of the therapeutic agent at the desired site of action such as solid tumours (Singh and Lillard 2009).

Nanoparticles possess certain unique features which make them attractive for application in drug delivery for cancer therapy (Davis et al. 2008). Nanoparticles have the capability to carry and protect a large payload of therapeutic agents (Davis et al. 2008). For instance, a nanoparticle (70 nm) was shown to carry about 2, 000 small interfering RNA (siRNA) molecules (Bartlett and Davis 2007) while an antibody conjugate could bear only about 6 siRNA molecules (Song et al. 2005). Other therapeutics such as small molecules or peptides could also be loaded into nanoparticles in similar manner and multiple classes of therapeutic agents can be incorporated within a nanoparticle to exert their various effects in a controlled manner (Davis et al. 2008). Also, the pharmacokinetic and biodistribution of nanoparticles are not affected by the type or number of payloads they carry since the loaded moieties are located within the particle. On the other hand, the pharmacokinetics of loaded therapeutic agent could be improved by the size and surface properties of the nanoparticle (Davis et al. 2008).

Furthermore, nanoparticles can be functionalised with multiple ligands for enhanced transport and site specific delivery. Thus a given nanoparticle could be functionalised with ligands that would enhance transport to and uptake at the site of action such as the brain (for example, a transporter molecule such as transferrin); targeting ligands for multivalent binding to specific receptors on the surface of target cells; antibodies against tumour markers for targeting and binding to target tumour cells which may potentially lead to improved efficacy and reduced toxicity; and appropriate fluorescent markers for tracking and imaging purposes (Hong et al. 2007; Bhaskar et al. 2010). In addition, modification of the surface properties of polymeric nanoparticles by coating them with surfactants such as polysorbate 80 or other polysorbates with 20 polyoxyethylene units and coating of non-viral gene delivery systems using poly ethylene glycol (PEG) attachment for siRNA delivery have been shown to be advantageous in brain targeting (Pardridge 2007; Bhaskar et al. 2010).
Nanoparticle-based delivery systems may deliver incorporated therapeutic agents to the brain mainly by either carrier-mediated transport (CMT) for small molecules or endocytotic transcytosis for macromolecules (Pardridge 2007; Abbott et al. 2010; Bhaskar et al. 2010).

1.6.4.2.2.1 Carrier-mediated transport (CMT) or carrier-mediated influx

CMT are forms of diffusion which may be active or passive (Bhaskar et al. 2010), involved in the transport of small molecules (Pardridge 2007). CMT mainly facilitates the transport of various essential polar molecules, with the aid of various carrier transporters (expressed on the plasma membrane of the brain endothelial cells) including glucose (GLUT1 glucose transporter), amino acids (LAT1 large neutral amino acid transporter) and nucleosides (CNT2 nucleoside transporter) into the brain (Pardridge 2005; Abbott et al. 2010; Bhaskar et al. 2010).

1.6.4.2.2.2 Endocytotic transcytosis

Endocytotic transcytosis represents the major route by which macromolecules such as peptides and proteins can gain access to the CNS intact (Abbott et al. 2010). Endocytotic transcytosis may occur by adsorptive mediated transcytosis (AMT) or receptor mediated transcytosis (RMT) (Abbott et al. 2010; Bhaskar et al. 2010).

1.6.4.2.2.2.1 Adsorptive mediated transcytosis (AMT)

AMT is based on electrostatic interaction between a positively charged molecule and the negatively charged binding sites on the surface of the brain endothelial cells (Abbott et al. 2010; Bhaskar et al. 2010). Thus, for molecules to be eligible for transport by the AMT mechanism, they must carry an excess of positive charge which would render them cationic for interaction with the negatively charged binding sites on the cell surface. Interaction of molecules with the cell surface binding sites induces endocytosis which is then followed by transcytosis (Sauer et al. 2005). Transport of molecules across the BBB may therefore be facilitated by coupling them to short (10 – 30 amino acid sequence) cationic peptides known as cell penetrating peptides (CPPs) such as SynB5 [originally deriving from protegrin (the SynB peptide vectors)] (Drin et al. 2003) or pAnt-[(43–58); also known as penetratin, a fragment of Antennapedia homeodomain] (Derossi et al. 1994; Drin et al. 2003); or cationised peptides such as cationised albumin (Pardridge et al. 1990).

1.6.4.2.2.2.2 Receptor mediated transcytosis (RMT)

RMT facilitates the transport of macromolecules such as peptides and proteins across the BBB by conjugating the molecules to ligands such as transferrin, insulin or lactoferrin which interact with specific receptors on the plasma membrane of the brain endothelial cells (Fishman et al. 1987; Baura et al. 1993; Fillebeen et al. 1999; Pardridge 2005; Abbott et al. 2010; Bhaskar et al. 2010).

In RMT, once the macromolecule-ligand conjugates bind to the specific receptors on the cell surface, an endocytotic event is triggered. The receptors and bound ligand cluster together and form a caveolus which breaks off into a vesicle. The ligand and receptors are then internalised into the endothelial cell and passes across the cytoplasm to be exocytosed at the opposite side of the cell. Subsequent dissociation of ligand from the receptor is thought to occur during cellular transit or during the exocytotic process (Abbott et al. 2010). RMT is a prominent transport mechanism which has attracted a great deal of interest in drug delivery (Bhaskar et al. 2010).

1.6.4.2.2.3 Application of nanoparticles in drug delivery to intracranial tumours

Steiniger and co-workers in their study investigated the possibility of a therapeutic success using a nanoparticle formulation of doxorubicin, a Pgp efflux pump substrate in a rat glioblastoma 101/8 model. The nanoparticle formulation employed in the study comprised doxorubicin bound to polysorbate 80 coated poly(butyl cyanoacrylate) nanoparticles. They carried out the study to assess the therapeutic efficacy of the nanoparticle formulation following previous studies which had shown that doxorubicin bound to the polysorbate 80 coated poly(butyl cyanoacrylate) nanoparticles was able to cross intact BBB and also achieved therapeutic concentrations of doxorubicin in the brain after intravenous administration (Gulyaev et al. 1999).

They evaluated two different doses of doxorubicin (3 X 1.5 mg kg^{-1} and 3 X 2.5 mg kg^{-1}) in the study. They reported a markedly increased survival in animals that received the formulation of doxorubicin bound to polysorbate 80 coated poly(butyl cyanoacrylate) nanoparticles at the two doses studied. In the higher dose (3 X 2.5 mg kg^{-1}) polysorbate 80 coated poly(butyl cyanoacrylate) nanoparticles group, there were long term survivors with survival up to 117 days and 163 days. Similarly, in the lower dose (3 X 1.5 mg kg^{-1}) polysorbate 80 coated poly(butyl cyanoacrylate) nanoparticles group, there was prolonged survival with some of the animals surviving for at least 120 days.

On the contrary, none of the animals treated with doxorubicin alone at the same dose levels survived for more than 65 days. Also, the nanoparticle formulation produced less peripheral toxicity after systemic administration compared to the formulation of doxorubicin alone. Healthy animals treated with doxorubicin alone showed slight signs of lung oedema (histologically confirmed), while animals treated with nanoparticles did not manifest this effect. Some tumour bearing animals treated with doxorubicin alone also showed slight lung oedema albeit without apparent histopathology (Steiniger et al. 2004).

A study by Zhang and co-workers demonstrated increased brain concentrations of paclitaxel, a P-gp efflux pump substrate by the administration of a nanoparticle formulation comprising cyclo-[Arg-Gly-Asp-D-Phe] {c[RGDfk]}-paclitaxel loaded hybrid micelles in a mouse model of glioma. Their nanoparticle delivery system combined the ability of transferrin to facilitate receptor mediated transcytosis (Fishman et al. 1987) of the drug delivery system with the targeting ability of c[RGdfk], a peptide known to bind specifically to integrin overexpressed in glioma cells (Bello et al. 2001; Desgrosellier and Cheresh 2010). Their results showed that the hybrid micelle produced a marked increase in survival time of intracranial U-87 MG (human glioblastoma) tumour bearing mice.

Tumour bearing mice treated with the transferrin modified c[RGDfk]-paclitaxel loaded hybrid micelles had a survival time of 42.8 days, while mice treated with transferrin modified paclitaxel loaded micelles (without c[RGdfk]) had a survival time of 39.5 days, mice treated with paclitaxel loaded micelles had a survival time of 34.8 days, those treated with Taxol had a survival time of 33.6 days, and saline treated mice had a survival time of 34.5 days. They also reported that the transferrin modified c[RGDfk]-paclitaxel loaded hybrid micelles did not lead to body weight loss compared with saline and was less toxic than transferrin modified paclitaxel loaded micelles (Zhang et al. 2012).

Also, Guo and co-workers evaluated the antiglioma effects of transferrin (Tf)-modified poly ethylene glycol-poly lactic acid (PEG-PLA) nanoparticles conjugated with resveratrol (Tf-PEG-PLA-RSV) in glioma bearing rats. Their studies showed that the nanoparticle formulation of resveratrol demonstrated superior antiglioma effects to the free resveratrol. Also, Tf-PEG-PLA-RSV with the transferrin targeted ligand showed improved activity compare to the nanoparticle formulation without transferrin. The data showed that both nanoparticle formulations of resveratrol produced significantly ($p < 0.05$) higher tumour inhibition at 15 days post-inoculation than free resveratrol, although the transferrin modified nanoparticles yielded better inhibition than the nanoparticles without transferrin. Also, glioma bearing rats treated with free resveratrol had a median survival time of 18 days, rats treated with the nanoparticle formulation without transferrin had a median survival time of 25 days while rats treated with the tranferrin modified nanoparticle formulation, Tf-PEG-PLA-RSV had a median survival time of 36 days. Thus, nanoparticle formulation of resveratrol resulted in prolonged survival times compared to free resveratrol (Guo et al. 2013).

Furthermore, Gao and co-workers demonstrated that the incorporation of lapatinib, a poorly water soluble dual EGFR and HER2 inhibitor into core–shell nanoparticles improved both the water solubility and anti-glioma effect of the drug. Their studies showed that incorporation of lapatinib into the core shell nanoparticles increased the water solubility of the drug from 0.007 mg mL^{-1} to over 10 mg mL^{-1}, which was better than what could be attained by most commercially available injection solvents. Evaluation of the anti glioma activities of the core shell nanoparticle formulation in glioma bearing mice showed prolonged increase in survival of mice treated with the nanoparticle formulation compared to the commercial lapatinib formulation (Tykerb). In their study, the mice treated with the high dose (30 mg kg^{-1}) nanoparticle formulation of lapatinib had a median survival time of 21.0 days, mice treated with the low dose (10 mg kg^{-1}) nanoparticle formulation had a median survival time of 22.0 days, while mice treated with Tykerb (100mg kg^{-1}) had a median survival time of 19.0 days and saline controls had a median survival time of 17.0 days. Therefore, their data showed that mice treated with lapatinib incorporated into the core shell nanoparticles at two dose levels (10 mg kg^{-1} and 30 mg kg^{-1}) had a significantly ($p < 0.05$) increased survival time compared to mice treated with Tykerb (100 mg kg^{-1}). Thus, administration of lapatinib incorporated into nanoparticles at a much lower dose than the commercial formulation resulted in better survival outcomes than the higher dose of the commercial formulation (Gao et al. 2014).

In another study, Qian and co-workers demonstrated that the administration of carmustine (BCNU) using chitosan surface modified poly (lactide-co-glycolides) nanoparticles loaded with BCNU along with O^6-benzylguanine (BG), which could directly deplete MGMT would improve the therapeutic efficacy of BCNU. They evaluated this nanoparticle formulation (BCNU + BG nanoparticle) in F98 glioma-bearing rats in comparison to a BCNU solution group, BCNU nanoparticles group, and BCNU + BG (intraperitoneal injection of BG 2 hours before intravenous injection of BCNU), with a saline group as the negative controls.

Their studies showed that the saline control group had a median survival time of 10.0 days, the BCNU nanoparticle group had a median survival time of 16.0 days which was not statistically different from the median survival time (14.5 days) of the BCNU solution group. On the other hand, the BCNU + BG nanoparticle group had a median survival time of 23.0 days which was statistically ($p < 0.05$) different from that for the BCNU + BG solution group (19.0 days) as well as the other treatment groups. Thus, the administration of BCNU and BG together in a nanoparticle formulation yielded superior survival outcomes compared to administration of the two drugs separately in solution as well as the nanoparticle containing BCNU alone (Qian et al. 2013).

From the foregoing, administration of therapeutics in nanoparticle formulations resulted in superior therapeutic outcomes compared to administration in conventional formulations.

The nanoparticle delivery system employed in the current study is based on quaternary ammonium palmitoyl glycol chitosan (GCPQ), a self-assembling chitosan amphiphile which had been previously shown to facilitate the delivery of molecules to the brain. Studies by Qu and co-workers showed that formulation of the intravenous anaesthetic propofol using GCPQ nanoparticles resulted in a more efficient encapsulation of propofol than obtained with conventional copolymers. Also, the nanoparticle formulation increased the brain activity of propofol by 10 times compared to commercial formulations of the drug (Qu et al. 2006).

Furthermore, Lalatsa and co-workers demonstrated the delivery of leucine^5-enkephalin, a hydrophilic peptide to the brain using the GCPQ based nanoparticle system. Their work showed that compared to leucine^5-enkephalin alone, brain exposure was increased by 67 % following oral administration of a novel derivative (palmitoyl leucine^5-enkephalin; TPLENK) of the peptide using GCPQ nanoparticle formulation while intravenous administration of this nanoparticle formulation increased brain exposure by 50 % (Lalatsa et al. 2012a). Also, intravenous administration of this nanoparticle formulation (10 mg kg^{-1}) produced considerably high antinociception in mice while leucine^5-enkephalin did not produce any analgesia at the same dose (Lalatsa et al. 2012a). Furthermore, their studies demonstrated that GCPQ nanoparticles increased the stability of leucine^5-enkephalin in the gut and the plasma by protecting the peptide from degradation. This facilitated the brain transport of the GCPQ nanoparticle stabilised peptide to the brain (Lalatsa et al. 2012a; Lalatsa et al. 2012b). In addition, studies have shown that GCPQ nanoparticles do not cross the BBB to any appreciable extent (Lalatsa et al. 2012a) and they do not open epithelial tight junctions (Siew et al. 2012). The GCPQ nanoparticles appear to deliver their payload to the brain by making contact with the brain endothelial cells following which loaded molecules are able to cross the BBB. Moreover, intravenously administered polymer have been known to remain in the circulation and adhere to the perivascular spaces of arterioles and venules and the inner surface of the blood vessels of brain endothelial cells (Garrett et al. 2012), which had allowed loaded peptide to cross the BBB (Lalatsa et al. 2012a).

1.7 Hypothesis

One of the major limitations to effective glioblastoma chemotherapy is dose limiting peripheral toxicity of clinically used therapeutic agents. This often leads to the necessity for dose delays, reductions or sometimes outright discontinuation (Cianfriglia et al. 1980; Kriegler et al. 1994; van den Bent et al. 1998; Gerber et al. 2007; Su et al. 2005; Tosoni et al. 2006; Vredenburgh et al. 2007; Friedman et al. 2009; Kreisl et al. 2009). This often compromises tumour response which may explain the poor clinical outcomes in the majority of cases (Hitron et al. 2011). Moreover resistance to chemotherapy (mainly mediated by AGAT), another challenge of effective chemotherapy may be overcome by continuous chemotherapy administration in order to deplete the resistance mechanism thereby increasing chemosensitivity (Tolcher et al. 2003).

This work is therefore based on the hypothesis that continuous administration of lomustine, a cytotoxic (DNA alkylating) nitrosourea compound in a high dose nanoparticle formulation will lead to improved therapeutic outcome whilst not increasing the incidence of myelosuppressive effects associated with the drug.

The nanoparticle formulation is based on GCPQ, a self-assembling chitosan amphiphile. GCPQ has been shown to exhibit a distinct distribution profile in vivo which suggests that the polymer formulation avoids the reticuloendothelial system (Lalatsa et al. 2012a). This indicates that nanoparticle-drug formulations based on GCPQ will not be readily taken up by the macrophages which are known to abound in the bone marrow (Leu et al. 1984; Moghimi et al. 2001; Chellata et al. 2005; Owens and Peppas 2006), [Figure 1-4], a major site of lomustine toxicity, due to the high susceptibility of the cells of the bone marrow to the toxic effects of cytotoxic agents (Pollak et al. 1988; Kriegler et al. 1994; Çetin et al. 2000).

Thus, the high dose lomustine-GCPQ nanoparticle formulation would lead to improved survival outcomes without attendant toxic effects (Figure 1-4)

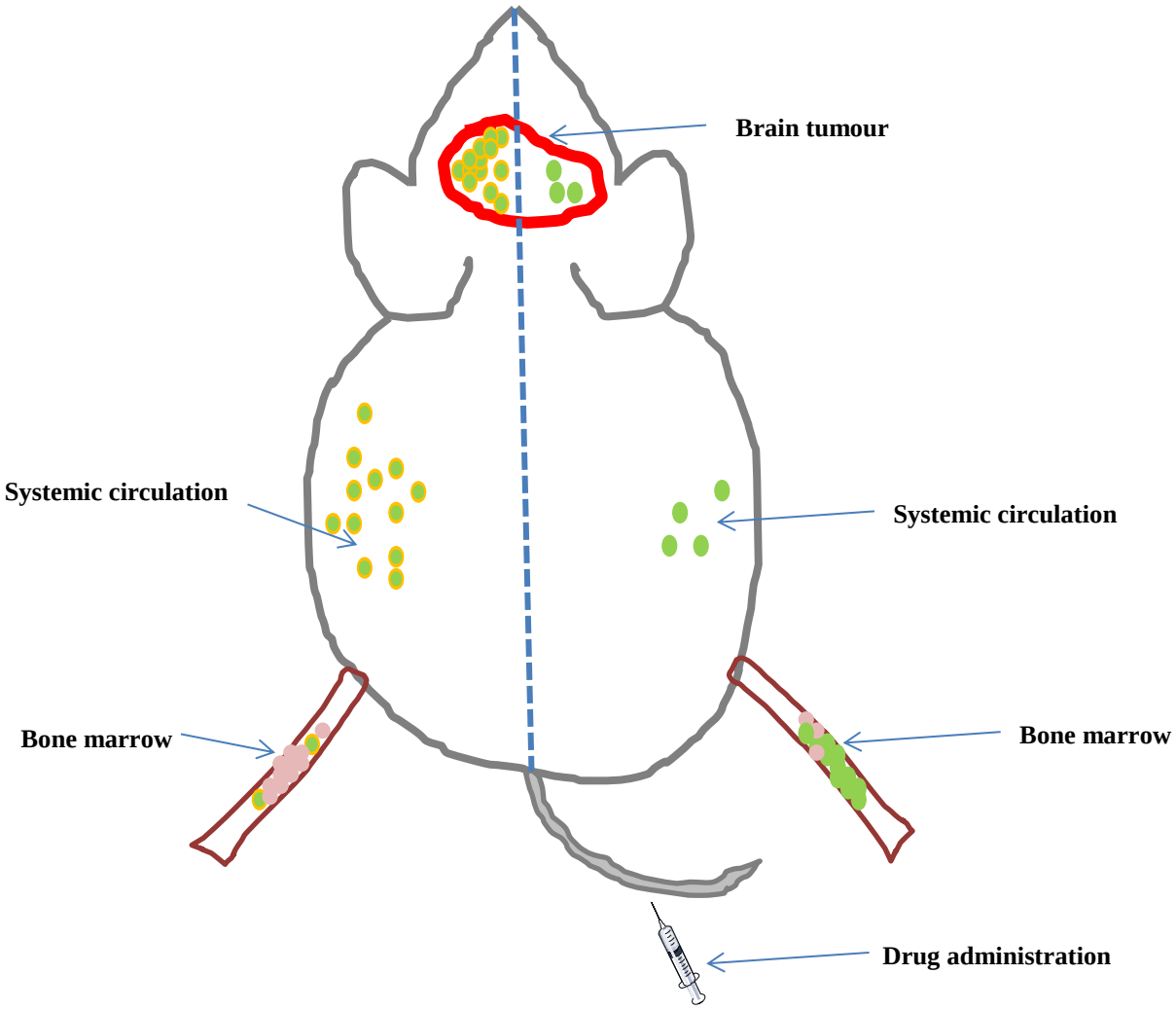

Figure 1-4: Schematic depicting administration of high dose chemotherapy using nanoparticle based drug formulation versus conventional aqueous drug formulation

Key:

Aqueous drug formulation

Nanoparticle based drug formulation

1.8 Aims and objectives

The aim of this study is to demonstrate that a high dose nanoparticle lomustine-GCPQ formulation will lead to improved survival outcomes without an increase in the incidence of toxic effects. This aim will be achieved through the following objectives:

1. To synthesise and characterise GCPQ
2. To prepare and characterise high dose lomustine-GCPQ nanoparticle (Q-LOM) formulation
3. To establish and characterise a mouse model of human glioblastoma
4. To assess in vivo anti-glioma activities of the Q-LOM formulation in tumour bearing mice
5. To assess the toxicity of the Q-LOM formulation in healthy mice
6. To study the in vitro uptake of GCPQ particles in macrophage cell line
7. To synthesise and characterise self-assembling peptide amphiphiles as potential delivery systems for anti-glioma agents
8. To synthesise and characterise a therapeutic peptide as a candidate for chemotherapy of intracranial tumours.

Chapter 2 Evaluation of Anti-tumour Activities of GCPQ-Lomustine (Q-LOM) Formulation

2.1 Introduction

Chemotherapy has become a component part of the standard of care for glioblastoma (Lonardi et al. 2005; Neider et al. 2006, Stupp et al. 2005; Stupp et al. 2009; Khasraw and Lassman 2010; Juralti et al. 2013) in spite of previous uncertainty about its value (Fine 1994; Gundersen 1998; Stewart et al. 2002; Grossman 2003; Khasraw and Lassman 2010) in improving therapeutic outcome. Currently, temozolomide is the first line chemotherapeutic agent employed in conjunction with and subsequent to surgical resection and radiotherapy in the management of newly diagnosed glioblastoma (Stupp et al. 2005; Gerber et al. 2007; Brandsma et al. 2008; Stupp et al. 2009; Brada et al. 2010; Raizer 2011; Khasraw et al. 2010; Grossman et al. 2010; Yust-Katz et al. 2013; Juratli et al. 2013; Lwin et al. 2013). Prior to the introduction of temozolomide, adjuvant glioblastoma chemotherapy was nitrosourea based, both as single agents and as combination regimens (Cianfriglia et al. 1980; Jakacki et al. 1998; Wong et al. 1999; Levin 1999; Jakacki et al. 2008; Brada et al. 2010; Chamberlain 2010; Florio and Barbieri 2012).

Lomustine [CCNU, 3-(2-chloroethyl)-1-cyclohexyl-3-nitrosourea)] is a synthetic alkylating nitrosourea compound. It is highly lipophilic and possesses BBB penetrating ability which makes it valuable in the treatment of intracranial tumours (Oliverio et al. 1970; Cheng et al. 1972; Weiss and Issell 1982; Jakacki et al. 2008; Batchelor et al. 2013).

Although lomustine bears only one chloroethylating unit on its structure, it is able to produce inter strand cross linking in DNA (Oliverio et al. 1970; Hoogstraten et al. 1973; Kohn 1977; Pratt et al. 1994).

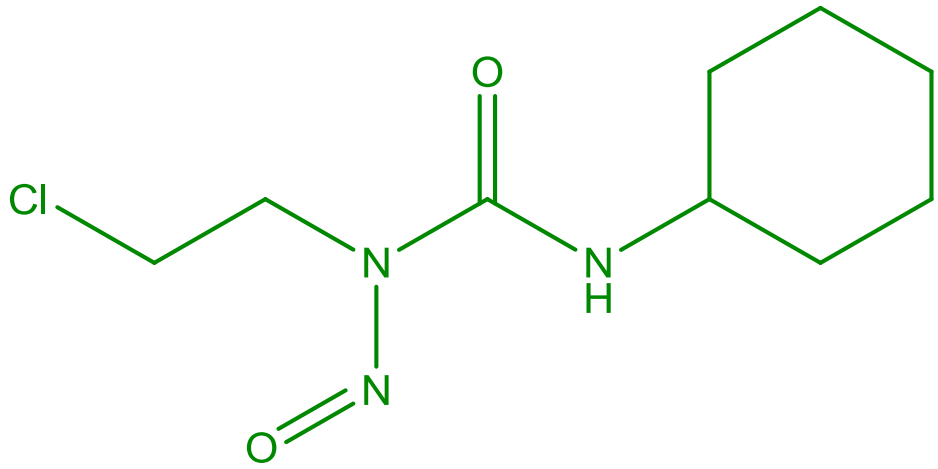

Figure 2-1: Lomustine [(CCNU; 3-(2-chloroethyl)-1-cyclohexyl-3-nitrosourea; molecular weight: 233.7]

Lomustine undergoes decomposition in physiologic conditions to produce 2-chloroethyl diazene hydroxide (alkylating) and an isocyanate (carbamoylating) intermediates. The major alkylating group, 2- chloroethyl carbonium ion is generated by spontaneous decomposition of the 2-chloroethyl diazene hydroxide intermediate at physiologic pH (Cheng et al. 1972; Reed et al. 1975; Montgomery et al. 1975; Weiss and Issell 1982; Pratt et al. 1994). Alkylation of nucleic acids (DNA and RNA) and proteins is as a result of the reaction of 2- chloroethyl carbonium ion with cellular constituents. The chloroethyl carbonium ion reacts with the O^6 and N^7 sites of guanine, with guanines in the midst of a run of guanines been more susceptible to attack than guanines in other base sequences, such as an isolated guanine.

The isocyanate on the other hand binds mainly to proteins by reacting with the lysine (ϵ- amino group) residues of proteins (Cheng et al. 1972; Weiss and Issell 1982; Briscoe et al. 1990; Pratt et al. 1994).

Antitumour activities of lomustine appear to be due mainly to DNA alkylation and cross linking, while carbamoylating activity does not contribute to any appreciable extent to antitumour activity (Panasci et al. 1977; Kann Jr. 1978). Interstrand DNA cross links are produced subsequent to alkylation of DNA by the 2 – chloroethyl carbonium ion. This proceeds via a two-step reaction in which there is an initial rapid chloroethylation of a guanine residue (at the O^6 position) in one strand of DNA, followed by a slower reaction in which there is elimination of the chloride (Cl^-) ion and subsequent alkylation of the opposite strand of DNA resulting in the formation of a cross link (Ewig and Kohn 1977; Kohn 1977).

Alkylation damage in DNA can be repaired by the O^6-alkylguanine-DNA alkyltransferase (AGAT), the DNA repair protein which removes alkyl groups from the O^6 position of guanine (a major site of alkylation) by alkylating agents. This leads to the development of resistance of tumour cells to alkylating agents which may result in lack of therapeutic success with these agents (Dumenco et al. 1989; Tano et al. 1990; Ochs and Kaina 2000; Kanugula and Pegg 2003; Gerson 2004; Hegi et al. 2005; Chamberlain 2010).

In clinical practice, an initial dose of lomustine (100 – 130 mg m^{-2}) is usually given, with a rest period of 6 – 8 weeks before doses are repeated. Dose reductions or delays may be necessary if there is myelosuppression which would be manifested in non-recovery of haematologic parameters (Cianfriglia et al. 1980; van den Bent et al. 1998; van den Bent et al. 2006; Jakacki et al. 1998). These dose reductions and treatment delays have been shown to compromise tumour response and overall survival (Hitron 2011).

2.2 Materials and methods

2.2.1 Materials

2.2.1.1 List of materials

S/n	Material	Supplier
1	Lomstine	Sigma; Sigma-Aldrich Corporation, St. Louis, MO, USA
2	Carmustine	Sigma
3	Etoposide	Sigma
4	Glycol Chitosan [≥ 60 % (titration)]	Sigma
5	Palmitic acid N- hydroxysuccinimide ester	Sigma
6	Hydrochloride acid	Fisher Scientific, UK, Loughborough, UK
7	Ethanol, Absolute (Analytical reagent grade)	Fisher Scientific, UK

S/n	Material	Supplier
8	Methanol (HPLC grade)	Fisher Scientific, UK
9	Water (HPLC grade)	Fisher Scientific, UK
10	Methanol- d_4	Sigma-Aldrich Corporation
11	1- Methyl- 2- pyrollidone	Sigma-Aldrich Corporation
12	Sodium bicarbonate	Sigma-Aldrich Corporation
13	Sodium hydroxide	Fluka; Sigma-Aldrich Corporation
14	Sodium iodide	Sigma-Aldrich Corporation
15	Iodomethane	Sigma-Aldrich Corporation
16	Amberlite IRA- 96	Fluka
17	Diethyl ether	Sigma-Aldrich Corporation
18	Dialysis membranes	Medicell membranes Ltd, London, GB
19	20 % Dextrose injection	AAH Pharmaceuticals Ltd, Coventry, GB

S/n	Material	Supplier
20	Water for injections (BP)	AAH Pharmaceuticals
21	U-87 MG cell line (ATCC® HTB-14™)	American Type Cell Culture Collection Manassas, VA, USA
22	Minimum essential medium	Life Technologies, Paisley, UK
23	Fetal bovine serum	Labtech International Ltd, Uckfield, East Sussex, UK
24	Trypsin- EDTA (0.05%)	Life Technologies
25	Dubelcco's phosphate buffered saline (DPBS)	Life Technologies
26	L- Glutamine	Life Technologies
27	Sodium pyruvate	Life Technologies

2.2.2 **Methods**

2.2.2.1 Synthesis and characterisation of GCPQ

GCPQ was synthesized according to methods described by Uchegbu et al. 2001 and characterised by NMR spectroscopy, the molecular weight was determined by multi-angle laser light scattering and gel permeation chromatography (GPC/ MALLS). ^{1}HNMR spectra were acquired on a Bruker AMX Ultrashield™ 400 MHz Spectrometer and molecular weight was determined by GPC/ MALLS using an Agilent 1200 system coupled to a Wyatt QELS Quasi light scattering laser.

2.2.2.2 Preparation and characterisation of lomustine [GCPQ-lomustine (Q-LOM) and ethanolic lomustine (LOM-ETOH)] formulations

2.2.2.2.1 Preparation of Lomustine (Q-LOM and LOM-ETOH) formulations

Lomustine nanoparticle formulation (Q-LOM) was prepared by probe sonicating a dispersion of GCPQ (20 mg mL^{-1}), lomustine (2 mg mL^{-1}), Soybean oil (10 mg mL^{-1}) and polysorbate 80 (5 mg mL^{-1}) in 5 % $^{w}/_{v}$ dextrose solution on ice for 30 minutes.

The ethanolic lomustine formulation was prepared by vortexing lomustine (2 mg) in absolute ethanol with polysorbate 80 (5 mg mL^{-1}) in 5 % $^{w}/_{v}$ dextrose solution (final ethanol concentration of 10 % $^{v}/_{v}$). The resulting colloidal mixture was then filtered (0.22 µm) to remove drug crystals and yield a non-particulate formulation.

2.2.2.2.2 Characterisation of Lomustine formulations

A calibration curve for lomustine (with carmustine as internal standard) was prepared for analysis of the drug content of the formulations. Chromatograms were acquired on an Agilent Technologies 1200 Series HPLC system using an Onyx C18 Monolithic (5 μm; 100 x 4.6 mm; Phenomenex UK) column with the temperature set at 40^{o} C. Samples were eluted using a methanol: water (60: 40) mobile phase at a flow rate of 1.5 mL min^{-1}, with detection at 230 nm. The formulation was dissolved in methanol and analysed using the same conditions.

Particle size for the formulation was determined by transmission light microscopy (TEM) imaging (Philips (FEI) CM 120 Bio Twin Transmission Electron Microscope) with an AMT digital camera (5 mega pixels; AMT Deben, UK Ltd) and dynamic light scattering (DLS) size measurements (Zetasizer Nano series, Malvern Instruments).

2.2.2.3 Preparation and characterisation of etoposide formulation

2.2.2.3.1 Preparation of etoposide formulation

GCPQ–etoposide nanomedicine formulations were prepared by probe sonicating GCPQ (10 mg mL^{-1}), etoposide (2 mg mL^{-1}), soybean oil (10 mg mL^{-1}) and Tween 80 (2 mg mL^{-1}) in 5 % $^{w}/_{v}$ dextrose solution on ice for 30 min. The formulation was then centrifuged at 5, 000 rpm for 15 minutes to remove free drug crystals. The supernatant was carefully collected into a separate vial immediately after centrifugation.

2.2.2.3.2 Characterisation of etoposide formulation

A calibration curve was prepared for etoposide to determine the drug content of the formulation. The chromatograms were acquired using the Agilent HPLC system and column as described above, with the column temperature set at 40^{o} C. The samples were eluted using a mobile phase comprising of methanol: water (50: 50) at a flow rate of 1 mL min^{-1} and the detection wavelength was set at 254 nm.

The particle size for the formulation was determined by TEM and DLS.

2.2.2.4 In vivo antitumour studies

2.2.2.4.1 Cell culture and preparation for tumour implantation

U-87 MG cells (ATCC® HTB-14™; originally from a 44 year-old male Caucasian glioblastoma patient) were cultured in Minimum Essential Medium (MEM) supplemented with FBS (10 % $^{v}/_{v}$); sodium pyruvate (1 mM) and L-Glutamine (2 mM). Cells were maintained in culture for up to 14 days (splitting every 2 – 3 days when 75 – 80% confluence was reached in the 75cm^2 tissue culture flask) before they were used for tumour implantation.

For tumour implantation, cells at 75 – 80 % confluence were trypsinized and centrifuged (800 g at 4 ^{o}C for 3 minutes) and then suspended in plain medium to a final concentration of 50 million cells mL^{-1} in a 2ml plastic tube (equipped with a push cap) and placed on ice until they were implanted.

2.2.2.4.2 Tumour implantation

Female CD1 nude mice [Charles River, UK Ltd, Kent, UK; (20 – 30 g)], housed in individually ventilated cages, with a maximum of 5 mice per cage and maintained in standard regulated laboratory conditions in the Biological Services Unit (BSU) within the School were used for the study. The mice were accommodated in the appropriate room with the temperature maintained at about 22 – 25 ^{o}C, humidity at 60 % and a 12 – hour light (from 07: 00 hours) and dark (from 19: 00 hours) cycle. The mice were acclimatized in the BSU for at least 5 – 7 days before studies commenced. All mice had access to food and water *ad libitum* as soon as they were housed in the BSU and throughout the period of study. The study was conducted in accordance with the policies and regulations of the Home Office as stipulated in the Animals and Scientific Acts 1986 UK, for the handling and care of laboratory animals used in scientific research, the recommendations of the BSU and with the approval of the ethics committee.

Mice were anaesthetised (inhaled isofluorane) and secured to a stereotaxic frame (BENCHmark^{TM}) with a mouse adaptor. An incision was made by opening the skin and inner membranes between the eyes towards the back of the cranium. After locating the bregma (the intersection of the coronal and sagittal sutures), a hole was drilled in the skull with the coordinates: + 0.5 mm anterior and – 2 mm lateral to the bregma (determined by a BENCHmark™ digital stereotaxic control panel), using a sterile (70 % ethanol) dental drill. A sterile (70 % ethanol) 10 µL Hamilton syringe loaded with 2µL cell suspension (100,000 cells) in plain medium was gently lowered into this hole to a depth of 3.3 mm below the skull surface. After 1 min, the syringe was withdrawn by 0.3 mm (final injection depth 3 mm) and the cell suspension was injected at a speed of 0.1 µL min^{-1} after which the syringe was left in place (3mm depth) for 5mins. Subsequently, the syringe was slowly withdrawn and the incision was closed using a 5 - 0 suture after which an analgesic (Rimadyl; 5 mg kg^{-1}) was administered by intraperitoneal injection.

The mice were weighed and reviewed on the following day for any signs of ill health or discomfort. Subsequently, they were weighed every 2- 3 days and monitored for any signs of ill health. Mice showing prolonged weight loss ≥ 15 % of their initial body weights were euthanized using a carbon dioxide (CO_2) chamber and the brains were harvested and fixed in formalin for 24 hours prior to MRI analysis.

2.2.2.4.3 Evaluation of antitumour activities of lomustine formulations

Following tumour implantation (as described above), mice were randomly assigned to one (n = 6) of three groups. The first group was treated with the high dose lomustine (13 mg kg^{-1}) nanomedicine formulation, the second group was treated with the low dose lomustine (1.2 mg kg^{-1}) ethanolic formulation, while the third group served as controls and received no drug treatment. Drug treatment was started on day 7 post tumour implantation and the formulations were administered to the mice by tail vein injection once daily for 10 consecutive days. Mice were weighed daily prior to drug administration to assess tolerability of the dosing regimen employed.

2.2.2.4.4 Evaluation of antitumour activities of etoposide formulations

Mice were randomly assigned to one (n = 5) of three groups after tumour implantation (as described above). The first group received 7.5 mg kg^{-1} (High Q-ETOP) of the nanomedicine formulation, the second group received 1.5 mg kg^{-1} (Low Q-ETOP) of the nanomedicine formulation, while the third group were the control mice and received no drug treatment.

Drug treatment was started 7 days post tumour implantation and the formulations were administered to the mice once daily by tail vein injection. Mice were weighed daily prior to drug administration to assess tolerability of dosing regimen employed.

2.2.2.4.5 Tumour analysis by MRI

Images were collected using a 1.5 T Phillips Intera scanner at the Exeter MR Research Centre, University of Exeter, UK. A high resolution T_2-weighted Turbo Spin-Echo (TSE) sequence was used (TR 3000 ms, TE 110 ms, flip angle 90 degrees, number of slices 54, voxel size 0.14 X 0.14 X 0.14 mm^3, 10 averages). High-resolution images were achieved by utilizing a microscopy coil (23 mm diameter).

Tumour bearing mice brains were embedded in a mixture (50 : 50) of agarose gel (1 % ^{w}/v) and formaldehyde solution (4 % $^w/_v$) prior to imaging, to fix the tissue and minimize shifting of the samples during measurement.

Image parameters were established in a preliminary experiment, so as to optimize tumour edge detection. OSIRIX software (Pixmeo SARL, Switzerland) was utilized to analyse the MRI images and to measure the tumour volume, after a manual determination of the edges in a slice-by-slice process.

2.2.2.4.6 Statistical analysis

Statistical analysis was performed using Minitab® 16 software (Minitab, Inc., Pennsylvania, USA). The treatment groups were compared two at a time for each time point using ANOVA followed by Tukey post hoc test. The significance level was set at $p < 0.05$.

2.3 Results

2.3.1 Synthesis and characterisation of GCPQ

GCPQ was successfully synthesised with 22 ± 2.1 % degree of palmitoylation and 13.4 ± 0.8 % degree of quaternisation as determined by ^{1}HNMR (Table 2-1; Figure 2-2). The molecular weight as determined by GPC/ MALLS (Figure 2-3) was: M_w: 9.4 ± 0.7 kDa; M_n: 7.7 ± 0.9 kDa and M_w / M_n: 1.3 ± 0.2 (Table 2-1)

	^{1}HNMR characterisation		Molecular weight determination		
GCPQ batch	% Palmitoylation	% Quaternisation	M_w (kDa)	M_n (kDa)	M_w / M_n
1	23.7	13.2	9.5	8.6	1.1
2	19.1	13.5	9.3	7.8	1.2
3	23.4	14.4	10.2	6.5	1.6
4	21.9	12.4	8.4	7.8	1.1
Mean	22	13.4	9.4	7.7	1.3
Standard deviation	2.1	0.8	0.7	0.9	0.2

Table 2-1: Characterisation data for GCPQ batches

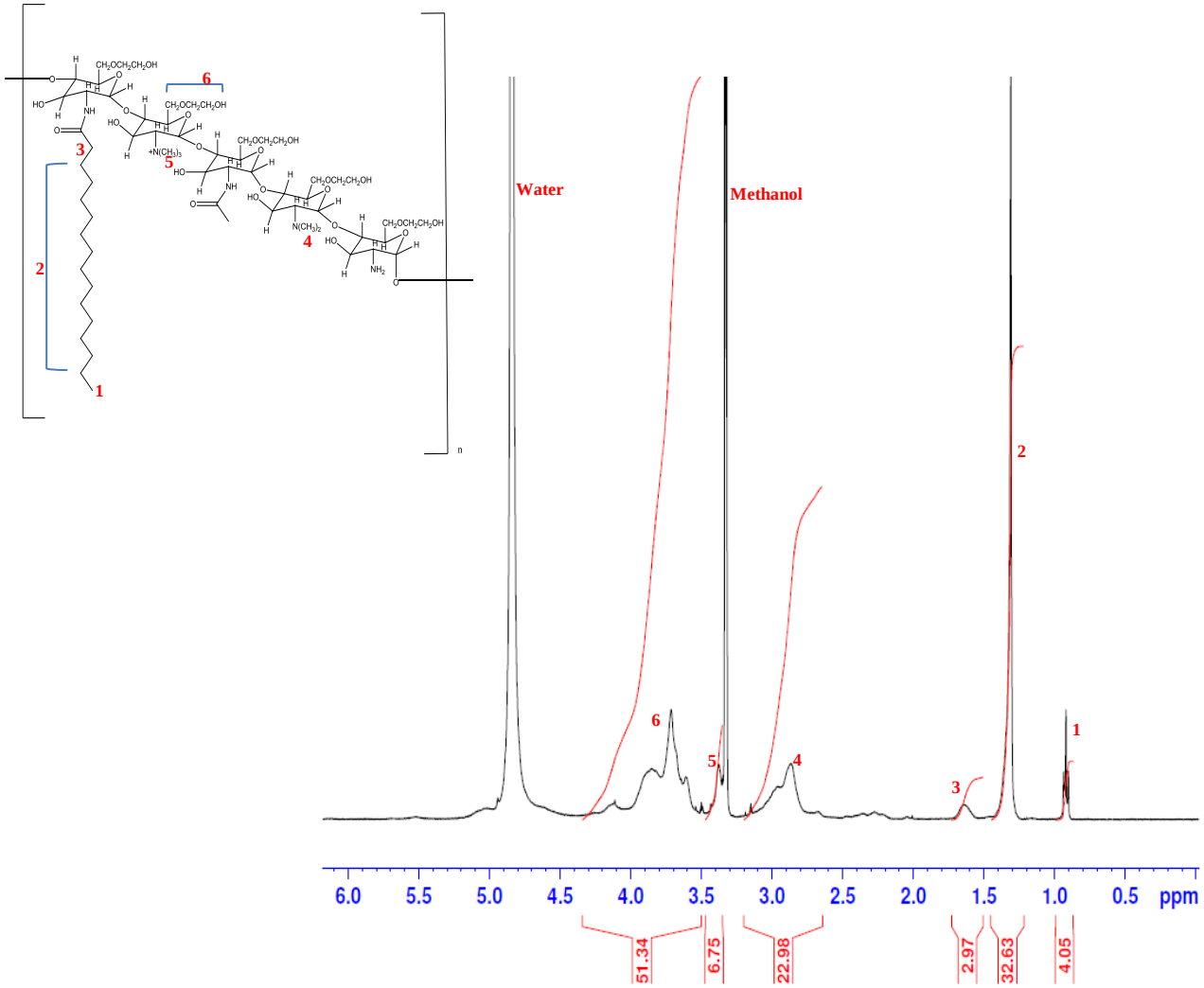

Figure 2-2: ^{1}H NMR spectra for GCPQ

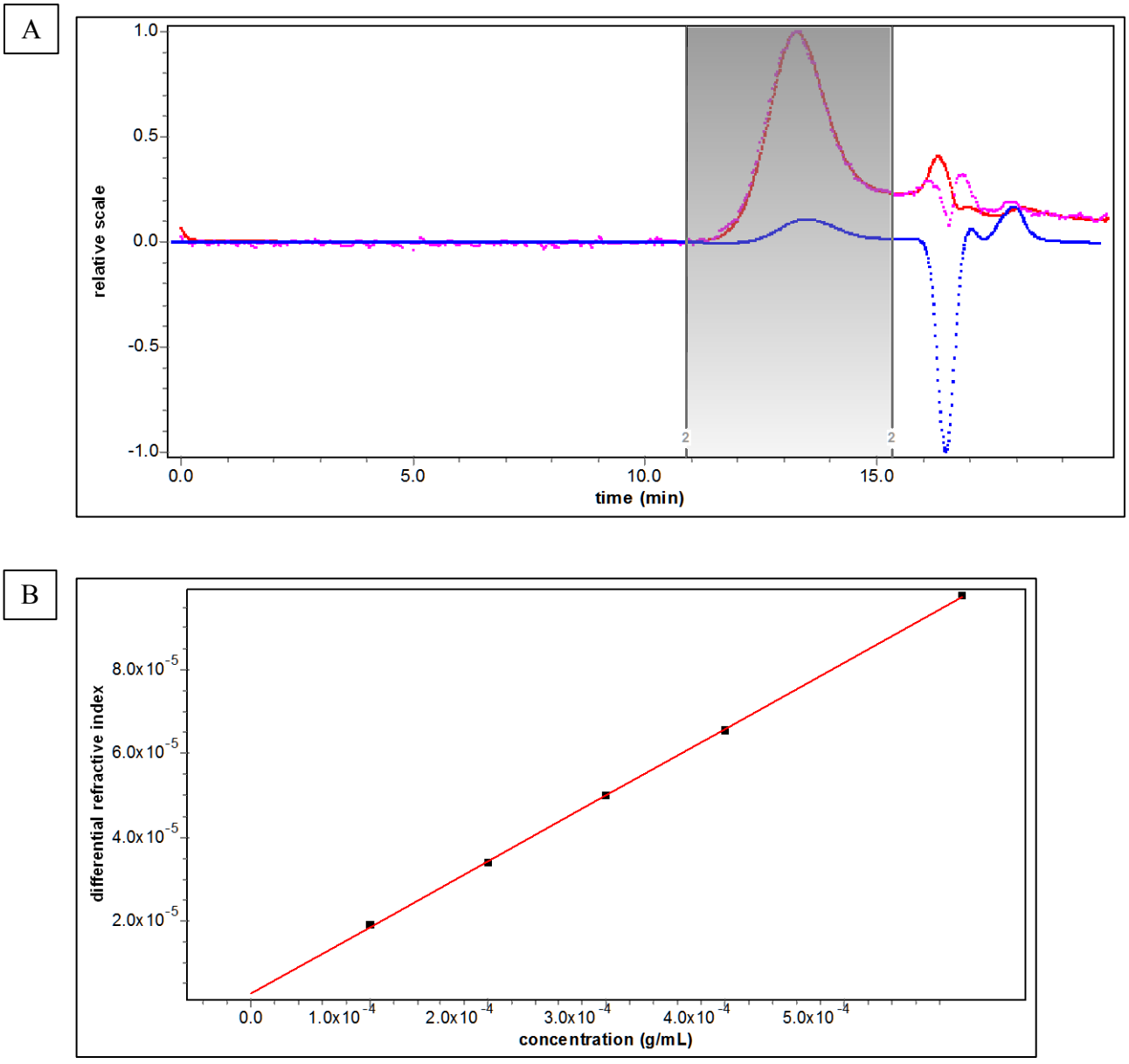

Figure 2-3: A: GPC/ MALLS chromatogram; B: dn/dc graph for GCPQ

Key: Red line: Light scattering detector signal; Blue line: Refractive index detector signal; Pink line: Quasi-elastic light scattering detector signal

2.3.2 Preparation and characterisation of lomustine (Q-LOM and ethanolic lomustine) formulations

2.3.2.1 Determination of drug content of lomustine formulations

A calibration curve was prepared for lomustine using carmustine as internal standard (Figure 2-4). This calibration curve yielded a lomustine / carmustine area ratio versus lomustine concentration line with the equation y = 0.1876x – 0.005 (R^2 = 0.9999), and a height ratio versus lomustine concentration line with equation y = 0.1091x – 0.0035 (R^2 = 0.9993).

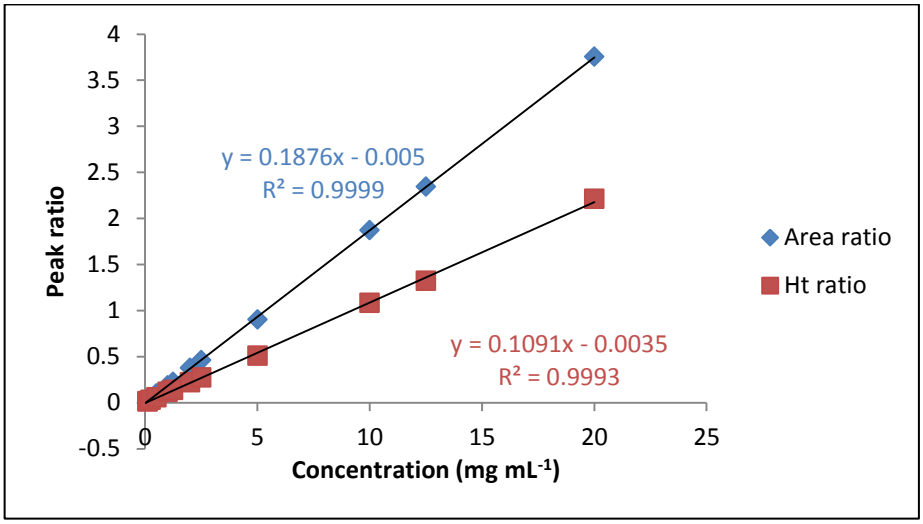

Figure 2-4: Calibration curve for lomustine with carmustine as internal standard

A calibration curve was also prepared using the concentration of lomustine alone (without carmustine as internal standard). This calibration curve yielded an area versus lomustine concentration line with the equation y = 9.8739x + 0.1585 (R^2 = 0.9998) and a height versus lomustine concentration line with the equation y = 0.9995x + 0.0673 (R^2 = 0.9999) (Figure 2-5).

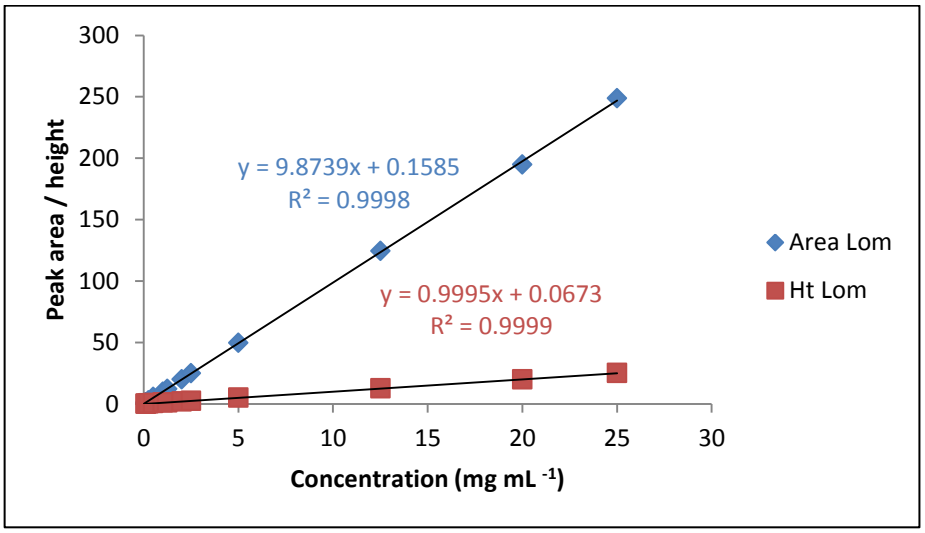

Figure 2-5: Lomustine calibration curve

Drug content of lomustine formulations was determined using the equation of the line produced by the area versus lomustine concentration (y = 9.8739x + 0.1585) from the calibration curve prepared using lomustine concentration alone (Figure 2-5).

2.3.2.2 Particle size determination for lomustine formulations

TEM images showed that Q-LOM formulation yielded particles in two distinct size ranges 80 – 470 nm and 0.2 – 1.1 µm (Figure 2-6).

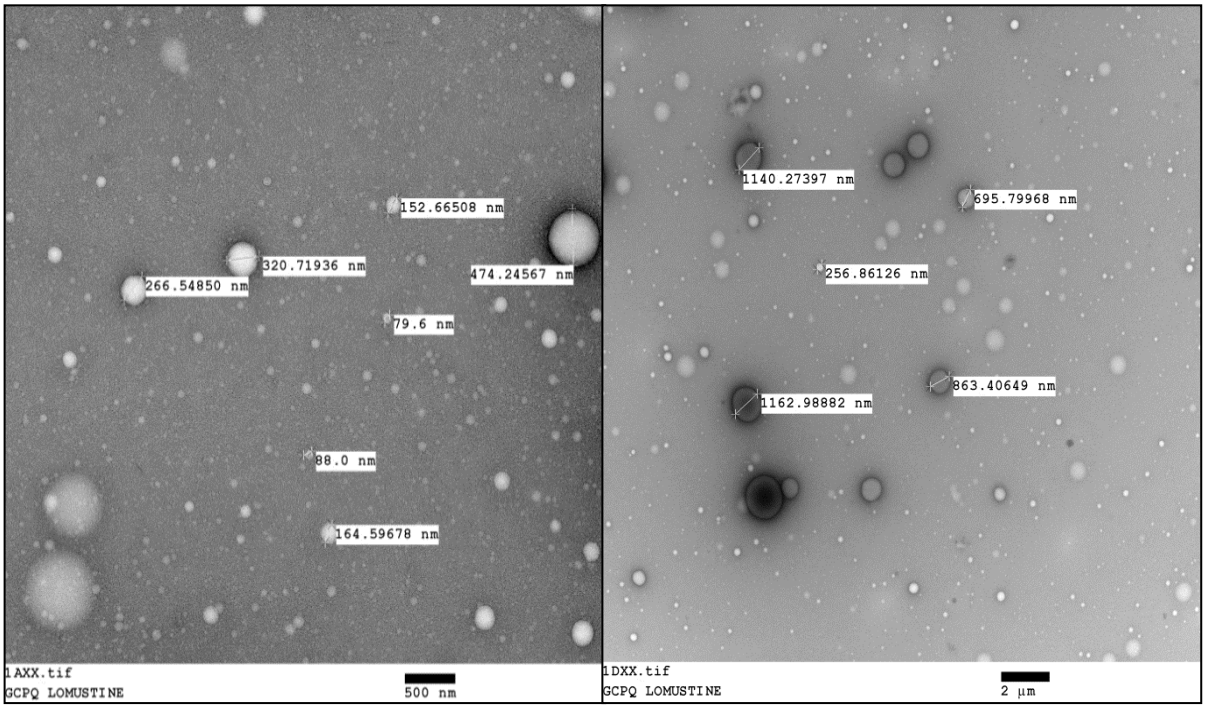

Figure 2-6: TEM images showing Q-LOM formulation

Freshly prepared nanoparticle formulation of lomustine containing: lomustine (2 $mgmL^{-1}$); GCPQ (20 $mg\ mL^{-1}$, 2 % w/v); polysorbate 80 (5 $mg\ mL^{-1}$, 0.5 % w/v); soya bean oil (10 $mg\ mL^{-1}$, 1 % w/v) in 5 % w/v dextrose solution. Particle size measurements are as generated by the AMT digital camera software.

However, DLS size data for the lomustine nanoparticle formulation revealed an average size of 271.4 nm with polydispersity index of 0.5 (Figure 2-7).

A

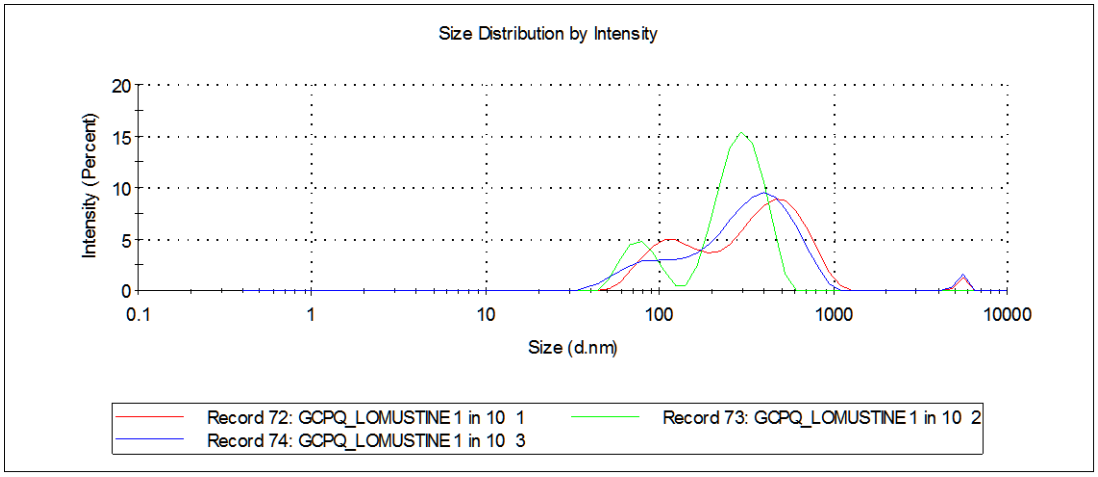

B

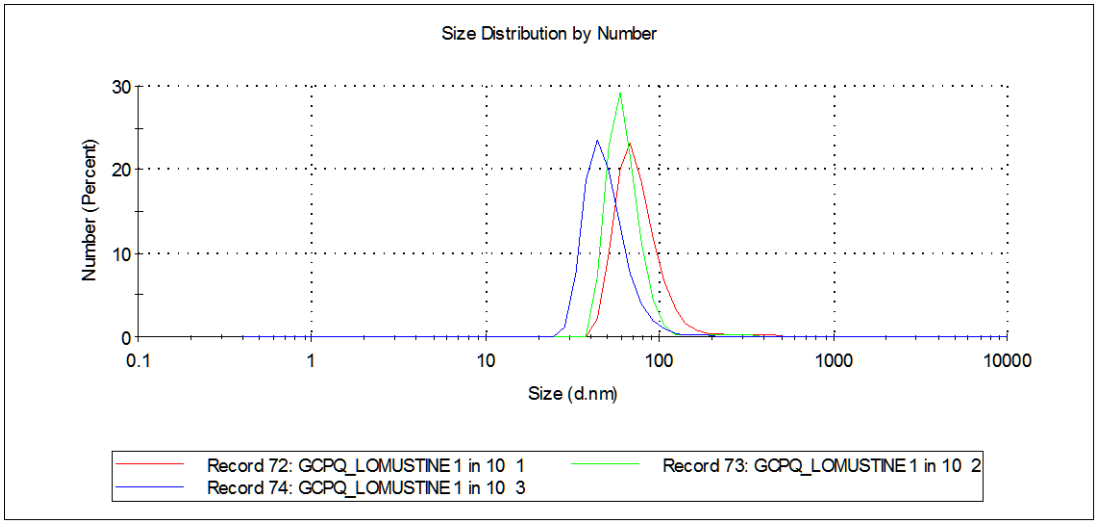

C

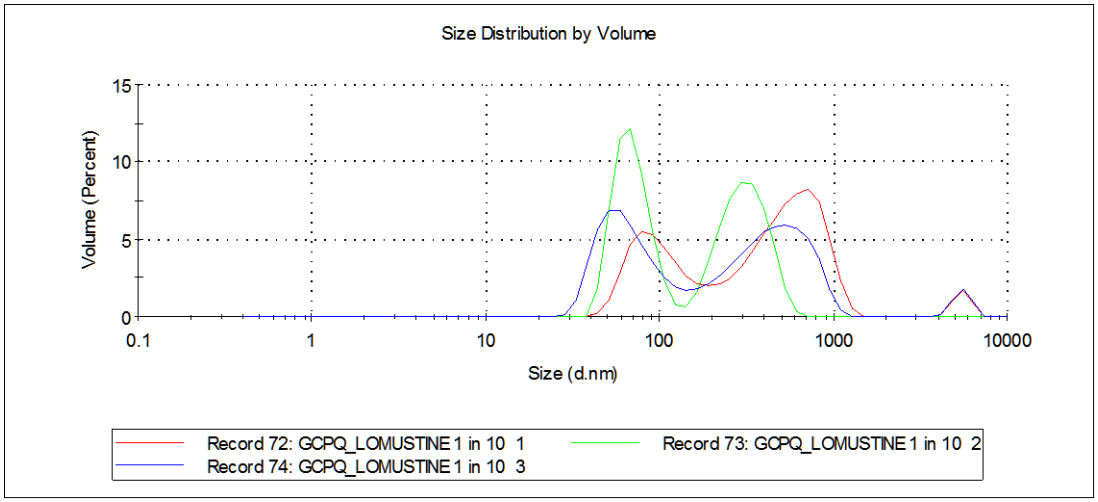

Figure 2-7: DLS graphs showing particle size distribution for Q-LOM by A: intensity; B: number; and C: volume

Freshly prepared nanoparticle formulation of lomustine containing: lomustine (2 mg mL^{-1}); GCPQ (20 mg mL^{-1}, 2 % $^{w}/_{v}$); polysorbate 80 (5 mg mL^{-1}, 0.5 % $^{w}/_{v}$); soya bean oil (10 mg mL^{-1}, 1 % $^{w}/_{v}$) in 5 % $^{w}/_{v}$ dextrose solution.

2.3.3 Preparation and characterisation of etoposide formulations

2.3.3.1 Determination of drug content of etoposide formulations

The calibration curve prepared for etoposide produced a line with the equation y = 6.1445x + 0.5063 (R^2 = 0.9998) for area of etoposide versus etoposide concentration and a line with equation y = 0.5092 + 0.0801 (R^2 = 0.9998) for height of etoposide versus concentration (Figure 2-8).

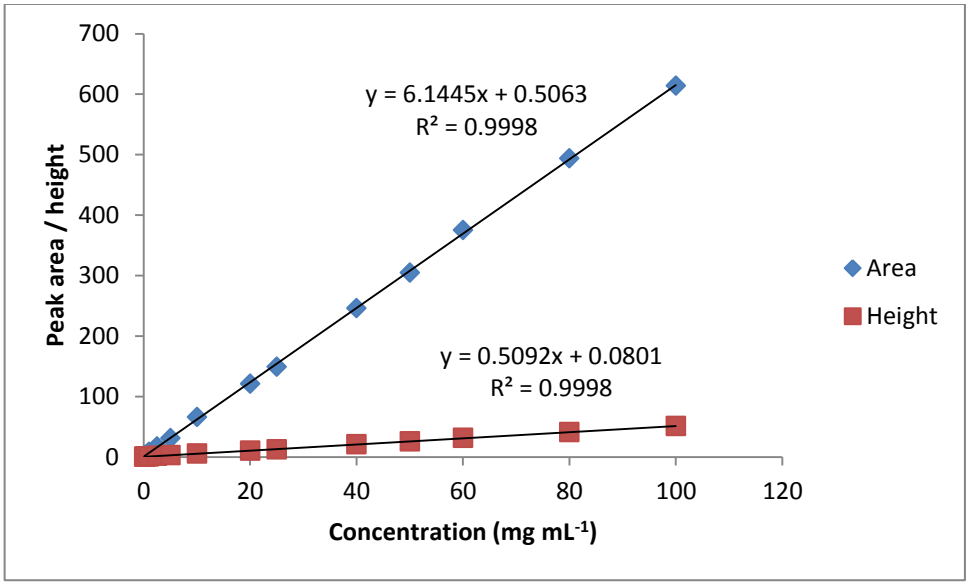

Figure 2-8: Calibration curve for etoposide

The equation of the line produced by the area versus etoposide concentration (y = 6.1445x + 0.5063) from the etoposide calibration curve (Figure 2-8) was used to determine the concentration of etoposide formulations.

2.3.3.2 Particle size determination for GCPQ- Etoposide Formulation

TEM images of the GCPQ- etoposide formulation revealed particle sizes in the range 15 – 300nm (Figure 2-9).

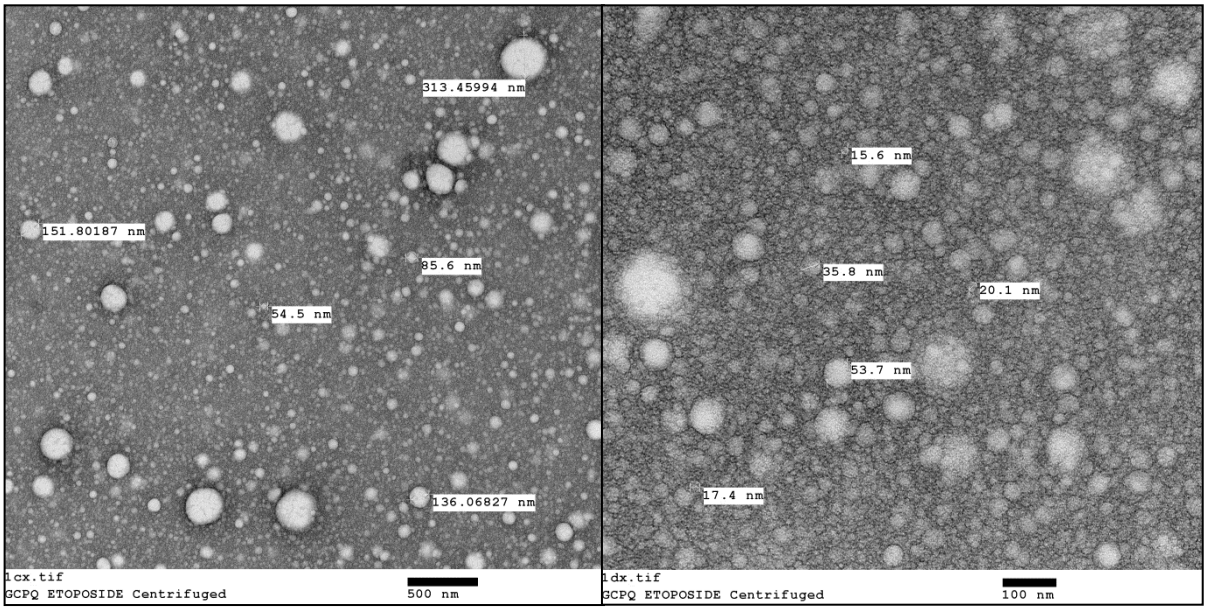

Figure 2-9: TEM images for GCPQ- etoposide formulation

Freshly prepared nanoparticle formulation of etoposide containing: etoposide (2 mg mL^{-1}); GCPQ (10 mg mL^{-1}, 1 % $^{w}/_{v}$); polysorbate 80 (2 mg mL^{-1}, 0.2 % $^{w}/_{v}$); soya bean oil (10 mg mL^{-1}, 1 % $^{w}/_{v}$) in 5 % $^{w}/_{v}$ dextrose solution. Particle size measurements are as generated by the AMT digital camera software.

DLS size data for the etoposide nanoparticle formulation revealed an average size of 176.7 nm with a polydispersity index of 0.2 (Figure 2-10).

A

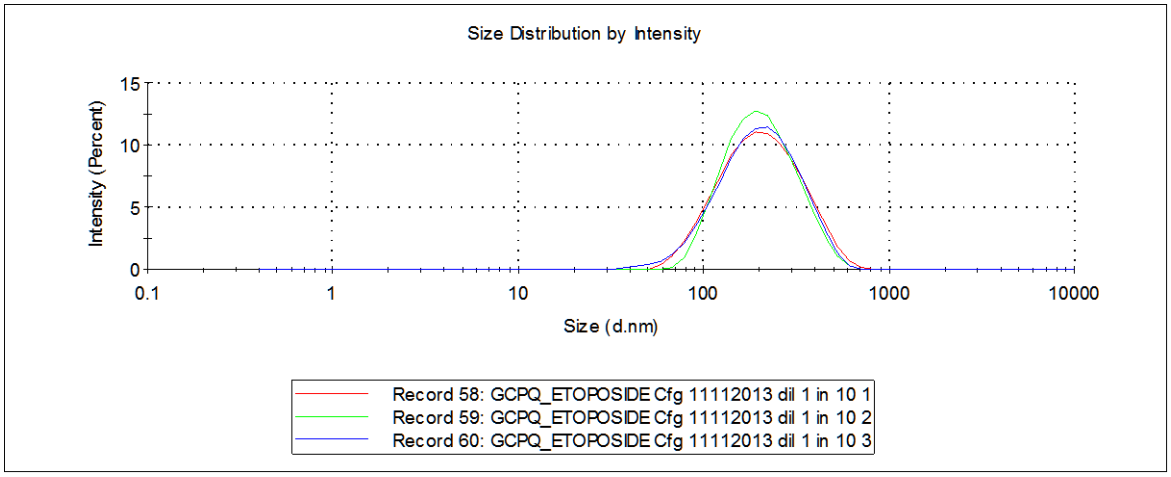

B

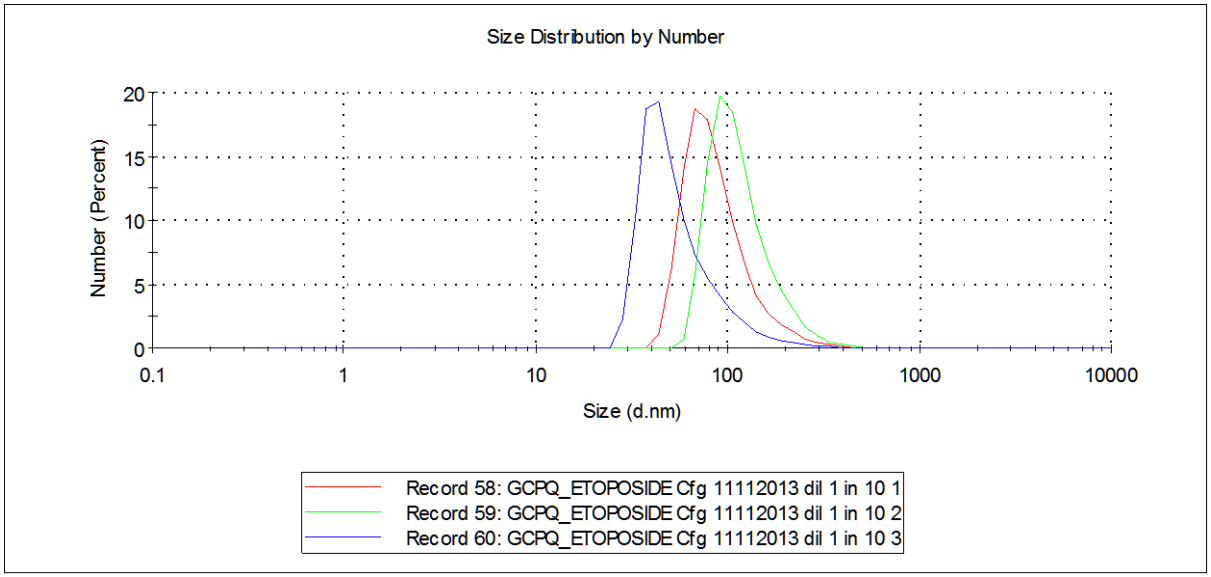

C

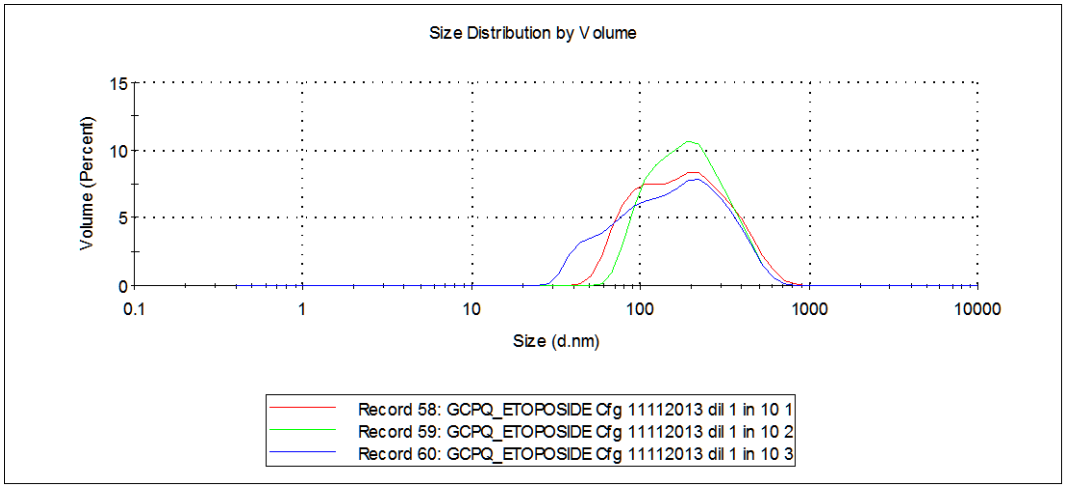

Figure 2-10: DLS graphs showing particle size distribution for GCPQ- etoposide formulation by A: intensity; B: number; and C: volume

Freshly prepared nanoparticle formulation of etoposide containing: etoposide (2 mg mL^{-1}); GCPQ (10 mg mL^{-1}, 1 % $^{w}/_{v}$); polysorbate 80 (2 mg mL^{-1}, 0.2 % $^{w}/_{v}$); soya bean oil (10 mg mL^{-1}, 1 % $^{w}/_{v}$) in 5 % $^{w}/_{v}$ dextrose solution.

2.3.4 **Tumour implantation**

MRI images acquired revealed successfully tumour implantation and establishment in the mice models (Figure 2-11)

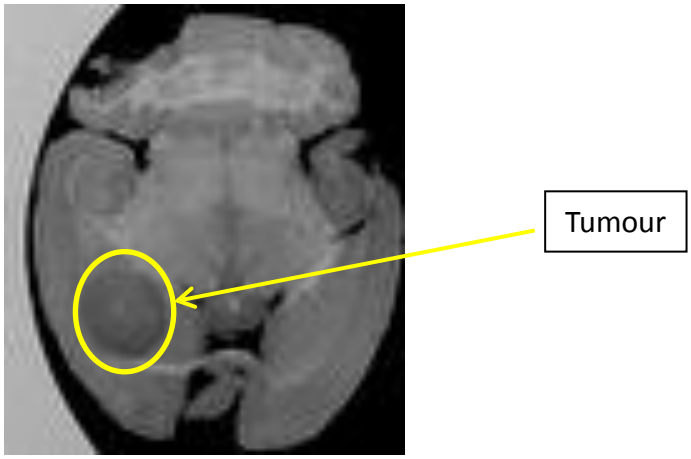

Figure 2-11: T_2 weighted image of an in situ brain tumour

2.3.5 **Tumour analysis by MRI**

MRI analysis data obtained for harvested tumour bearing mice brains revealed the presence of established intracranial tumours at 7 days post implantation (Figure 2-12), with the tumour volumes determined to be 2.12 ± 0.37 mm^3. The tumour sizes increased progressively over time until about 20 days (tumour volume = 91.8 ± 7.57 mm^3), the time point at which untreated tumour bearing mice reach the 15 % weight loss and are culled (Figure 2-13).

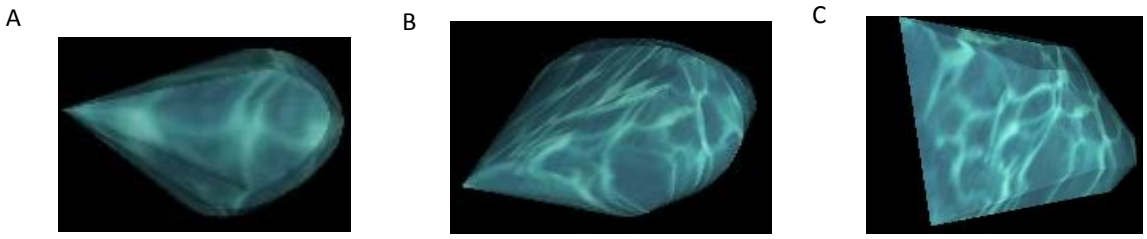

Figure 2-12: 3D MR images of 7 days post implantation intracranial tumours

Tumour volumes: A = 2.5 mm^3; B = 2.0 mm^3; C=1.8 mm^3.

Figure 2-13: 3D MR images of fully developed intracranial tumours

Tumour volumes: A = 98.1 mm^3; B = 93.9 mm^3; C= 83.4 mm^3.

The tumour images (Figure 2-12; Figure 2-13) show high resolution 3D MR images of the harvested mice brain tumours as generated by the Osirix software (MAC application) from the slices generated from individual tumours during the MRI process. In order to compute the volume for each tumour, regions of interest (ROI) are defined in all the slices with detectable tumour area. The ROI is defined by drawing a polygon around the tumour area in each slice with the aid of the appropriate Osirix software command. Initially, ROIs are defined in some representative slices from the first slice through the slices in the middle until the last slice. Importantly, ROIs must be defined in the first and the last slices. Once the ROIs are defined in the representative slices, ROIs are automatically generated for all the other slices using the appropriate Osirix software command. The ROIs are then checked to make sure they are accurately defined for the tumour area in each slice and adjusted where necessary. Following the satisfactory generation of all the ROIs, the tumour volume is then computed automatically for the tumour using the appropriate Osirix software command which also simultaneously generates the 3D tumour images shown above (Figure 2-12; Figure 2-13).

2.3.6 In vivo anti-tumour studies

2.3.6.1 Evaluation of antitumour activities of lomustine formulations

Mice were successfully treated with the appropriate lomustine formulation once daily for 10 consecutive days. Weight measurements revealed that this dosing regimen was well tolerated in the mice (Figure 2-14 A – C).

A

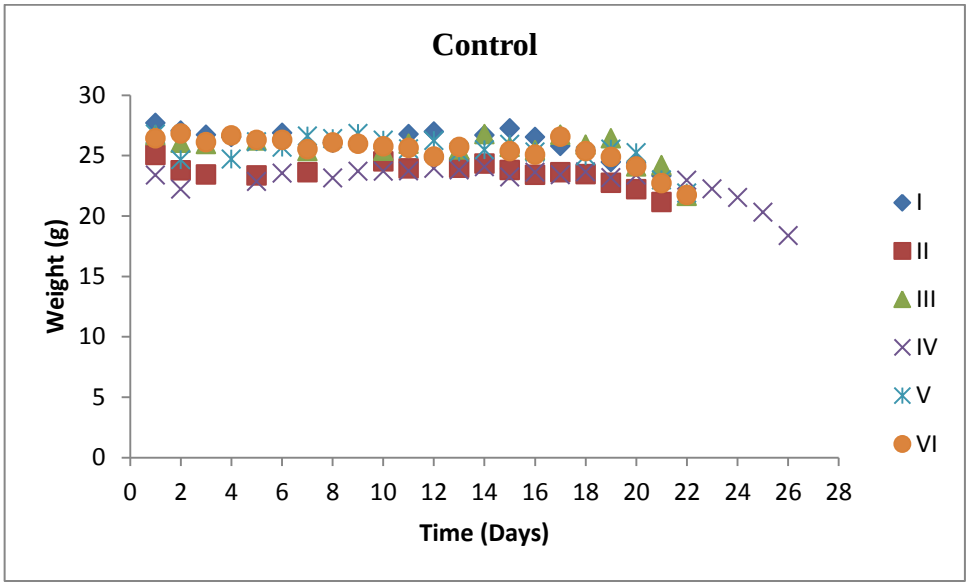

B

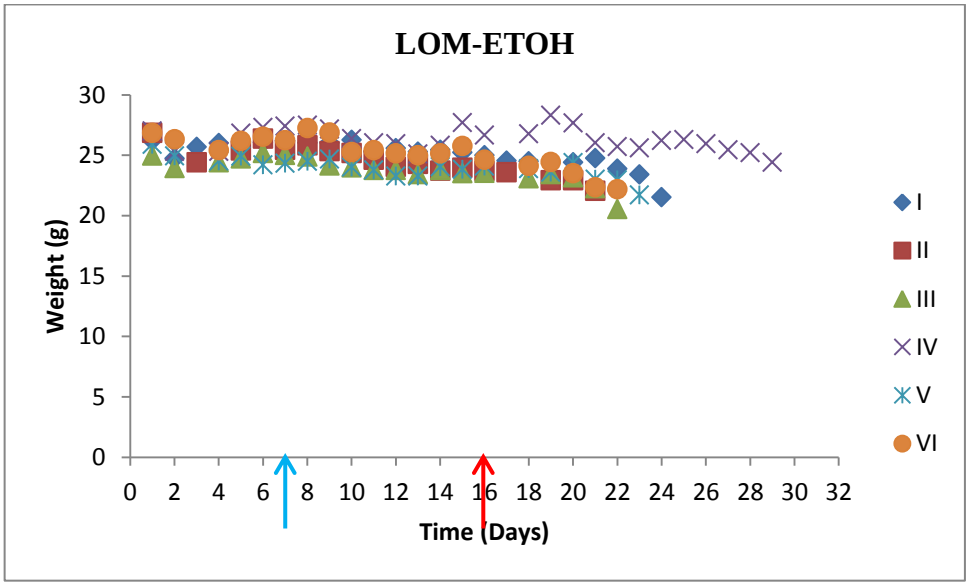

C

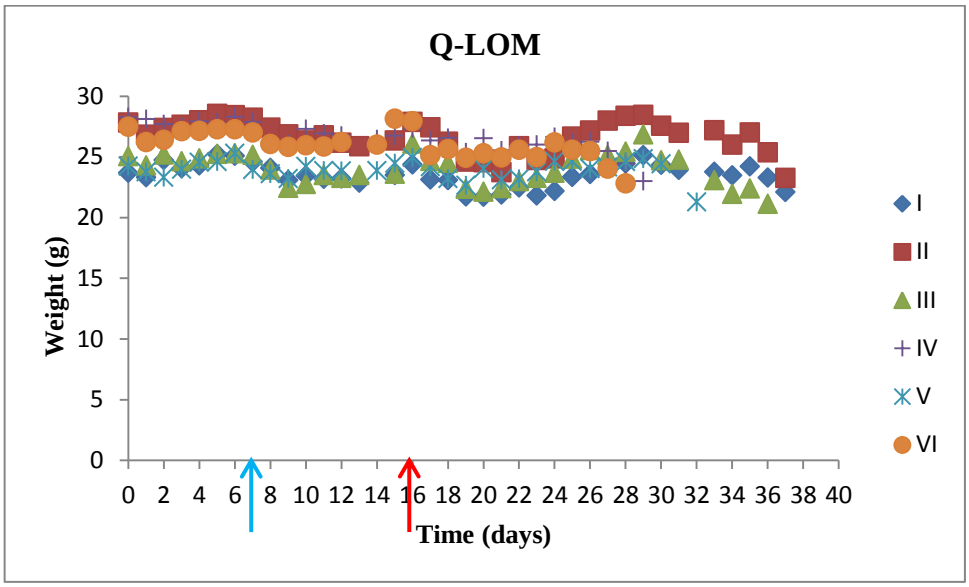

Figure 2-14: Weight measurement of treated and untreated tumour bearing mice over time.

Treatment groups: Q-LOM group: 13 mg kg^{-1} lomustine nanoparticle formulation, injected (tail vein) once daily for 10 consecutive days (≈ 200 µL of formulation, volume adjusted according to the weight of each mouse); LOM-ETOH group: 1.2 mg kg^{-1} ethanolic lomustine formulation, injected (tail vein) once daily for 10 consecutive days (≈200 µL of formulation, volume adjusted according to the weight of each mouse); CONTROL group: No treatment.

Key: Blue arrow: Treatment start date (Day 7); **Red arrow:** Treatment end date (Day 16).

Mice treated with the high dose lomustine (13 mg kg^{-1}) nanomedicine formulation had a mean survival time of 33.2 days, while mice treated with the ethanolic lomustine (1.2 mg kg^{-1}) formulation had a mean survival time of 22.5 days and the untreated control mice had a mean survival time of 21.3 days (Figure 2-15)

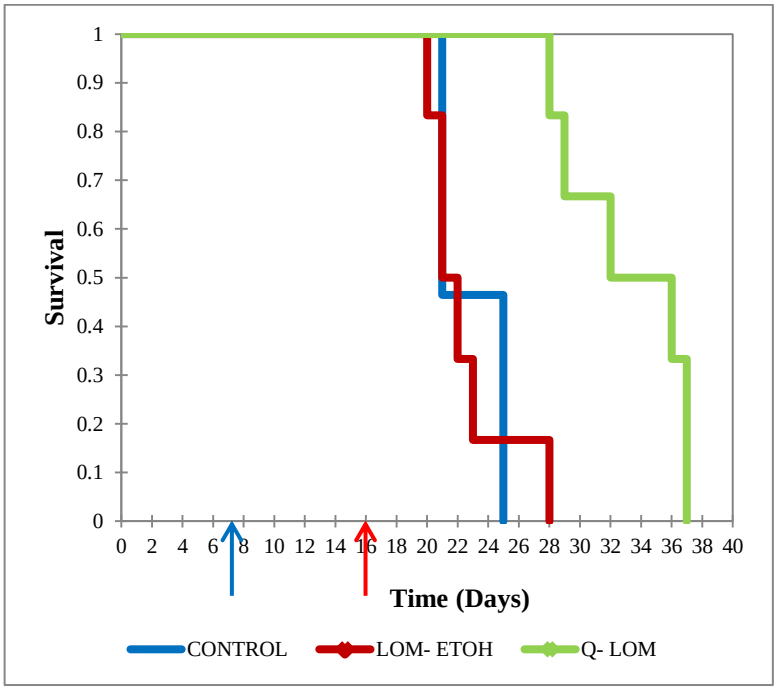

Figure 2-15: Kaplan Meier plot for tumour bearing mice from tumour implantation to time of cull (humane end point)

Treatment groups: Q-LOM group: 13 mg kg^{-1} lomustine nanoparticle formulation, injected (tail vein) once daily for 10 consecutive days (≈200 µL of formulation, volume adjusted according to the weight of each mouse); LOM-ETOH group: 1.2 mg kg^{-1} ethanolic lomustine formulation, injected (tail vein) once daily for 10 consecutive days (≈200 µL of formulation, volume adjusted according to the weight of each mouse); CONTROL group: No treatment.

Key: Blue arrow: Treatment start date (Day 7); **Red arrow:** Treatment end date (Day 16).

2.3.6.2 Evaluation of antitumour activities of etoposide formulations

Mice in this study could not be injected on consecutive days as planned because of the weight loss recorded. The dosing regimen had to be altered to allow one or two days of rest between doses for all the mice in the high dose etoposide nanomedicine group. The frequency and total number of doses administered depended on the recovery of each mouse as determined by recovery of body weight. Also, two mice in the low dose etoposide nanomedicine group were not injected on consecutive days due to loss in body weight. One of these was culled on dosing day 7 due to loss of body weight (Figure 2-16 A – C).

A

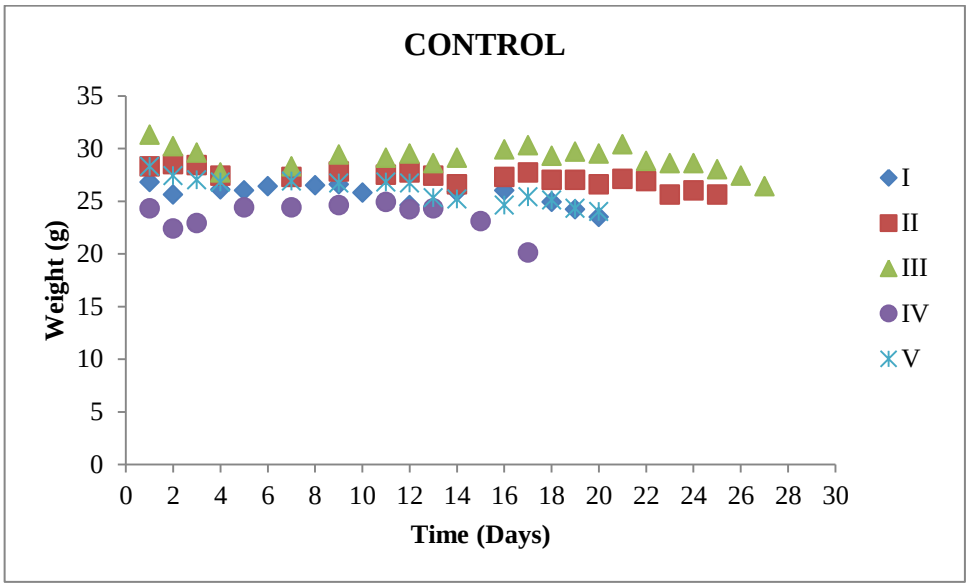
CONTROL
Weight (g)
Time (Days)
I
II
III
IV
V

B

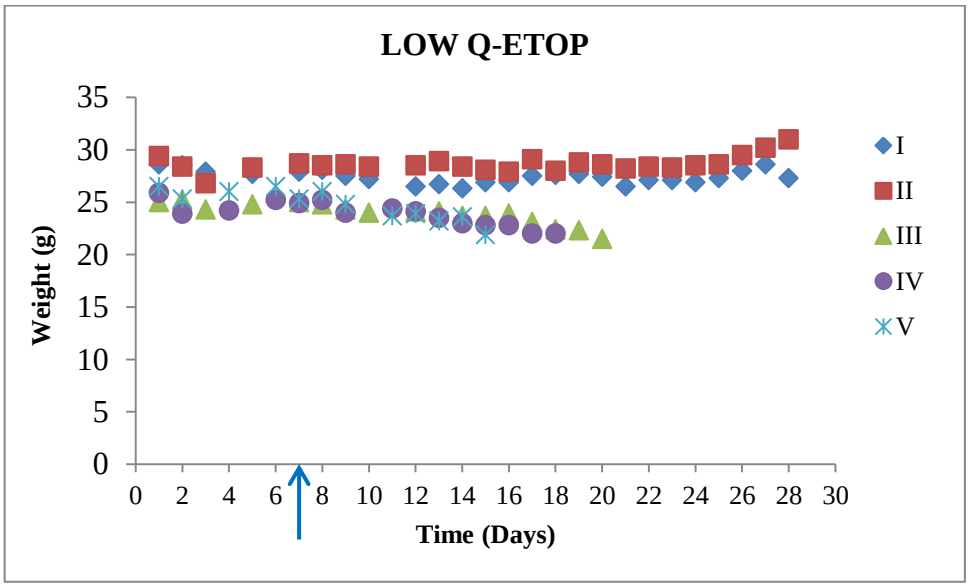
LOW Q-ETOP
Weight (g)
Time (Days)
I
II
III
IV
V

C

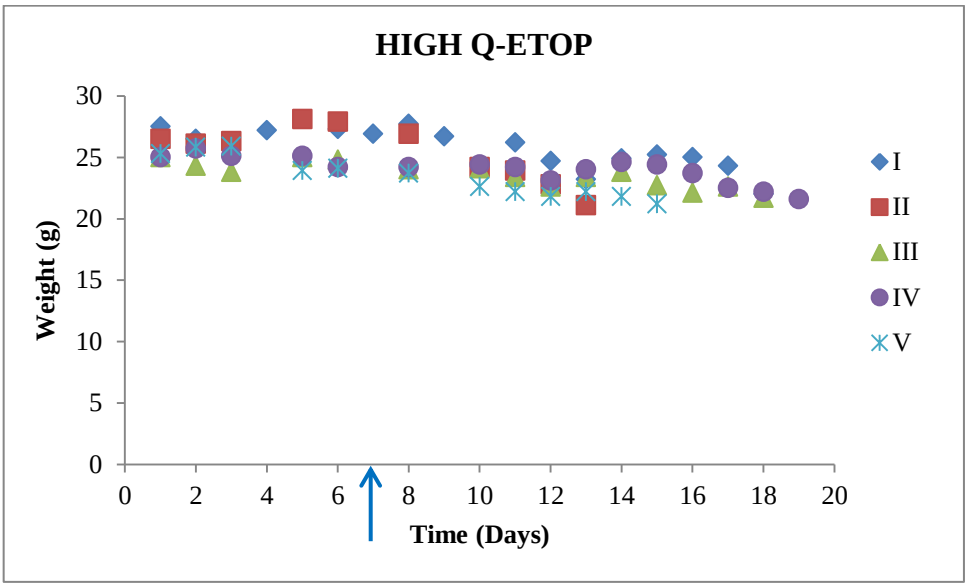

Figure 2-16: Weight measurement of treated and untreated tumour bearing mice over time

Treatment groups: High Q-ETOP group: 7.5 mg kg^{-1} etoposide nanoparticle formulation, injected (tail vein) once daily (≈ 200 µL of formulation, volume adjusted according to the weight of each mouse); Low Q-ETOP group: 1.5 mg kg^{-1} etoposide nanoparticle formulation, injected (tail vein) once daily (≈200 µL of formulation, volume adjusted according to the weight of each mouse); CONTROL group: No treatment. Planned consecutive (once) daily dosing was not achieved in this experiment due to weight loss observed in all the mice in the high dose nanomedicine (High Q-ETOP) as well as 2 mice in the low dose nanomedicine (Low Q-ETOP) groups

Key: Blue arrow: Treatment start date (Day 7).

Mean survival time for the High Q-ETOP group was 15.6 days, while the untreated control mice had a mean survival time of 20.8 days (Figure 2-17).

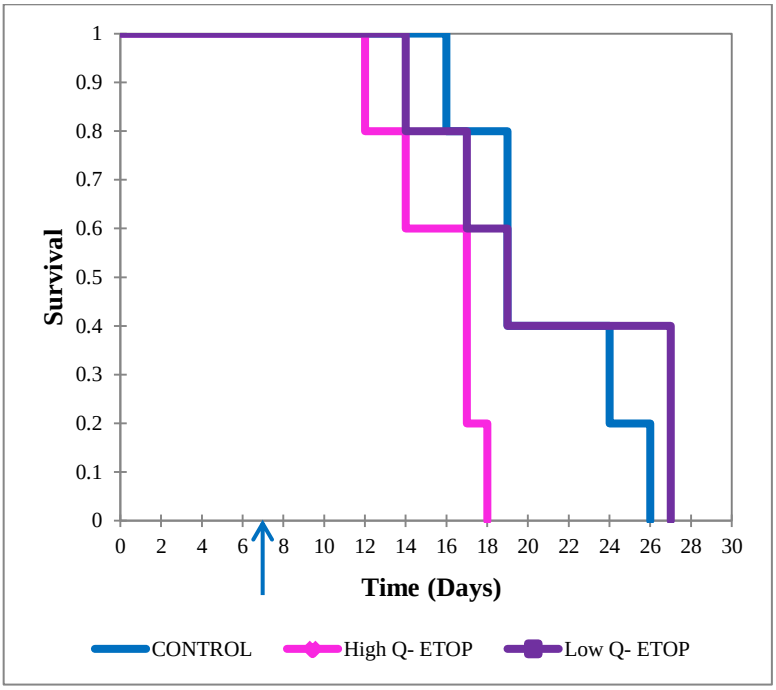

Figure 2-17: Kaplan Meier plot for tumour bearing mice from tumour implantation to time of cull (humane end point)

Treatment groups: High Q-ETOP group: 7.5 mg kg^{-1} etoposide nanoparticle formulation, injected (tail vein) once daily (≈ 200 µL of formulation, volume adjusted according to the weight of each mouse); Low Q-ETOP group: 1.5 mg kg^{-1} etoposide nanoparticle formulation, injected (tail vein) once daily (≈200 µL of formulation, volume adjusted according to the weight of each mouse); CONTROL group: No treatment. Planned consecutive (once) daily dosing was not achieved in this experiment due to weight loss observed in all the mice in the high dose nanomedicine (High Q-ETOP) as well as 2 mice in the low dose nanomedicine (Low Q-ETOP) groups

Key: Blue arrow: Treatment start date (Day 7).

2.4 Discussion and conclusions

Animal models have long been employed in the study of cancer. These studies include the development and evaluation of anticancer therapies before introducing such therapies in humans (Burger and Fiebig 2002; Sausville and Burger 2006; Teicher 2006). The cancer models may be murine tumours (Steiniger et al. 2004; Qian et al. 2013) or human tumour xenografts established by transplantation of either human cancer cell lines or biopsies from cancer patients in immunodeficient host animals (Lee and Weinmann 2008; Baklaushev et al. 2012) to preclude the incidence of host rejection of the transplant (Selek et al. 2014). Lomustine had been evaluated in various animal models for brain tumours.

Tamura and co-workers evaluated lomustine in a rat glioma model. They studied the effect of different total dose levels and the effect time of initiation of treatment on the effectiveness of chemotherapy. They reported that lomustine was highly effective when a dose of 3 x 40 mg kg^{-1} (total dose of 120 mg kg^{-1}) was administered intraperitoneally. This dose was found to increase the life span of tumour bearing animals by 53 – 86 %. Their data also showed that small total doses of 15 mg kg^{-1} and 30 mg kg^{-1} did not prolong the survival of animals treated with these doses of the drug. Also, single injections of lomustine at larger doses of 90 mg kg^{-1} and 120 mg kg^{-1} which are higher than the LD10 [approximately 60 mg kg^{-1} (Levin et al. 1970)] were toxic and decreased rather than increase the life span of treated animals by 38 % and 65 % respectively. Also, there were no significant differences in survival times between groups of animals in which treatment had been initiated earlier and and those in which treatment was initiated later. They concluded that in the assessment of the beneficial or detrimental effects of lomustine in animal brain tumour models, single doses of lomustine corresponding to 60 – 80 % of the LD10 given in several injections proved to be adequate (Tamura et al. 1979).

Also, Bethune and co-workers demonstrated improved therapeutic efficacy of a liposome formulation of lomustine in a 36B-10 (malignant rat astrocytoma) tumour model without a concomitant increase in toxicity. Rats bearing established subcutaneously implanted 36B-10 tumours were treated with either free lomustine or the liposomal lomustine formulation by intraperitoneal injection on day 14 following tumour implantation. Their pharmacokinetic studies suggested a two-fold plasma exposure resulting from the liposomal formulation compared to the free drug. Also, single dose as well as multiple dose (three weekly doses) treatments with the liposomal formulation resulted in approximately two-fold reduction in tumour progression compared to the free drug. In addition, they also reported that drug concentration in the tumours were found to be 10-fold greater than that in plasma following administration of the liposomal formulation. On the contrary, tumour drug concentration after administration of the free drug was similar to that in the plasma. Their data therefore suggests that the improved efficacy of the liposomal formulation of lomustine may be as a result of increased accumulation of the drug within the tumours (Bethune et al. 2001).

Furthermore, etoposide a semisynthetic podophyllotoxin derivative which has demonstrated pronounced antitumor activity against a variety of cancers such as testicular cancer, monocytic or myelomonocytic leukemia, non-Hodgkin's lymphomas and hepatocellular carcinoma (Cavalli 1982) has also been employed in animal studies.

For instance, in a fairly recent study, etoposide loaded poly(ethylene glycol)-co-poly(sebacic acid) [PEG–PSA) particles (Etop/PEG–PSA) was shown to demonstrate enhanced efficacy in a xenograft mouse model of human small cell lung cancer compared to the free drug. Intratumoural administration of a single dose of Etop/PEG–PSA (on day 14 following tumour implantation) in mice bearing subcutaneously implanted NCI-H82 (human lung tumour) cells resulted in effective suppression of tumour growth. There was 100 % survival of mice treated with Etop/PEG–PSA by day 31. On the other hand, mice treated with multiple doses of the free drug either by intratumoural or intraperitoneal injection had to be humanely sacrificed by day 24. In contrast to multiple doses of the free drug which resulted in median survival times of 11 days (intraperitoneal) and 16 days (intratumoural), a single intratumoural (bolus) dose of Etop/PEG–PSA resulted in a significantly ($p < 0.05$) increased median survival time of 47 days for treated mice (Tang et al. 2010).

In the current studies, GCPQ nanomedicine formulations improved the solubility of lomustine, a poorly aqueous soluble drug. The GCPQ formulation afforded a 2 mg mL^{-1} formulation of the drug thus enabling the Q-LOM formulation to be administered at a higher dose (13 mg kg^{-1}) which was 10 times what could be administered using the ethanolic formulation. The dose (1.2 mg kg^{-1}) employed for the ethanolic formulation was limited by the poor aqueous solubility of lomustine and the drug level achievable with the 10 % $^{v}/_{v}$ ethanol and polysorbate 80 (5 mg mL^{-1}) formulation.

Weight loss is a general indicator of drug-associated toxicity (Hofland et al. 2005), thus the extent of weight loss induced by a drug would be an indication of the toxic effects of that drug. Weight loss amongst other side effects had been found to constitute a restriction in therapy with lomustine in a sizeable number of patients (van den Bent et al. 2003). In the present study, weight measurements revealed no difference in mice that had received the high dose Q-LOM formulation compared to the controls and those that received the low dose ethanolic formulation (Figure 2-14). Also, this group of mice did not manifest signs of discomfort or ill health throughout the treatment period.

The mice that were treated with the high dose Q-LOM formulation had a mean survival time of 33.2 days which was significantly different ($p < 0.05$) from the mean survival time (22.5 days) for mice treated with the low dose ethanolic formulation and the untreated control mice (21.3 days) [Figure 2-15]. Thus, the Q-LOM formulation produced therapeutic and survival benefit as it enabled dose intensification by enabling the administration of a higher dose in a continuous dosing regimen, which produced prolonged survival in the mice that received this formulation compared to the other groups, without leading to additional gross toxicity.

Drugs employed as anticancer agents can exert either cytostatic or cytotoxic effects. Therefore, their effects can be assessed by their ability to produce a reduction in tumour volumes and/ or prolongation of survival (Raizer 2011). The prolonged survival provided by the Q-LOM formulation demonstrates the cytostatic efficacy of the drug using the nanomedicine formulation and the dosing regimen employed in this study.

The daily dosing regimen afforded continuous and prolonged exposure of tumour cells to the drugs thereby leading to an increase in chemosensitivity (Dolan et al. 1990; Tolcher et al. 2003; Tosoni et al. 2006). This strategy could be used to lead to an increased depletion or consumption of the AGAT protein and an increase in tumour penetration by the drug (Raizer, 2011). Moreover, findings from the work of Wick and co-workers demonstrated that administration of temozolomide in a dose-dense schedule of 150 mg m^{-2}/day in an alternate weekly (days 1 through 7 and days 15 through 21; every 4 weeks) regimen resulted in clinically important improved treatments outcomes. The alternate weekly dosing regimen was found to result in a 6-month progression-free survival (PFS-6) rate of 43.8 % and median PFS of 24 weeks in glioblastoma patients (Wick et al. 2007). The treatment outcome resulting from this dose dense regimen (PFS-6: 43 %; median PFS: 24 weeks) was superior to treatment outcomes (PFS-6 rate: 21 %; median PFS: 12 weeks) obtained in a large (225 patients) multicentre phase II study of temozolomide (versus procarbazine) in glioblastoma patients at first relapse (Yung et al. 2000) as well as the treatment outcomes (PFS-6 rate: 15 %; median PFS: 9 weeks for glioblastoma patients) in a large (375 patients) meta-analysis of eight consecutive clinical trials (Wong et al. 1999). Also, the treatment outcome obtained from the alternate weekly regimen was superior to that resulting from a low-dose temozolomide protracted schedule of 75 mg m^{-2}/day for 21 days every 28 days (three weeks on, one week off). This dosing schedule produced PFS-6 rate of 30.3 % and overall median PFS was 16.1 weeks (Brandes et al. 2006). The survival outcomes resulting from the alternate weekly regimen and the three weeks on, one week off dosing schedules were found to be independent of the MGMT gene promoter methylation status (Brandes et al. 2006; Wick et al. 2007), as a methylated MGMT gene promoter in tumour tissue was not associated with prolonged PFS (Wick et al. 2007).

Thus, from these two studies employing dose intensification in the form of increasing the dosing frequency, the lack of correlation of the MGMT gene promoter methylation status with survival outcomes indicates that the increased exposure of tumours to the drug may have resulted in increased depletion of MGMT such that tumours possessing an unmethylated MGMT gene promoter (more chemoresistant tumours) also became more sensitive to chemotherapy.

The superior outcomes (PFS-6: 43 %; median PFS: 24 weeks) resulting from the higher dose (150 mg m^{-2}/day) temozolomide in an alternate weekly regimen (Wick et al. 2007) demonstrates that the administration of chemotherapy at higher dose intensity could potentially lead to more beneficial treatment outcomes. This indicates that depletion of MGMT resulting from the alternate weekly administration of temozolomide (150 mg m-2/day) may overcome the chemotherapeutic challenges of an unmethylated MGMT promoter (Wick et al. 2007).

Therefore, the significantly ($p < 0.05$) increased survival time of 33.2 days (without additional gross toxicity) resulting from the high dose lomustine (Q-LOM; 13 mg kg^{-1}) nanomedicine formulation compared to survival time (22.5 days) in the low dose lomustine (1.2 mg kg^{-1}) ethanolic formulation in the present study, can be linked to the increased exposure of the tumours to the drug as a result of the administration of 10 consecutive daily injections of the formulation at the high (13 mg kg^{-1}) dose. This suggests that continuous tumour exposure to lomustine using the high dose nanomedicine formulation in a continuous dosing regimen may result in depletion of MGMT in tumour cells thereby increasing tumour response to the therapy.

This indicates that the administration of the high dose lomustine formulation (Q-LOM; 13 mg kg^{-1}) in a dose intense regimen may result in beneficial therapeutic outcomes in the chemotherapy of tumours with an unmethylated MGMT gene promoter as well as tumours expressing a methylated promoter.

The nanomedicine formulation of lomustine (Q-LOM) thus enabled the administration of the drug in a dose intense regimen which produced therapeutic and survival benefits, producing a mean survival time that is 1.5 times longer than the low dose ethanolic treatment group and untreated control mice, while not leading to additional toxicity. This formulation therefore has potential as a dose intensification therapeutic, in that lomustine may be given at a higher dose and in more frequent doses provided it is encapsulated in nanoparticles. This will avoid the usual rest periods of 6 – 8 weeks (or longer in some cases), employed in chemotherapy with lomustine (Cianfriglia et al. 1980; van den Bent et al. 1998; van den Bent et al. 2006; Jakacki et al. 1998). Moreover, dose intensification with lomustine in the past had been unsuccessful due to haematologic toxicity which led to dose delays and reduction (Caincross et al. 1994), and the overall achievable dose was not different from the standard regimen (Jackaki et al. 1998).

On the contrary, dose intensification with etoposide nanomedicine formulation was not feasible using the nanomedicine formulation. There was no therapeutic or survival benefit associated with the high dose (7.5 mg kg^{-1}) nanomedicine formulation of the drug. Firstly, once daily dosing was not achievable with the nanomedicine formulation. All the mice in high dose (7.5 mg kg^{-1}) nanomedicine (High Q-ETOP) treatment group experienced loss of body weight which necessitated alteration of the initial planned dosing regimen. The weight loss observed in this treatment group necessitated an alteration of the planned consecutive daily dosing schedule to allow for rest periods of one or two days (as appropriate, based on body weight measurements) between doses.

Two out of the five mice in the high dose etoposide nanomedicine (High Q-ETOP; 7.5 mg kg^{-1}) treatment group could receive a total of only 3 doses due to a drop in body weight close to 15 % of the initial body weight, which is the severity limit for the experiment. Furthermore, the remaining three mice in the group could receive only 5 doses, also with days of rest in between due to the loss in body weight recorded for the mice. Also, two mice in the low dose nanomedicine (Low Q-ETOP; 1.5 mg kg^{-1}) group could not receive the planned daily doses due to a drop in their body weight. The body weight loss recorded could be attributed to etoposide treatment related gross toxicity, as weight loss is a known toxic effect associated with etoposide therapy (Holm et al. 1996; Hofland et al. 2005).

Secondly, the mice that had been treated with the high dose nanomedicine formulation (High Q-ETOP; 7.5 mg kg^{-1}) did not derive a survival benefit from the therapy. Mice treated with the high dose nanomedicine formulation had a shorter mean survival time (15.6 days) compared to untreated control mice (20.8 days) [Figure 2-17]. Moreover, the experiment was terminated as the high dose nanomedicine formulation (High Q-ETOP; 7.5 mg kg^{-1}) did not yield any therapeutic benefit. Two mice in the low dose nanomedicine (Low Q-ETOP; 1.5 mg kg^{-1}) treatment group were culled prior to reaching the end point of 15 % loss of body weight when the experiment was terminated. Thus, the nanomedicine formulation of etoposide did not lead to a protection of treated animals from the toxic effects of the drug as the mice treated with the high dose etoposide nanomedicine experienced gross toxicity while not deriving any survival benefit (Figure 2-17).

Therefore, in contrast to the high dose lomustine (13 mg kg^{-1}) nanomedicine formulation that permitted continuous drug administration for 10 consecutive days with attendant therapeutic benefit, a high dose etoposide (7.5 mg kg^{-1}) nanomedicine formulation produced gross toxic effects in mice without providing any therapeutic or survival benefit.

Chapter 3 Evaluation of Myelosuppressive Effects of Q-LOM Formulations

3.1 Introduction

Myelosuppression is the major dose limiting toxicity associated with most clinically used cytotoxic agents employed in cancer chemotherapy. This puts a restraint on the extent of potentially advantageous dose intensification with chemotherapeutic agents as it curtails both the dose and frequency of administration (Newlands et al. 1992; Peters et al. 1993; Carey 2003; Tolcher et al. 2003; Stupp et al. 2005; Su et al. 2005; Chamberlain 2010; Gerber et al. 2007; Combs et al. 2008; Chamberlain and Raizer 2009). Myelosuppression results from the indiscriminate toxic effects of cytotoxic agents on normal cells as well as tumour cells (Maxwell and Maher 1992; Kriegler et al. 1994; Raizer 2011) with rapidly proliferating cells such as the haematopoietic cells being the most sensitive (Pollak et al. 1989; Kriegler et al. 1994; Çetin et al. 2000). Toxicity is as a result of obliteration of cycling progenitors in the bone marrow which in turn leads to reduced peripheral blood cell count which does not recover until there is replenishment by the quiescent progenitors and stem cells (Maxwell and Maher 1992; Kriegler et al. 1994; Dale 2002). Also, in patients receiving long term adjuvant chemotherapy, there is a risk of permanent damage to self-renewal tissues such as the bone marrow. Once damaged, the bone marrow has reduced proliferative potential, which constitutes a significant challenge in the event of a requirement for the use of further chemotherapy for eradication of gross metastasis (Smaaland et al. 2002).

Neutropenia and thrombocytopenia are two clinically important myelosuppressive effects of cytotoxic drugs which can lead to fatal complications, sepsis in the case of neutropenia and haemorrhage in the case of thrombocytopenia (Schofield 1986; Dale 2002; Hitron et al. 2010; McMahon and Kwaan 2012; Lyman et al. 2013).

Neutropenia arises as a result of reduction in the number of granulocytes in peripheral circulation. As granulocytes are involved in the body's defence against infections, neutropenia puts patients at risk of life threatening infections (Morstyn et al. 1988; Lyman et al. 1998; Dale 2002; Crawford et al. 2004). Risk of developing infections is determined by the degree as well as the duration of neutropenia (Lyman et al. 1998; Crawford et al. 2004). Development of febrile neutropenia necessitates hospitalisation and aggressive treatment with intravenous antibiotics as the risk of development of septicaemia is increased (Lyman et al. 1998; Crawford et al. 2004).

Thrombocytopenia arising from reduced platelet counts is also very significant as it may lead to thrombotic and bleeding complications. This often makes hospitalisations and platelet transfusions necessary as supportive measure in chemotherapy (Intile et al. 2009; Hitron et al. 2011; McMahon and Kwaan 2012).

Chemotherapy induced myelosuppression often leads to the need for dose delays and reductions which compromise tumour response and the overall survival of patients (Hitron et al. 2011). Measures taken to reduce the extent and duration of myelosuppression usually include autologous bone marrow support, such that myelosuppression does not determine the maximal tolerated dose (MTD) of a chemotherapeutic regimen. The MTD would then be determined by effects of chemotherapy on the non-haematopoietic organs. Infusion of committed peripheral blood progenitor cells (PBPC) have also been used which results in cells that are enriched with large numbers of circulating committed myeloid progenitors (Peters et al. 1993). The additional treatments required to combat these myelosuppressive effects lead to increased expense, have limited success and may not prevent chemotherapy-induced genetic damage to cycling progenitor cells (Intile et al. 2009).

The greatest concern in the use of high dose chemotherapy is the duration of suppression, that is if the stem cells will recover quickly enough to prevent fatalities resulting from sepsis and haemorrhage associated with prolonged neutropenia and thrombocytopenia (Schofield 1986; Smaaland et al. 2002).

This study has demonstrated a potential for dose intensification with lomustine using a nanomedicine formulation of the drug without leading to a proportionate increase in toxicity.

3.2 Materials and methods

3.2.1 Materials

3.2.1.1 List of materials

S/n	Material	Supplier
1	Lomustine	Sigma
2	GCPQ	Synthesised
3	Cholesterol	Sigma
4	L- α- Phosphatidyl choline (from egg yolk)	Sigma
5	Nile red (Bioreagent, suitable for fluorescence)	Sigma
6	CD45–Vioblue mouse antibody	MACS; Miltenyi Biotech, GmbH, Germany
7	CD61–APC Mouse and rat antibody	MACS; Miltenyi Biotech
8	Anti-TER–119 PE mouse antibody	MACS; Miltenyi Biotech

S/n	Material	Supplier
9	MACSQuant™ Running buffer	MACS; Miltenyi Biotech
10	Dubelcco's Phosphate buffered saline (DPBS)	Life Technologies
11	J774A.1 cell line	European Collection of Cell Cultures (ECACC); Culture Collections, Public Health England, Salisbury, UK
12	Dulbecco's Modified Eagle's Medium (DMEM) (ATCC® 30-2002™)	LGC Standards, Teddington, Middlesex, UK
13	Ringer's Solution	Thermo Scientific; Oxoid Limited, Basingstoke, Hampshire, UK
14	Ethanol, Absolute (Analytical reagent grade)	Fisher Scientific, UK,
15	Chloroform (HPLA grade)	Fisher Scientific, UK,
16	50 % Dextrose solution	AAH Pharmaceuticals

S/n	Material	Supplier
17	Water for injections (BP)	AAH Pharmaceuticals
18	Fetal bovine serum	Labtech International Ltd, Uckfield, East Sussex, UK
19	Phosphate buffered saline (PBS) – EDTA	Lonza Group Ltd, Verviers, Belgium
20	Glass bottom tissue culture dishes	MatTek, Corporation, Ashland, MA, USA

3.2.2 **Methods**

3.2.2.1 Drug treatment for evaluation of myelosuppressive effects of lomustine formulations

Male CD-1 mice (Harlan Laboratories Limited, Derbyshire, UK) housed in plastic cages, with a maximum of 5 mice per cage, maintained in standard regulated laboratory conditions in the Biological Services Unit (BSU) within the School were used for the study. The mice were accommodated in suitable rooms with the temperature maintained at about 22 – 25 ^{o}C, humidity at 60 % and a 12 – hour light (from 07: 00 hours) and dark (from 19: 00 hours) cycle. The mice were acclimatized in the BSU for 5 – 7 days before studies commenced. All mice had access to food and water *ad libitum* as soon as they were housed in the BSU and throughout the period of study. The study was conducted in accordance with the policies and regulations of the Home Office as stipulated in the Animals and Scientific Acts 1986, UK, the recommendations of the BSU for the handling and care of laboratory animals and with the approval of the ethics committee.

Lomustine formulations for administration to the mice were prepared as described in the preceding chapter (2.2.2.2.1).

Mice were assigned to one (n = 5) of three groups to receive either the high dose formulation (QLOM; 13 mg kg^{-1}), the low dose formulation (Lom- ETOH; 1.2 mg kg^{-1}), or no drug treatment (Control). Mice were administered the appropriate formulation by tail vein injection once daily for 10 consecutive days and were subsequently sacrificed at pre-determined time points after completion of the dosing regimen for analysis of blood parameters.

3.2.2.2 Sample collection for analysis of blood parameters

To obtain blood samples for analysis, mice were administered a terminal dose of anaesthetic agent (Euthatal) by intraperitoneal injection and allowed to become fully anaesthetised. Once confirmed to be fully under anaesthesia (pinching the hind limb with a pair of forceps and eliciting no response), the skin was cut open from the abdominal region up to the thoracic region to expose the rib cage. The heart was then exposed by carefully cutting open the sternum and blood was withdrawn by cardiac puncture. The blood was immediately transferred into an ethylenediaminetetraacetic acid (EDTA) treated blood collection tube and mixed to prevent the formation of clots. The blood samples were analysed using an automated clinical haemocytometer for the determination of cell counts for different blood components. A portion of the samples were further analysed by flow cytometry for the determination of absolute cell counts.

3.2.2.3 Preparation and analysis of blood samples by flow cytometry

Absolute blood cell counts were determined by staining blood samples with mouse specific antibodies for the different blood components (leucocytes, erythrocytes and platelets). Blood samples were stained with CD45- Vioblue for of leucocyte count (for white blood cells), Anti-TER- 119 PE for erythrocyte count (for red blood cells) and CD61- APC for platelet count. Blood sample for each mouse (60 µL) was transferred into a 5 ml FACS tube and 10 µL of the appropriate antibody was added. The mixture was incubated at 4 ^{o}C (refrigerator) for 10 minutes, after which 1 ml of MACS Quant running buffer was immediately added to stop staining (prevent over staining). Further dilution of the samples was then made to achieve the required dilution for analysis. For erythrocytes and platelets, a final sample dilution of 1 in 1000 was made while a dilution of 1 in 20 was made for leucocytes. The samples were then analysed on the flow cytometer for determination of the cell counts for each blood component.

3.2.2.4 Cell uptake studies

3.2.2.4.1 Preparation and characterisation of Nile red loaded nanoparticles

3.2.2.4.1.1 Preparation of Nile red loaded GCPQ (GCPQ NR) formulation

GCPQ NR formulation for cell treatment for flow cytometry analysis was prepared by probe sonicating Nile red (50 µg mL^{-1}) and GCPQ (1 mg mL^{-1}) in 5 % $^{w}/_{v}$ dextrose solution on ice for 30 minutes. This was followed by centrifugation at 1,000 g for 30 minutes at 4^{o} C to eliminate free precipitated dye. The supernatant was then carefully collected immediately after centrifugation. A GCPQ NR formulation for cell treatment and for confocal microscopy imaging was prepared by adding 100 µL of a solution of Nile red (100 µg ml^{-1}) in ethanol to a dispersion of GCPQ (1 mg mL^{-1}), in 5 % $^{w}/_{v}$ dextrose solution with free precipitated dye removed as described above.

3.2.2.4.1.2 Preparation of Nile red loaded liposome (Liposome NR) formulation

Liposome NR formulations for cell treatment for flow cytometry analysis were prepared as described by McPhail et al. 2000, with some modifications. Briefly, Nile red (50 µg mL^{-1}), egg phosphatidylcholine (3 mg mL^{-1}) and cholesterol (1.4 mg mL^{-1}) were dissolved in chloroform (10 mL) and the resulting solution evaporated to dryness at 40° C using a rotary evaporator. The thin lipid film obtained was then hydrated with 5 % $^{w}/_{v}$ dextrose solution (5 mL) by shaking for 30 min at room temperature to yield a homogenous dispersion of egg phosphatidylcholine liposomes. This dispersion was subsequently probe sonicated on ice for 15 minutes to yield nano sized liposome formulation. This formulation was then centrifuged at 1,000 g for 30 minutes at 4^{o} C to eliminate precipitated free dye and the supernatant was carefully collected immediately after centrifugation.

A Liposome NR formulation for cell treatment and for confocal microscopy imaging was prepared by adding 100 µL of a solution of Nile red (100 µg mL $^{-1}$) in chloroform to egg phosphatidylcholine (3 mg mL^{-1}) and cholesterol (1.4 mg mL^{-1}) dissolved in chloroform (10 mL). The resulting solution was evaporated to dryness at 40° C using a rotary evaporator (IKA® HB 10 Digital, IKA®-Werke GmbH & Co. KG, Staufen, Germany). The thin lipid film obtained was then hydrated with 5 % w/v dextrose solution (5 mL) by shaking for 30 min at room temperature to yield a homogenous dispersion of egg phosphatidylcholine liposomes. This dispersion was subsequently probe sonicated on ice for 15 minutes to yield nano sized liposome formulation. Precipitated free dye was removed as described above.

The concentration of Nile red (fluorescence) in both GCPQ NR and Liposome NR were adjusted to give similar concentrations in both formulations before cell treatment.

3.2.2.4.1.3 Characterisation of Nile red loaded nanoparticles

A calibration curve for determination of Nile red content of nanoparticle formulations was prepared by measuring the fluorescence intensity of serial dilutions of Nile red in methanol using a fluorescence spectrometer (LS – 50 B, Perkin Elmer Inc, USA) with FL WinLab (Perkin Elmer Inc, USA) software. The equation of the line produced by plotting the fluorescence intensity versus Nile red concentration was used to determine the concentration (as a measure of intensity) of Nile red in GCPQ and Liposome NR formulations.

To determine the fluorescence intensity, hence the concentration of Nile red in GCPQ NR and Liposome NR formulations, the formulations were diluted 1 in 10 with methanol and the Nile red intensity was then measured using the fluorimeter. The fluorescence intensity of the formulations was adjusted by diluting with 5 % $^{w}/_{v}$ dextrose solution so that both GCPQ NR and Liposome NR formulations had similar fluorescence intensities prior to cell treatment.

The Nile red loaded nanoparticle (GCPQ NR and Liposome NR) formulations were characterised using TEM and DLS to determine particle size.

3.2.2.4.2 Evaluation of uptake of Nile red loaded nanoparticles in macrophage (J774A. 1) cell line

J774A. 1 cells were cultured in Dulbecco's Modified Eagle's Medium (ATCC-DMEM) modified to contain 4 mM L-glutamine, 4500 mg/L glucose, 1 mM sodium pyruvate, and 1500 mg/L sodium bicarbonate, and supplemented with 10 % fetal bovine serum. The cells were maintained in culture for at least 14 days before they were used for uptake experiments. Uptake of Nile red loaded nanoparticles in J774A. 1 cells was assessed quantitatively by flow cytometry and qualitatively by confocal microscopy.

For flow cytometry and confocal microscopy imaging, cells were seeded and prepared for analysis according to methods described by Fernado et al. 2010 and Kim et al. 2012 with some modifications.

3.2.2.4.2.1 Evaluation of uptake of Nile red loaded nanoparticles in J774A. 1 cell line by flow cytometry

J774A. 1 cells were seeded in 6 – well plates at a density of 300, 000 cells / well (working volume of 2 mL / well) and incubated for 72 hours before treatment with 200 µL of either GCPQ NR or Liposome NR formulation, with some wells left untreated as control. Cells were treated for predetermined time periods of 5 minutes, 10 minutes, 30 minutes, 1 hour, 2 hours, or 4 hours. Cells were then washed 3 times with DPBS solution [calcium chloride anhydrous ($CaCl_2$; 0.9 mM), magnesium chloride ($MgCl_2.6H_2O$; 0.5 mM), potassium chloride (KCl; 2.7 mM, potassium phosphate monobasic (KH_2PO_4; 1.5 mM), sodium chloride (NaCl 137.9 mM), sodium phosphate dibasic ($Na_2HPO_4.7H_2O$; 8.1 mM), pH 7.0 – 7.2] (2 mL / well) and then incubated in cold PBS – EDTA [KH_2PO4 (1.9 mM), NaCl (138.9 mM), $Na_2HPO4.2H_2O$ (6.6 mM), Titriplex III (EDTA Na_2; 1.4 mM), lithium chloride (LiCl; 10.1 mM); pH 7.5)] (1 mL / well) for 1 – 2 minutes.

Cells were then harvested by gently scraping and pipetting the cell suspension which was then centrifuged and resuspended in cold Ringer solution [Sodium chloride (38.5 mM), Potassium chloride (1.4 nM), Calcium chloride hexahydrate (0.5 mM), Sodium bicarbonate (0.6 mM); pH 7]. Nanoparticle uptake was quantified as determined by Nile red fluorescence detection using the flow cytometer (MACSQuant Analyzer, Miltenyi Biotec, Germany). A total of 20, 000 cells (events) were measured in each sample within the Nile red positive channel. The experiment was carried out in quadruplet for each formulation and the untreated control cells.

3.2.2.4.2.2 Evaluation of uptake of Nile red loaded nanoparticles in J774A.1 cell line by confocal microscopy

For confocal microscopy imaging, the cells were seeded in glass (thickness no. 1.0 cover slip) bottom 35 mm tissue poly–d–lysine coated tissue culture dishes at a density of 75,000 cells / dish and incubated for 48 hours. Cell uptake of the Nile red formulations was then monitored in a time lapse experiment set up on a Zeiss LSM 710 laser scanning microscopy imaging unit (LASOS Laserteknik GmbH, Carl Zeiss Promenade 10). Images were captured first at 3 minutes after treatment with the appropriate Nile red formulation and subsequently after every 5 minutes. The images were analysed using Zen 2009 software.

3.2.2.4.3 Statistical analysis

Statistical analysis was performed using Minitab® 16 software (Minitab, Inc., Pennsylvania, USA). The treatment groups were compared two at a time for each time point using ANOVA followed by Tukey post hoc test. The significance level was set at $p < 0.05$. Error bars represent the standard deviations of the mean values for each group.

3.3 Results

3.3.1 Drug treatment for evaluation of myelosuppressive effects of lomustine formulations

All mice received the total number (10) of doses planned for the study on time without any necessity for dose delay or reduction in the any of the treatment groups. There was no manifestation of gross toxic symptoms by animals across the treatment groups as weight measurement did not reveal unacceptable reduction in body weight in the treated animals (Figure 3-1 A – E)

A

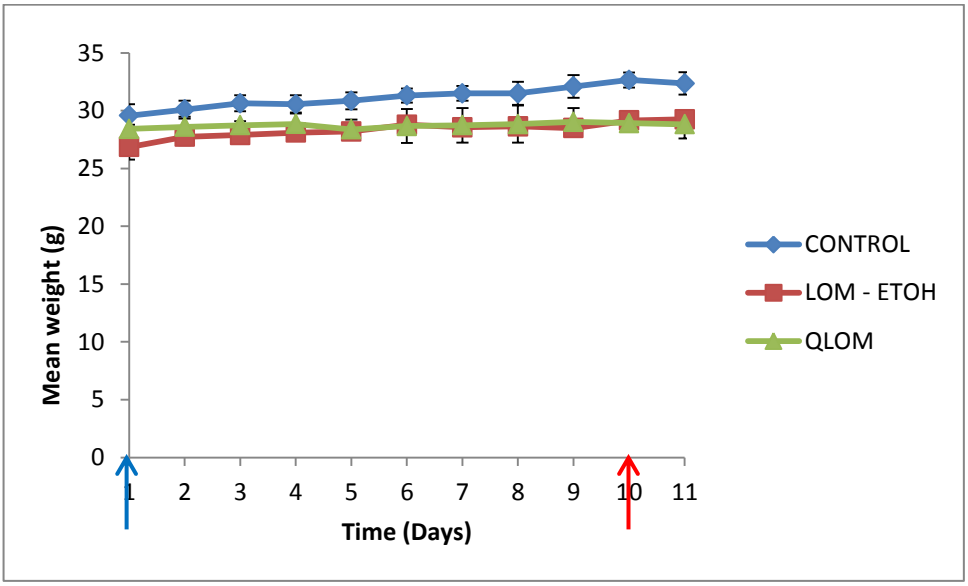

B

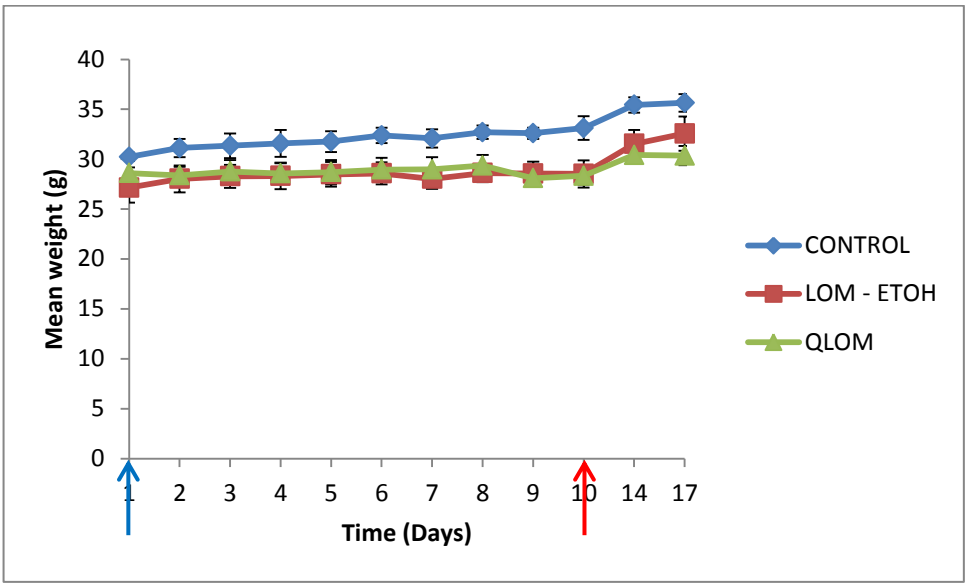
Mean weight (g)
0
5
10
15
20
25
30
35
40
1
2
3
4
5
6
7
8
9
10
14
17
Time (Days)
CONTROL
LOM - ETOH
QLOM

C

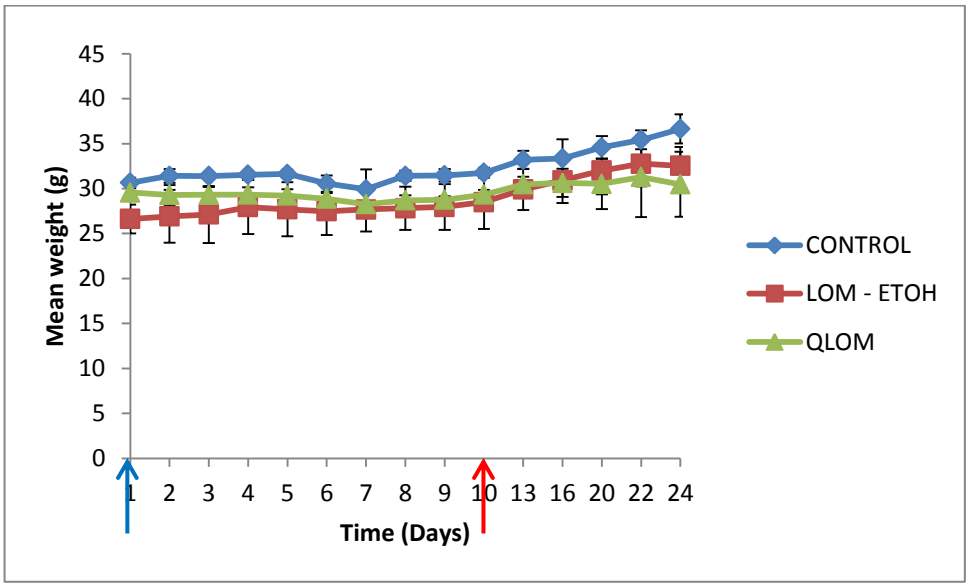
Mean weight (g)
0
5
10
15
20
25
30
35
40
45
1
2
3
4
5
6
7
8
9
10
13
16
20
22
24
Time (Days)
CONTROL
LOM - ETOH
QLOM

D

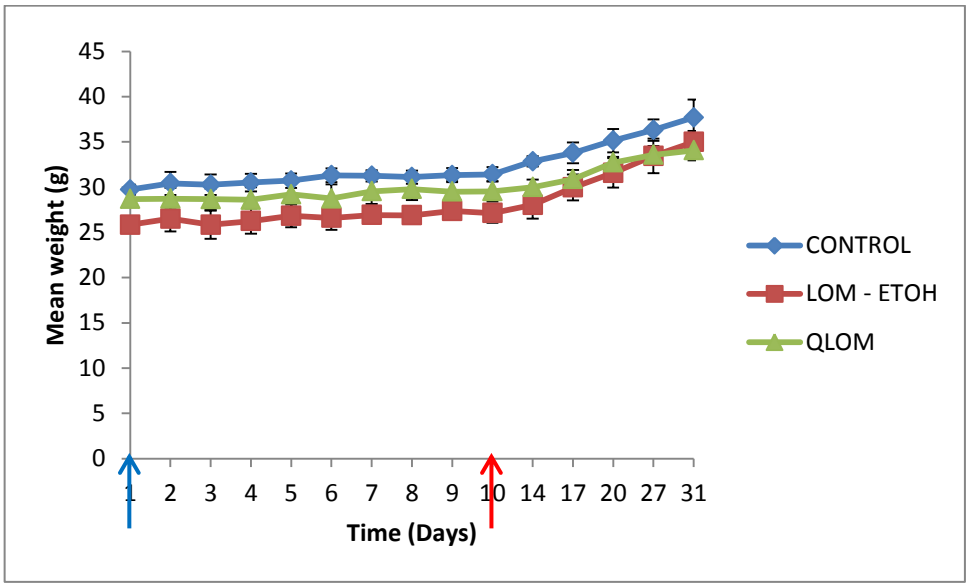

E

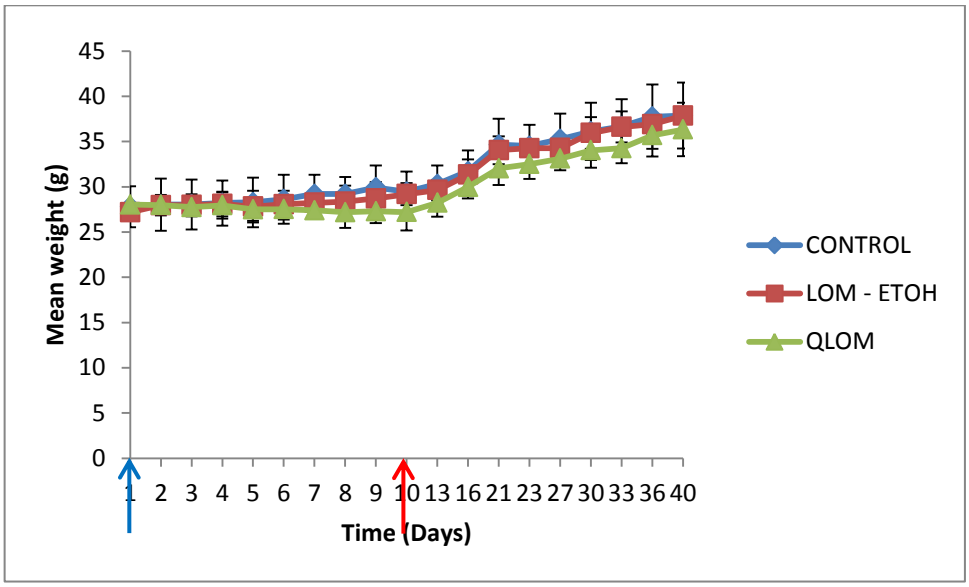

Figure 3-1: Weight measurement for animals culled for analysis of blood samples at A: Day 1; B: Day 7; C: Day 14; D: Day 21 and E: Day 30 after completion of 10 consecutive daily doses of lomustine formulations

Key: Blue arrow: Treatment start date; **Red Arrow:** Treatment end date. Weights were recorded from commencement of dosing until mice were culled for collection of blood samples for analysis. Days 1, 7, 14, 21 and 30 correspond to number of days following completion of 10 consecutive daily doses of lomustine formulations.

3.3.2 **Analysis of blood samples using the haemocytometer**

Analysis of blood samples after completion of 10 consecutive daily doses for lomustine formulations treated and untreated control animals for full blood cell counts revealed no effect of either the higher dose (13 mg kg^{-1}) nanoparticle lomustine formulation or the low dose (1.2 mg kg^{-1}) ethanolic formulation of lomustine on the white blood cell counts of treated animals (Figure 3-2 A).

A

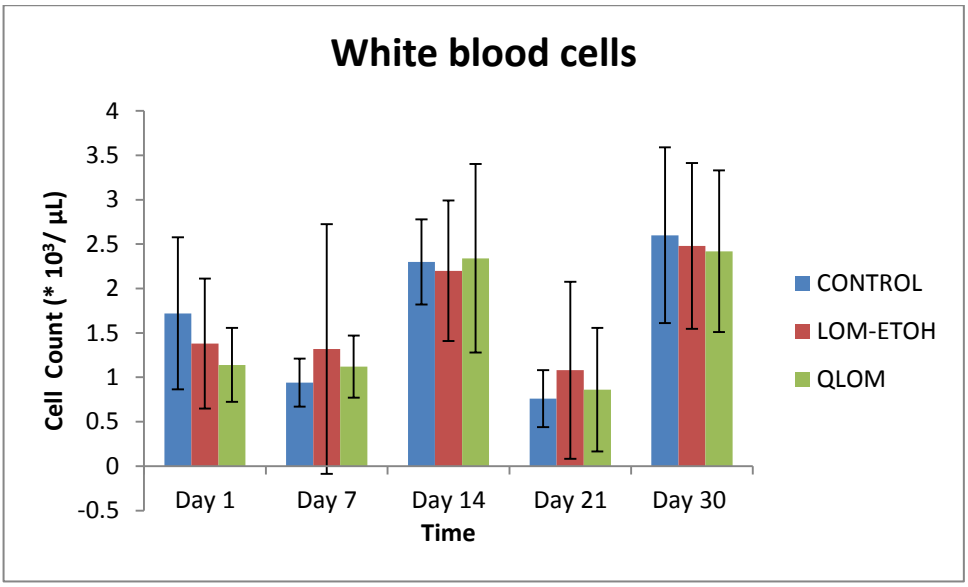

B

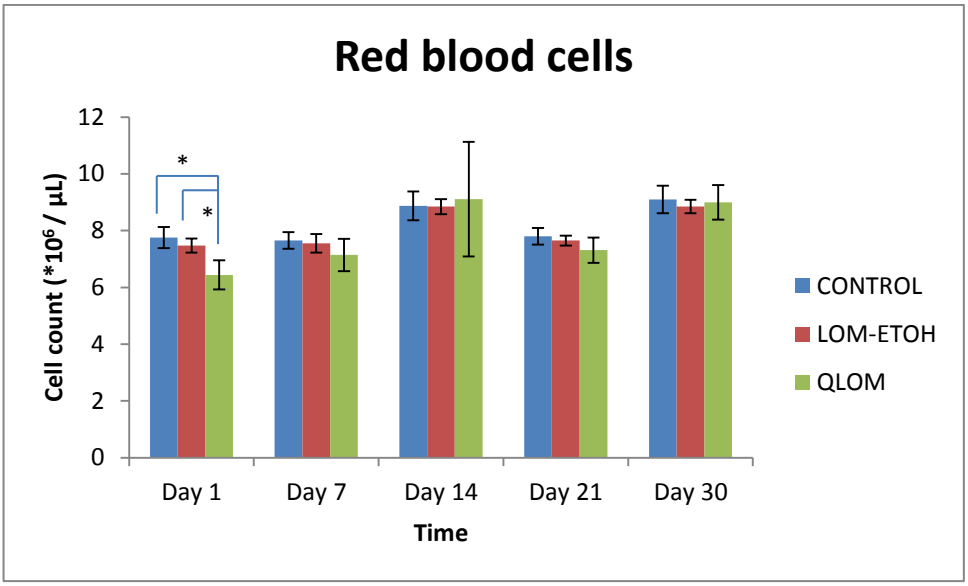
Red blood cells
Cell count (*10⁶ / µL)
12
10
8
6
4
2
0
*
*
Day 1
Day 7
Day 14
Day 21
Day 30
Time
CONTROL
LOM-ETOH
QLOM

C

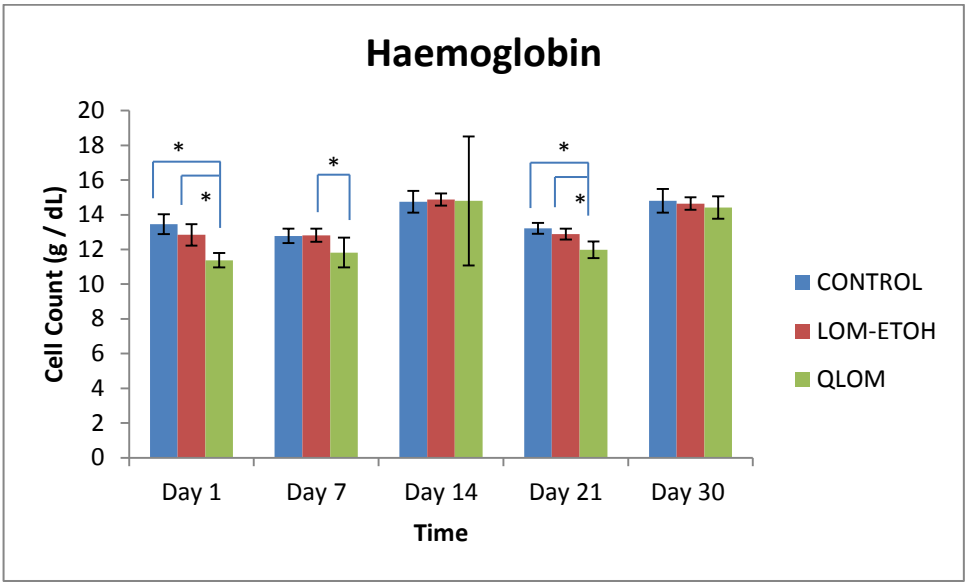
Haemoglobin
Cell Count (g / dL)
20
18
16
14
12
10
8
6
4
2
0
*
*
*
*
Day 1
Day 7
Day 14
Day 21
Day 30
Time
CONTROL
LOM-ETOH
QLOM

D

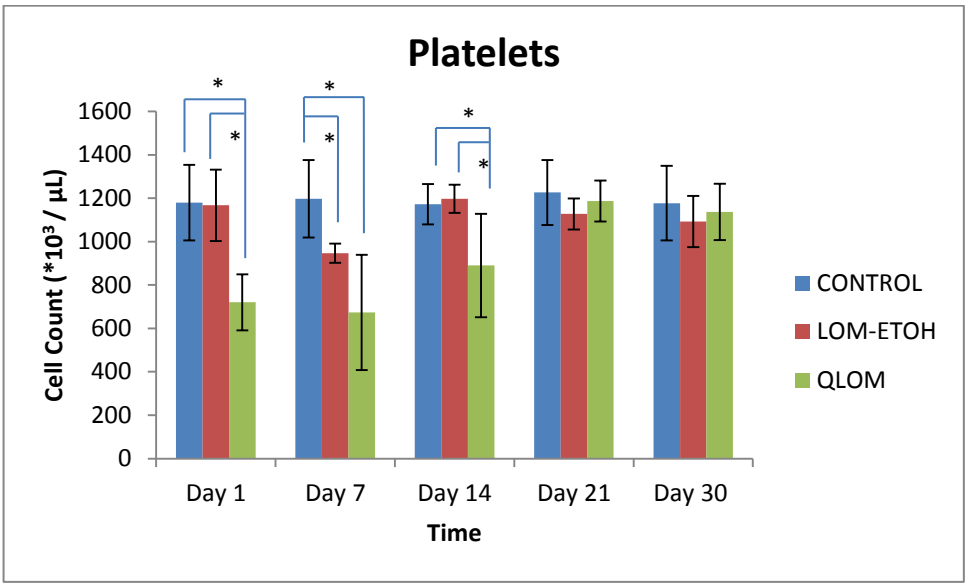

Figure 3-2: Full blood count parameters for treated (lomustine formulations) and control (untreated) animals

Days 1, 7, 14, 21 and 30 correspond to number of days following completion of 10 consecutive daily doses of lomustine formulations.

Key: *: Significantly different $p < 0.05$ (One-way ANOVA with Tukey post hoc test)

Conversely, there was a transient drop in the red blood cell counts of animals that received the high dose nanoparticle formulation which had recovered by day 7. However, there was a persistent drop in haemoglobin levels for animals in this treatment group and recovery was confirmed after 21 days (Figure 3-2 C).

Also, there was a reduction in platelet counts for both high dose (13 mg kg^{-1}) nanoparticle formulation and low dose (1.2mg kg^{-1}) ethanolic formulation treated groups of animals. The low dose formulation treated animals recovered after 7 days while the high dose formulation treated animals recovered after 14 days (Figure 3-2 D).

3.3.3 **Analysis of blood samples by flow cytometry**

Flow cytometry analysis of blood samples for determination of the counts for different cell populations in the whole blood of the treated and untreated animals revealed no effect of either formulation on the leucocyte and erythrocyte counts of the animals. On the other hand, the high dose formulation treated animals experienced a transient drop in their platelet counts which had recovered by Day 7 (Figure 3-3 C).

A

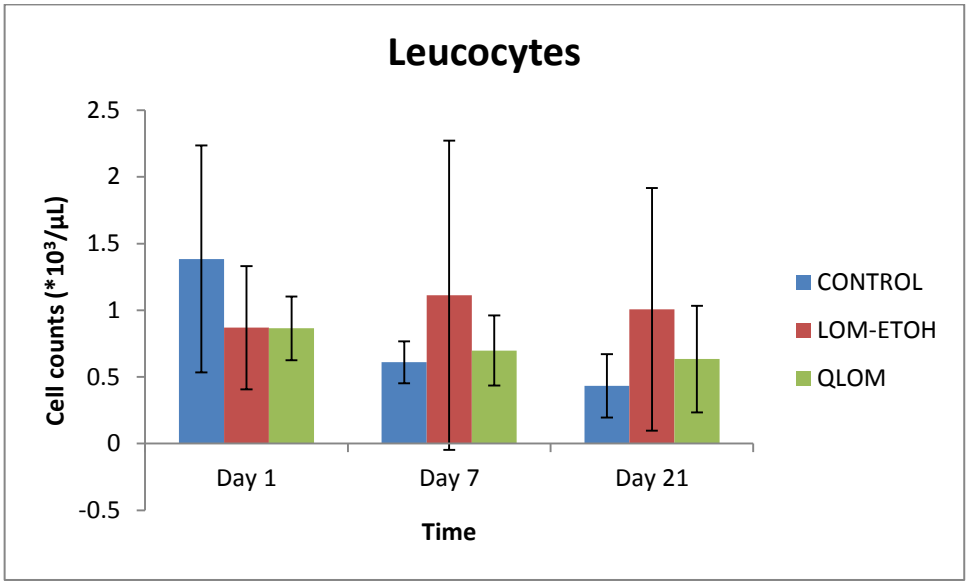

B

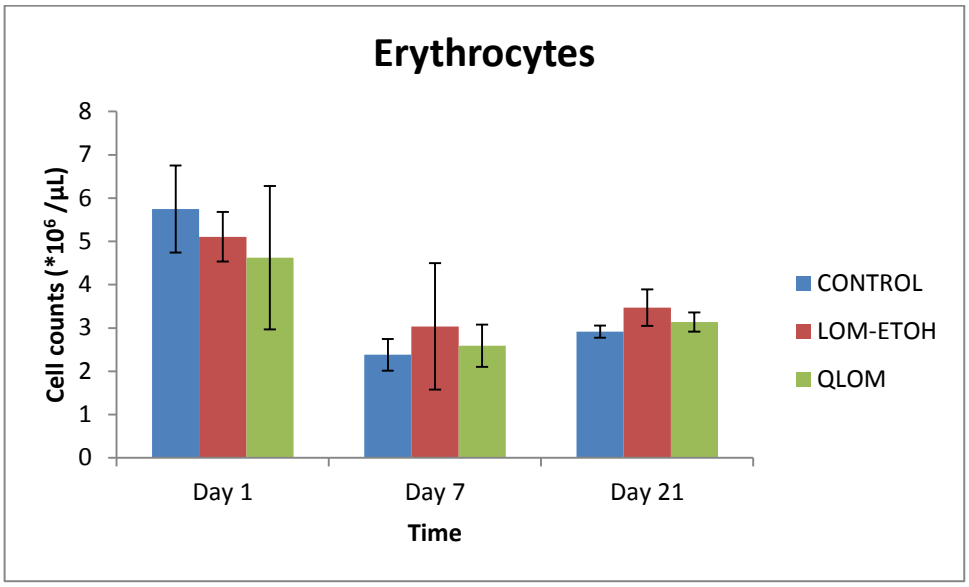

C

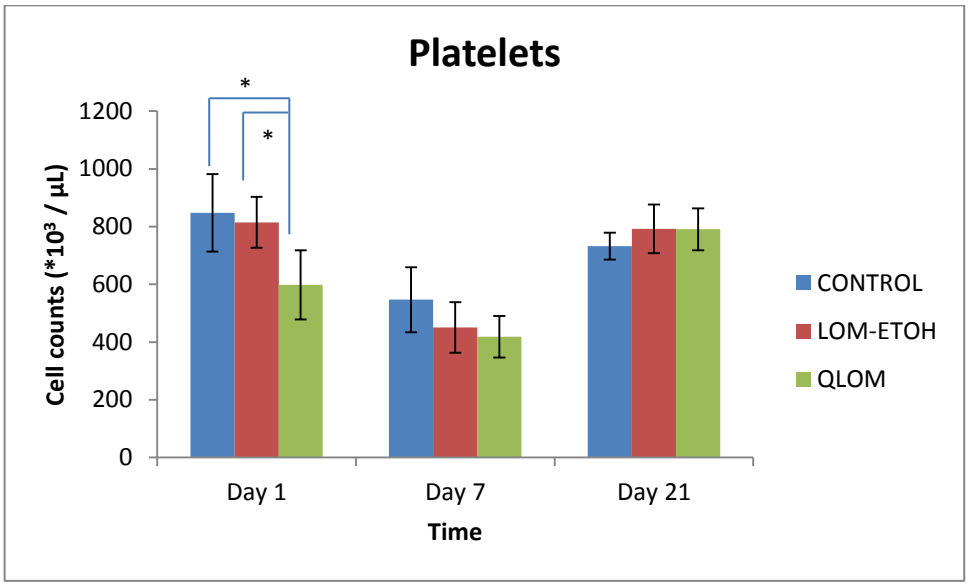

Figure 3-3: Blood cell counts for determination of leucocytes, erythrocytes and platelets counts for treated (lomustine formulations) and control (untreated) animals using a flow cytometer

Days 1, 7, and 21 correspond to number of days following completion of 10 consecutive daily doses of lomustine formulations.

Key: ∗ : Significantly different $p < 0.05$ (One-way ANOVA with Tukey post hoc test).

3.3.4 Evaluation of uptake of Nile red loaded nanoparticles in macrophage (J774A.1) cell line

3.3.4.1 Preparation and characterisation of Nile red loaded nanoparticles

3.3.4.1.1 Determination of Nile red content of nanoparticles

The calibration curve for Nile red fluorescence intensity versus concentration yielded a straight line with the equation y = 247.18x + 3.348 (R^2 = 0.9991). This calibration curve was used to determine the concentration of Nile red encapsulated within the nanoparticles prepared (Figure 3-4)

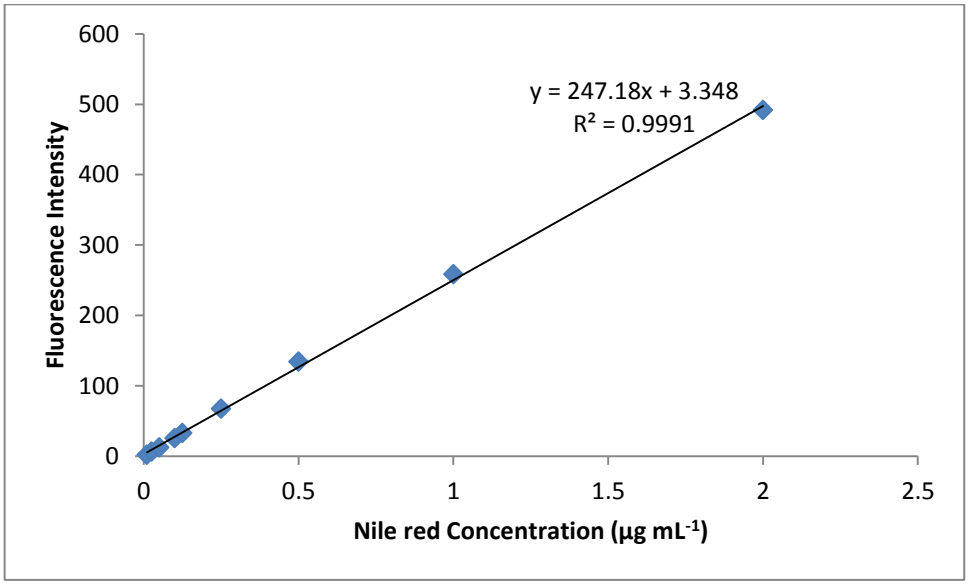

Figure 3-4: Calibration curve for Nile red

3.3.4.1.2 Determination of particle size for Nile red loaded nanoparticles

TEM images for GCPQ NR formulations showed nanoparticles in the size range 100 – 370 nm in diameter (Figure 3-5)

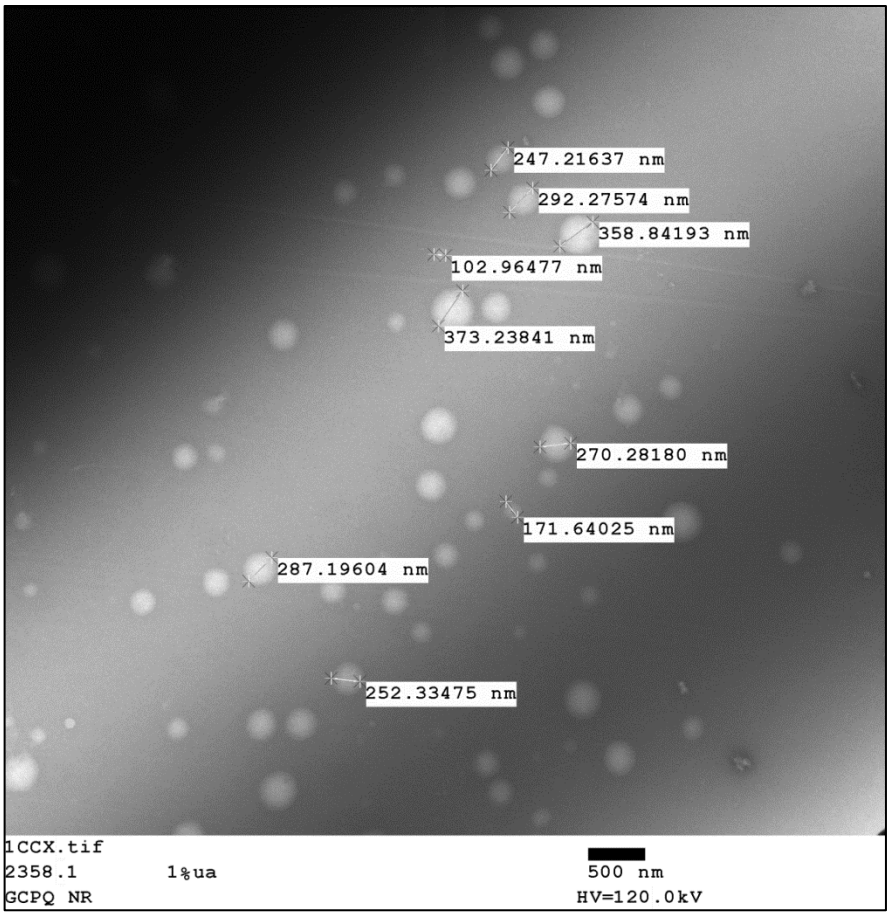

Figure 3-5: TEM micrograph for GCPQ NR formulation

Nile red (50 µg mL^{-1}) with GCPQ (1 mg mL^{-1}) in 5 % $^{w}/_{v}$ dextrose solution, vortexed for 30 seconds, then probe sonicated (QSonica, Connecticut, USA) on ice for 30 minutes at amplitude 25. Particle size measurements are as generated by the AMT digital camera software.

Particle size measurements by DLS yielded an average size of 211.6 nm with polydispersity index of 0.6 (Figure 3-6 A – C).

A

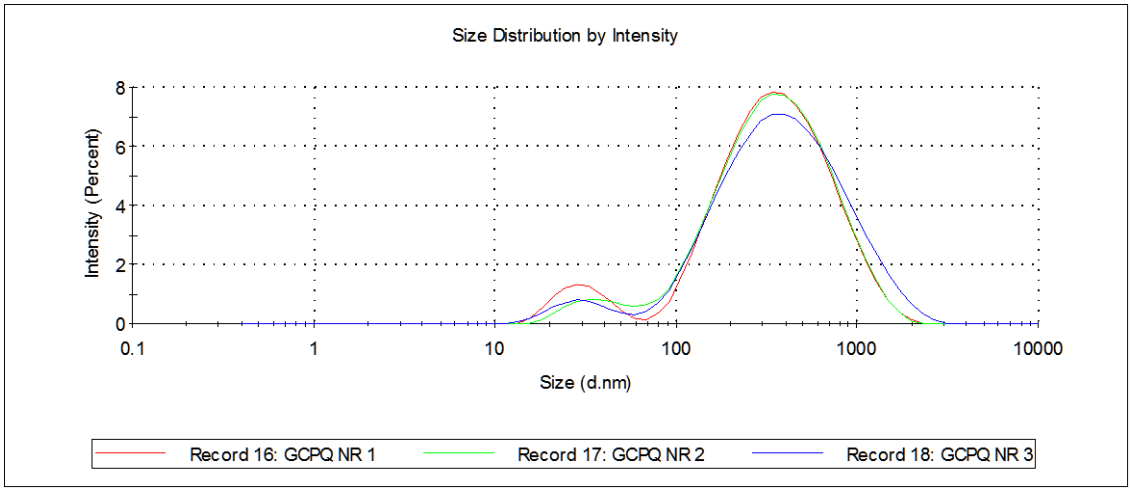

B

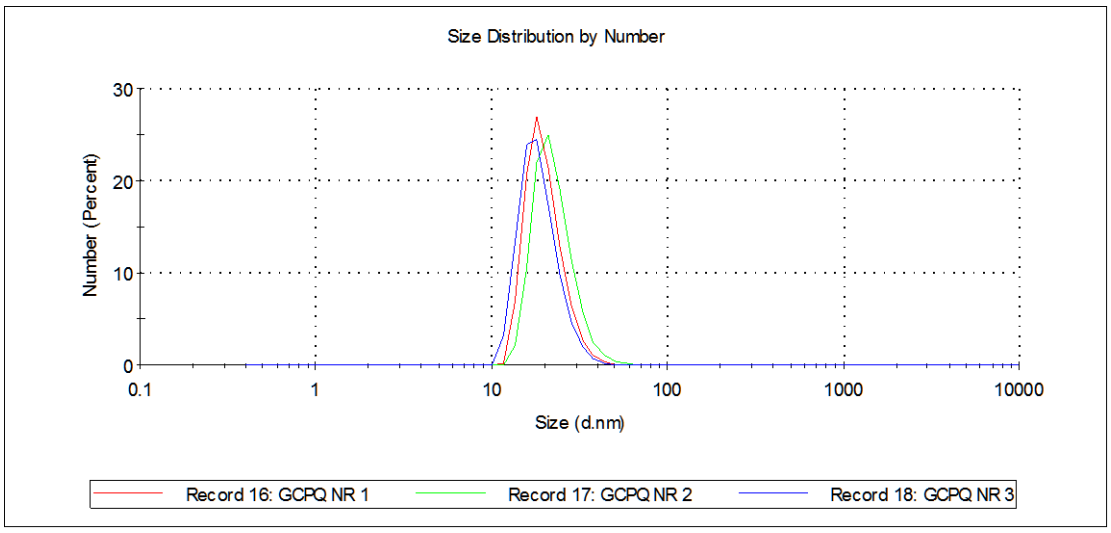

C

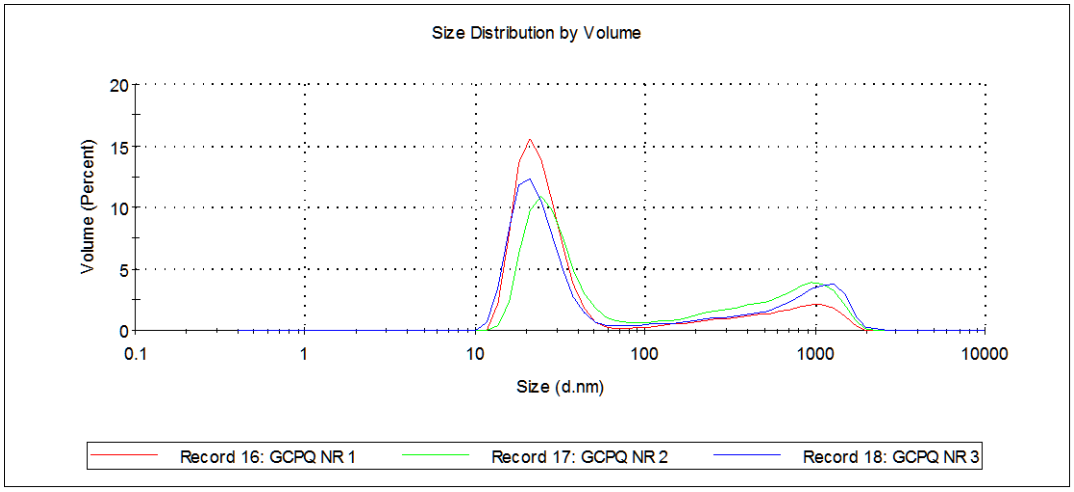

Figure 3-6: DLS graphs showing particle size distribution for GCPQ NR by A: intensity; B: number; C: volume

Nile red (50 µg mL^{-1}) with GCPQ (1 mg mL^{-1}) in 5 % w/v dextrose solution, vortexed for 30seconds, then probe sonicated (QSonica, Connecticut, USA) on ice for 30 minutes at amplitude 25.

TEM micrograph for Liposome NR formulations on the other hand revealed particles of 51.5 – 147.5 nm in diameter (Figure 3-7).

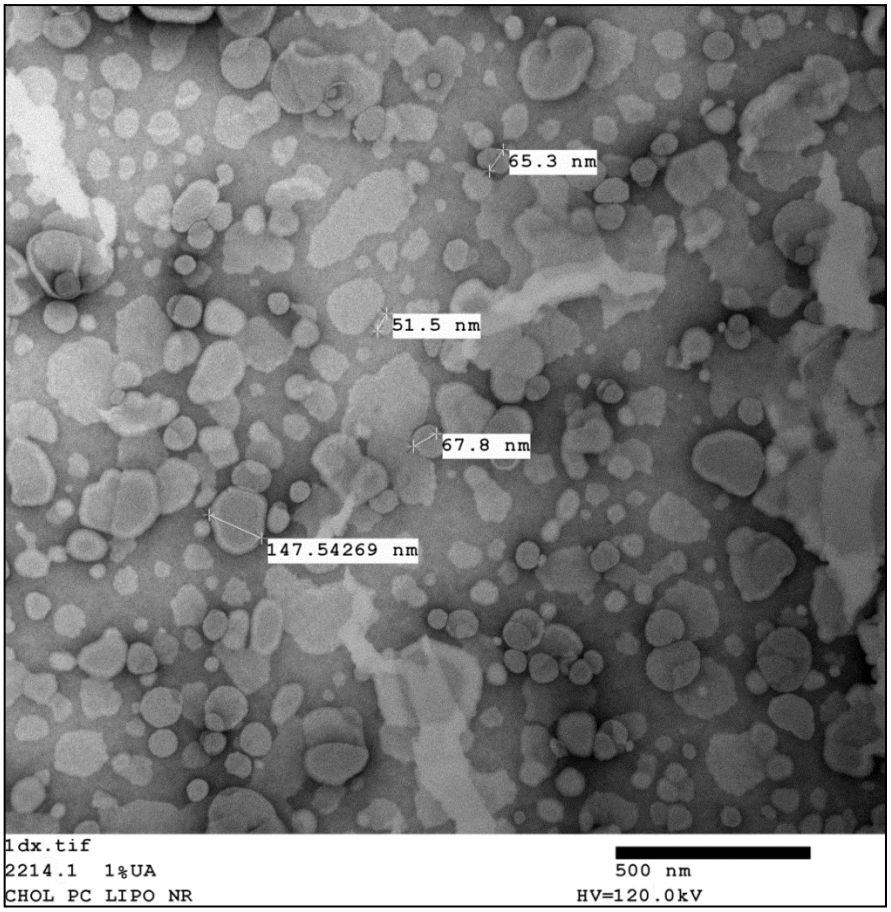

Figure 3-7: TEM micrograph for Liposome NR formulation

Nile red (50 µg mL^{-1}) with egg phosphatidylcholine (3 mg mL^{-1}) and cholesterol (1.4 mg mL^{-1}) in 5 % w/v dextrose solution. Probe sonicated (QSonica, Connecticut, USA) on ice for 15 minutes at amplitude 25 after liposome preparation. Particle size measurements are as generated by the AMT digital camera software.

DLS size measurements for this formulation revealed an average size of 160.5 nm with polydispersity index of 0.2 (Figure 3-8 A – C).

A

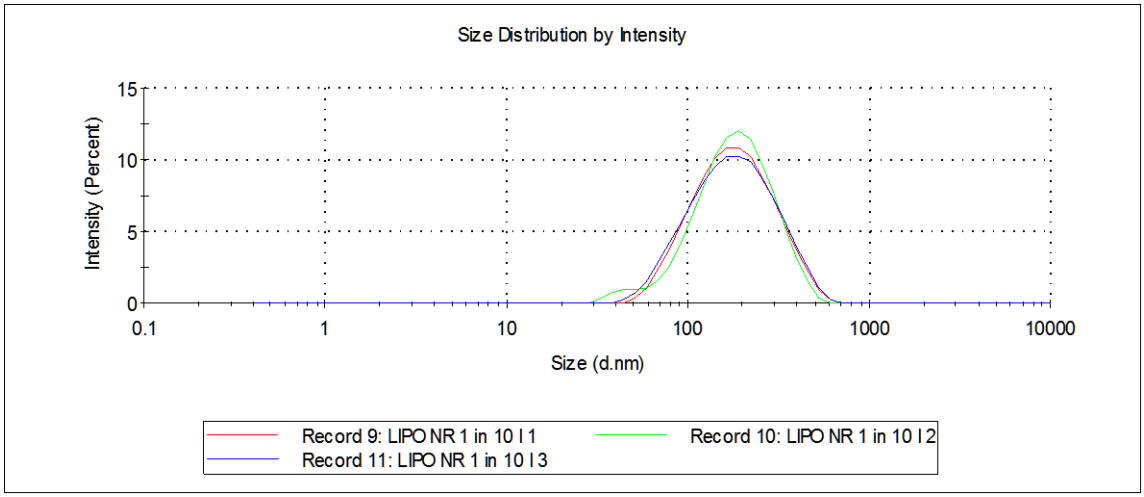

B

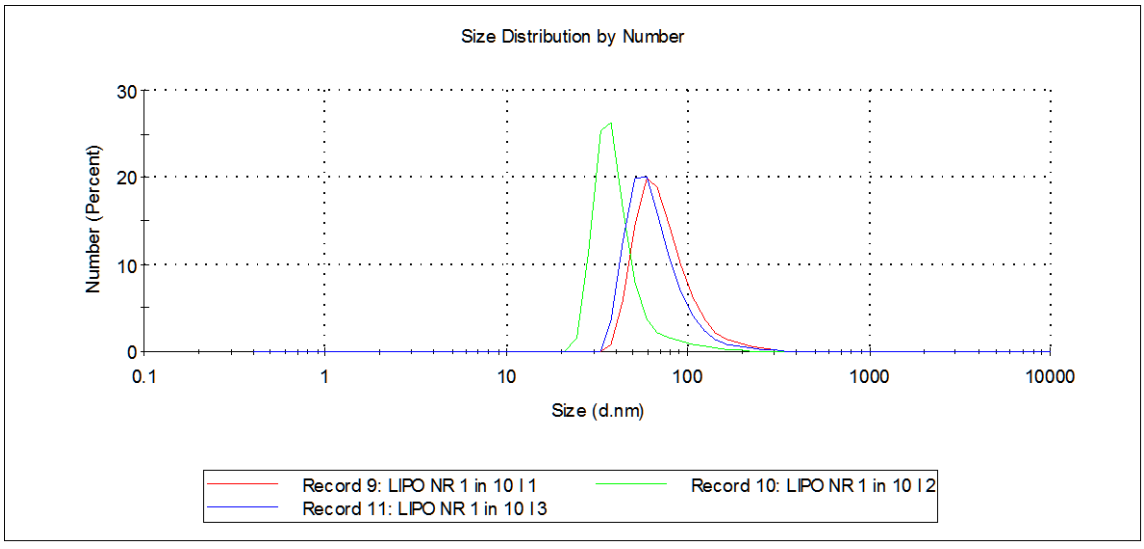

C

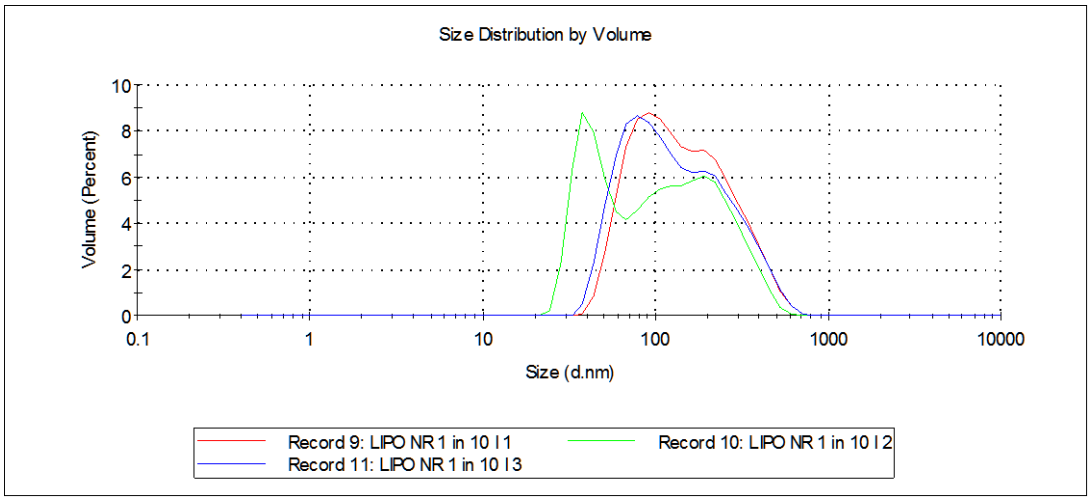

Figure 3-8: DLS graphs showing particle size distribution for Liposome NR by A: intensity; B: number; C: volume

Nile red (50 µg mL^{-1}) with egg phosphatidylcholine (3 mg mL^{-1}) and cholesterol (1.4 mg mL^{-1}) in 5 % w/v dextrose solution. Probe sonicated (QSonica, Connecticut, USA) on ice for 15 minutes at amplitude 25 after liposome preparation.

3.3.4.2 Evaluation of uptake of Nile red loaded nanoparticles in J774A.1 cell line by flow cytometry

Analysis of the uptake of Nile red loaded nanoparticles in macrophage cell line revealed a more rapid uptake of the liposome formulation (Liposome NR) than the GCPQ formulation (Figure 3-9).

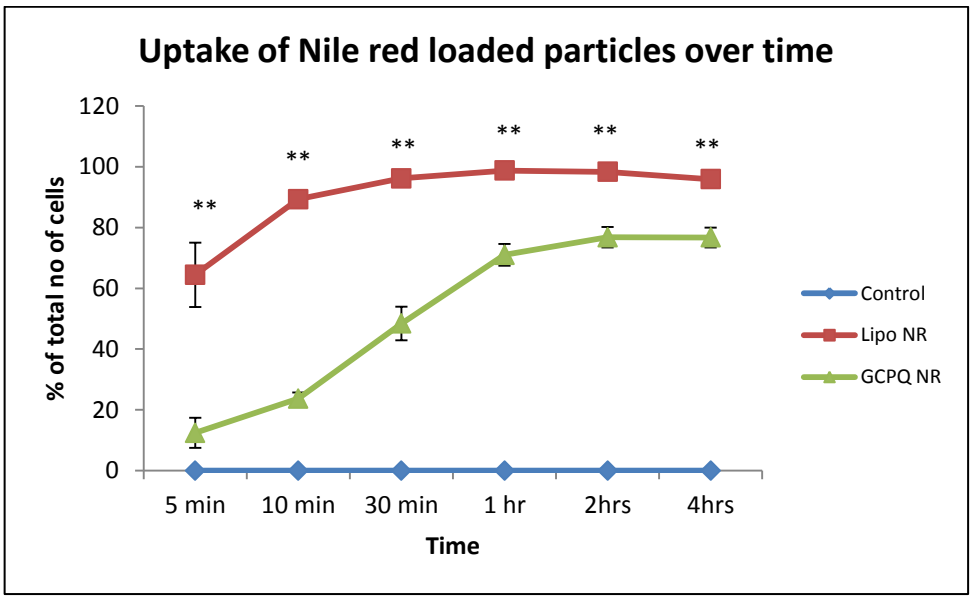

Figure 3-9: Flow cytometry analysis of the uptake of GCPQ NR and Liposome NR in J774A.1 cells over time

[Nile red (50 µg mL^{-1}) with GCPQ (1 mg mL^{-1}) in 5 % w/v dextrose solution, vortexed for 30seconds, then probe sonicated (QSonica, Connecticut, USA) on ice for 30 minutes at amplitude 25] and Liposome NR [Nile red (50 µg mL^{-1}) with egg phosphatidylcholine (3 mg mL^{-1}) and cholesterol (1.4 mg mL^{-1}) in 5 % w/v dextrose solution. Probe sonicated (QSonica, Connecticut, USA) on ice for 15 minutes at amplitude 25 after liposome preparation] particles in J774A.1 cells over time.

Key: **: Significantly different from Nile red loaded GCPQ particles $p < 0.01$ (One-way ANOVA with Tukey post hoc test).

Time	Control (n = 4)		Liposome NR (n = 4)		GCPQ NR (n = 4)	
	Mean (%)	Standard deviation	Mean (%)	Standard deviation	Mean (%)	Standard deviation
5 mins	0.01	0.01	64.46	10.58	12.41	4.96
10 mins	0	0	89.34	2.71	23.70	2.00
30 mins	0.01	0.01	96.15	1.82	48.40	5.55
1 hr	0	0	98.72	0.47	70.99	3.59
2 hrs	0	0	98.31	0.93	76.76	3.38
4 hrs	0	0	95.92	1.65	76.73	3.28

Table 3-1: Uptake of GCPQ NR and Liposome NR in J774A.1 cells over time

3.3.4.3 Assessment of the uptake of Nile red loaded nanoparticles in J774A. 1 cell line by confocal microscopy imaging

Confocal microscopy images in time lapse experiments for both GCPQ NR and Liposome NR treated cells showed intracellular location of the nanoparticles from the earliest time point in which images were captured (Figure 3-10).

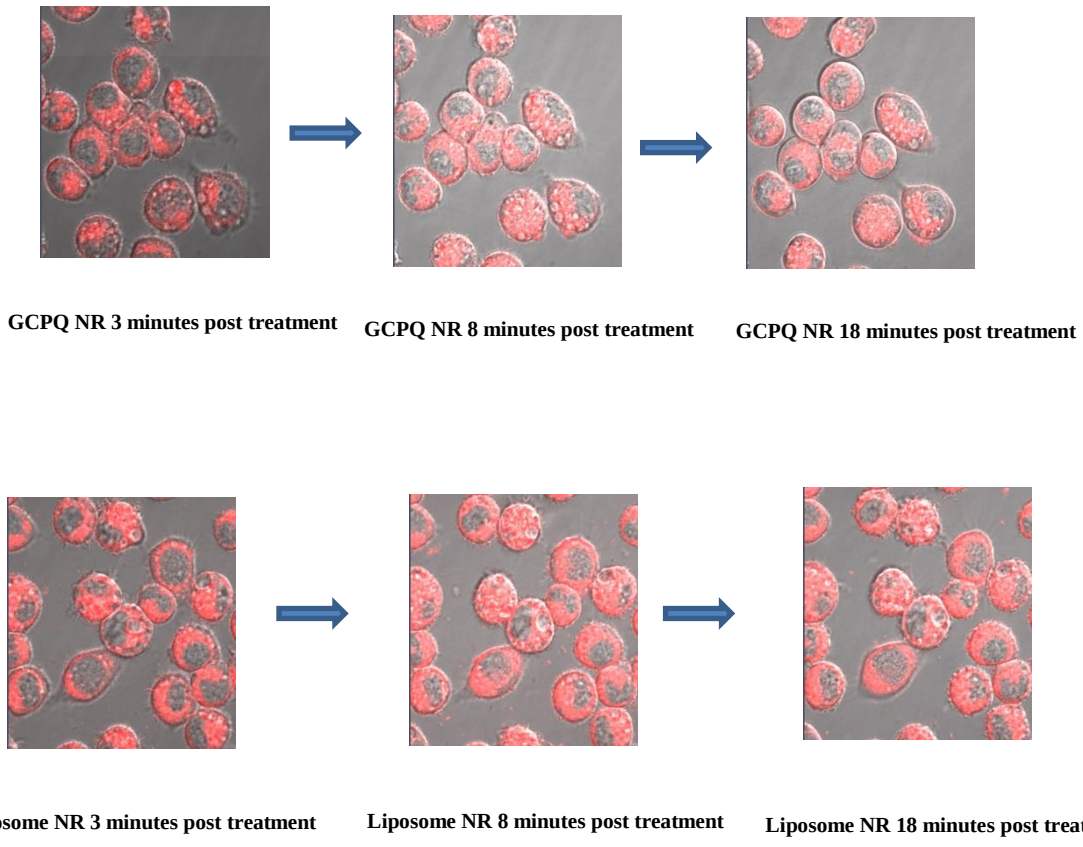

Figure 3-10: Confocal microscopy images showing uptake of GCPQ NR and Liposome NR in J774A.1 cells over time

3.4 Discussion and conclusions

Chemotherapy induced myelosuppression represents a great limitation to the extent of potentially beneficial dose intensification with most clinically used cytotoxic agents (Tolcher et al. 2003; Su et al. 2005; Tosoni et al. 2006; Gerber et al. 2007) although increasing the dose intensity leads to an increase in response rates (Boesen et al. 1994; Crawford et al. 2004).

In this study, the effect of continuous exposure to high dose chemotherapy with GCPQ based nanomedicine formulation of lomustine on the haemopoietic system was evaluated. Due to the myelosuppressive effects of lomustine, chemotherapy with the drug is usually associated with rest periods to allow for recovery of patients haematological parameters (Cianfriglia et al. 1980; van den Bent et al. 1998; van den Bent et al. 2006; Jakacki et al. 1998).

All doses were administered as scheduled without the need for dosing delays or reduction throughout the study. The animals were monitored for any signs of ill health or weight loss throughout the period of study. Weight measurements revealed that the high dose (13 mg kg^{-1}) nanomedicine formulation was well tolerated by the animals that received this formulation (Figure 3-1). An excessive weight loss (≥ 15 % of initial body weight; severity limit for the study) would have been an indication of toxicity and would have necessitated dosing delay or outright disruption, as weight loss is a side effect of lomustine therapy (van den Bent et al. 2003). Thus the animals that received the nanomedicine formulation administered at a dose 10 times higher than the ethanolic formulation did not manifest gross toxic effects compared to the latter.

Analysis of blood samples for determination of blood cell counts using an automated clinical haemocytometer showed no effect of either the low dose or high dose formulations on the white blood cells of treated animals (Figure 3-2 A). Thus, administration of a high dose of lomustine using the nanomedicine formulation in a continuous daily dosing regimen did not induce a suppression of the white blood cells in the treated animals. This is could be of clinical significance as neutropenia has been considered to be the commonest and most important toxicity arising from chemotherapy with cytotoxic agents (Dale 2002; Crawford et al. 2004). Neutropenia is usually the first haematologic toxicity to arise from cytotoxic chemotherapy due to the short (6 – 14 hours) life span of granulocytes (Nathan 1987). Neutropenia is of great clinical importance as it poses the risk of predisposing patients to infections which may lead to sepsis which may be potentially fatal (Lyman et al. 1998; Dale 2002).

The platelets are the next cell type to be affected after the granulocytes due to their life span of 7 – 10 days in humans (4 – 5 days in mice). This is reflected in the current study as haemocytometer cell counts showed that all animals in both the low and high dose treatment groups experienced a significant reduction in their platelet counts compared to untreated controls at Day 7 following completion of the dosing regimen (Figure 3-2 D). The platelet counts on this day represent the nadir for both treatment groups. Although the high dose treatment group had a lower nadir value than the low dose group, there was no significant difference between the platelet counts for both groups. The platelet counts for the low dose group had recovered by day 14, while for the high dose group the counts were recovered by day 21 (Figure 3-2 D). Reduced platelet counts are of clinical significance as chemotherapy induced thrombocytopenia leads to an increase in the risk of bleeding complications which may necessitate treatment delays or dose reductions. It also leads to the need for platelet transfusions and hospitalisation (Gerber et al. 2007; Intile et al. 2009; Hitron et al. 2011; McMahon and Kwaan 2012).

Toxic effects of chemotherapy on red blood cells are the last to be observed owing to their relatively longer life span of 100 – 120 days (Smaaland et al. 2002). In this study, there was a transient drop in red blood cell counts in animals that received the high dose nanoparticle formulation with a recovery by day 7 after dosing had been completed (Figure 3-2 B). On the other hand, there was a persistent drop in haemoglobin levels of this group of animals with recovery after 21 days (Figure 3-2 C). Haemoglobin synthesis (in red blood cells) begins at an early stage in the formation and differentiation of the red blood cells and by the time they leave the bone marrow (as reticulocytes), they continue to form only minute quantities of haemoglobin for one or two days until they become matured red blood cells. Thus red blood cells at maturation are already carrying their maximum haemoglobin content (Hall 2011). Therefore, since the red blood cell counts were recovered by day 7 (Figure 3-2 B), the persistent drop in haemoglobin counts recorded may not necessarily be clinically significant. Moreover, the haemoglobin levels were at least 90 % of the cell counts recorded for the control animals by day 7 and onwards after dosing had been completed.

On the other hand, analysis of blood cell counts by flow cytometry using cell type specific antibodies showed a significant drop in the platelet counts of high dose formulation treated animals only on Day 1 (Figure 3-3 C) while both leucocyte and erythrocyte counts were unaffected. Although the platelet counts seemed not to be fully recovered by day 7, there was no statistical difference in the platelet counts in this group compared to the low dose group ($p = 0.541$) and the untreated controls ($p = 0.065$). This may be an indication of a quicker recovery of these cell counts than have been reflected by counts determined using the clinical haemocytometer. However, further studies are required to confirm this.

Nitrosoureas including lomustine are known to produce cumulative and delayed myelosuppression, producing nadir counts later than most other cytotoxic agents (Pratt et al. 1994; Jakacki et al. 1998; Smaaland et al. 2002). This study has demonstrated an alteration in the expected pattern of myelosuppression with lomustine. The animals were seen to recover from the myelosuppressive effects of the high dose nanomedicine formulation rather than experience delayed effects as would be expected from a conventional formulation of the drug. This is demonstrated in weight measurements (Figure 3-1 A – E) and the data obtained by analysis of the haematologic parameters (Figure 3-2 A – D). For instance, mice in the later time points (Days 14 – 30) would be expected to experience progressive weight loss and lower blood cell counts than those in the earlier time points due to delayed myelosuppression. On the contrary, in both sets of mice treated with the high dose (13 mg kg^{-1}) nanomedicine and the low dose (1.2 mg kg^{-1}) ethanolic formulation, there was no indication of increasing myelosuppressive effects of the drug (lomustine). The mice showed an increase in their body weights (Figure 3-1 A – E; Appendix I A – E) and recovery of blood cell counts (Figure 3-2 A – D) with time after dosing had been completed.

Furthermore, cellular uptake of Nile red loaded nanoparticles was studied in J774A.1 (murine macrophage cell line) cells. The uptake of GCPQ nanoparticles using GCPQ NR in the J774A.1 cells was studied as a surrogate for the pattern of uptake of the nanoparticles in vivo by macrophages. The uptake of GCPQ NR nanoparticles by J774A.1 cells was compared to that of Nile red loaded liposome nanoparticles (Liposome NR). Liposomes are one of the most widely studied carriers for targeted delivery of materials to macrophages (Ahsan et al. 2002). Therefore, Liposome NR was a suitable nanoparticle system for comparison with GCPQ NR.

Flow cytometry analysis of the uptake of Nile red loaded nanoparticles reveal a more rapid uptake of Liposome NR than the GCPQ NR formulations. At the earliest time (5 min) point recorded, the cell uptake of the liposome particles was greater than 60 % of the total number of cells. This is in contrast to GCPQ particles for which there was only 12 % uptake at the same time point. At 10 minutes post treatment, uptake of liposome particles was already greater than 80 % and had become saturated (96.88 %) after 30 minutes. For GCPQ particles on the other hand, uptake after 30 mins was just approaching 50 % and even after 4 hours was just getting to 80 % (Figure 3-9).

Confocal microscopy images (Figure 3-10) confirmed the cytoplasmic localisation of the Nile red loaded particles. Semi-quantitative assessment of fluorescence intensity in the cells by ImageJ (Windows) software was done in an attempt to determine a time-based increase in nanoparticle uptake by the cells. The analysis showed an initial increase in the calculated mean intensity in the early time points (3 minutes to 8 minutes) for both GCPQ NR and Liposome NR.

Subsequently, there was no further increase as later time points showed a decrease rather than an increase in the fluorescence intensity (Appendix II A, B). This may be attributed to quenching of the fluorescence of the dye or bleaching due to the exposure of the samples to the laser. Moreover, images captured at the later time points showed less fluorescence (reduced brightness) than the earlier images (Appendix III A, B). However, this analysis is interpreted with caution as the current experiment was not specifically set up to do this semi-quantitative analysis. Therefore, although the confocal microscopy images did not show a time-based increase in nanoparticle uptake, they confirmed that the fluorescence signal measured by flow cytometry was due to nanoparticles that had been taken up into the cells.

J774A.1 cells exhibit many properties of macrophage cells (Fernando et al. 2010) and thus permit the study of the uptake of nanoparticles by macrophages (Fernando et al. 2010; Missirlis and Hubbell 2010).

In a study, the in vitro uptake of amphiphilic (polymeric) hydrogel nanoparticles formulated from PEG and Pluronic® F127 was investigated. Flow cytometry data showed a time (and dose) dependent increase of fluorescence in the J774A.1 cells, which could be correlated with nanoparticle association over time. Also, the uptake of the fluorescently (fluorescein) labelled amphiphilic hydrogel nanoparticles by J774A.1 cells was compared to that of commercial anionic Fluospheres® of similar average size. Uptake of the amphiphilic hydrogel nanoparticles was greatly reduced compared to that of the commercial anionic Fluospheres®. After 4 hours of incubation of nanoparticles with J774A.1 cells, fluorescence measurements in buffered cell lysates revealed a 50-fold higher association of the commercial anionic Fluospheres® with the cells compared to the amphiphilic hydrogel nanoparticles (Missirlis and Hubbell 2010).

Macrophages abound in many tissues including the Kupffer cells of the liver, bone marrow, brain, lungs, spleen, and guts and are involved in the uptake and subsequent clearance of nanoparticles from systemic circulation (Leu et al. 1984; Moghimi et al. 2001; Chellata et al. 2005; Owens and Peppas 2006).

Haematopoietic stem cells (HSCs), which produce all the necessary cells for replenishing the blood and immune systems are known to reside in the bone marrow which is the preferred site for haematopoiesis in adults (Chow et al. 2011; Winkler et al. 2010). The functions of the HSCs is maintained under strictly controlled processes to sustain a constant number of the different blood cell types (red blood cells, leukocytes and platelets) in the circulation (Winkler et al. 2010). Macrophages have been identified as a constituent part of the haematopoietic microenvironment (Mori et al. 1990). In particular, macrophages play an important role in erythropoiesis as they are have been found to form part of the erythroblastic islands, which are specialised microenvironments where mammalian erythrocytes proliferate and differentiate. Erythroblastic islands comprise a central ("nurse") macrophage surrounded by erythroblasts at different stages of maturation. The erythroblasts are connected to the central macrophage through cytoplasmic protrusions from the macrophage and the cell interaction at the erythroblastic island is crucial for both early and late stages of erythroid maturation (Manwani et al. 2008).

Also, some recent studies have demonstrated the significance of bone marrow macrophages in the haemostasis of red blood cells (Chow et al. 2013; Ramos et al. 2013). In their studies, both groups of workers (separately) depleted macrophages (CD 169^{+}) in adult mice.

The data from both groups showed that macrophage depletion in the steady state did not produce significant anaemia. However, both studies reported that in the presence of anaemia, macrophage depleted mice showed delayed haematocrit recovery and reticulocytosis compared to mice that did not have macrophage depletion (Chow et al. 2013; Ramos et al. 2013). Also, the studies by Chow and co-workers showed that sustained (3 – 4 weeks) macrophage depletion in the steady state resulted in decreased serum iron concentration, transferrin saturation, mean corpuscular haemoglobin and reticulocyte haemoglobin content. Their studies also showed that depletion of the macrophages was accompanied by delayed recovery of erythroblast and peripheral erythrocyte following challenge with a myeloablative agent (5-fluorouracil) (Chow et al. 2013). In addition, Ramos and co-workers showed that there was reduced erythroid expansion in the bone marrow and spleen after phlebotomy in macrophage depleted mice, compared to controls. Based on their studies, they reiterated that although iron is crucial in sustaining stress erythropoiesis, the pathways triggered by macrophages are quantitatively important in the erythropoietic response after phlebotomy-induced anaemia (Ramos et al. 2013).

Furthermore, bone marrow macrophages have been shown to be involved in maintaining the HSC niche. A study by Mori and co-workers had previously shown that some bone marrow resident macrophages stained positively for anti-Forssman glycosphingolipid antibody which is known to be positive for resident macrophages of hematopoietic foci and negative for monocytes, peritoneal macrophages, Kupffer cells and macrophages derived from granulocyte-macrophage colony forming cells. Based on their findings, they suggested that bone marrow resident macrophages may have a role in haematopoiesis (Mori et al. 1990).

Also, more recent studies have implicated bone marrow macrophages in promoting the retention of HSCs through interaction with some Nestin expressing cells in the niche (Chow et al. 2011), and depletion of bone marrow macrophages was found to result in mobilisation of HSCs into the blood (Winkler et al. 2010; Chow et al. 2011).

The pattern of uptake of GCPQ nanoparticles by macrophage cells has not been previously reported. Thus, this in vitro study elucidated the fate of GCPQ nanoparticles when exposed to macrophage cells, which could be an indication of what would be expected upon in vivo administration of GCPQ nanoparticles. The most clinically important dose limiting toxicity for cytotoxic drugs including lomustine is myelosuppression involving bone marrow cells which is known to be populated by macrophages. Therefore, the relatively low toxicity observed following administration of the high dose lomustine (13 mg kg^{-1}) nanoparticle formulation in may be due to the low and slow uptake of the formulation by the bone marrow.

The work by Chow et al. (2013) showed that following myeloablative therapy in the presence of macrophage depletion, there was delayed recovery of peripheral erythrocytes and decreased reticulocyte haemoglobin content. In this study, it was observed that there was a persistent drop in the haemoglobin levels of mice that were treated with the high dose nanomedicine (Q-LOM) formulation, with recovery after 21 days (Figure 3-2 C). This would have suggested that the slow recovery of the haemoglobin levels was possibly an effect of the drug formulation on the bone marrow macrophages of the treated mice, leading to additional toxic effects on the haemoglobin of the treated mice. However, the red blood cells of the treated mice were recovered by day 7 after dosing was completed (Figure 3-2 B). Also, the haemoglobin levels recorded at all the time points were at least 90 % of the levels recorded for untreated control mice. Taken together, these points reinforce the possibility that the observed drop in haemoglobin levels may not be clinically significant.

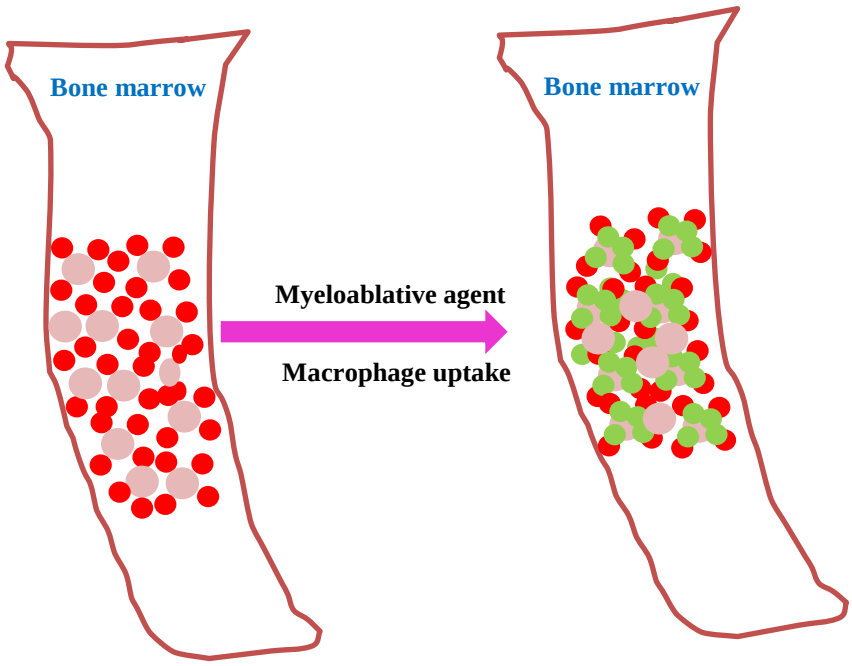

Figure 3-11: Schematic showing macrophage uptake resulting in blood cells exposure to myeloablative agent

Key:

Blood cell

Macrophage

Myeloablative agent

In addition, it has been previously shown that chloroethylnitrosoureas with glucose carriers produced reduced myelosuppressive effects; particularly, they did not produce significant depression in peripheral neutrophil count in mice when administered at an LD_{10} dose (Anderson et al. 1975; Panasci et al. 1977). Thus, the presence of the sugar moieties in the GCPQ backbone may also have contributed to the relatively low myelosuppressive effects of the high dose nanoparticle formulation of lomustine employed in this study. Moreover, it has been previously shown (Lalatsa et al. 2012a) in the distribution kinetics of GCPQ nanoparticles following intravenous administration that the particles do not accumulate to an appreciable extent in the liver and spleen and were not detected in the lungs and heart. This distribution pattern exhibited by GCPQ nanoparticles suggests that GCPQ particles (Lalatsa et al. 2012a) unlike other particulate systems and other polymeric nanoparticles like liposomes seem to avoid the reticuloendothelial system (Moghimi et al. 2001; Vauther et al. 2003).

Thus, the results of this study indicates that the administration of the cytotoxic drug lomustine using a GCPQ nanoparticle based formulation leads to a reduction in the myelosuppressive effects of the drug by changing the mode of tissue or organ distribution of this drug. This has permitted the administration of the drug at a much higher dose in a continuous manner. This is potentially beneficial for the administration of the drug in a dose intense manner which would lead to greater therapeutic benefits while avoiding a commensurate increase in toxic effects.

Chapter 4 Synthesis and Characterisation of Self-assembling Peptide Amphiphiles

4.1 Introduction

The optimal therapy of glioblastoma as well as other intracranial neoplasia is still very much an enigma as there still exixts a great need for the development of more effective therapeutic agents (Chamberlain 2010; Agarwal et al. 2011a; Raizer 2011; Malmström et al. 2012). A number of small molecule therapeutics has been clinically employed in the chemotherapy of brain tumours with varying degrees of sucess. However, their usefulness is greatly limited by their myelosuppressive side effects (Carey 2003; Chamberlain 2010). Also, in spite of tremendous research efforts up till the present time, which has resulted in a better understanding of the molecular basis of glioblastoma, as well as the discovery and introduction of various targeted therapies, advancement is far from rapid (Olar and Adalpe 2014). Thus, this leaves a lot to be desired as far as a cure or even optimal management is concerned. In light of this, it is imperative to exploit all possible avenues for the development of novel therapies aimed at the effective treatment of glioblastoma and other intracranial tumours.

Therefore, this chapter is aimed at the development of peptide-based molecules as potential candidates for application in the delivery of therapeutic molecules to the brain for the treatment of intracranial tumours. This aim will be achieved through the synthesis and characterisation of three self-assembling peptide amphiphiles (PAs). Two of these PAs were designed to be potential drug delivery systems for anti-glioma agents. The third PA is an analogue of a therapeutic peptide designed as a potential bio-therapeutic agent for the treatment of intracranial tumours.

4.2 Peptides and proteins

Peptides are molecules comprising amino acids covalently linked through the formation of an amide bond and may vary in size from 2 amino acids (dipeptide) to high molecular weight proteins (Pardridge 1991; Audie and Boyd 2010) containing up to 100 or more amino acid residues, termed polypeptides (Koolman and Roehm 2005). The term peptide is usually applied to molecules comprising 50 amino acid residues or less (Sato et al. 2006; Watt 2006; McGregor 2008; van der Walle and Olejnik 2011) while larger molecules are referred to as proteins (van der Walle and Olejnik 2011). However, there is no unanimous agreement on the definition of terms for the two categories as there are borderline molecules such as insulin (51 amino acid residues) which is usually regarded as a peptide but is referred to as a protein by others (van der Walle and Olejnik 2011).

Peptides and proteins have been implicated in many pathological conditions including but not limited to those of the central nervous system. For instance, insulin resistance resulting from defective expression and dysfunctions in insulin signalling pathways is implicated in type 2 diabetes and cardiovascular disease (Sasso et al. 2004; Neeland et al. 2012; Henriksen and Prasannarong 2013). Similarly, the β-amyloid polypeptide with diphenylalanine peptide as the core recognition motif is implicated in the pathologies of neurological diseases such as Alzheimer's disease and transmissible spongiform encephalopathies (TSEs) (Harper and Lansbury 1997; Zhang 2003; Adler-Abramovich et al. 2006).

It is particularly striking that short peptide sequence domains (active site) within protein systems such as enzymes are responsible for performing their biological functions (Lucchese et al. 2007).

4.3 Peptides and proteins drugs (Bio-pharmaceuticals)

Peptides and proteins have been employed as therapeutics from the 1920s forward with the approval of insulin, thyroid hormone and factor VIII (Lee 1991; van der Walle and Olejnik 2011), and they remain promising target molecules for the treatment and management of many pathological conditions (Audie and Boyd 2010; van der Walle and Olejnik 2011).

Peptide and protein drugs, categorised as bio-pharmaceuticals or biological drugs (Watt 2006; Antosova et al. 2009) may emerge as the back bone of therapy for diseases previously regarded as pharmaceutically untreatable by conventional methods (Johnson-Léger et al. 2006; Watt 2006) such as chronic renal failure, dwarfism and infertility for which successful management using protein therapeutics have now been achieved (Johnson-Léger et al. 2006).

The most frequently commercialised of this class of therapeutics includes insulin for the treatment of diabetes, therapeutic vaccines for anti-hepatitis A and/or B immunisation, growth hormones and monoclonal antibodies for anticancer and autoimmune diseases therapy (Johnson-Léger et al. 2006; Walsh 2006) with monoclonal antibodies making up half of the molecules in development (Johnson-Léger et al. 2006).

4.3.1 **Peptides as bio-pharmaceuticals**

Peptides possess some unique advantages compared to antibodies and other proteins as well as small molecule therapeutics. Advantages of peptide drugs compared to small molecules include: ability to disrupt protein – protein interactions; frequently highly potent receptor agonists and they may overcome the undruggable targets barrier; higher target selectivity, specificity and affinity; minimal systemic toxicity since their degradation products are amino acids; they do not usually accumulate in tissues due to their short half-life, thus reducing the risk of complications arising from their metabolites (Loffet 2002; Ladner et al. 2004; Hummel et al. 2006; Sato et al. 2006; McGregor 2008; Vlieghe et al. 2010).

Peptides also offer certain advantages relative to proteins such as antibodies including: activity of small peptides will normally depend on the functional groups of constituent amino acids whereas for proteins their activity will also depend on the maintenance of specific 3-D structures (van der Walle and Olejnik 2011); smaller size which permits better tissue or tumour penetration; lower immunogenicity; higher activity per unit mass (15 – 60 fold) compared to proteins and antibodies; higher stability (room temperature storage for long periods is acceptable); lower royalty stack than antibodies; and lower production cost since they can be synthesised chemically rather than expressed by recombinant technology (Graff and Wittrup 2003; Ladner et al. 2004; Sato et al. 2006; McGregor 2008; Vlieghe et al. 2010).

4.4 Self-assembly

Self-assembly is a free energy–driven process involving the organisation of components into well-defined, organized, and functional patterns or structures at multiple length scales, as a consequence of specific and local non covalent molecular interactions with little or no external intervention (Zhang and Altman 1999; Rajagopal and Schneider 2004; Whitesides and Grzybowski 2002; Lehn 2002; Ayres et al. 2010; Cui et al. 2010; Stupp and Palmer 2014). Self-assembly is a practical solution for fabricating a wide range of nanostructures (Service 2005), and is also simple in application, thus it holds great promise in the construction of nano-sized materials (Palmer and Stupp 2008; Palmer et al. 2007; Cui et al. 2010).

Self-assembly in aqueous medium is driven by weak intermolecular forces like hydrophobic interactions, van der Waals bonds, electrostatic interactions, hydrogen and coordination bonding (Cui et al. 2010; Whitesides 2002; Zhang 2003; Stendahl et al. 2006). Even though each of the various interactions mediating self-assembly is weak in isolation, if there are an adequate number of these interactions in operation, they can produce remarkably stable structures (Cavalli et al. 2010).

4.4.1 Peptide based nanostructures

Peptides have been identified as excellent starting materials for the design of self-assembling nanostructures for a number of reasons namely: they are biocompatible and biodegradable; their structures are relatively simple compared to other bio molecules such as proteins and nucleic acids; they can be synthesized quite easily on a large scale; they offer a great level of versatility in chemical and biological modifications; (Zhang 2002; Cui et al. 2010; Colombo et al. 2007). In addition, the capability of peptides for adopting specific secondary structures creates a distinct opportunity for the design of structurally controllable nanomaterials (Cui et al. 2010).

A certain class of peptides, β-sheet forming peptides exhibits an intriguing capability to assemble into one dimensional (1D) nanostructures through the formation of intermolecular hydrogen bonds (Hartgerink et al. 2001), which can interact further to bring about the formation of higher order (3D) networks. The biodegradable feature of peptides can be further exploited for building bioactive hydrogels that can mimic the native extracellular matrix (ECM) both structurally and functionally by the incorporation of specific amino acid sequences or by controlling their self-assembly (Cui et al. 2010).

4.4.1.1 Self-assembling peptides

Zhang and co-workers serendipitously discovered a novel class of self-assembling peptides which comprise alternating hydrophilic and hydrophobic amino acid residues (ionic self-complementary) within the same peptide molecule. They found that the self–complementary peptide $(Ala\text{-}Glu\text{-}Ala\text{-}Glu\text{-}Ala\text{-}Lys\text{-}Ala\text{-}Lys)_2$ (EAK16) from a region of alternating hydrophobic and hydrophilic residues in zuotin (a yeast protein that had been previously identified for its ability to bind preferentially to left-handed Z-DNA), forms very stable β-sheet structures in water and spontaneously assemble to form stable macroscopic membranes in the presence of monovalent salts and serum (Zhang et al. 1993).

A second class of self-assembling peptides comprising a broad class of peptide amphiphiles (PAs) was developed by the Stupp laboratory. These PAs typically consist of an alkyl chain which is attached to a short peptide sequence capable of forming intermolecular hydrogen bonding and which drives self-assembly into nanofibers through the formation of β-sheets.

These PAs also possess a region of charged amino acids for enhanced solubility in water and for the design of pH and salt-responsive nanostructures and networks. In addition, these PAs possess a fourth portion which is used for the presentation of bioactive signals, usually through epitopes that can interact with cells or proteins (Hartgerink et al. 2001; Palmer et al. 2007; Palmer and Stupp 2008; Webber et al. 2009; Webber et al. 2011). These PAs combine the structural features of amphiphilic surfactants with the functions of bioactive peptides. These PAs self-assemble into high-aspect-ratio nanofibers under specific solution conditions such as pH, ionic strength and temperature (Cui et al. 2010).

Furthermore, another class of self-assembling PAs has been shown to self-assemble into high axial ratio nanofibres. This class of PAs was described recently by Mazza and co-workers. Their work showed that a PA comprising only a β-sheet forming short peptide sequence covalently linked to an alkyl chain was able to self-assemble into high axial ratio nanofibres in aqueous solution. In this class of PAs, the β-sheet forming peptide region also serves as the active epitope (Mazza et al. 2013).

4.4.1.1.1 Peptide amphiphiles

Peptide amphiphiles (PAs) comprise the class of the most commonly studied self-assembled nanofibers (Ayres et al. 2010). Peptides that form β-sheets are able to assemble into nanofibres through intermolecular hydrogen bonding. Further interaction of these nanofibres can in turn lead to formation of three-dimensional networks (Beniash et al. 2005; Webber et al. 2009; Cui et al. 2010). These peptide based nanostructures are amenable to the design of bioactive hydrogels that can mimic the structure and function of the native ECM due to their biodegradability and tunability for incorporation of specific amino acid sequences and control over their self-assembled structures (Cui et al. 2010).

4.4.1.1.1.1 Mechanism of PA self-assembly

Self-assembly of PAs in aqueous medium is governed by forces that arise from energy contributions including: hydrophobic interaction of the alkyl tails; hydrogen bonding among the β-sheet forming peptide segments, both of which favour aggregation of the PA molecules; and electrostatic repulsion between charged amino acid residues which does not favour aggregation. Thus, the assembly can be controlled by factors such as the amino acid sequence, concentration of the peptide, pH of the solution, temperature, ionic strength and nature of the solvent (Fung et al. 2008; Cui et al. 2010). Consequently, the final structure and properties of the assembled material such as size, shape and interfacial curvature depends on a balance of the contributing (attractive and repulsive) forces (Cui et al. 2010; Paramonov et al. 2006).

Tsonchev and co-workers have demonstrated that self-assembly of a class of PAs into cylindrical micelles rather than spherical micelles which would have been the energetically favoured shape if the assembly were driven only by hydrophobic interactions as previously thought (Tsonchev et. al. 2003; Paramonov et al. 2006) is as a result of the electrostatic interactions of the PA headgroups. Their work revealed that a unique directional electrostatic attraction occurs between the PA headgroups contrary to the expected repulsive interactions. This electrostatic attraction prevails over hydrophobic attraction of the alkyl tail resulting in the formation of cylindrical micelles.

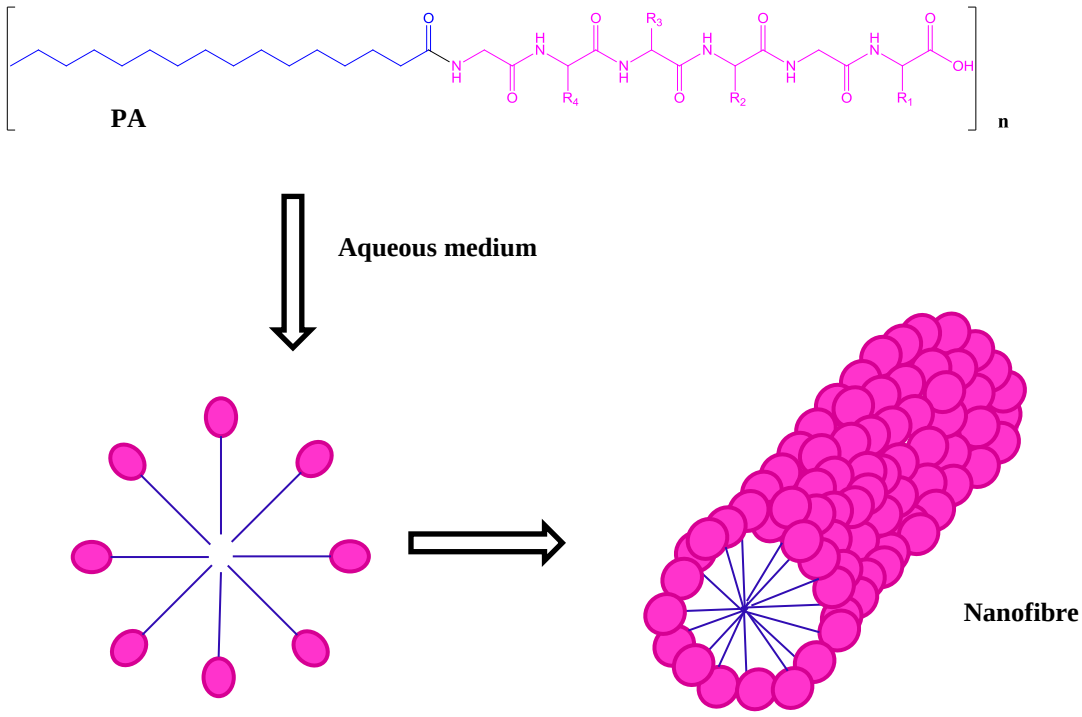

Figure 4-1: Schematic depicting self-assembly of PA in aqueous medium

Key:

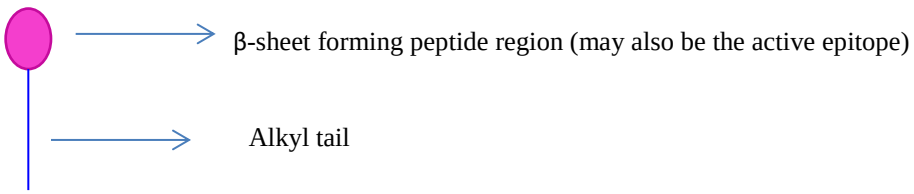

They considered a PA possessing an arginine residue and a phosphate group in the PA molecule. At pH values of about 3, the headgroup exists as an amphiphilic zwitterion in which the carboxylic acid is neutralized, the arginine is positively charged and the phosphate group is negatively charged. As a result, the headgroup bears a net charge of zero, but the two charges present create a large dipole that is approximately perpendicular to the backbone of the molecule. This creates the platform for attractive interactions between the hydrophilic headgroups in the self-assembly (Tsonchev et al. 2004).

Also, Velichko and co-workers in their simulation study showed that in a system comprising both hydrophobic interactions and hydrogen bonding (such as in a PA), phase behaviour and assembly mechanisms would depend on the strength of intermolecular bonding. In these systems, although the critical micelle temperature (CMT) is the most important parameter, formation of hydrogen bonds by the peptide blocks leads to significant changes in the phase behaviour. Hydrogen bonding below the CMT leads to the formation of β-sheets with large size polydispersity. The connection of amphiphilic molecules into β-sheets leads to an increase in the local concentration of hydrophobic units. Consequently, there is strengthening of the hydrophobic interaction between β-sheets, and rolls or stacks of β-sheets are formed. Formation of hydrogen bond above the CMT leads to changes in the micellar structure with formation of β-sheets randomly distributed in the entire micellar corona. With an increase in hydrogen bonding energy however, the spherical symmetry becomes unstable leading to the formation of cylindrical fibres with the β-sheets aligned parallel to the fibre axis (Velichko et al. 2008).

Furthermore, Paramonov and co-workers (2006) have demonstrated that hydrogen bonding by the four amino acids closest to the core of the nanofibre is crucial in the formation of elongated cylindrical nanostructures. Interruption of hydrogen bonding in this part of the PA molecule would lead to a loss of ability to form the elongated cylindrical structures and spherical structures would be preferentially formed.

In addition, simulation studies on a self-assembling PA developed by Mazza and co-workers showed that PAs comprised only of a β-sheet forming short peptide sequence and an alkyl chain would also preferentially assemble into nanofibres. Their work revealed that in this kind of PA, the peptide backbone wraps around and lines the exterior of the fibre, while the alkyl chains form the hydrophobic core of the nanofibre. The alkyl chains lie perpendicular to the long axis of the fibre, pointing towards the centre of the nanofibre (Mazza et al. 2013). Thus, their work showed a pattern of arrangement uniquely different from the conventional cylindrical micelle-like structure previously reported (Hartgerink et al. 2001) to be the characteristic pattern of arrangement of self-assembling PAs (Mazza et al. 2013).

Hence, assembly of PAs to cylindrical nanofibers in aqueous solution is a product of the combined effects of hydrophobic collapse of the alkyl tails and tendency for hydrogen bonding among the β-sheet forming peptide segment (Cui et al. 2010). Hydrophobic collapse leads to aggregation of the alkyl tails away from the aqueous media and packing in the centre of the micelle leaving the peptide segments exposed to the aqueous environment. The peptide segments in turn form intermolecular hydrogen bonds parallel to the long axis of the fibre (Webber et al. 2009; Paramanov et al. 2006; Hartgerink et al. 2001). The driving force for self-assembly may also be enhanced by intermolecular contact of the side chains of adjacent hydrophobic amino acids through close association of the hydrophobic side chains (Beniash et al. 2005).

4.4.1.1.1.2 Applications of PAs

Self-assembled PA nanofibers have potential applications in tissue engineering, material sciences, molecular electronics, molecular medicine and drug delivery (Colombo et al. 2006) and this has been demonstrated by various workers.

Hartgerink and co-workers used pH-induced self-assembly of a PA to make nanostructure scaffold similar to ECM. The PA was designed to permit reversible cross-linking through intermolecular disulfide bridge formation to increase chemical robustness of the fibre. The resulting cross-linked fibres can direct mineralization of hydroxyapatite (HA) to form a composite material with the same alignment as that found between collagen fibrils and HA crystals in bone (Hartgerink et al. 2001).

Guler and co-workers in their study demonstrated the encapsulation of pyrene, a small hydrophobic molecule, within the cores of self-assembling PAs. Encapsulation and aggregation of pyrene within the hydrophobic cores was demonstrated by the formation of pyrene excimers using fluorescence spectrofluorometry. Excimer formation was found to be more efficient in cylindrical nanofibre forming PAs covalently functionalized with pyrene linked to the hydrophobic cores but was less efficient in similar molecules that assembled into spherical aggregates. This was thought to be as a result of the formation of well-organized nanofibers, which may enable closely packed, geometrically organized pyrene segments leading to an increased local concentration of pyrene within the nanofibers. The spherical (micelle-like) supramolecular aggregates however, would provide a liquid-like environment for the pyrene rather than the well-ordered β-sheet structures found in the nanofibers.

Moreover, excimer formation requires direct contact between two pyrene units, thus the extent and rate of excimer formation would reflect the internal dynamics of the macromolecule to which the pyrene moieties are covalently attached (Duhamel 2012). This study indicates that encapsulation can lead to solubilisation of hydrophobic drugs such as pyrene in the core of nanostructures creating the possibility of combining encapsulation of hydrophobic drugs with presentation of bioactive epitopes for targeted drug delivery (Guler et al. 2005).

Beniash and co-workers have demonstrated the use of PA nanofibers in cell transplantation and tissue engineering. They developed PA molecules that can assemble into robust nanostructured networks when added to synthetic physiological fluids or cell culture media in the presence of polyvalent metal ions. Self-assembly of the PA can entrap cells suspended in the fluid in the nanofibre matrix, and the cells survive, proliferate, and internalize the fibres, suggesting they may be utilizing the PA molecules in their metabolic processes (Beniash et al. 2005).

Nagai and co-workers have reported the potential for self-assembling peptide nanofibers based on an ionic self- complementary peptide sequence to provide controlled release kinetics. They demonstrated this using diffusion property in hydrogels and used phenol red, bromophenol blue, 8-hydroxypyrene-1, 3, 6-trisulfonic acid trisodium salt (pyranine, 3-PSA), 1, 3, 6, 8-pyrenetetrasulfonic acid tetrasodium salt (4-PSA), and Coomassie Brilliant Blue G-250 (CBBG). They found from their work that the diffusivities of the dyes decreased with increasing peptide concentration, indicating that the release kinetics can be managed by controlling molecular interactions of the nanofibers and the dyes (Nagai et al. 2006).

Furthermore, Huang and co-workers demonstrated the competence of an artificial matrix composed of self- assembling PA nanofibers displaying high density RGDS epitopes to provide both permissive and inductive signals to the enamel organ epithelium it comes in contact with. The matrix was able to induce the proliferation and differentiation of ameoblasts capable of synthesizing, organizing and biomineralization of an enamel nodule separated physically from the authentic enamel. This demonstrates that authentic enamel may be synthesised and used as a replacement for enamel lost as a result of disease, trauma or congenital defects (Huang et al. 2010).

Tysseling-Mattiace and co-workers have demonstrated the possibility of inhibition of glial scar formation and regeneration after spinal cord injury by employing three-dimensional nanostructures formed by PAs displaying high densities of the pentapeptide laminin epitope, Isoleucine-lysine-valine-alanine-valine (IKVAV), which is known to promote neurite sprouting and to direct neurite growth (Tashiro et al. 1989; Schense et al. 2000) on their surfaces. In vivo treatment with the PAs reduced astrogliosis, cell death and led to an increase in the number of oligodendria at the site of injury as well as promoting regeneration of ascending sensory fibres and descending motor fibres. PA treatment also led to significant behavioural improvement based on the Basso, Beattie and Bresnahan (BBB) locomotor scale (Basso et al. 1996; Joshi and Fehlings 2002). They found that from 5 weeks of IKVAV PA treatment and beyond following experimental spinal cord injury, animals that had received the PA treatment displayed significant behavioural improvement compared to a glucose control group. By the ninth week, the mean BBB score for the control group was 7.03 ± 0.8, compared to a score of 9.2 ± 0.5 ($p < 0.04$) for the PA treatment group. This shows significant recovery because a score of 7 implies no functional movement despite an extensive range of movement in all three joints in the hindlimb, whereas a score of 9 indicates dorsal stepping in which the animal steps on the dorsal side of its foot during locomotion, that is, the hindlimb movement has a functional use (Tysseling-Mattiace et al. 2008).

In addition, Webber and co-workers have developed a synthetic cell-free VEGF-mimetic therapy based on PA nanostructures. The PA nanofibers displayed the VEGF-mimetic peptide on their surfaces at high density after self-assembly. The VEGF-mimetic filaments were found to induce VEGF receptors phosphorylation and promote proangiogenic behaviour in vitro. Furthermore, the murine hind-limb ischemia model was used to evaluate the potential of the VEGF- mimetic PA nanostructures as therapy for ischemic disease. There was increased tissue perfusion, functional recovery, limb salvage and treadmill endurance in mice that had received VEGF- mimetic PA compared to those treated with a mutant PA (with systematic replacement of four specific residues known to be near the peptide–receptor-binding interface with structurally distinct amino acids), VEGF peptide alone, and saline. Also, the VEGF-mimetic PA performed as well or better than the recombinant protein ($VEGF_{165}$) in every measured outcome. Their results suggest that the bioactive nanostructures could provide a synthetic therapeutic strategy for regeneration of microcirculation and restoration of perfusion to ischemic tissue in cardiovascular disease and could be an alternative to VEGF protein-based strategies (Webber et al. 2011).

Also, Mazza and co-workers have demonstrated the delivery of an active peptide to the brain using a self-assembling PA comprising an alkyl (C_{16}) chain linked to a β-sheet forming peptide (dalargin) which was also the active peptide. Their results showed that following intravenous administration, brain levels of the PA (palmitoyl dalargin; pDal) with respect to plasma increased steadily for up to 90 minutes and pDal was detected in the brain for up to 4 hours post administration (Mazza et al. 2013).

4.5 Peptide synthesis

Peptide synthesis (chemistry) is based on the reaction of a carboxylic acid and an amino group of alpha (α) - amino acids leading to the formation of an amide bond and liberation of water yielding a peptide as the product (Gesellchen and Santerre 1991). Peptide synthesis emerged from the works of Emil Fischer in his attempts at total chemical synthesis of molecules which possessed properties similar to "albumoses" (proteins). He also introduced the term "peptide" in 1906 (Kent 1988; Gesellchen and Santerre 1991) based on the nomenclature of saccharides ('ide') and the word peptone ('pept'; the products of enzymatic cleavage of proteins) to describe the product of amino acids linkage through amide bonds (van Nispen 1987).

For successful synthesis of desired peptide sequences, it is imperative to take measures to prevent unintended reaction of other carboxylic acid and amino groups present in the reaction medium otherwise there would be formation of any number or combination of unwanted products. This necessitates the employment of suitable protecting groups for various functionalities of amino acids not directly involved in the formation of amide bonds. Thus for a coupling reaction to lead to the formation of a desired dipeptide, the N^{α} – amino group of one amino acid and the C – terminal carboxylic acid group of the other amino acid are protected with suitable groups. In this way, the desired amide bond can be formed once the free carboxyl group is activated to yield the desired dipeptide (van Nispen 1987; Lloyd-Williams et al. 1997; Gesellchen and Santerre 1991). The development of the carbobenzyloxy or Cbz (an amide) protecting group (which can be selectively removed after amide bond formation) by Bergmann and Zervas in 1932 produced a great boost to successful and predictable synthesis of desired peptides (Gesellchen and Santerre 1991). Further advances over the next decade climaxed in the successful synthesis of oxytocin by du Vigneaud and co-workers in 1954 (du Vigneaud et al. 1954), which many consider to mark the milestone in the field of peptide synthesis research (Gesellchen and Santerre 1991).

4.5.1 **Peptide synthesis techniques**

In biological systems, ribosomal peptide synthesis occurs in the N to C direction that is the peptide chain grows from the amino end towards the carboxyl end. In chemical peptide synthesis however, synthesis is usually carried out in the reverse (C to N) direction that is from the carboxyl end towards the amino end. This is due to the inherent risk of racemisation (via oxazolone formation) when chemical peptide synthesis is carried out in the N to C direction. (Felix and Merrifield 1970; Gesellchen and Santerre 1991; Henkel et al. 1997; Johansson et al. 2000). Racemisation occurs upon activation of the carboxyl end (C terminus) of the second amino acid (that is activation after formation of a dipeptide) for coupling to the third amino acid. Activation of the C terminus of the dipeptide leads to oxazolone formation between the carbonyl group of the first amino acid and the activated C-terminus of the second amino acid (Gesellchen and Santerre 1991; Henkel et al. 1997). Although several attempts have been made at chemical peptide synthesis in the N to C direction with varying degrees of success (Felix and Merrifield 1970; Henkel et al. 1997; Johansson et al. 2000), chemical synthesis in the C to N direction remains the most widely utilised procedure in routine chemical peptide synthesis (Johansson et al. 2000).

Peptide synthesis can be carried out using either solution or solid phase techniques. Solution phase synthesis was the conventional technique employed for peptide synthesis (Gesellchen and Santerre 1991; Corradin et al. 2010). In solution phase peptide synthesis, the formation of a dipeptide from two amino acids in a controlled manner necessitates that one of the amino acids is protected at the N- terminus while the other is protected at the C- terminus. The resultant protected dipeptide is then isolated after amide bond formation for purification and characterisation. Subsequently, the N^{α} – protecting group can be removed if necessary and the dipeptide can be isolated, purified and characterised.

The dipeptide can then be further coupled with another amino acid with the resulting protected tripeptide isolated, purified and characterised. This cycle could be repeated until the desired peptide is obtained and this is termed linear synthesis. Conversely, in another strategy termed convergent synthesis, protected peptide segments are coupled to form the desired peptide (Kent 1988; Lloyd-Williams et al. 1997). The opportunity for isolation and characterisation of intermediate products during the process of solution synthesis makes detection of side reactions, incomplete deprotection or coupling reactions easy, such that undesired products can be removed before advancing with subsequent steps. Nevertheless, these procedures slow down the overall synthesis process such that an appreciable amount of time and energy will be needed for the synthesis of comparatively small peptides. Furthermore, synthesis in solution is greatly affected by solubility problems especially due to the poor solubility of larger protected intermediate products, such that in some cases chemical reaction for amide bond formation cannot occur. Racemisation of the C-terminal amino acid of activated peptide fragments is also a challenge in solution phase synthesis (Kent 1988; Lloyd-Williams et al. 1997).

4.5.1.1 Solid phase peptide synthesis (SPPS)

SPPS involves the synthesis of peptide chains on an insoluble solid support to which the C- terminal amino acid is attached by means of its carboxyl group (Merrifield 1963; Gesellchen and Santerre 1991; Bodanszky 1993; White and Chan 2000). The supports employed are resins that swell in the solvents used, forming a porous gel structure (which allows reagents to readily penetrate) within which the peptide synthesis occurs (Merrifield 1963; Lloyd-Williams et al. 1997). This technique was developed by Robert Merrifield in 1962 (Gesellchen and Santerre 1991) in an attempt to overcome the technical problems of solution phase synthesis such as solubility and purification in the synthesis of large peptides.

Subsequently, he published the synthesis of a tetrapeptide (L-leucyl-L-alanylglycyl-L-valine) on a solid support (resin) composed of chloromethylated copolymer of styrene and divinylbenzene (200 – 400 mesh) beads in January 1963 to demonstrate the feasibility of the approach (Merrifield 1963).

By design, in SPPS the problem of solubility no longer exists since the peptide chain is assembled on an insoluble support (Kent 1988; Lloyd-Williams et al. 1997). Also, isolation of intermediate products is no longer feasible since the growing peptide chain is firmly attached to the resin, however this is not necessarily consequential if coupling reactions are pushed to completion (Lloyd-Williams et al. 1997). Moreover in SPPS, intermediate peptide products can be easily separated from excess reagents (including starting materials) and products of side reactions by filtration and washing with appropriate solvent (Kent 1988; Gesellchen and Santerre 1991; Bodanszky 1993; Lloyd-Williams et al. 1997; White and Chan 2000; Corradin et al. 2010).

4.5.1.1.1 General Scheme for SPPS

In SPPS, the C-terminal amino acid is chemically attached to the solid support which acts as protecting group for the carboxyl group (Lloyd-Williams et al. 1997), with its α- amino group (N^{α}) protected with a "temporary" protecting group while other side chain functionalities are protected with "permanent" protecting groups. To proceed with synthesis, the "temporary" N^{α}- protecting group is removed and an excess of the next N^{α}-protected amino acid with its carboxyl group activated by a coupling reagent is introduced and left to react with the preceding amino acid in the presence of a weak organic base leading to formation of the amide bond. After the coupling (amide bond formation) reaction, excess reagents are removed by washing and the protecting group at the N-terminus is removed before the next amino acid is added. The use of large excesses of N^{α}-protected amino acids can function to push coupling reactions to completion (Lloyd-Williams 1997; Chan and White 2000) with little or no racemisation (Lloyd-Williams et al. 1997).

Coupling and deprotection steps are repeated until the target peptide sequence is achieved. The synthesised peptide is then liberated from the resin with the permanent protecting groups for side chain functionalities removed simultaneously (Kent 1988; Gesellchen and Santerre 1991; Bodanszky 1993; Lloyd-Williams et al. 1997; White and Chan 2000; Corradin et al. 2010) [Figure 4-2: General SPPS method]. The crude free peptide is then isolated, purified and characterised (Lloyd-Williams et al. 1997).

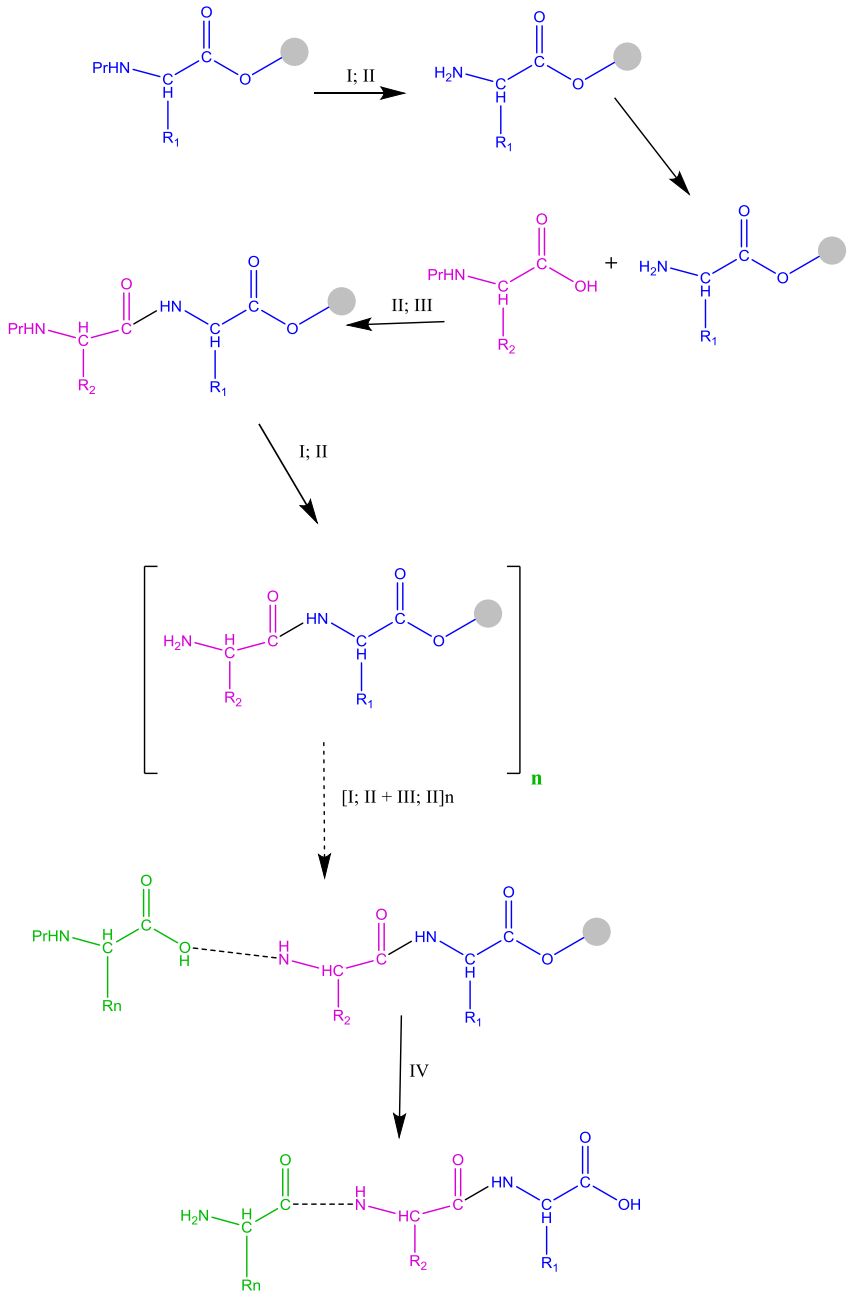

Figure 4-2: General SPPS method

Key:

Pr: N^{α}- protecting group; I: Deprotection conditions for N^{α}- protecting group; II: Wash step; III: Coupling reaction conditions for amide (peptide) bond formation; IV: Cleavage reaction conditions for liberation of target peptide

Due to the success of peptide synthesis on insoluble polymeric supports developed by Merrifield, most peptides are now synthesised using solid phase techniques (Lloyd-Williams et al. 1997; Albericio 2000) and SPPS has remained the method of choice for synthesis of small peptide hormones up to 20 amino acids in length (van der Walle and Olejnik 2011).

SPPS can be carried out using one of two major techniques namely: Merrifield's SPPS (Merrifield 1963) and 9-fluorenylmethoxycarbonyl (Fmoc) SPPS (Lloyd-Williams 1997; Chan and White 2000); depending on the choice of protecting scheme (Albericio 2000).

4.5.1.1.2 Merrifield SPPS

In contemporary Merrifield SPPS, peptide assembly occurs on a hydroxymethylphenylacetamidomethyl polystyrene (PAM) resin to which the C-terminal amino acid is anchored through a benzyl ester linkage with the resin. The original chloromethyl polystyrene is now rarely used due to high incidence of side reactions during synthesis of longer peptides (Chan and White 2000). In this technique, the tert- butyloxycarbonyl (Boc) group is employed as N^{α}-protecting group while the side chain functionalities are protected by benzyl- or cyclohexyl – based protecting groups (Lloyd-Williams 1997; Chan and White 2000). Merrifield SPPS depends on a system of graduated acidolysis for selective removal of temporary and permanent protecting groups (Meienhofer et al. 1979; Lloyd-Williams 1997; Chan and White 2000; Merrifield 1986). Hence, the Boc group for α-amino group protection is removed by neat trifluoroacetic acid (TFA) or 33% TFA in dichloromethane (DCM), while the Bzl group for side chain protection is removed by strong acids such as anhydrous hydrogen fluoride (HF) or trifluoromethanesulfonic acid, with concurrent release of the peptide from the resin (Chan and White 2000; Lloyd-Williams 1997; Albericio 2000).

Although it is possible to cleave the Boc group without significant damage to the benzyl ester resin linkage, a small but not trivial part of amino acid or peptide is lost to cleavage from the resin during each deprotection step (Bodanszky 1993). Also, prolonged exposure of peptide chains to TFA for deprotection to remove the Boc group may be detrimental in the synthesis of long peptides and proteins (Atherton et al. 1978), and may result in premature removal of the Bzl group (Albericio 2000). In addition, the strong acidic conditions required to remove the Bzl group may be deleterious for peptides containing fragile sequences and these may not be able to survive such conditions (Albericio 2000).

Peptide synthesis using the Merrifield technique is on a decline as the need for the use of special polytetrafluoroethylene (PTFE) - lined apparatus for containment of the highly toxic liquid HF has been a deterrent to many in the adoption of this strategy for SPPS (Chan and White 2000).

4.5.1.1.3 Fmoc SPPS

Fmoc SPPS strategy was developed in order to eradicate the need for repetitive acid treatment required for removal of the N^{α}-protecting group (Atherton et al. 1978) such that the N^{α}-protecting group can be removed using a different strategy such as base treatment (amongst other strategies). The Fmoc group was selected as a suitable candidate based on its favourable properties including rapid quantitative cleavage in mild conditions such as piperidine in aprotic solvents like dimethylformamide (DMF). This also permitted the use of acid labile tert-butyl (tBu) group as protecting group for side chain functionalities as it is known to be completely stable to base treatment.

This combination of "temporary" and "permanent" protecting groups for the N^{α} and side functionalities respectively thus allows for an orthogonal (chemical selectivity) strategy in the removal of the different groups (Atherton et al. 1978; Meienhofer et al. 1979). Since the protecting groups belong to unrelated classes of compounds, each can be removed independently and in any order, in the presence of the other groups by different mechanisms. As a result of this, the Fmoc strategy allows for the use of milder reaction conditions and greater flexibility than the Boc strategy (Albericio 2000).

Thus, in contemporary Fmoc SPPS, the N^{α} groups are protected by the base labile Fmoc group which can be removed by treatment with piperidine in DMF, while the side chain functionalities are protected with acid labile groups such as tBu and trityl-based protecting groups which can be removed by TFA treatment (Gesellchen and Santerre 1991; Bodanszky 1993; Chan and White 2000).

This orthogonal (Fmoc/tBu) strategy employed provides a number of advantages over the Merrifield (Boc/Bzl) strategy. Firstly, the repeated base treatment required for deprotection of the N^{α} groups during synthesis has no impact on the integrity of the resin and the side chain protecting groups (Gesellchen and Santerre 1991). Secondly, there is no need for a neutralisation step after deprotection by acidolysis as the amino group is released in the free form for amide bond formation with the next amino acid after deprotection by base treatment. Also, the number of washing steps are reduced since deprotection and coupling reactions are carried out in the same solvent (DMF). Lastly but importantly, the use of the tBu group as side chain protecting group removes the need for the use of final deprotection and cleavage with the highly toxic and strongly acidic liquid HF (Gesellchen and Santerre 1991; Bodanszky 1993).

4.5.1.2 Purification of synthetic peptides

High performance (or high pressure) liquid chromatography (HPLC) is the most commonly used method for purification of peptides of different origins (including synthetic peptides), quantity and complexity. HPLC has been found to be especially applicable in purification of a peptide of interest from the crude mixture from SPPS which normally contains impurities that are frequently very similar to the target peptide (Mant et al. 1997; Smith and Hanly 1997; Aguilar 2004a). Such impurities are usually terminated sequences, deletion or chemically modified peptides which may be different from the target peptide by missing only one amino acid residue (Mant et al. 1997; Aguilar 2004a).

HPLC has been particularly successful owing to several intrinsic characteristics of the technique which are correlated to reproducibility, typically high recovery, ease of manipulation for required selectivity and the exceptionally high level of resolution achievable under various conditions for molecules possessing very similar properties and structurally dissimilar molecules (Aguilar 2004a).

Detection of peptide eluents from HPLC analysis can be achieved at wavelength values between 210 – 220 nm due to the characteristic absorbance of peptide bonds in this range (far ultraviolent; < 220 nm). However, peptides containing amino acids such as tyrosine and tryptophan which possess aromatic side chains may be detected at higher wavelengths of 250 – 290 nm (Shaw 1994; Mant and Hodges 1996; Aguilar 2004b; Mant et al. 2007).

There are different HPLC modes that can be employed in the peptide separations such as size exclusion HPLC which effects separation based on size (SEC), ion-exchange HPLC which exploits the net charge to effect separation and reversed-phase HPLC in which separation of molecules and hence purification depends on hydrophobicity. The levels of separation or purification may be optimised by making subtle changes in the chromatographic conditions (such as the mobile phase) specifically for each mode employed. A combination of different modes may also be necessary in some cases for optimal purification (Mant et al. 1997; Aguilar 2004a).

4.5.1.2.1 Reversed-phase HPLC (RP HPLC)

RP HPLC is recognised as the method of choice for the purification (Shaw 1994; Mant et al. 1997; Smith and Hanly 1997; Aguilar 2004; Mant et al. 2007) as well as assessment of purity of synthetic peptides (Smith and Hanly 1997). RP HPLC usually gives better results than other modes of HPLC in terms of speed and efficiency and it is the mode that presents the greatest platform for controlling specific characteristics of both mobile and stationary phases to obtain optimal separation of peptides (Mant et al. 1997). The stationary phase employed in RP HPLC is micro particulate silica beads derivatised with covalently bonded alkyl chains such as octyl (C_8), octadecyl (C_{18}) or phenyl groups (Fallon et al. 1987; Shaw 1994; Smith and Hanly 1997; Mant et al. 2007). Elution of peptides is effected using a mixture of water and water – miscible organic solvents such as acetonitrile or methanol as mobile phase with the addition of ionic modifiers such as TFA (Fallon et al. 1987; Mant and Hodges 1996; Smith and Hanly 1997; Aguilar 2004b). In RP HPLC, separation is a function of hydrophobic interaction of component molecules (in the mixture to be purified) present in the mobile phase with the hydrophobic groups attached to the surface of the stationary phase (Aguilar 2004b).

In purification of peptides, elution is carried out using gradient methods whereby the concentration of the organic component of the mobile phase is increased over a pre-set time period (Aguilar and Hearn 1996; Mant and Hodges 1996; Aguilar 2004b) and peptides are eluted in order of increasing net hydrophobicity (Aguilar 2004b; Mant et al. 2007).

The mobile phase systems usually employed in RP HPLC have advantages such as volatility which translates to ease of removal without the need for desalting procedures following preparative purification procedures (Mant and Hodges 1996; Mant et al. 1997; Lindner and Helliger 2004; Mant et al. 2007). Also, TFA commonly used in the mobile phase is volatile and it eliminates ionic interaction between with residual underivatised silanol silica groups (negatively charged at pH ≥ 3 – 4) of the stationary phase and positively charged amino acid by preventing their ionisation at the low pH values generated (Mant et al. 2007).

RP HPLC presents various advantages which make it an attractive HPLC mode. The inertness of the stationary phase employed may be considered to be the most important of these advantages. This permits the use and manipulation of various solvent systems and additives as well as different pH and temperature conditions (Fallon et al. 1987). Also, RP HPLC mode provides exceptional resolution of closely related as well as structurally dissimilar molecules in varying chromatographic conditions; mobile phase characteristics may be varied relatively easily in order to achieve the desired selectivity and RP HPLC usually gives high recoveries leading to high product yields (Aguilar 2004b).

4.5.1.3 Characterisation of synthetic peptides

4.5.1.3.1 Mass spectrometry

Mass spectrometry (MS) is a sensitive and robust micro analytical technique valuable for selective detection and determination of the amount of analyte samples based on the separation of the ionized analyte sample molecules according to their mass to charge ratios (m/z) by the application of electric and magnetic fields (Wait 1993; Watson and Sparkman 2007). MS originated from experimental works by Sir J. J. Thompson (Thomson 1913) in his study into the passage of electricity through gases, which led to his discovery of the electron and his measurement of the charge – to – mass ratios in 1897 (Nobel Prize in Physics 1906). In subsequent works, he studied positive ions using similar methods and built the first "mass spectrometer" (parabola spectrograph) which enabled the separation of narrow ray beams into positive ray parabolas, each of which correspond to a specific charge – to – mass ratio (Griffiths 1997; Suizdak 2006).

MS is indispensable in the characterisation of synthetic peptides for the determination of their molecular weight. This is necessary to confirm that the synthetic product obtained by RP HPLC purification (prominent peak) actually corresponds to the target peptide as this is not always the case (Smart et al. 1996).

In order to carry out MS analysis of analyte compounds, it essential to first generate gas phase ions of such compounds, which can then be separated based on their different mass – to – charge ratios and detected by a detector (Smith et al. 1990; Ho et al. 2003; de Hoffmann and Stroobant 2007; Watson and Sparkman 2007). The process of ion formation determines the scope and applicability of the method (Smith et al. 1990).

MS is a reasonably sensitive technique with capability for detection limits down to the picomole and femtomole scales and lower (Hillenkamp and Karas 1990; Wait 1993; Suizdak 1994; Solouki et al. 1995; Morris et al. 1997; Watson and Sparkman 2007), thus requiring very small amount of analyte (picomole or nanomole quantities) for analysis (Wait 1993). MS is an attractive analytical technique for bio molecules owing to the very high sensitivity limits obtainable, the potential for highly accurate mass determination, and the ability for structural elucidation of molecules under investigation (Hillenkamp and Karas 1990). Nevertheless, MS is a destructive technique as analytes are invariably consumed in the process of analysis (Wait 1993; Jonsson 2001).

4.5.1.3.1.1 Ionisation in MS

Ionisation in MS comprises both the methods by which ionisation can be achieved and the ionisation sources which refer to the mechanical devices that allow ionisation to take place (Suizdak 2006).

4.5.1.3.1.1.1 Ionisation in methods MS

Ionisation of analytes for MS analysis can be achieved through various mechanisms such as protonation, deprotonation, cationisation, transfer of a charged molecule to the gas phase, electron ejection and electron capture. Each mechanism of ionisation has applications in the ionisation of various analyte types to which they are particularly suited (Suizdak 2006).

4.5.1.3.1.1.1.1 Protonation

Ionisation of analytes by protonation involves the addition of a proton to the molecule (Suizdak 2006; de Hoffmann and Stroobant 2007) resulting in a net positive charge (1+ for each proton added). The positive charges are usually localised on the more basic residues (like amines) of such molecules to produce stable cations. Ionisation of peptides for MS is frequently achieved by the protonation method. Protonation can be accomplished through matrix assisted laser desorption ionisation (MALDI), electrospray ionisation (ESI) and atmospheric pressure chemical ionisation (APCI) (Suizdak 2006).

4.5.1.3.1.1.2 Ionisation sources in MS

Historically (before 1970), electron ionisation (EI) and chemical ionisation (CI) served as the main ionisation sources for MS analysis (Harrison and Cotter 1990; Suizdak 2006; Watson and Sparkman 2007). However, these techniques are applicable only to significantly volatile and thermally stable analytes as they produce gas phase ions only from gas phase molecules. Thus they cannot be applied to thermo labile analytes and those that lack sufficient vapour pressure (Wait 1993; Williams and Fleming 1996; de Hoffmann and Stroobant 2007; Watson and Sparkman 2007). Also, EI produces extensive fragmentation such that the molecular ion may sometimes not be observed (Wait 1993; Williams and Fleming 1996; de Hoffmann and Stroobant 2007). The associated fragmentation is usually reproducible and distinctive for each molecule, providing an important tool for structural elucidation of unknown compounds. However, fragmentation is sometimes so much that comparatively non informative low–mass ions are predominant in the resulting spectra (Wait 1993).

In addition, the application of EI has been restricted to small molecules with masses falling outside the mass range of typical bio molecules (Wait 1993; Suizdak 2006; Watson and Sparkman 2007). Nevertheless, EI and CI remain important in combination with techniques such as gas chromatography/ MS (GC/MS) and liquid chromatography MS (LC/MS) techniques (Watson and Sparkman 2007).

Subsequently, more recent techniques such as fast atom/ ion bombardment (FAB), MALDI and ESI were developed which have broadened the scope of application of MS (Suizdak 2006; Watson and Sparkman 2007). The development of these techniques which has brought about many advances in the analysis of biomolecules including larger molecules up to 100 kDa (Harrison and Cotter 1990; Williams and Fleming 1996; Suizdak 2006) was inspired by the attendant constraints of the earlier techniques such as EI (Suizdak 2006).

Albeit, ESI and MALDI have emerged as the methods most favoured for MS analysis of biomolecules (Suizdak 1994; Suizdak 2006; Watson and Sparkman 2007). These techniques provide the platform for the simple, rapid and accurate generation of molecular weight information for a wide variety of analytes. This has enabled conventional characterisation in small molecule and protein synthesis as well as compounds such as those derived directly from biological matrices (Suizdak 1994).

4.5.1.3.1.1.2.1 ESI MS

ESI is commonly applied in the analysis of a wide variety of molecules including peptides, proteins, oligonucleotides, carbohydrates, lipids, synthetic and biopolymers, as well as small polar molecules (Smith et al. 1990; Loo 2000; Suizdak 2006; de Hoffmann and Stroobant 2007), although it was initially regarded as an ionisation source solely for protein analysis (de Hoffmann and Stroobant 2007). In ESI MS, gas phase ions are produced directly from the liquid phase, eliminating the need for analytes to be volatile and thermo stable (Kebarle 2000; Ho et al. 2003; Suizdak 2006; Watson and Sparkman 2007).

In the ESI process, a fine spray of highly charged droplets is generated in the presence of a strong electric field applied at atmospheric pressure to a liquid (analyte) passing through a capillary tube at low flow rate of about 1 – 10 µl min^{-1}. The electric field results from applying a potential difference (3 – 6 kV) between the spraying capillary and a counter electrode separated by a distance of 0.3 – 2 cm, this generates electric fields of about 10^6 V m^{-1} in strength. The field causes accumulation of charges at the surface of the liquid present at the end of the capillary which will break up into highly charged droplets. Subsequently, the droplets will pass through either heated inert gas (usually nitrogen) or a heated capillary to remove any remaining solvent molecules (Wait 1993; Williams and Fleming 1996; Kebarle 2000; Ho et al. 2003; Suizdak 2006; de Hoffmann and Stroobant 2007). The polarity bias of the spraying capillary will result in the electrosprayed droplets having an excess of positive or negative charges (Williams and Fleming 1996; Ho et al. 2003). Evaporation of the solvent from the droplets leads to the droplets shrinking and an increase in their charge per unit volume (Suizdak 1994; Ho et al. 2003; Suizdak 2006; de Hoffmann and Stroobant 2007).

The reduction in droplet size also leads to an increase in the forces of repulsion between the excess charges in the droplets such that the mutual "Coulombic repulsion" between the particles exceeds the surface tension and the ions are ejected through what is called a "Taylor cone" (Suizdak 2006; de Hoffmann and Stroobant 2007; Watson and Sparkman 2007).

Although ESI favours the formation of singly charged molecular ions of small molecules, the generation of multiply charged species from larger molecules is a widely recognised feature of this ionisation source. Such multiply charged ions are produced with large molecules that possess a number of ionisable sites. For instance, proteins would usually bear approximately one charge per thousand daltons, the number of charges may be less if very few basic amino acids are present in the molecule. The generation of multiply charged ions provide the advantage of improved sensitivity at the detector and permits the analysis of high molecular weight compounds using analysers with a relatively small mass range (Wait 1993; Suizdak 1994; Suizdak 2006; de Hoffmann and Stroobant 2007; Watson and Sparkman 2007).

ESI is recognised as a "soft" ionisation technique which permits accurate mass determination for small molecules and ionisation of macromolecules without disrupting covalent bonds. Also, ESI is particularly suited for the study of biological complexes because it maintains weak non-covalent interaction of macromolecules like proteins (Loo 2000; Watson and Sparkman 2007).

4.5.1.3.1.1.2.2 Tandem MS

Tandem MS, abbreviated as and often referred to as MS/MS, generically describes MS involving at least two stages of mass analysis (de Hoffmann and Stroobant 2007). The term MS/MS (for mass spectrometry/mass spectrometry) was invented by William F. Haddon in 1978 to describe the method of inducing the decomposition of a stable ion by forcing it to collide with neutral gas atoms or molecules (Watson and Sparkman 2007).

Frequently in MS/MS experiments, a precursor ion is first isolated using a first analyser, this ion then undergoes fragmentation either spontaneously or by activation to yield product ions and neutral fragments. The product ions are then analysed in a second analyser (Ho et al. 2003; de Hoffmann and Stroobant 2007; Watson and Sparkman 2007). This is commonly achieved by positioning a collision cell between the first and second (MS_1 and MS_2 respectively) mass analysers (Ho et al. 2003; Watson and Sparkman 2007). However, the number of steps can be increased depending on the required application (MS_n). Thus for a three step experiment, ions of a first mass would be selected, followed by selection of ions of a second mass (from the previously generated fragments), the fragments from the last selected ions are then analysed. Such an experiment would thus be an MS/MS/MS or MS_3 experiment (de Hoffmann and Stroobant 2007).

MS/MS is a widely recognised method for determination of protein sequences mostly due to the great level of structural diversity of peptides and the limitations of other conventional methods (Gross 1990). Also, MS/MS allows more structural information to be obtained from ionic species of interest (de Hoffmann and Stroobant 2007). MS/MS is generally applicable for determination of the amino acid sequence of peptides.

For instance, cleavage of the same bond such as the CO – NH of consecutive peptide linkages (with retention of the positive charge on the CO – group) would generate a series of ions of increasing mass. Thus, the identities of consecutive amino acids in the peptide sequence would be revealed by the mass difference between consecutive pairs (Biemann 1990).

4.5.1.3.2 Nuclear magnetic resonance (NMR) spectroscopy

NMR is a phenomenon that was first observed in 1946 (Williams and Fleming 1996; Stepišnik 2006) separately by Felix Bloch and Edward Mills Purcell (Nobel Prize in Physics 1952) (Smith and Blandford 1995; Stepišnik 2006) and has found routine application in organic chemistry as far back as 1960. The influence and adaptability of NMR has continued to increase from then onwards and notably since the introduction of Fourier Transform (FT) NMR spectroscopy in the late 1970s (Williams and Fleming 1996). NMR has the unique advantage over most other spectroscopic techniques in the capability to acquire structural and dynamic information at atomic resolution (Barber et al. 1993).

NMR alludes to the absorption and release of radio frequency energy by a nucleus in a magnetic field (Smith and Blandford 1995). NMR spectroscopy is based on the possession of nuclear spin (I) by some atomic nuclei which confers on them behaviour similar to that of bar magnets. These nuclei can orient themselves in $2I + 1$ ways when placed in a magnetic field (Günther 1995; Smith and Blandford 1995; Williams and Fleming 1996; Guthrie 1997). The applied external magnetic field causes a polarisation in the spin of the constituent protons and neutrons of such atomic nuclei which can be aligned (Jones and Mulloy 1993; Stepišnik 2006) parallel or antiparallel to the applied field.

The spin alignment thus causes the quantum mechanically allowed energy levels of such nucleus to split and the nucleus can absorb electromagnetic radiation at a frequency corresponding exactly to the difference between the energy levels (Stepišnik 2006).

In practical applications of NMR, the most important nuclei are ^{1}H and ^{13}C (Williams and Fleming 1996), with ^{1}H being the most commonly studied (Williams and Fleming 1996; Guthrie 1997). Both ^{1}H and ^{13}C have a spin of ½, so they can only present one of two orientations (from 2I + 1). Thus, they either have a low energy orientation aligned with the applied field or a high energy orientation opposed to the applied field (Williams and Fleming 1996). The difference in energy is given by the equation:

$$\Delta E = hyB_0/2\pi \qquad \textbf{Equation 4-1}$$

where: h is Planck's constant; y is the magnetogyric ratio (a proportionality constant (differs for each nucleus) which essentially measures the strength of the nuclear magnets; B_0 is the strength of the applied magnetic field (Williams and Fleming 1996).

The difference in the number of nuclei in the low energy state (N_α) and the high energy state (N_β) is determined by the Boltzmann distribution, represented in the equation:

$$N_\beta/N_\alpha = \exp(-\Delta E/kT) \qquad \textbf{Equation 4-2}$$

where k is the Boltzmann constant; T is the temperature in Kelvin.

The distribution changes when an applied radio frequency signal matches the frequency at which the nuclear magnets naturally precess in the magnetic field B_0 such that some N_α nuclei are promoted from the low energy state to the high energy state, leading to an increase in N_β (Williams and Fleming 1996).

The frequency [in Hertz (Hz)], known as the resonance frequency is given by the equation:

$\nu = yB_0/2\pi$ **Equation 4-3**

where ν is the frequency

The resonance frequency therefore depends on both the strength of the applied field and the nature of the nucleus under consideration (Williams and Fleming 1996; Hinds and Norton 1997).

The difference between the N_α and N_β is usually very small (of the order of 1 in 10^5 protons in a 200 MHz instrument), making NMR a relatively insensitive technique compared to techniques such as ultraviolet (UV) and infrared (IR) spectroscopy, thus NMR requires very sensitive electronics. The difference between the N_α and N_β increases with increasing field strength B_0 (equations 2.1 and 2.2), this implies that high-field (200 – 500 MHz) instruments are intrinsically more sensitive than the older (60 – 100 MHz) instruments (Günther 1995; Smith and Blandford 1995; Williams and Fleming 1996).

4.5.1.3.2.1 Measurement of NMR Spectrum

To acquire an NMR spectrum, a radio frequency pulse is applied to the sample to be analysed. Subsequently, the NMR signal (free induction decay or FID) is changed from an analog to a digital signal by an analog to digital converter and stored in a computer. After this, the magnetisation of the sample is allowed to relax before the next scan starts. The signal-to-noise ratio of a spectrum is directly proportional to the square root of the number of scans acquired. This is of great importance in when handling small samples as reducing concentration significantly increases the length of time needed to generate a spectrum with the same signal-to-noise ratio (Hinds and Norton 1997).

The NMR spectrum is measured using one of two methods namely: continuous wave (CW) NMR or Fourier transform (FT) NMR (Jones and Mulloy 1993; Günther 1995).

In conventional CW method, some of the N_α nuclei are promoted to the higher energy state by absorbing a small portion of the applied signal and the response is detected in a receiving coil. The range of frequency being considered is scanned steadily from one extreme end to the other by varying either the frequency of the transmitter or the magnetic field. The spectrum acquired is then plotted directly (as it is generated) to show the absorption (upwards) versus frequency (increasing to the left, as found in UV and IR spectroscopy) (Günther 1995; Williams and Fleming 1996).

In the FT method, the radio frequency signal is applied to the sample as a single powerful pulse lasting for a period of time (t_P) usually a few microseconds. This pulse which effectively covers the whole frequency range generates an oscillating magnetic field (B_1) along the x axis, at right angles to the applied magnetic field (B_0), which is defined along the z axis (Jones and Mulloy 1993; Günther 1995; Williams and Fleming 1996).

Due to the small difference between N_α and N_β, the sample to be analysed has a net magnetisation (M), initially aligned in the direction of the magnetic field. The magnetisation is tipped by the applied pulse through an angle given by the equation:

$$\theta = \gamma B_1 t_P \qquad \textbf{Equation 4-4}$$

The time (t_P) is usually chosen such that θ is 90^o and these kinds of pulses are termed $^{\pi}/_{2}$ pulses (Williams and Fleming 1996).

The magnetisation thus disturbed from its orientation along the z axis precesses in the xy plane and the magnetisation orientated along the y axis is detected in a receiver coil (Günther 1995; Williams and Fleming 1996). Hence, after the application of the pulse, the signal detected starts as a positive signal in the + y axis, precesses to the x axis (zero signal) and then to the – y axis (negative signal). Usually, the signal is detected for times in the order of one second. The frequency of oscillation detected is the difference between the excitation frequency and the NMR resonance frequency (Williams and Fleming 1996).

In FT NMR, emissions are recorded and stored in a computer as the nuclei relax and go back to the ground state. The data recorded is then converted from the time domain (FID) to the frequency domain (spectrum) by mathematical manipulation which is the Fourier transformation (Günther 1995; Guthrie 1997; Hinds and Norton 1997). FT NMR possesses an important advantage over CW NMR which derives from the acquisition of the spectrum by the excitation of all the resonances simultaneously using a single pulse for a few seconds. This allows the collation of data obtained from many acquisitions which gives in turn greatly enhances the signal-to-noise ratio, making FT NMR much more sensitive than CW NMR (Jones and Mulloy 1993; Williams and Fleming 1996; Guthrie 1997). This is particularly important for the study of relatively insensitive nuclei such as ^{13}C (also with a low occurrence; 1 in 100 carbon atoms) in biological samples, which would have otherwise been practically impossible (Williams and Fleming 1996; Guthrie 1997).

Currently, CW spectra are seldom used except to obtain the first spectrum of a product from a reaction mixture, typically for ^{1}H spectra on samples $\geq$ 50 mg. On the other hand FT NMR is used to acquire all ^{13}C spectra and for small samples quantities. FT NMR is also employed when accurate and well resolved spectra are required. For a typical ^{13}C, a sample of about 50 – 100 mg is required while for FT ^{1}H spectrum, a sample of 1 – 10 mg would normally suffice (Williams and Fleming 1996).

For acquisition of an NMR spectrum, the sample to be analysed is usually dissolved in a solvent which would not give rise to additional signals in the spectrum. For this purpose, deuterated (in which most of the ^{1}H have been replaced with ^{2}H, that is deuterium) solvents are employed with the choice of solvent determined by the solubility of the sample to be analysed (Williams and Fleming 1996; Guthrie 1997).

4.5.1.3.2.2 Chemical Shift

The exact frequency at which an atom will experience resonance is determined by both the applied field (B_0) and the very small differences in the magnetic environment experienced by each nucleus (Günther 1995; Williams and Fleming 1996; Guthrie 1997). Such differences are a result of the variation in electron density surrounding each nucleus so that each chemically different atom (^{1}H or ^{13}C) in the structure under investigation would come into resonance at a frequency slightly different from the other nuclei (Williams and Fleming 1996). For each atomic nucleus in a magnetic field surrounded by other atoms, the electron clouds from the surrounding atomic nuclei will exert a small but significant effect which will create a "shielding effect" on the reference atom. The extent of the shielding effect will determine the precessional frequency of the reference atomic nucleus, such that the greater the shielding effect on the atomic nucleus (more dense electric cloud) the lower the precessional frequency and vice versa (Smith and Blandford 1995; Guthrie 1997). In practise, it is rather cumbersome to characterise individual peaks by assigning a specific frequency to each of them, which would all be very close to the resonance frequency. The practicable alternative is to measure the difference in the frequency (ν_s) of the peak from that of a chosen internal standard (both in Hz). This difference is then divided by the operating frequency (in MHz) to get a field independent number in a convenient range.

More often than not tetramethylsilane (TMS) is used as internal standard in spectra acquisition. The chemical shift is defined by the equation:

$\delta = [\nu \text{ sample} - \nu \text{ reference}] / \text{operating frequency}$ **Equation 4-5**

This yields a dimensionless quantity and is expressed in parts per million (ppm) (Jones and Mulloy 1993; Günther 1995; Smith and Blandford 1995; Williams and Fleming 1996; Guthrie 1997).

4.6 Materials and methods

4.6.1 Materials

4.6.1.1 List of materials

S/n	Material	Supplier
1	Fmoc- Phe- OH	Novabiochem; Merck Schuchardt, OHG, Hohenbrunn, Germany
2	Fmoc- Gly- OH	Novabiochem
3	Fmoc- Leu- OH	Novabiochem
4	Fmoc- Tyr- OH	Novabiochem
5	Fmoc- Arg(Pbf)- OH	Novabiochem
6	Fmoc- Tyr (2- ClTrt)- OH	Novabiochem
7	Fmoc- Leu- Wang resin [(0.64 mmole/g); (100- 200 mesh)]	Novabiochem
8	Fmoc- Phe- Wang resin [(0.65mmole/g); (100- 200 mesh)]	Novabiochem

S/n	Material	Supplier
9	Fmoc- Met- Wang resin [(0.70 mmole/g); (100 – 200 mesh)]	Novabiochem
10	2-(1 H- Benzotriazole- 1- yl)- 1,1,3,3-tetramethyluronium hexafluorophosphate (HBTU)	Novabiochem
11	N,N- Dimethylformamide (DMF)	Rathburn Chemicals Ltd, Walkerburn, Scotland
12	Dichloromethane (DCM)	GPR Rectapur; VWR Chemicals, Fontenay-sous-Bois, France
13	Dry DCM	Sigma-Aldrich
14	N,N-Diisopropylethylamine (DIEA)	Sigma-Aldrich
15	Trifluoroacetic acid (TFA)	Sigma-Aldrich
16	Triethylamine	Sigma

S/n	**Material**	**Supplier**
17	Palmitic acid N- hydroxysuccinimide ester	Sigma
18	Piperidine	Sigma-Aldrich
19	Triisopropylsilane (TIS)	Sigma-Aldrich
20	Methyl sulfoxide- d_6	Sigma-Aldrich
21	Acetonitrile (MeCN; HPLC grade)	Sigma-Aldrich
22	Water (H_2O; HPLC grade)	Sigma-Aldrich
23	Diethyl ether	Sigma-Aldrich

4.6.2 **Methods**

4.6.2.1 Synthesis of PAs

Three PAs (Peptides A, B and C) were synthesized manually by Fmoc SPPS protocols. Peptides A and B comprised essentially the same amino acid residues and differed only in the sequence and position of the acyl chain. Peptide A (O-Palm-Y-G-G-L-R-F) possessed a terminal acyl substituent while peptide B (G-G-Y- (O-Palm)-F-R-L) possessed a mid-chain acyl substituent. Peptide C is a novel analogue of the natural neuropeptide methionine enkephalin modified at the N- terminus with an acyl chain attached to the hydroxyl (OH) side chain of the tyrosyl residue (O-Palm-Y-G-G-F-M). Peptide assembly for the three PAs was done on Wang resin pre-coupled with the C- terminal amino acid.

For the synthesis of O-Palm-Y-G-G-L-R-F (0.5 mmole), Fmoc- Phe-Wang resin (770mg, 0.65 mmole/g substitution) was weighed in a glass weighing boat and transferred to a glass reaction vessel (sealable sintered glass funnel) and allowed to swell in DMF (10 mL) for 1 hour. The DMF was then drained off and the resin was washed with 2 further portions of DMF and drained (left wet). The Fmoc protecting group of the resin was removed by reacting the resin with piperidine in DMF (20 % $^{v}/_{v}$) for 20 (2 X 10) minutes. Successful deprotection of the N-terminus was confirmed by performing the ninhydrin (Kaiser's) test. A few resin beads were transferred from the reaction mixture unto a small sintered glass funnel and washed with a DCM and methanol (1 : 1) mixture and dried under vacuum. The resin beads were then transferred into a glass test tube to which was added 2 drops of Solution A (80 % $^{w}/_{v}$ phenol in ethanol); 4 drops of Solution B (2 % $^{v}/_{v}$ potassium cyanide in 1mM pyridine) and 2 drops of Solution C (5 % $^{w}/_{v}$ ninhydrin in ethanol).

The test tube was then transferred to a heating block that had been pre- heated to 120^{o} C for 3 – 5 minutes. Dark blue colouration of the resin beads indicates the presence of free primary amines on the resin, hence successful deprotection (Chan and White 2000). The deprotected resin was then washed thoroughly with copious amounts of DMF to ensure complete removal of piperidine and drained till just wet with minimum DMF.

To the deprotected resin, N,N-diisopropylethylamine [(DIEA); 425 µL, 5 mmol)] was added, followed by Fmoc- Arg(Pbf)-OH (811 mg, 2.5 mmol) and 2-(1 H-benzotriazole- 1- yl)- 1,1,3,3- tetramethyluronium hexafluorophosphate [(HBTU); 474 mg, 2.5 mmol)] dissolved in DMF (7 mL). The reaction vessel was capped and the reaction was left to proceed with constant agitation for 45 – 60 minutes. The reaction mixture was then washed off and the coupling process was repeated to ensure complete coupling of the amino acid. The ninhydrin test was performed to check the success of the coupling reaction. Production of a yellow to orange colouration of the resin beads indicates that coupling has been successful and a dark blue colour indicates unsuccessful coupling in which case coupling was repeated. Coupling of the other amino acids proceeded as described with the N^{α} protected Fmoc- amino acids [5 (2 X 2.5) molar equivalents] and HBTU [5 (2 X 2.5) molar equivalents] dissolved in DMF and DIEA (5 molar equivalents at each coupling), for 30 minutes until the sequence was complete (Figure 4-3). Coupling and deprotection reactions were qualitatively monitored with the ninhydrin test.

When peptide assembly was completed, the peptidyl-resin was washed thoroughly with DMF and drained, then with DCM and finally with a DCM and methanol (1 : 1) mixture and dried under vacuum. The resin was then transferred into a pre- weighed glass vial with the cap perforated and left in a dessicator (*in vacuo*) overnight.

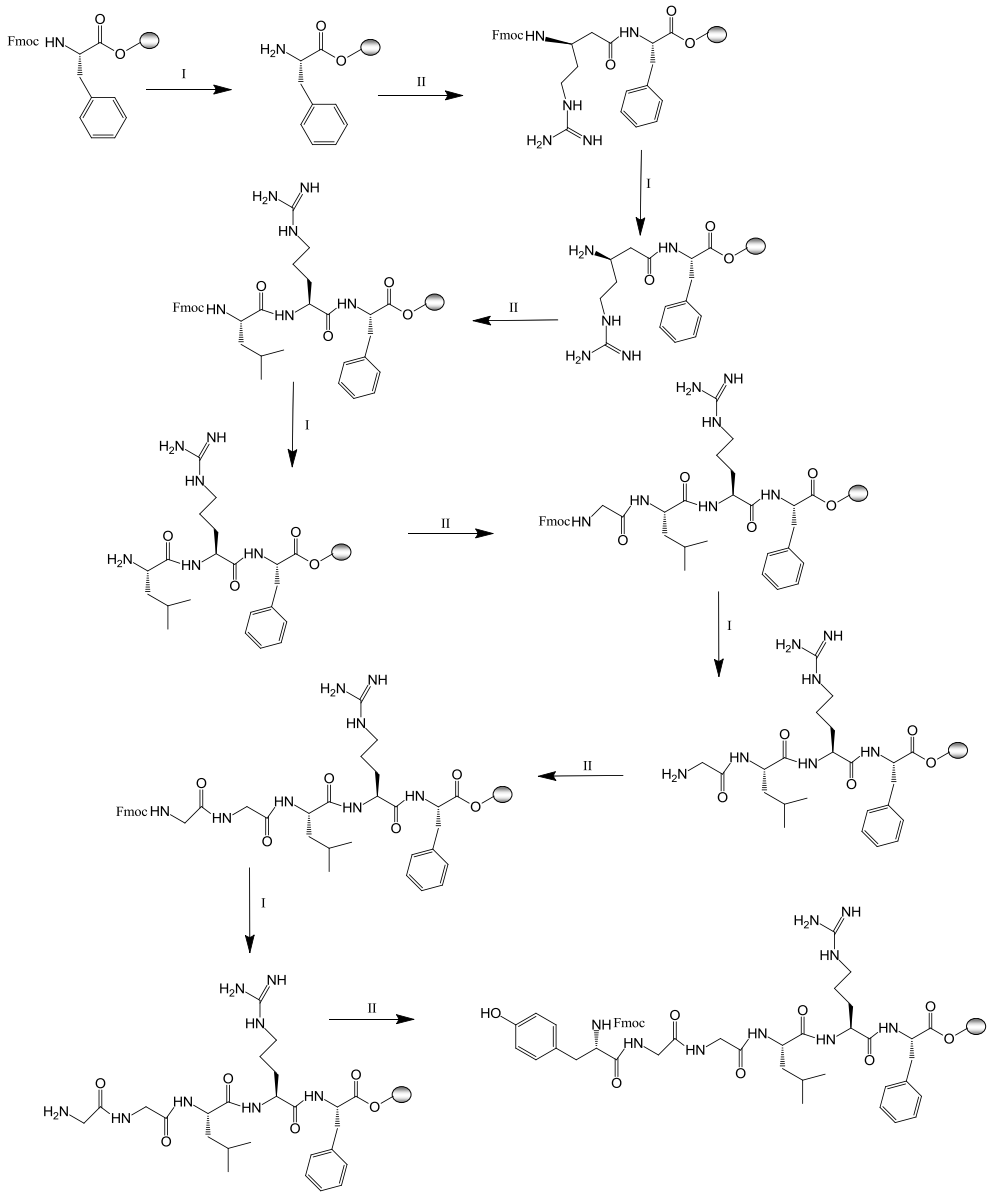

Figure 4-3: Reaction scheme for peptide synthesis

Key:

I: Deprotection [piperidine/DMF (10 % $^{v}/_{v}$); followed by washing (DMF); II: Coupling [HBTU (2.5 mmol) + N^{α}- protected amino acid (2.5 mmol) + DIEA (5 mmol)] X 2; followed by washing (DMF)

Acylation of the peptides was achieved by coupling a palmitoyl (C_{16}- alkyl) chain to the hydroxyl (OH) side chain of the tyrosyl residue of the peptides.

For acylation of O-Palm-Y-G-G-L-R-F (0.2 mmol), the required peptidyl- resin (511.73 mg) was weighed and transferred into a the glass reaction vessel and swelled in DMF (10 mL) for 45 – 60 minutes; triethylamine (1.4 mL; 5 mmol) was added and to this mixture, palmitic acid N-hdroxysuccinimide ester (565.62 mg, 0.8 mmol) dissolved in DMF was added in a drop wise manner. The vessel was capped, and the reaction was left to proceed for 18 – 24 hours with constant agitation. Subsequently, the resin was filtered and washed thoroughly with DMF and deprotection of the N^{α} group was carried out using piperidine in DMF (20 % $^{v}/_{v}$) for 20 (2 X 10 minutes. The acylated peptidyl- resin was then washed thoroughly with DMF, drained and then washed with DCM followed by washing with a DCM and methanol (1 : 1) mixture, dried under vacuum and transferred into a pre-weighed glass vial (cap perforated) and left overnight in a dessicator (*in vacuo*) [Figure 4-4].

Synthesis of G-G-Y-(O-Palm)-F-R-L and O-Palm-Y-G-G-F-M were carried out as described above.

However, to achieve acylation of G-G-Y-(O-Palm)-F-R-L, containing a side chain protected tyrosyl residue [Tyr (2- ClTrt)- OH], the protecting group had to be removed to make the OH group of the tyrosyl (side chain) residue available for the acylation reaction. Selective deprotection of the tyrosyl residue was achieved by weighing and transferring the required amount of the peptidyl resin (534 mg, 0.2 mmole) into the glass reaction vessel. The resin was swelled in dry DCM (10 mL) for 45 – 60 minutes. The resin was then drained and a mixture of TFA/TIS/DCM (1/5/94 % $^{v}/_{v}$; 5 mL) was added, the vessel was capped and the resin was agitated for 2 minutes.

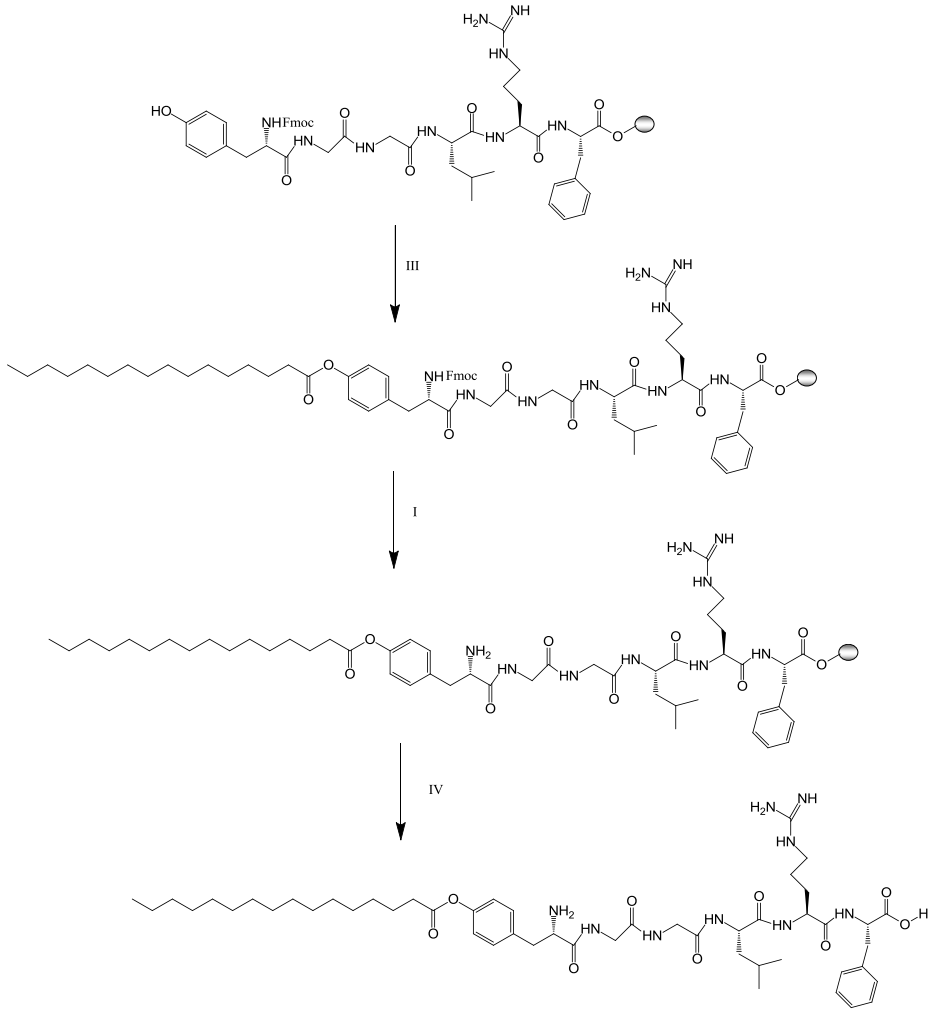

Figure 4-4: Reaction scheme for palmitoylation and final cleave to yield target PA

Key:

III: Palmitoylation reaction [N^{α}-protected peptide (0.2 mmol) + triethylamine (5 mmol) + palmitic acid N-hdroxysuccinimide ester (0.8 mmol)]; followed by washing; I: Deprotection [piperidine/DMF (10 % $^{v}/_{v}$); followed by washing (DMF); IV: Cleavage reaction: TFA/TIS/water (95/2.5/2.5 % $^{v}/_{v}$)

A bright yellow colouration was observed, indicating the liberation of the 2- ClTrt group which is in turn scavenged by the TIS component of the cleavage mixture. The resin was drained and washed with dry DCM and the reaction was repeated until complete disappearance of the yellow colouration and then one more time to ensure complete removal of the Trt group. Subsequently, the resin was washed thoroughly with DCM and drained, then with DMF after which it was left to swell in DMF (10 mL) for 30 minutes before proceeding with the acylation reaction as described above.

In the case of O-Palm-Y-G-G-L-R-F and G-G-Y-(O-Palm)-F-R-L, acylated peptide was liberated from the resin using a high concentration TFA cleavage mixture consisting of TFA/TIS/H_2O (95/2.5/2.5 % $^{v}/_{v}$). Dry peptidyl resin was placed in a dry round bottom flask and the required amount of cleavage mixture (1mL per 0.1g of resin) was added, the flask was capped, and left to stand at room temperature with occasional swirling for 2.5 hours. The resin was then filtered and washed with further portions of TFA and the filtrate collected in a round bottom flask. The cleavage mixture was then evaporated off under reduced pressure using a rotary evaporator (IKA® HB 10 Digital, IKA®-Werke GmbH & Co. KG, Staufen, Germany) until an oily residue was left in the flask. The crude peptide was precipitated by drop wise addition of ice-cold ether using a glass pipette. The first layer of ether (containing residual cleavage mixture) was carefully removed with a glass pipette. The peptide was then washed with two further portions of ether. The ether was removed using a glass pipette and the peptide was dispersed in a mixture of acetonitrile and water (80 : 20) and lyophilised.

In the case of O-Palm-Y-G-G-F-M, a cleavage mixture consisting of TFA/ethanedithiol/thianisole/anisole (90/3/5/2 % $^{v}/_{v}$) was added to the dry peptidyl resin (1 mL per 0.1g of resin) in a dry glass vial, the vial was capped, sealed with parafilm and placed in a water bath (25^{o} C; 120 rpm) for 2 hours. The resin was then filtered and washed with further portions of TFA and the filtrate collected in a round bottom flask. The cleavage mixture was then evaporated off under reduced pressure (rotary evaporator; IKA® HB 10 Digital, IKA®-Werke GmbH & Co. KG, Staufen, Germany) until an oily residue was left and the crude peptide was precipitated out by drop wise addition of cold double deionised (Millipore) water with a glass pipette and left in the fridge overnight. Cold ethanol was added to this and placed in the water bath (35^{o} C) for 45 minutes and a further portion of cold water (double deionised) was added to complete precipitation.

The peptide was obtained by centrifugation (4^{o} C; 5000 rpm) for 30 minutes with careful removal of the supernatant (with a glass pipette), this was repeated 3 times and the peptide washed with fresh portions of cold water after the second centrifugation. The peptide was recovered by dissolving the sediment in a mixture of acetonitrile and water (80 : 20) and then lyophilised.

4.6.2.2 Purification of synthesised PAs

The crude PAs were purified by preparative RP HPLC on a C_{18} derivatised silica gel based column (Atlantis, USA: 10 µm; 19 mm X 250 mm) in a Waters HPLC system consisting of a Waters 2487 Dual λ Absorbance Detector, Waters 600 Controller and Waters Delta 600 pump. The peptides were injected at a concentration of approximately 5 mg mL^{-1} and eluted using the gradient method of elution with the mobile phase comprising two solvent systems: 0.02% TFA/H_2O (Line A) and 90% MeCN /0.016% TFA/ H_2O (Line B).

For O-Palm-Y-G-G-L-R-F and G-G-Y-(O-Palm)-F-R-L, the peptides were first dissolved in Line B (and 90% MeCN /0.016% TFA/ H_2O) at low concentration (1 mg mL^{-1}), followed by centrifugation (30 minutes; 2000 rpm). The supernatant was carefully collected and then concentrated using a rotary evaporator (IKA® HB 10 Digital, IKA®-Werke GmbH & Co. KG, Staufen, Germany) to give a final concentration of approximately 5 mg mL^{-1}. The peptides were then purified using a gradient elution method in which the concentration of the organic phase (Line B) of the solvent system was increased over a period of 52 minutes (55 % - 100 %), at a flow rate of 15 mL min^{-1} (Appendix IV).

For O-Palm-Y-G-G-F-M on the other hand, the peptide was dissolved by first adding DMSO (100µL/ 20 mg sample) to the peptide and vortexing vigorously for about 30 seconds. Subsequently, MeOH was added to give a final peptide concentration of 5 mg mL^{-1}. The gradient elution was carried out by increasing the concentration of the organic phase (Line B) over a period of 40 minutes (55 % - 100 %) at a flow rate of 20.4 mL min^{-1} (Appendix V).

The eluent peaks (absorbance $\geq$ 0.2) at different retention times were collected in glass tubes and subjected to mass spectrometry analysis to identify the peak corresponding to the desired peptide mass. The fraction identified as the peptide peak was then freeze- dried and stored in the freezer (-20^{o}C).

4.6.2.2.1 Determination of purity

The level of purity for the purified PAs was determined by analytical RP HPLC using an analytical C_{18} derivatised silica gel based (Onyx Monolithic: 5 μm; 100 x 4.6 mm; Phenomenex UK) column using an Agilent Technologies 1200 Series HPLC system. The PAs were eluted using a gradient method comprising solvent systems: 0.02% TFA/H_2O (Line A) and 90% MeCN /0.016% TFA/ H_2O (Line B), by increasing the concentration of the organic phase (Line B) over a period of 20 minutes (0 – 100%) at a flow rate of 1.2 mL min^{-1} (Appendix VI). The chromatograms were acquired with the column temperature set at 40^o C and wavelength of detection was set at 214 nm. Following acquisition of chromatograms, all peaks were integrated and the percentage area under the curve (AUC) for the peptide peak was taken as the percentage purity for the peptide.

4.6.2.3 Characterisation of PAs

The PAs were characterised by mass spectrometry (MS), nuclear magnetic resonance (NMR), and self-assembly was studied by electron microscopy.

4.6.2.3.1 Mass Spectrometry (MS)

The eluent peptide peak (from prep RP HPLC) was submitted (1 mL) for MS analysis by ESI MS and tandem MS/MS. The samples were analysed by a direct infusion ESI-MS^n using an LTQ (Thermo Scientific, Hemel Hempstead, UK) linear ion trap mass spectrometer. The direct infusion was performed through a 250 µL Hamilton syringe at 15 $\mu Lmin^{-1}$ flow rate. The LTQ was operated so that the MS^2 event was performed after the MS scan. MS^2 was performed on $[M+H]^+$ ions. The scan time was 200 ms with 3 microscans. The collision energy was set to 35 (35 % of the output) for the MS^2 experiments.

4.6.2.3.2 Nuclear Magnetic Resonance (NMR)

The PAs were subjected to NMR analysis. The peptides (8mg) were dissolved in deuterated DMSO (0.7mL), bath sonicated and transferred into the NMR tubes. The NMR spectra were acquired on a Bruker AMX Ultrashield^{TM} 400 MHz Spectrometer.

4.6.2.3.3 Self-assembly

The self-assembly of the PAs was studied by TEM imaging using a Philips (FEI) CM 120 Bio Twin Transmission Electron Microscope (Philips, Eindhoven, The Netherlands) and scanning electron microscopy (SEM) using a FEI QUANTA 200 F microscope (Eindhoven, The Netherlands). Also, molecular dynamics (MD) simulations was carried out on O-Palm-Y-G-G-L-R-F and G-G-Y- (O-Palm)-F-R-L.

4.6.2.3.3.1 TEM

PAs nanofibres were prepared by vortexing for 30 seconds and then probe sonication (QSonica sonicator, Connecticut, USA) of the aqueous peptide (1mgmL^{-1} in double deionised water) dispersions on ice at amplitude of 15. The PAs were probe sonicated for a total time of 5 minutes and 15 minutes for each PA to assess the ease with which they self-assemble into nanofibers. For TEM imaging, a drop of the peptide dispersion was placed on a formvar/ carbon coated grid and excess sample was blotted off on a filter paper (Whatman No 1). The samples were then negatively stained (uranyl acetate 1 % $^{w}/_{v}$) and left for 1 – 2 minutes to air dry. Subsequently, images were captured on the TE microscope using an AMT digital camera (5 mega pixels; AMT Deben, UK Ltd).

4.6.2.3.3.2 SEM

For SEM imaging, the PA dispersions were prepared as described above and then diluted (1 in 10) with double deionised water to avoid excessive clumping. A thin layer of the dispersion for each PA was then applied unto a microscope stub and left in a desiccator (*in vacuo*) to dry. The resulting film on the stub was subsequently coated with a layer of gold (10 nm) using a sputter coater prior to imaging. SEM micrographs were subsequently acquired on the SE microscope.

4.6.2.3.3.3 Molecular dynamics (MD) simulations of PA self-assembly

MD simulations was employed to study the molecular organisation of O-Palm-Y-G-G-L-R-F and G-G-Y- (O-Palm)-F-R-L into nanofibres. To be able to assess the microsecond timescales required for observation of self-assembly, the MARTINI 2.1 coarse-grained (CG) potential for lipids (Marrink et al. 2007) and proteins (Monticelli et al. 2008) were employed, with slight refinement which made it possible to capture the chemistry of the PAs more accurately.

4.6.2.3.3.3.1 Atomistic MD simulation

To refine the CG model, 50 ns of atomistic MD simulation of O-Palm-Y-G-G-L-R-F (linear PA) and G-G-Y- (O-Palm)-F-R-L ("T"-PA) were initially performed in TIP3P (Jorgensen et al. 1983) water using the CHARMM all atom force field (Brooks et al. 1983). The partial charges on the modified tyrosyl residues were defined based on parameters obtained for a related PA, palmitoyl dalargin (Mazza et al. 2013). A timestep of 2 fs was used for the simulations and the temperature was coupled to 300 K using the Nose-Hoover thermostat (Nose 1984; Hoover 1985) while the pressure was coupled to 1 bar using the Parrinello-Rahman barostat (Nose 1983; Parrinello and Rahman 1981). Lennard-Jones interactions were cut off at 1.0 nm and electrostatic interactions were calculated using the particle-mesh Ewald approach with a real-space cut off of 1.0 nm. Following the simulations, the bond angle distributions were calculated from the trajectory and used as target data for refinement of the CG models (Appendix VII).

4.6.2.3.3.3.2 CG MD simulation

CG linear and "T"-PAs were built using a mapping scheme (Figure 4-5). Essentially this follows the standard mapping for amino acid residues in the MARTINI 2.1 protein force field (Brooks et al. 1983) except for the modified TYR residue which was represented by three hydrophobic particles (aromatic ring), one polar particle (ester group) and four additional hydrophobic particles (hydrocarbon tail) [Figure 4-5]. As the MARTINI protein force field requires secondary structure information as an input parameter, the peptide backbone was initially assumed to adopt an extended β-sheet structure. The bond angle distributions from the atomistic simulations were then used to refine the equilibrium bond angles in the CG models.

To achieve this, simulations of a single CG peptide in water were carried out and the bond angle parameters (equilibrium bond angle and force constant) were iteratively modified until optimal agreement with the bond angle distributions from the atomistic simulations was achieved. The final set of bond angle parameters (Appendix VII), bond (length) parameters, bond constraints and improper dihedrals on the aromatic rings were unchanged from the native MARTINI force field. This optimal set of parameters was used in all subsequent simulations of PA self-assembly.

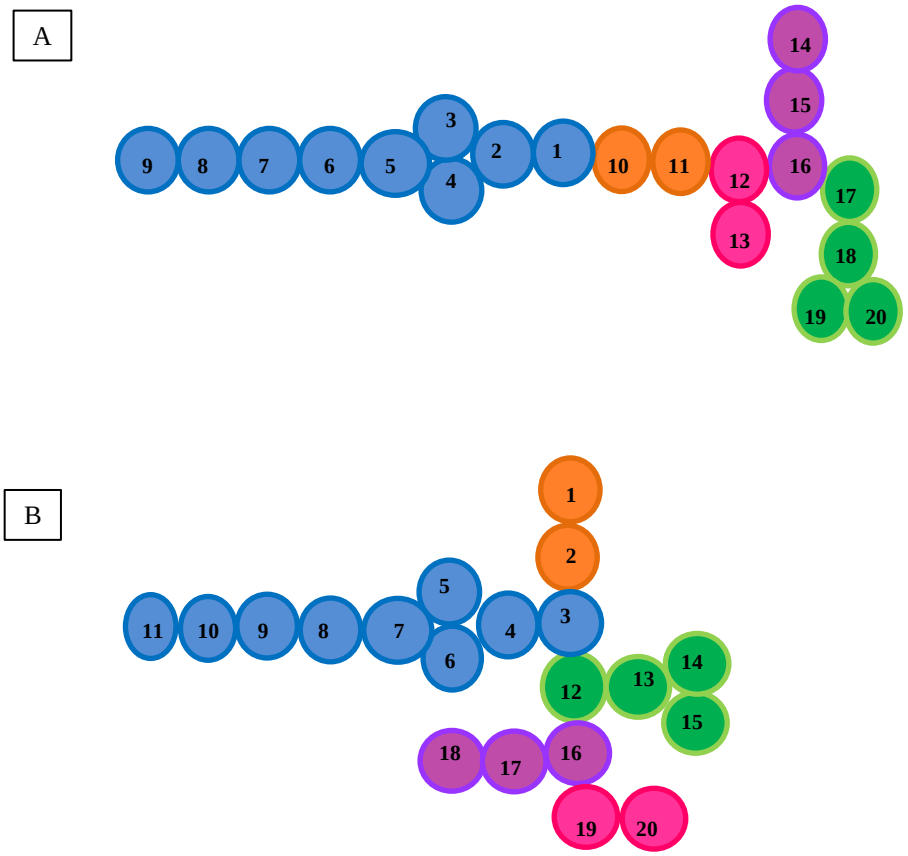

Figure 4-5: Coarse-grained mapping scheme for A: O-Palm-Y-G-G-L-R-F (Linear PA) and B: G-G-Y- (O-Palm) - F-R-L ("T"-PA)

Key: Blue beads: Palmitoyl-Tyrosine residue; orange beads: Glycine residues; pink beads: Leucine residue; purple beads: Arginine residue; green beads: Phenylalanine residue.

4.6.2.3.3.3.3 Initial configurations

Initial configurations for the self-assembly simulations were generated by randomly inserting 512 PAs into a cubic box and then solvating with 25600 CG water particles (each CG water particle represents four real water molecules) and 512 chloride counterions. Three different random configurations were generated for each of the PAs.

To reveal the structure of the ends of the nanofibres we performed two additional simulations (one each of the linear and "T"-PA) of a more dilute solution of 512 PAs in 51200 CG water particles and 512 chloride counterions. Enlarging the simulation box in this way prevented the growing nanofibre from spanning the boundaries of the periodic simulation cell and thus it was possible to simulate the assembly of an isolated nanofibre and observe the arrangements of the peptide amphiphiles at the ends of the nanofibres.

4.6.2.3.3.3.4 CG simulation parameters

Simulations were carried out in the isothermal – isobaric (Gibbs) ensemble (NPT) in which the temperature and pressure are constrained, that is, they have specified average values (Hünenberger 2005). The temperature of the system was maintained at 300 K and isotropic pressure coupling was applied to maintain a pressure of 1 bar using the Berendsen thermostat and barostat (Berendsen et al. 1984). Electrostatic and Lennard-Jones interactions were shifted to zero between 0.9 nm and the cut-off distance, which was 1.2 nm. Coordinates were saved every 5000 steps for analysis. To equilibrate the solvent around the peptides, MD simulations were carried out for 900 ns, with position restraints of 1000 kJ mol^{-1} on all peptide particles, followed by 600 ns, with position restraints of 10 kJ mol^{-1} on all peptide particles. Over this time the volume of the simulation cell shrank from 20.0 nm^3 to 17.3 nm^3. The time step for all the CG simulations was 30 fs. Following equilibration, MD simulations of self-assembly was carried out for at least 5 μs for each PA.

4.6.3 **Results**

The three peptides: O-Palm-Y-G-G-L-R-F, G-G-Y- (O-Palm)-F-R-L, and Palm- Y-G-G-F-M were successfully synthesized. Characterisation data confirmed synthesis and the ability of the PAs to assemble into nanofibers in aqueous medium was revealed by TEM and SEM micrographs.

4.6.3.1 Mass spectrometry

Mass spectrometry revealed the expected mass for the compounds: electrospray ionization m/z calculated for $C_{50}H_{79}N_9O_9$ = 950.22; found 950.75 $(M+H)^+$ for O-Palm-Y-G-G-L-R-F (Figure 4-6) and 950.87 $(M+H)^+$ for G-G-Y- (O-Palm)-F-R-L (Figure 4-9) and m/z calculated for $C_{43}H_{65}O_8S$ = 812.07; found 834.62 $(M+Na)^+$ for O-Palm-Y-G-G-F-M (Figure 4-12). Also, MS/MS spectra showed correct amino acid sequence for the three peptides (Figure 4-7; Figure 4-10; Figure 4-13) as deduced from the resulting fragment peaks (Table 4-1; Table 4-2; Table 4-3).

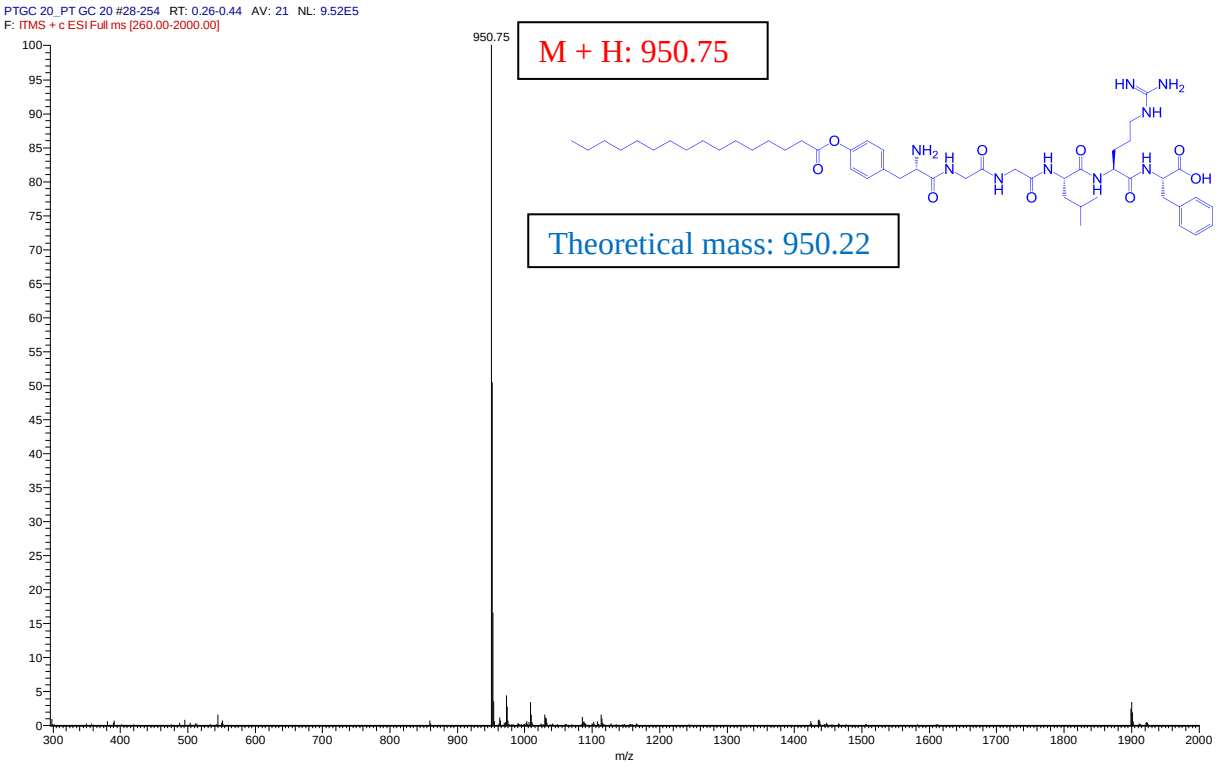

Figure 4-6: ESI MS spectra for O-Palm-Y-G-G-L-R-F

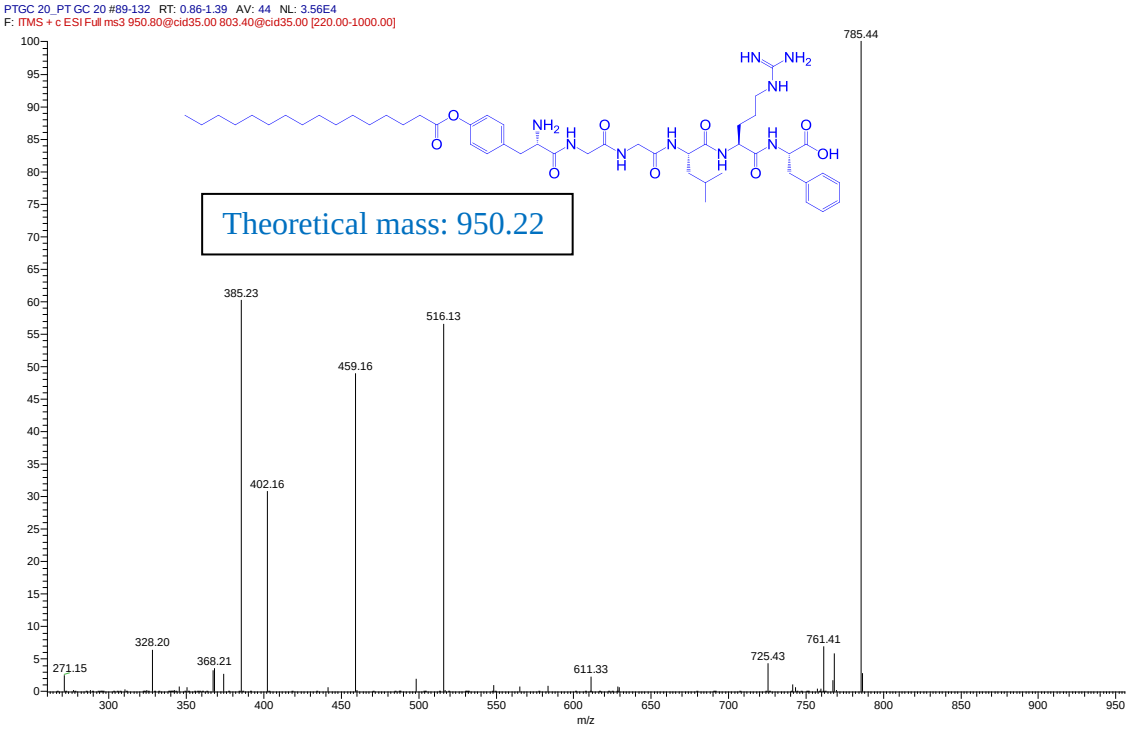

Figure 4-7: MS/MS spectra for O-Palm-Y-G-G-L-R-F

m/z	**Corresponding fragment ion**
915.47	(M + H) – $2H_20$
785.44	(M + H) – F
516.13	[(M + H) – F] – R- L
459.16	{[(M + H) – F] – R- L} – G
402.16	{[(M + H) – F] – R- L} – G – G = Y-(O- palmitoyl)
385.23	Y-(O- palmitoyl) – OH

Table 4-1: MS/MS peak assignment for O-Palm-Y-G-G-L-R-F

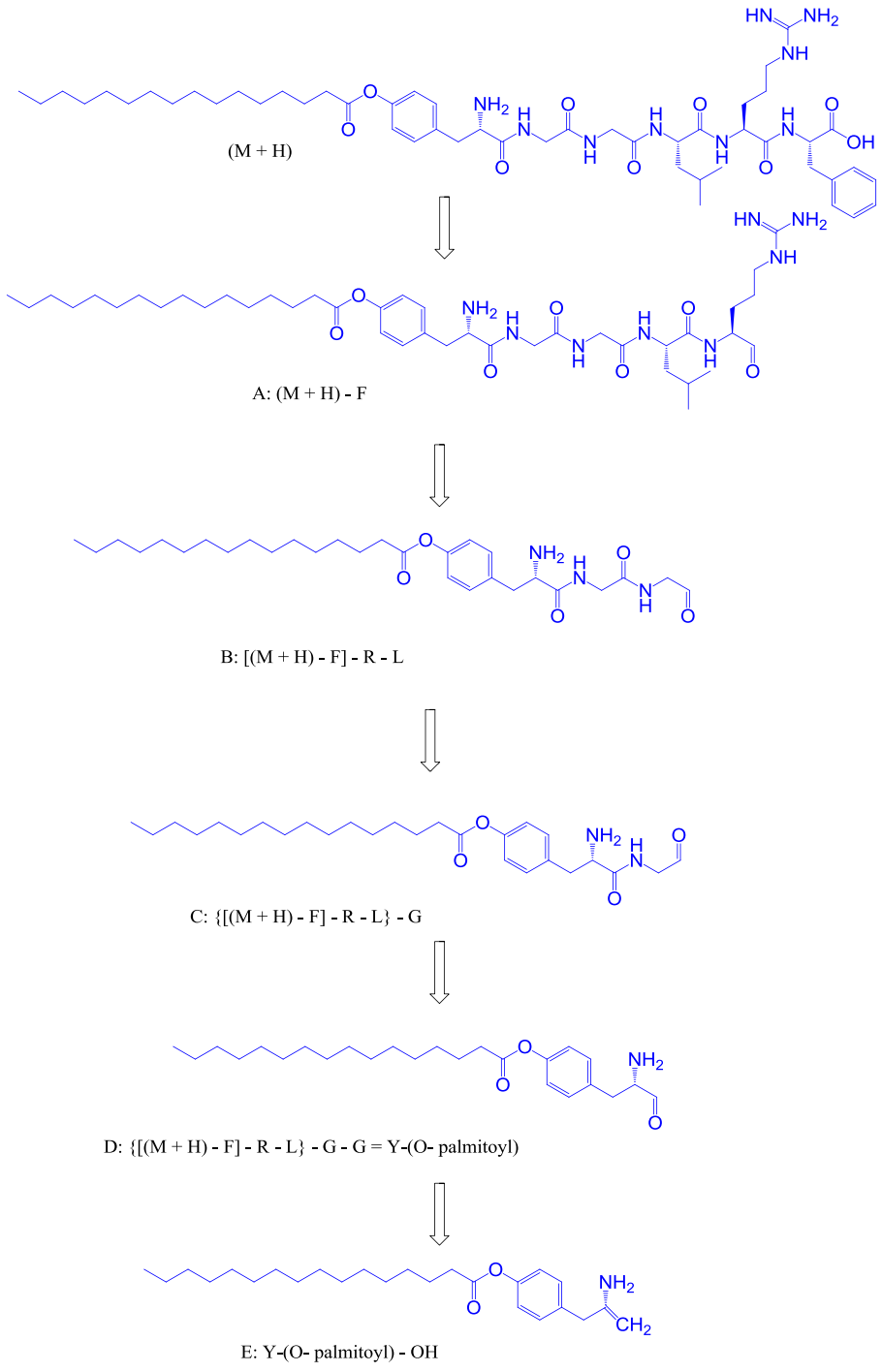

Figure 4-8: Major MS/MS fragment ions for O-Palm-Y-G-G-L-R-F

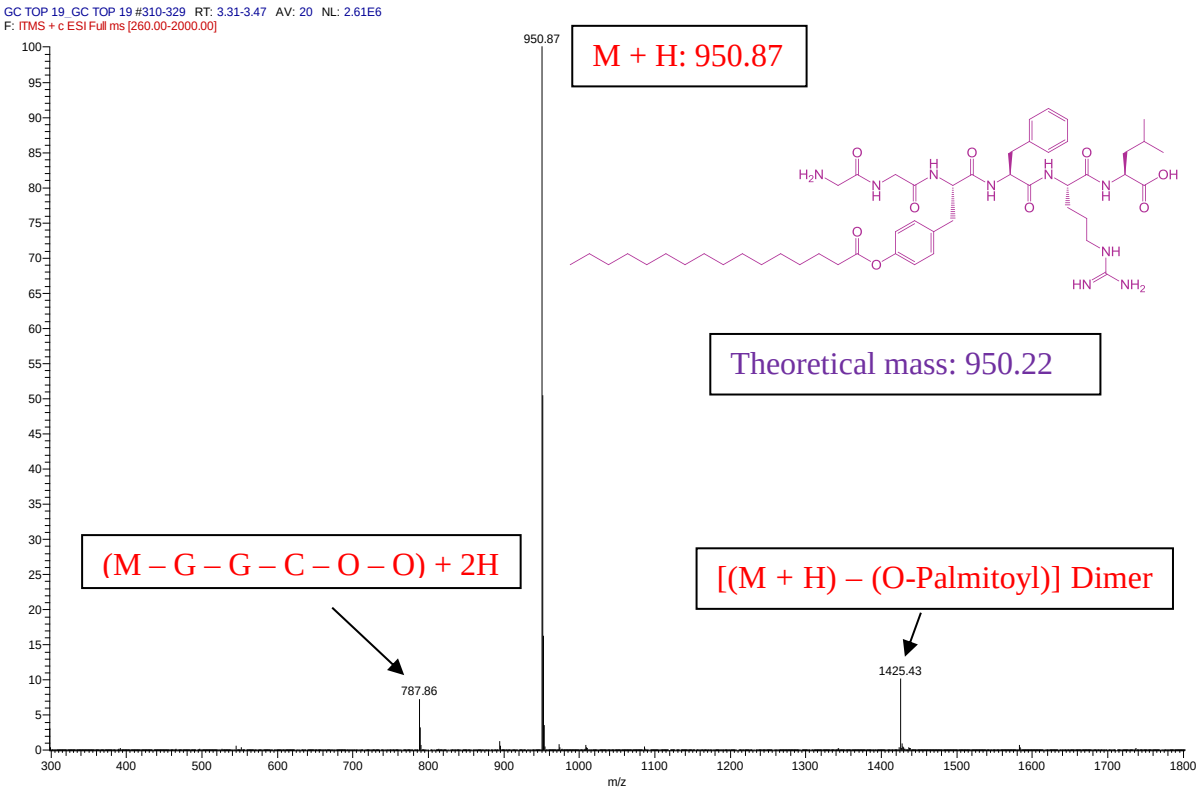

Figure 4-9: ESI MS spectra for G-G-Y- (O-Palm) - F-R-L

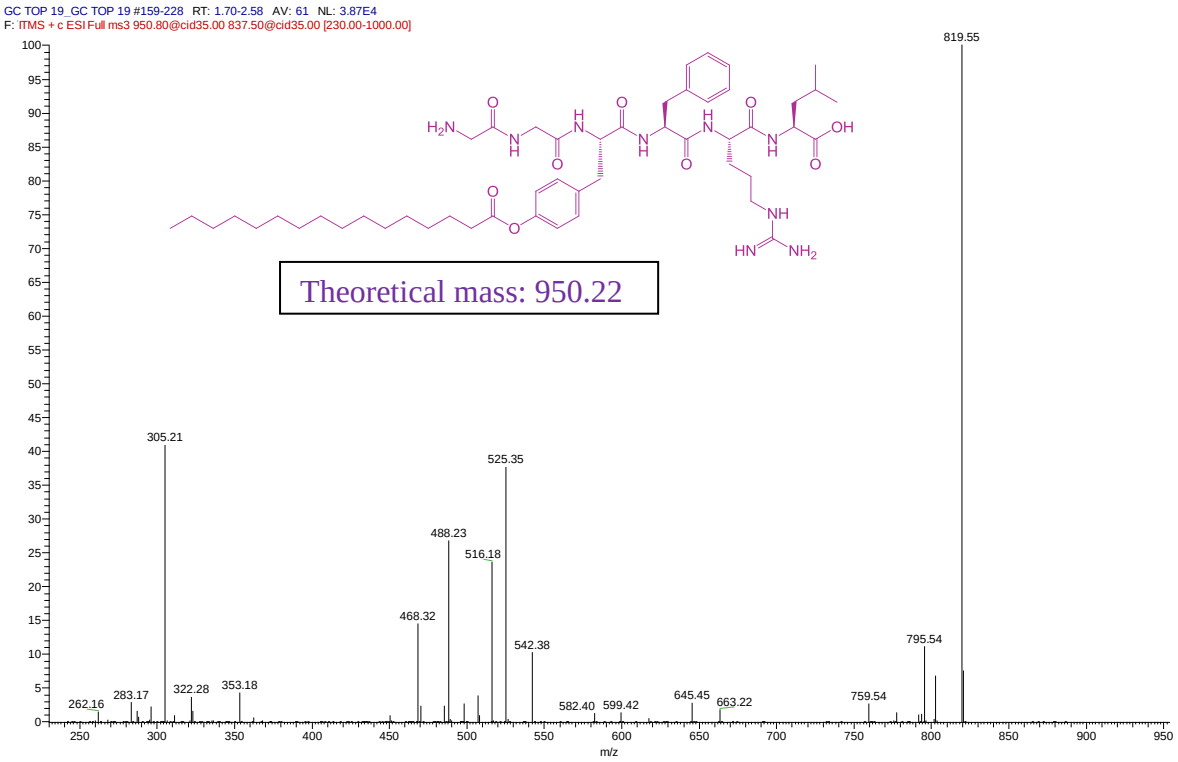

Figure 4-10: MS/MS spectra for G-G-Y- (O-Palm) - F-R-L

m/z	**Corresponding fragment ion**
819.55	$(M + H) – L – H_2O$
795.54	$[(M + H) – L – H_2O] – CN + 2H^+$
759.54	$\{[(M + H) – L – H_2O] – CN + 2H^+\} – 2(H_2O)$
542.38	$\{[(M + H) – L – H_2O] – CN + 2H^+\} – 2(H_2O) – R – CNO – H_2O – H^+$
525.35	$\{[(M + H) – L – H_2O] – CN + 2H^+\} – 2(H_2O) – R – CNO – H_2O – H^+ – OH$
516.18	$[(M + H) – L – H_2O] – R – F$
488.23	$\{[(M + H) – L – H_2O] – R – F\} – CO$
468.32	$\{[(M + H) – L – H_2O] – R – F\} – CO – H_2O – 2H^+$
305.21	$\{[(M + H) – L – H_2O] – R – F\}$ – (O-Palmitoyl) + (CHO) = G-G-Y + CHO

Table 4-2: MS/MS peak assignment for G-G-Y- (O-Palm) - F-R-L

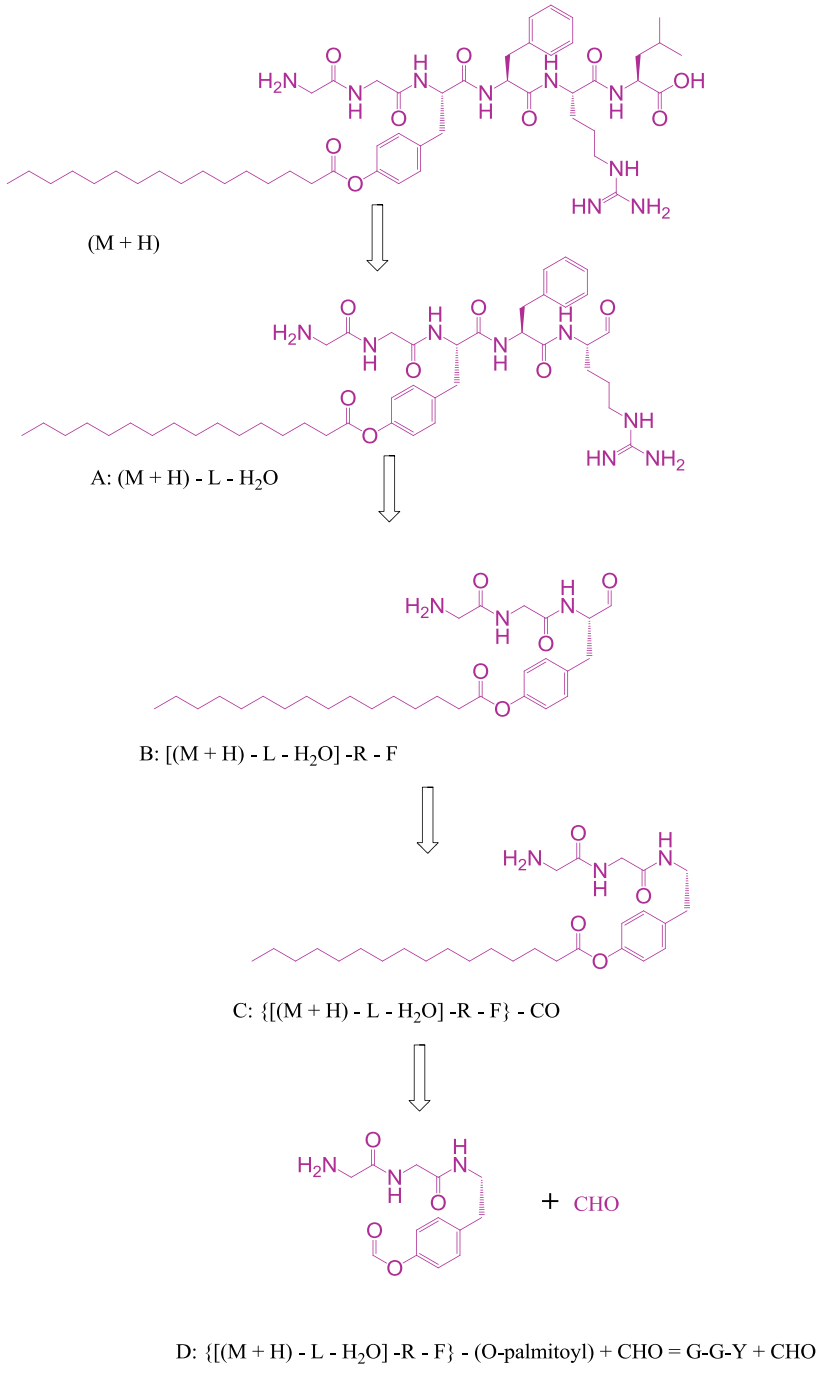

Figure 4-11: Major MS/MS fragment ions for G-G-Y- (O-Palm) - F-R-L

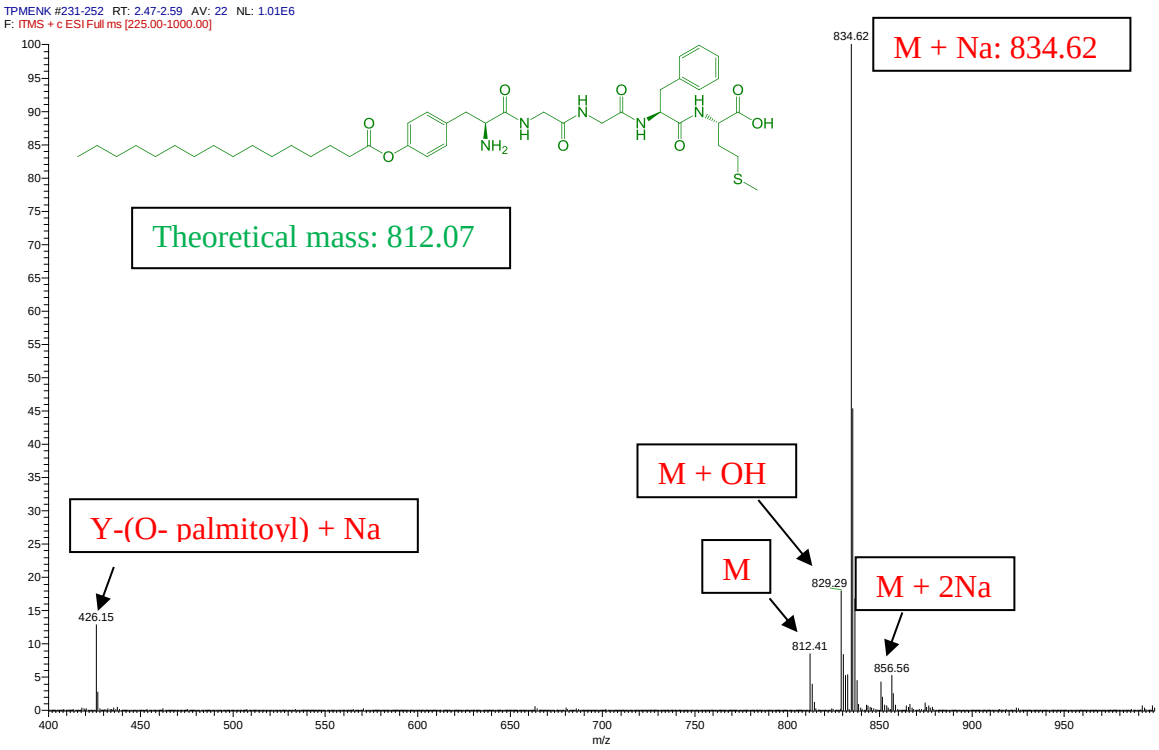

Figure 4-12: ESI spectra for O- Palm-Y-G-G-F-M

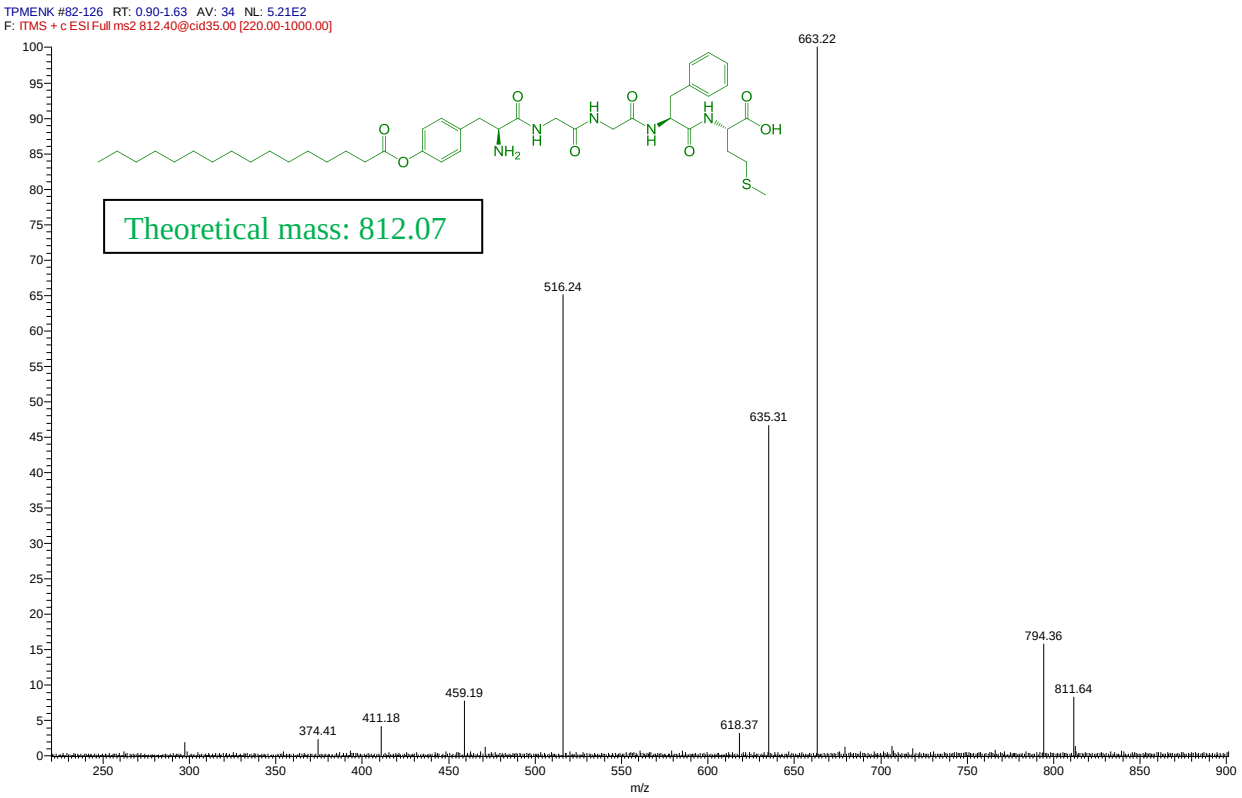

Figure 4-13: MS/MS spectra for O- Palm-Y-G-G-F-M

m/z	**Corresponding fragment ion**
811.64	M – H
794.36	M – H_2O
663.22	(M- H_2O) – M^5
635.31	[(M- H_2O) – M^5] – CO
618.37	{[(M- H_2O) – M^5] – CO} – OH
516.24	(M- H_2O) – M^5 – F
459.19	{(M- H_2O) – M^5 – F] – G
411.18	[(M- H_2O) – M^5 – F] – G – C – $2H_2O$
374.41	{[(M- H2O) – M^5 – F] – G – C – $2H_2O$ – G} + H_2O + 2H = Y-(O- palmitoyl) – CO

Table 4-3: MS/MS peak assignment O- Palm-Y-G-G-F-M

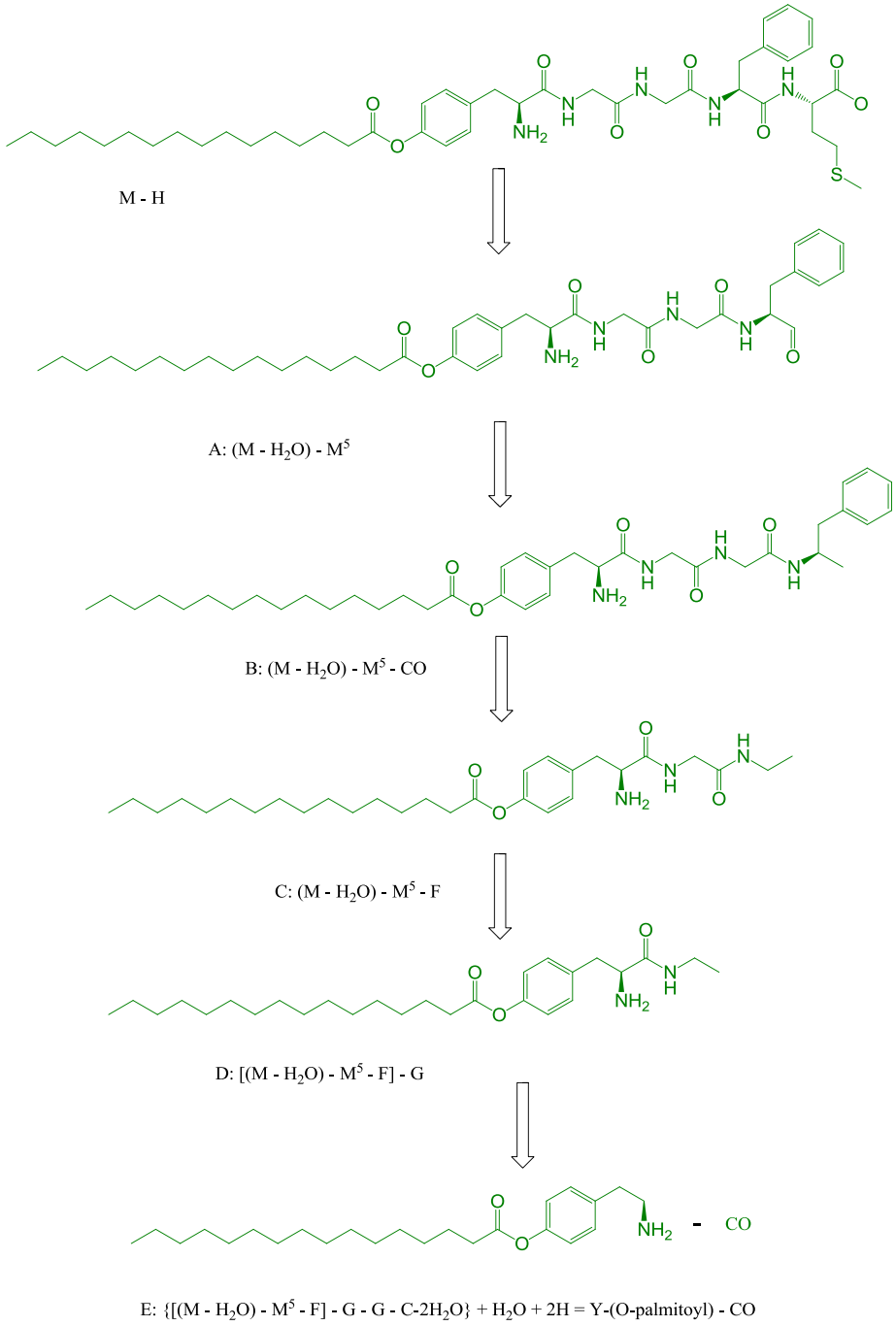

Figure 4-14: Major MS/MS fragment ions for O- Palm-Y-G-G-F-M

4.6.3.2 Nuclear magnetic resonance (NMR)

The ^{1}HNMR spectra [interpreted with the aid of COSY (fixed) spectra] acquired for the peptides revealed the relevant proton peaks in the synthesised PAs (Figure 4-15; Figure 4-16; Figure 4-17; Appendix IX A – C).

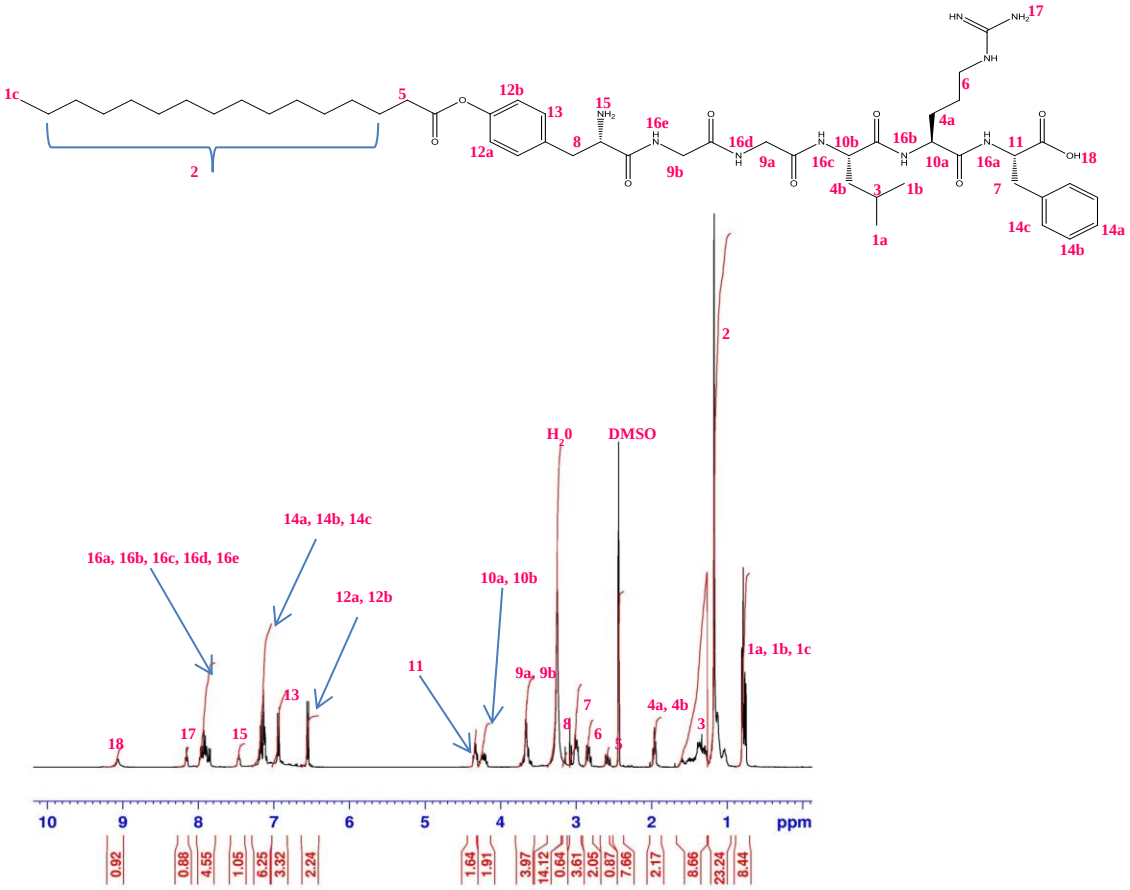

Figure 4-15: ^{1}HNMR spectra for O-Palm-Y-G-G-L-R-F

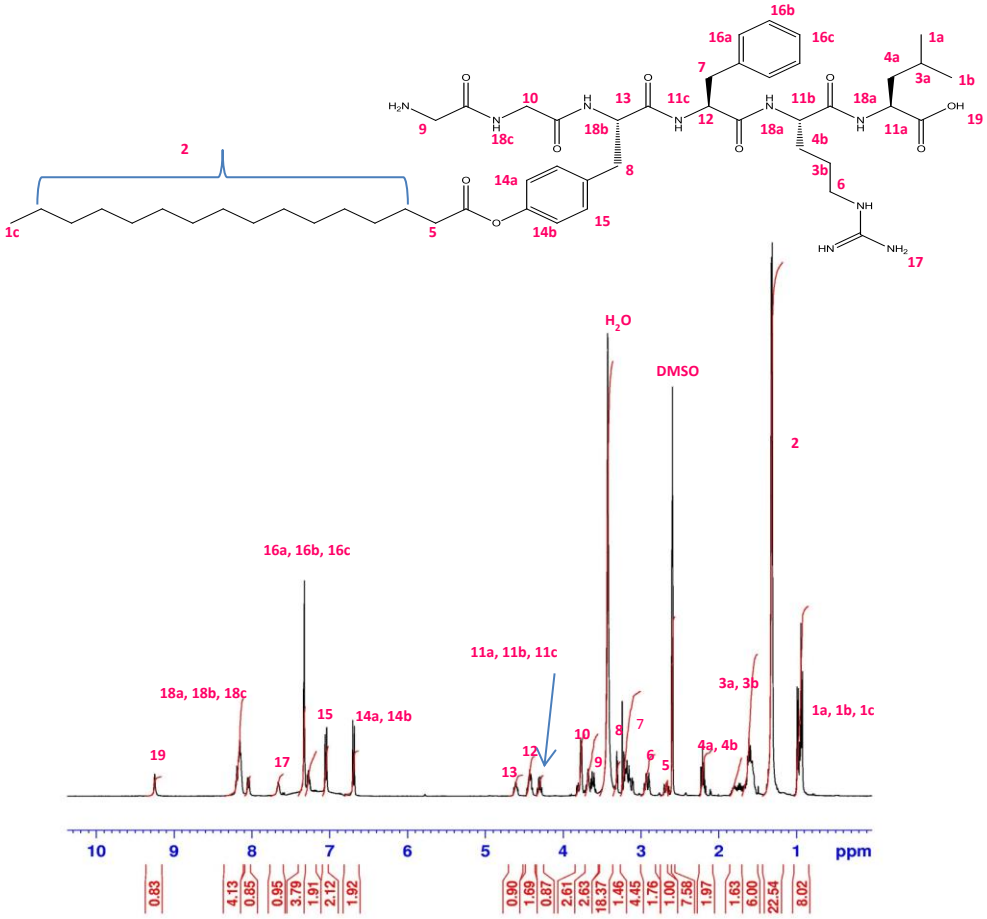

Figure 4-16: ^{1}HNMR spectra for G-G-Y- (O-Palm) - F-R-L

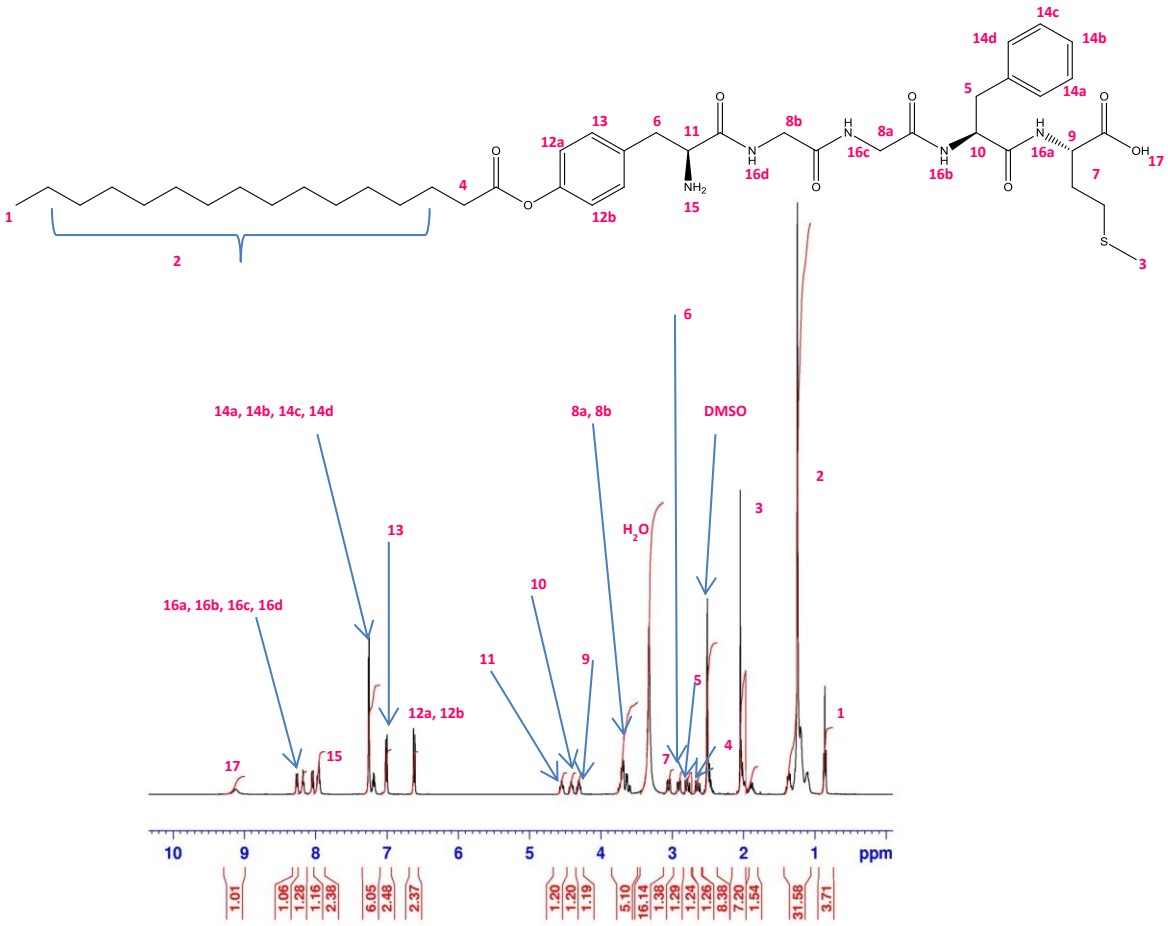

Figure 4-17: ^{1}HNMR spectra for O- Palm-Y-G-G-F-M

4.6.3.3 Determination of purity

Analytical RP HPLC of the purified PAs showed that a purity level higher than 90 % was achieved for the three PAs following preparative RP HPLC purification (Figure 4-18; Figure 4-19; Figure 4-20)

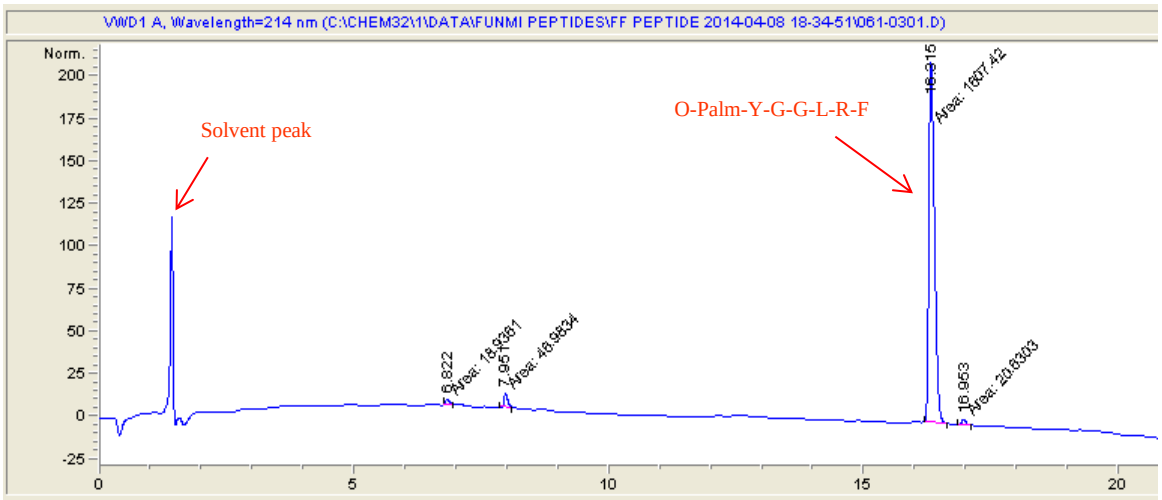

#	Time	Area	Height	Width	Area%	Symmetry
1	6.822	18.9	3.5	0.0914	1.118	0.583
2	7.951	47	8.6	0.0916	2.774	0.574
3	16.315	1607.4	211.8	0.1265	94.891	0.554
4	16.953	20.6	3.6	0.096	1.218	1.013

Figure 4-18: Analytical RP HPLC chromatogram for O-Palm-Y-G-G-L-R-F

Linear gradient 0 – 100 % organic phase (90 % MeCN/0.016 % TFA/H_2O) over 20 minutes.

The HPLC chromatograph showed that the purity level achieved for O-Palm-Y-G-G-L-R-F was 95 %, with a retention time of 16.315 minutes using the gradient system employed (Figure 4-18).

For G-G-Y- (O-Palm) - F-R-L, analytical HPLC revealed a purity of 91 % with a retention time of 16.893 minutes (Figure 4-19).

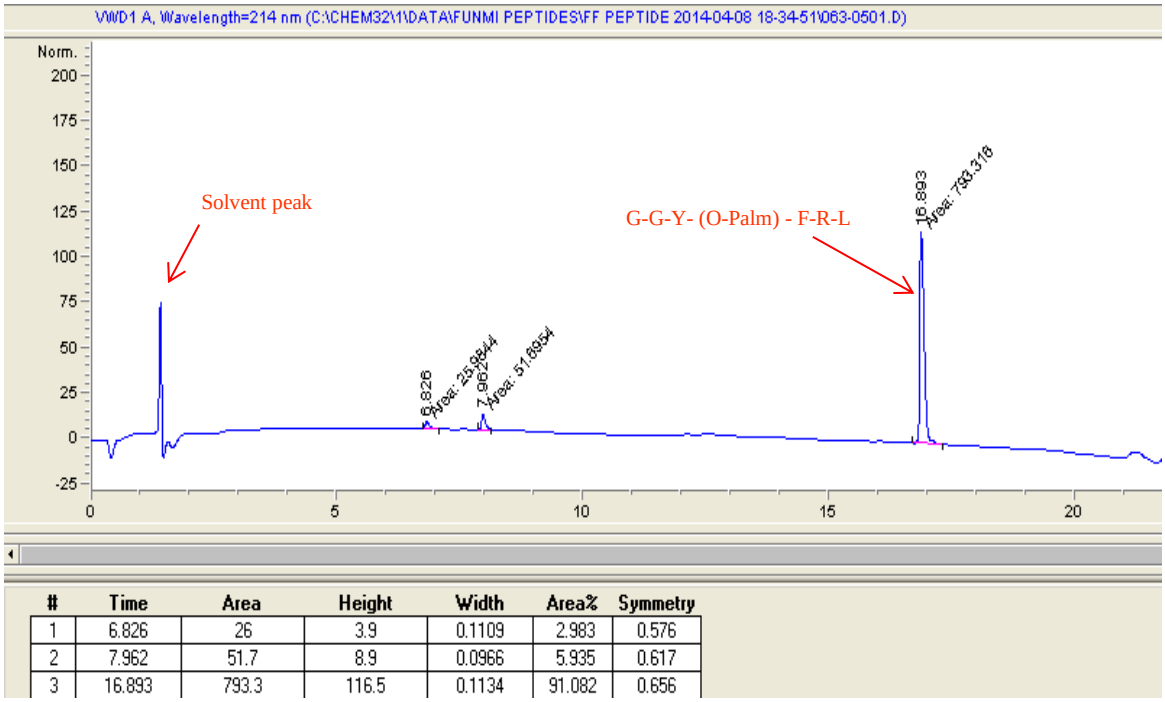

#	Time	Area	Height	Width	Area%	Symmetry
1	6.826	26	3.9	0.1109	2.983	0.576
2	7.962	51.7	8.9	0.0966	5.935	0.617
3	16.893	793.3	116.5	0.1134	91.082	0.656

Figure 4-19: Analytical RP HPLC chromatogram for G-G-Y- (O-Palm) - F-R-L

Linear gradient 0 – 100 % organic phase (90 % MeCN/0.016 % TFA/H_2O) over 20 minutes.

Analytical RP HPLC for O-Palm-Y-G-G-F-M also showed the purity to be 94 % with a retention time of 18.241 minutes (Figure 4-20).

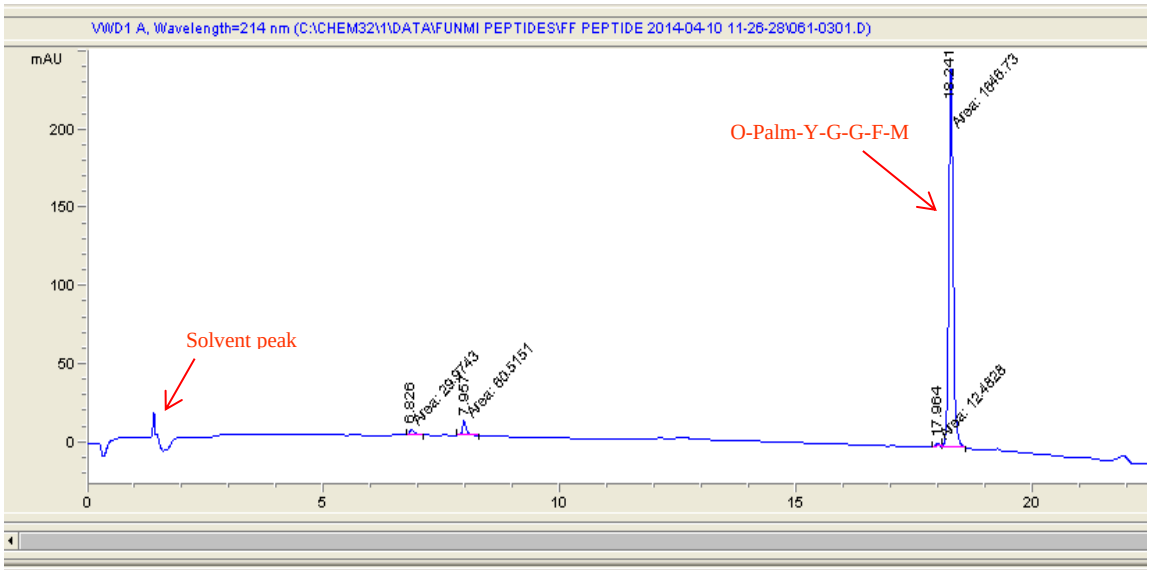

#	Time	Area	Height	Width	Area%	Symmetry
1	6.826	30	4	0.1239	1.713	0.462
2	7.957	60.5	9.5	0.1062	3.459	0.633
3	17.964	12.5	2.3	0.0895	0.713	1.154
4	18.241	1646.7	242.6	0.1131	94.115	0.762

Figure 4-20: Analytical RP HPLC chromatogram for O-Palm-Y-G-G-F-M.

Linear gradient 0 – 100 % organic phase (90 % MeCN/0.016 % TFA/H2O) over 20 minutes.

4.6.3.4 Self-assembly

4.6.3.4.1 TEM

TEM micrographs have shown that all three PAs synthesised can self-assemble into nanofibres in aqueous medium (Figure 4-21; Figure 4-22; Figure 4-23), irrespective of the position of the acyl chain.

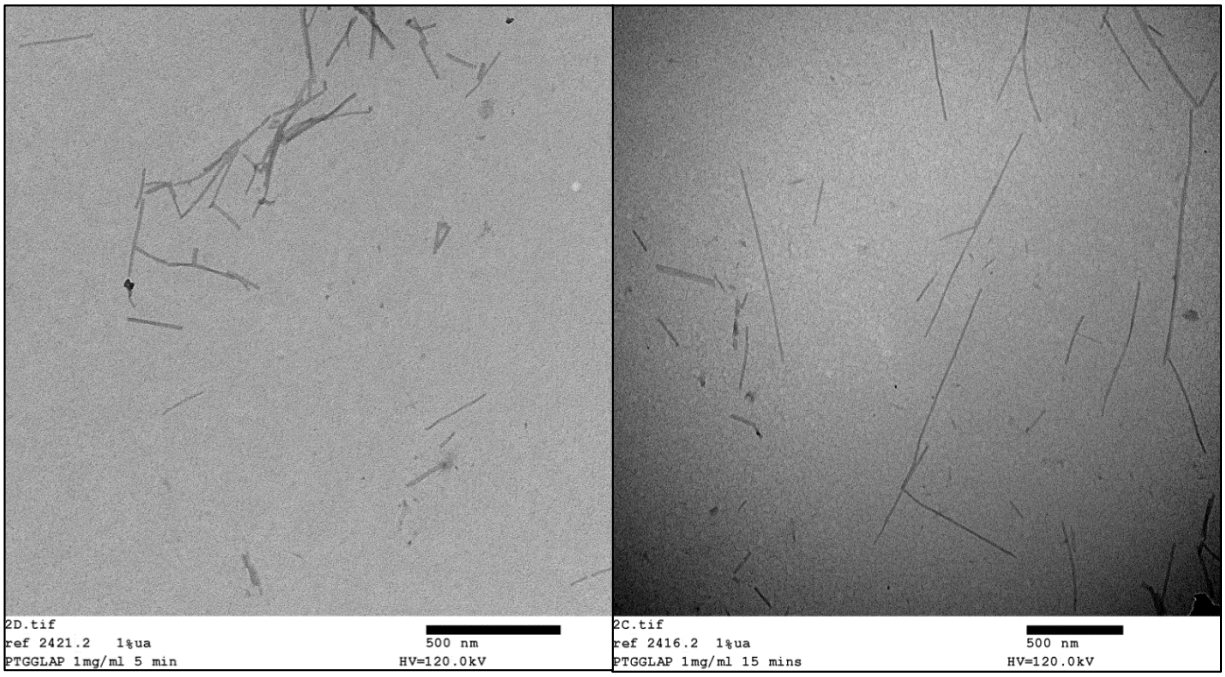

Figure 4-21: TEM micrographs for O-Palm-Y-G-G-L-R-F (1 mg mL^{-1})

O-Palm-Y-G-G-L-R-F (1 mg mL^{-1}) in double deionised water, vortexed for 30 seconds then probe sonicated (QSonica sonicator, Connecticut, USA) on ice for 5 minutes (left) or 15 minutes (right) at amplitude of 15.

The TEM micrographs show formation of nanofibres measuring 10 – 12 nm in diameter with variable length up to 1 µm. The nanofibres are formed mostly as individual fibres with straight needle-like morphology [Figure 4-21; Appendix X (A)].

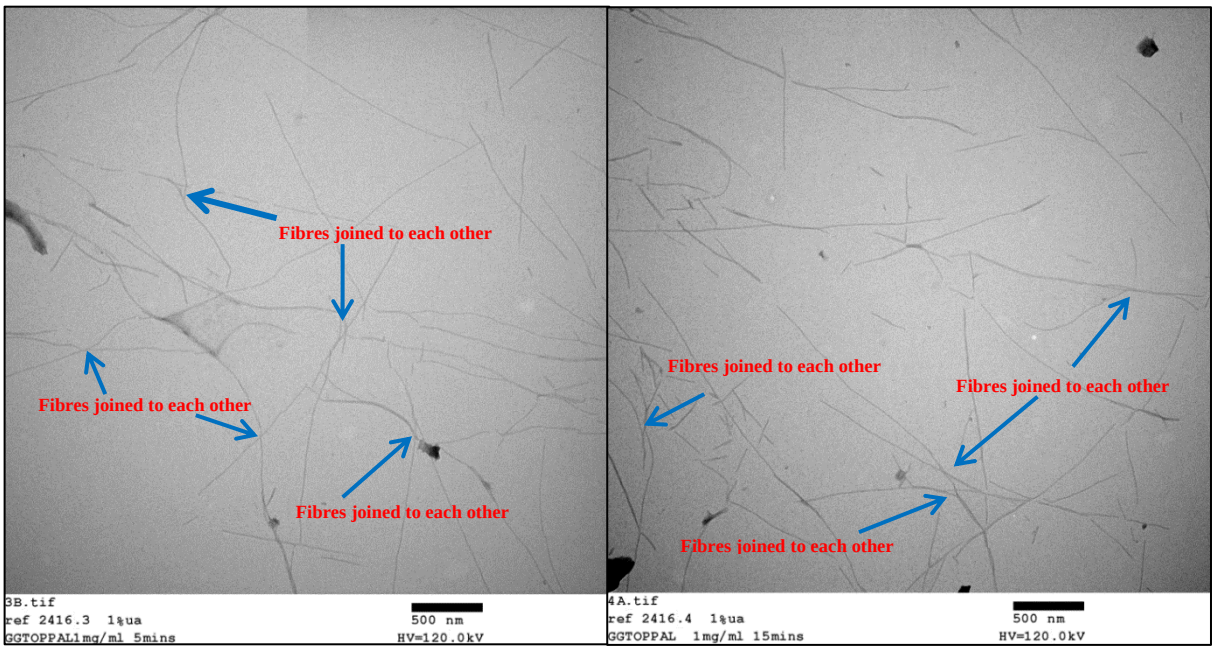

Figure 4-22: TEM micrographs for G-G-Y- (O-Palm) - F-R-L (1 mg mL^{-1})

G-G-Y- (O-Palm) - F-R-L (1 mg mL^{-1}) in double deionised water, vortexed for 30 seconds then probe sonicated (QSonica sonicator, Connecticut, USA) on ice for 5 minutes (left) or 15 minutes (right) at amplitude of 15.

The TEM micrographs reveal formation of nanofibres approximately 10 nm in diameter while the length varies up to almost 1.5 µm. The nanofibres show an extensive network of fibres which are well formed even from the short sonication time of 5 minutes [Figure 4-22; Appendix X (B)].

Although both O-Palm-Y-G-G-L-R-F (linear PA) and G-G-Y- (O-Palm) - F-R-L ("T"-PA) have been shown to self-assemble into nanofibres, the resulting assemblies from the two PAs possess distinct morphologies as seen in the TEM micrographs (Figure 4-21; Figure 4-22). While O-Palm-Y-G-G-L-R-F self-assemble to form mostly straight individual fibres in aqueous medium, G-G-Y- (O-Palm) - F-R-L forms thinner, slightly curved and longer fibres which are joined to each other appearing to form a network of fibres (Figure 4-22). This might be the result of the difference in the molecular architecture of the two PAs. Although they comprise the same amino acids and so would be expected to possess more or less the same properties, O-Palm-Y-G-G-L-R-F has a linear arrangement while G-G-Y- (O-Palm) - F-R-L is shaped like a "T". The mid-chain location of the acyl chain in the "T"-PA may lead to enhanced hydrophobic as well as $\pi - \pi$ interactions of the tyrosyl and phenylalanyl side chains, leading to the formation of extensive fibre networks at a concentration as low as 1 mg mL^{-1} (0.1 % $^{w}/_{v}$) in aqueous medium. This might be indicative of the possibility for gel formation at an even lower concentration than the concentrations (0.25 – 0.5 % $^{w}/_{v}$) that had been previously reported in literature.

At these relatively low concentrations (0.25 – 0.5 % $^{w}/_{v}$), ionic PAs had been shown to self-assemble into nanofibres which can then entangle into networks to form self-supporting gels as a result of lowering the pH or addition of metal ions (Beniash et al. 2005; Stendahl et al. 2006). The induction of gelation in the PAs as a result of lowering the pH or addition of metal ions implies that their self-assembly is initiated by the screening of their charges by counterions in the medium, leading to a reduction in the double layer repulsive forces. Subsequently, other non-covalent attractive forces such as such as van der Waals and hydrophobic forces, ionic bridging, coordination and hydrogen bonding promote close association of the amphiphilic molecules to form the nanofibres (Stendahl et al. 2006).

Therefore, apart from metal ions, self-assembly and stability of nanofibre gels formed by the PAs are also greatly influenced by the interplay of factors related to the chemistry of each individual PA such as hydrophobic interactions including attraction between hydrophobic tails, intermolecular interaction of the side chains of hydrophobic amino acid residues, hydrophilic repulsion, hydrogen bonding in the peptide region, and the molecular geometry in relation to amphiphilic packing (Beniash et al. 2005; Stendahl et al. 2006). In these PAs, the formation of supramolecular nanofibres which impede the thermal motion of the solution and resist external shear stress, lead to the transition from the liquid state to a self-supporting gel (Stendahl et al. 2006).

Thus, in contrast to a linear PA comprising the same amino acids (O-Palm-Y-G-G-L-R-F), the "T"-PA [G-G-Y- (O-Palm) - F-R-L] demonstrated the ability to form extensive nanofibre networks in aqueous medium (double deionized water) at a concentration as low as 0.1 % $^{w}/_{v}$, which may be attributed to the unique molecular architecture ("T"-shape) of G-G-Y- (O-Palm) - F-R-L.

The TEM micrographs for O-Palm-Y-G-G-F-M reveal the formation of short, slightly twisted nanofibres approximately 10 nm – 20 nm in diameter and less than 500 nm in length. The nanofibres tend to occur with two or three fibres close together and they also lie across each other to form short nanofibre networks [Figure 4-23; Appendix X (C)].

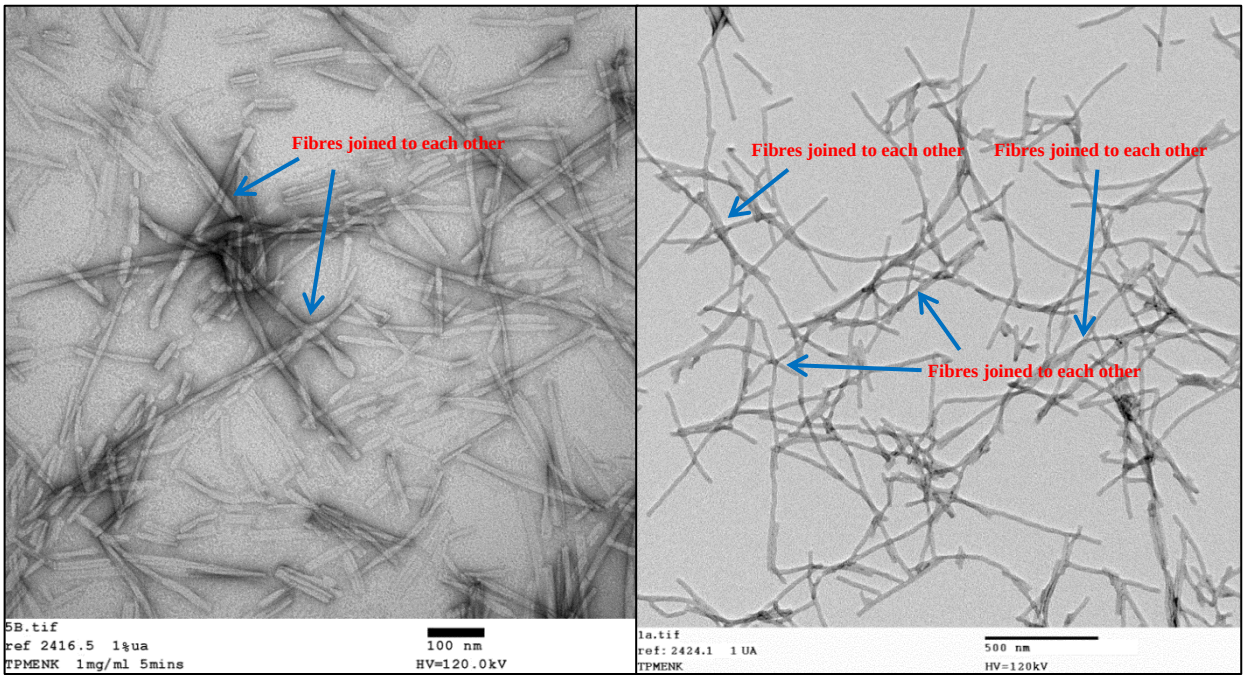

Figure 4-23: TEM micrographs for O-Palm-Y-G-G-F-M (1 mg mL^{-1})

O-Palm-Y-G-G-F-M (1 mg mL^{-1}) in double deionised water, vortexed for 30 seconds then probe sonicated (QSonica sonicator, Connecticut, USA) on ice for 5 minutes (left) or 15 minutes (right) at amplitude of 15.

4.6.3.5 SEM

SEM micrographs also show that all the three PAs synthesized self-assemble into nanofibers (Figure 4-24; Figure 4-25; Figure 4-26).

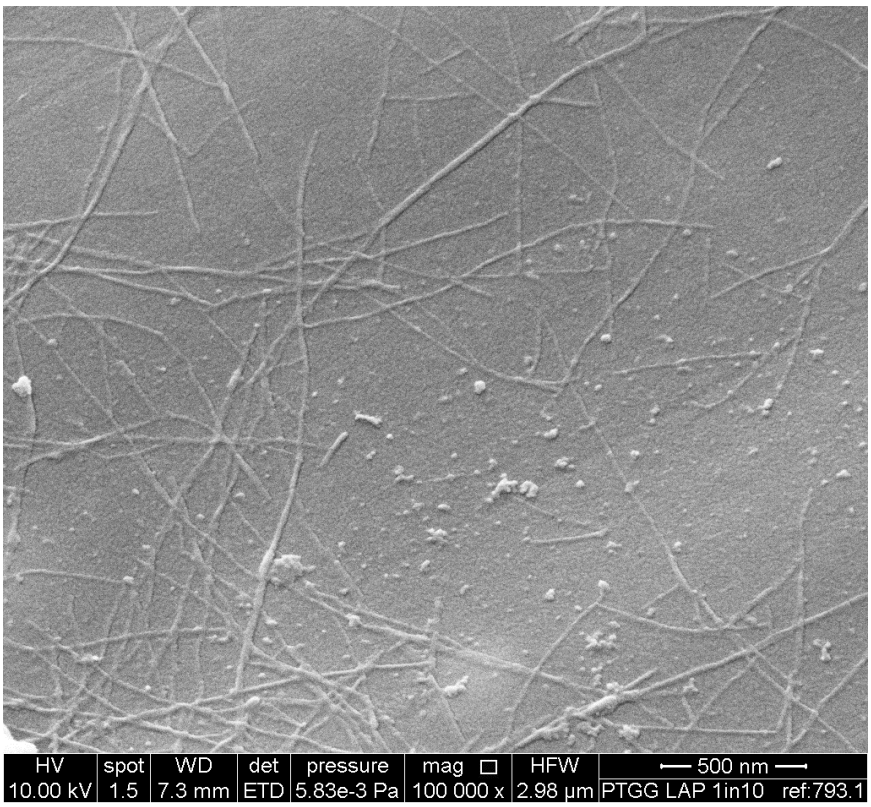

Figure 4-24: SEM micrograph for O-Palm-Y-G-G-L-R-F (1 mg mL^{-1})

O-Palm-Y-G-G-L-R-F (1 mg mL^{-1}) in double deionised water, vortexed for 30 seconds then probe sonicated (QSonica sonicator, Connecticut, USA) on ice for 15 minutes at amplitude of 15; diluted 1 in 10 before preparation for imaging.

The SEM micrograph shows nanofibers of the PA as well as clumps of the PA on the stub surface (Figure 4-24).

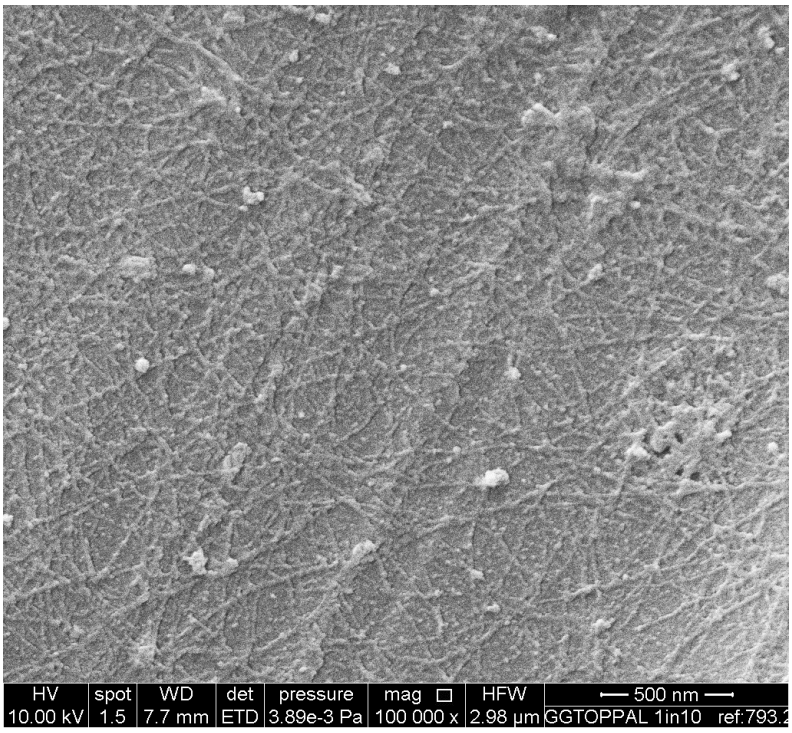

Figure 4-25: SEM micrograph for G-G-Y- (O-Palm) - F-R-L (1mg mL^{-1})

G-G-Y- (O-Palm) - F-R-L (1 mg mL^{-1}) in double deionised water, vortexed for 30 seconds then probe sonicated (QSonica sonicator, Connecticut, USA) on ice for 15 minutes at amplitude of 15, diluted 1 in 10 before preparation for imaging.

The SEM micrograph show nanofibers of the PA as well as some clumps of dried PA on the stub surface (Figure 4-25).

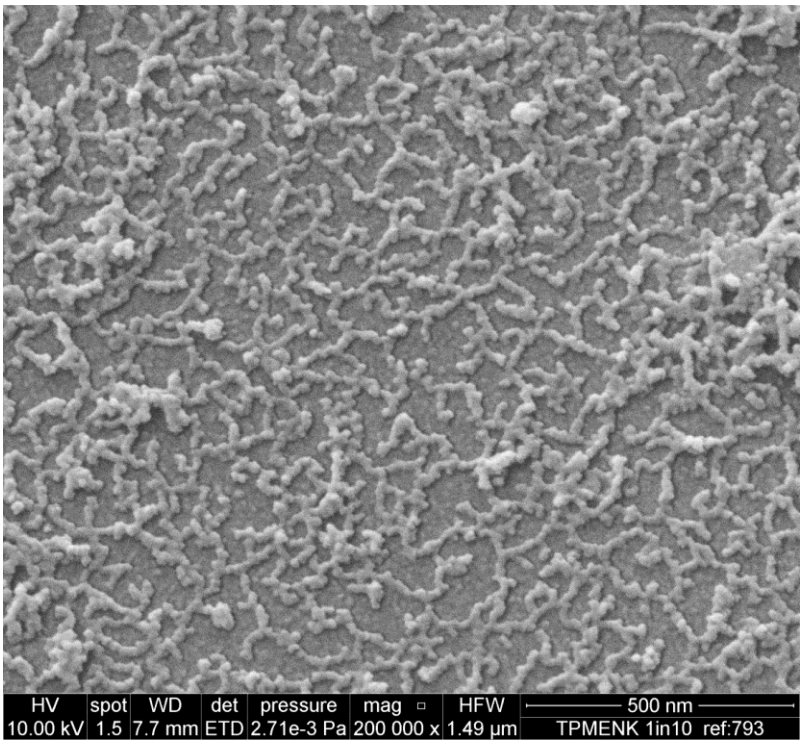

Figure 4-26: SEM micrographs for O-Palm-Y-G-G-F-M (1 mg mL^{-1})

O-Palm-Y-G-G-F-M (1 mg mL^{-1}) in double deionised water, vortexed for 30 seconds then probe sonicated (QSonica sonicator, Connecticut, USA) on ice for 15 minutes at amplitude of 15, diluted 1 in 10 before preparation for imaging

The SEM micrographs show nanofibers of the PA as well as a few clumps from aggregates in the sample (Figure 4-26).

The SEM micrographs for O-Palm-Y-G-G-F-M reveal the formation of short networks of twisted PA nanofibres. Although O-Palm-Y-G-G-F-M is also able to form fibre networks in aqueous medium (double deionized water) at low concentration (0.1 % w/v), the fibre networks observed in the case of O-Palm-Y-G-G-F-M are short and are not continuous (Figure 4 26) as the networks observed for G-G-Y- (O-Palm) - F-R-L (Figure 4 25).

4.6.3.6 Molecular Dynamics (MD) modelling

4.6.3.6.1 Coarse-grain MD modelling simulations

MD modelling using coarse-grained (CG) models was successfully applied to model the self-assembly of O-Palm-Y-G-G-L-R-F: terminal acyl chain and G-G-Y- (O-Palm) - F-R-L: mid-chain located acyl chain.

The CG MD simulations data showed nanofibre formation for both the linear PA (O-Palm-Y-G-G-L-R-F) with terminal acyl chain (Figure 4-27) and the "T"-PA [G-G-Y-(O-Palm) - F-R-L] with mid-chain located acyl chain (Figure 4-28).

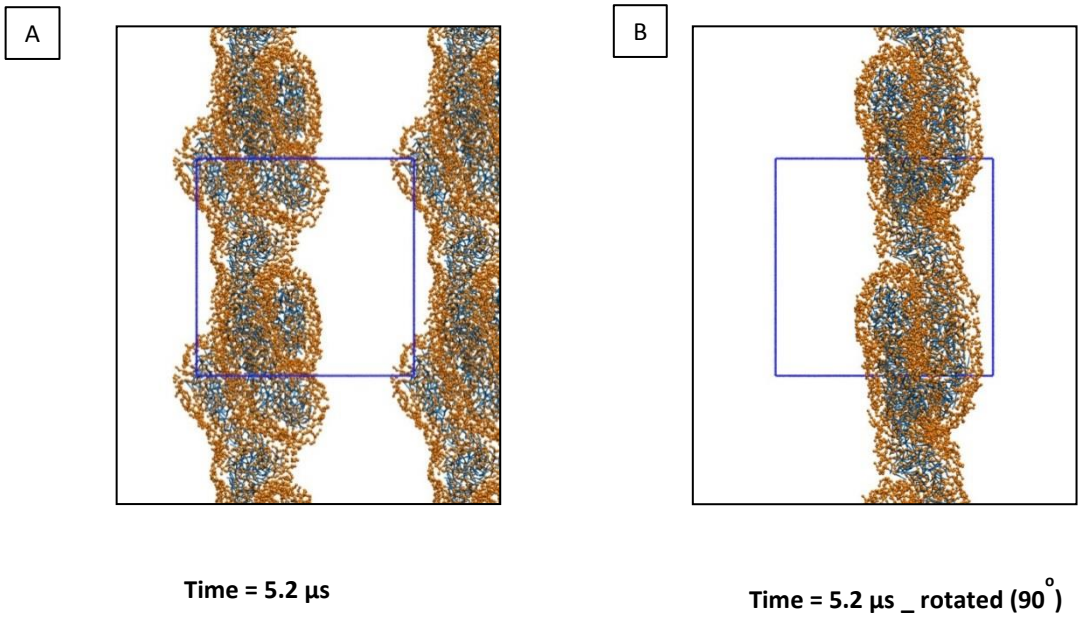

Figure 4-27: Snapshots of the simulations of nanofibre formed through self-assembly of O-Palm-Y-G-G-L-R-F (Linear PA)

Key: Orange spheres: Peptide backbone; blue lines: acyl chain. Side chain particles, water and ions are removed for clarity.

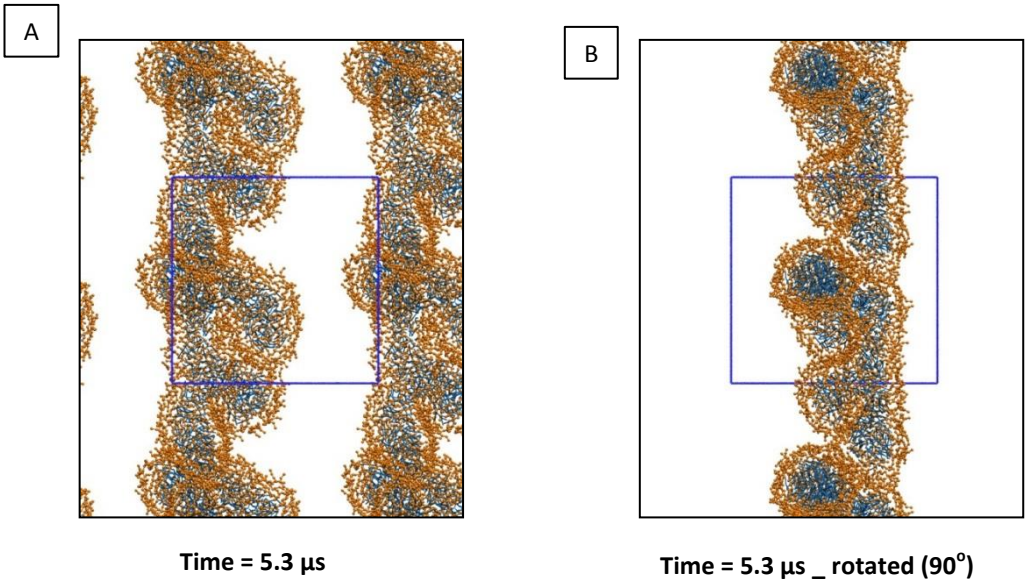

Figure 4-28: Snapshots of the simulations of nanofibre formed through self-assembly of G-G-Y-(O-Palm) - F-R-L ("T"-PA)

Key: Orange spheres: Peptide backbone; blue lines: acyl chain. Side chain particles, water and ions are removed for clarity.

In the self-assembly process, the "T"-PA seemed to have a tendency to aggregate more quickly and to a greater extent, with the final assembled fibre showing the formation of multiple inter-chain contacts (networks). Also, the fibres appear to exhibit what looks like a branch to varying extents in the final assembly, which was observed in three independent simulation runs for the peptide (Figure 4-29; Appendix XI). The linear PA on the other hand exhibited somewhat slower aggregation with lower degree of inter-chain contacts (Figure 4-30). Branching was observed in one out of three simulation runs for the linear PA (Appendix XII). The branching and networks observed in the "T"-PA may be the result of the architecture of this PA.

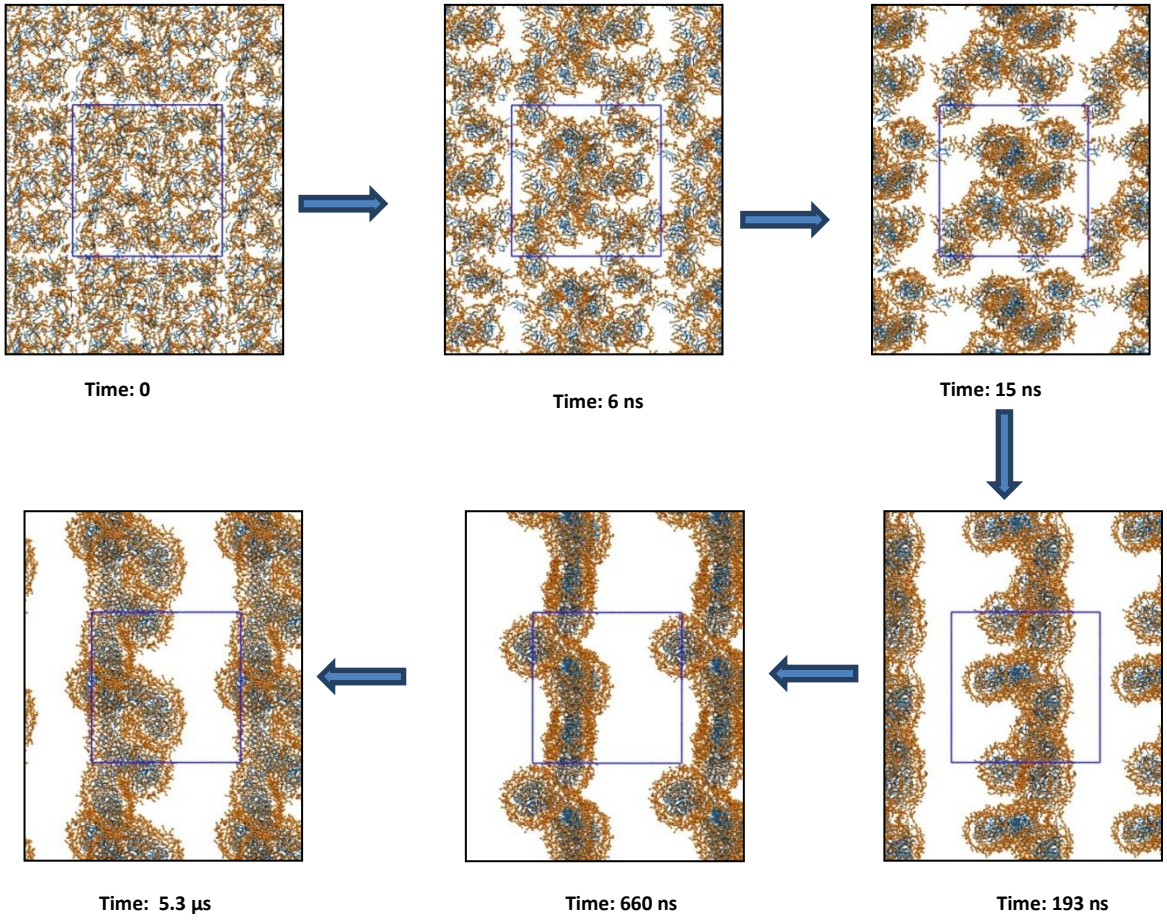

Figure 4-29: Snapshots of the simulation of the self-assembly process for G-G-Y-(O-Palm) - F-R-L at different time intervals during the simulation

Key: Orange spheres: Peptide backbone; blue lines: acyl chain. Side chain particles, water and ions are removed for clarity.

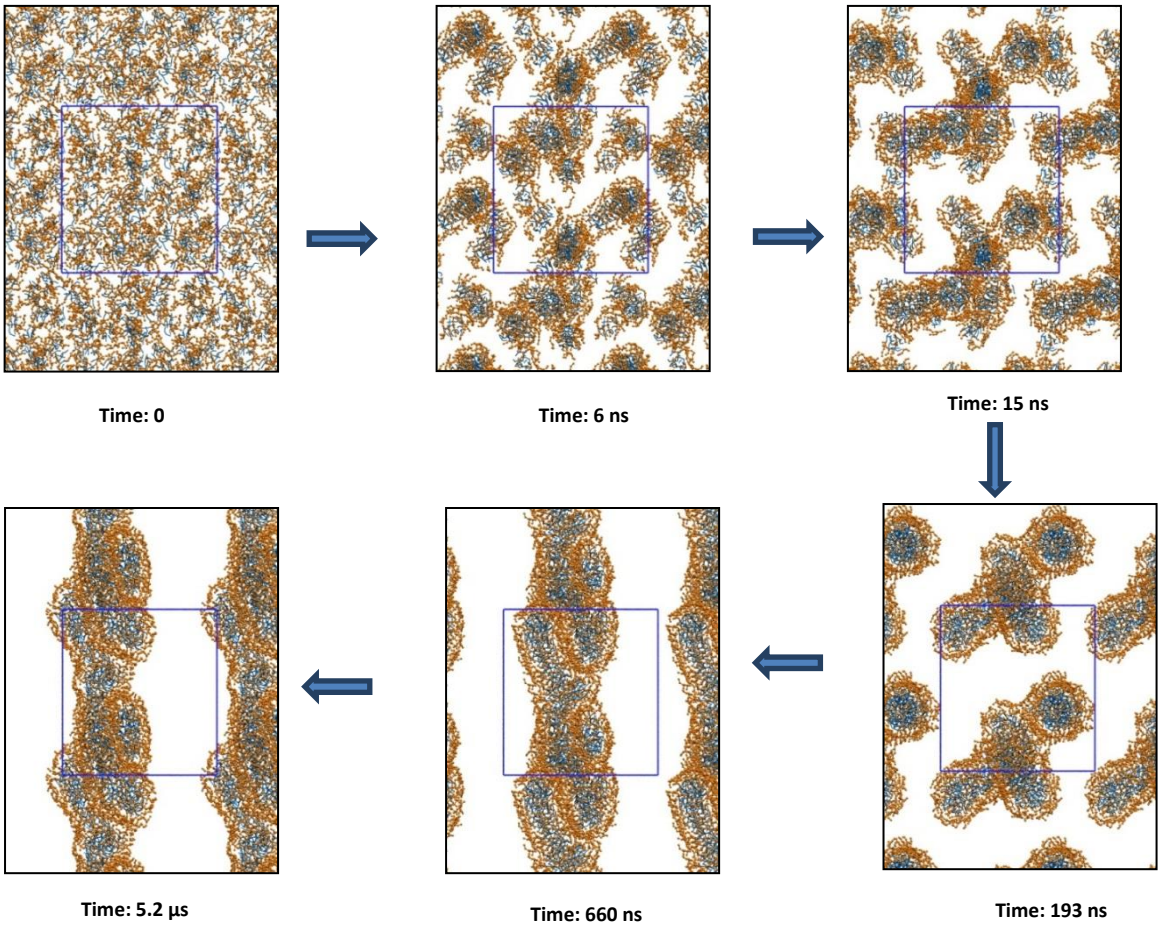

Figure 4-30: Snapshots of the simulation of the self-assembly process for O-Palm-Y-G-G-L-R-F

Key: Orange spheres: Peptide backbone; blue lines: acyl chain. Side chain particles, water and ions are removed for clarity.

In the "T"-PA, the acyl chain-modified tyrosyl residue is located in the mid-region rather than at the end of the molecule and is next to the phenylalanyl residue which also has a phenyl side chain. Thus, in the "T"-PA, the bulky groups are located in the middle of the PA while there is no bulky group at the end of the molecule. Intermolecular contact of the hydrophobic side chains of amino acid residues of PA may enhance the driving force for the self-assembly of PAs (Beniash et al. 2005). The location of the phenyl side chains for both the tyrosyl and phenyalaninyl residues in the mid-region will also result in the $\pi - \pi$ interactions of the phenyl rings which also contribute to the self-assembly (Reches and Gazit 2003; Paramonov et al. 2006; Yan et al. 2008) to be concentrated in the mid-region. Thus in the "T"-PA, the multiple inter-chain contacts observed may be the result of the localization of the hydrophobic as well as $\pi - \pi$ interactions in the mid-region of the PA molecule which fostered multiple inter-chain bonding of the PA molecules. This resulted in the formation of the extensive fibre networks and branching observed for the "T"-PA. In the linear PA on the other hand, the acyl chain-modified tyrosyl residue and the phenylalanyl residue are located far apart in the PA molecule thus resulting in the reduced inter-chain contacts observed in this PA.

4.6.3.6.2 Radial distribution function (RDF)

The RDFs for O-Palm-Y-G-G-L-R-F and G-G-Y- (O-Palm) - F-R-L suggest the formation of antiparallel β- sheets by the two peptides (Figure 4-31; Figure 4-32).

RDFs serve as a means of determining the probability of finding a particular atom type within a specified distance of another atom chosen as the reference. The peaks generated reveal the extent of the interaction between the two atoms such that a big and sharp peak is indicative of a strong interaction (Langham et al. 2007).

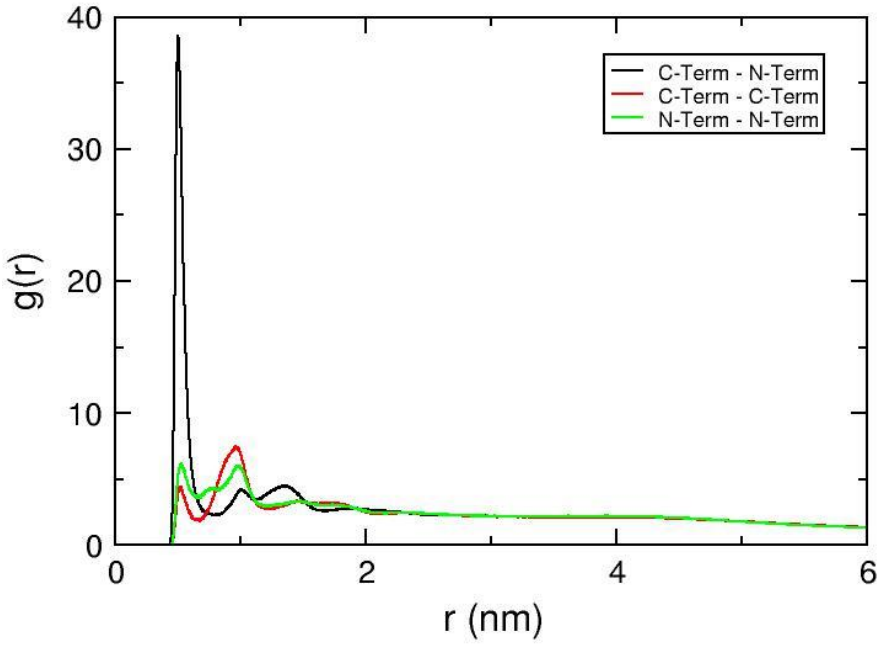

Figure 4-31: Radial distribution function for O-Palm-Y-G-G-L-R-F

Key: r is the distance in nm; g(r) is the probability of finding an atom within the distance tested

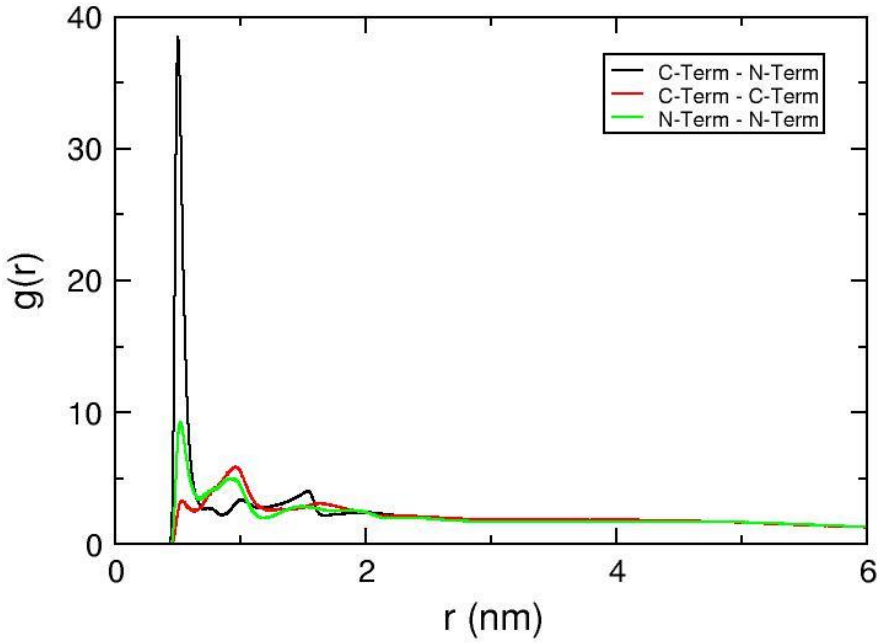

Figure 4-32: Radial distribution function for G-G-Y- (O-Palm) - F-R-L

Key: r is the distance in nm; g(r) is the probability of finding an atom within the distance tested

The RDFs for both O-Palm-Y-G-G-L-R-F and G-G-Y- (O-Palm) - F-R-L showed similar peak patterns for the termini tested. (Figure 4-31; Figure 4-32).

The RDFs reveal a sharp peak for C- terminus and N- terminus atoms for both peptides. However, there are some differences in the heights of the peaks for the other termini interactions. For O-Palm-Y-G-G-L-R-F, there was a slightly higher peak for the C- terminus and C- terminus atoms whereas for G-G-Y- (O-Palm) - F-R-L, the peak for N- terminus and N- terminus atoms was higher than that for O-Palm-Y-G-G-L-R-F (Figure 4-31; Figure 4-32).

The RDFs suggest antiparallel β-sheet formation for both O-Palm-Y-G-G-L-R-F and G-G-Y- (O-Palm) - F-R-L as the peak obtained for the interaction of the C- terminus and the N- terminus is sharp indicating that there is a strong interaction as would be expected for atoms in close proximity (Langham et al. 2007). The differences obtained for the peak of the interaction for the other termini may be as a result of the differences in their molecular architecture.

4.6.4 **Discussion and conclusions**

The PAs synthesized were successfully purified to relatively high purity levels (Figure 4-18; Figure 4-19; Figure 4-20). The PAs (O-Palm-Y-G-G-L-R-F and G-G-Y- (O-Palm) - F-R-L) which comprise essentially the same amino acids but with modifications in the sequence and architecture of the molecules show some differences in hydrophobicity as shown in their retention times in RP HPLC. O-Palm-Y-G-G-L-R-F showed a retention time of 16.315 minutes (Figure 4-18) while G-G-Y- (O-Palm) - F-R-L showed a retention time of 16.893 minutes (Figure 4-19). This suggests that O-Palm-Y-G-G-L-R-F is somewhat more hydrophobic than G-G-Y- (O-Palm) - F-R-L. Also, TEM micrographs of the PAs negatively stained with uranyl acetate (1 %) show that O-Palm-Y-G-G-L-R-F (Figure 4-21) was more stained than G-G-Y- (O-Palm) - F-R-L (Figure 4-22), also indicating that G-G-Y- (O-Palm) - F-R-L being less stained with uranyl acetate is more hydrophobic than O-Palm-Y-G-G-L-R-F (Beniash et al. 2005).

Furthermore, the novel methionine^{5}- enkephalin analogue, O-Palm-Y-G-G-F-M showed a retention time of 18.241 minutes (Figure 4-23) and less staining on TEM micrographs (Figure 4-23), implying that this PA is even more hydrophobic than O-Palm-Y-G-G-L-R-F and G-G-Y- (O-Palm) - F-R-L.

PAs comprising a short hydrophobic portion, usually an alkyl chain bonded to a short peptide sequence (hydrophilic in comparison to the alkyl chain), have been shown to self- assemble into high- aspect- ratio nanofibres under defined solution conditions, such as pH, temperature and ionic strength (Hartgerink et al. 2001; Hartgerink et al. 2002; Cui et al. 2010).

These PAs are usually designed to possess a β-sheet forming peptide region which facilitates intermolecular hydrogen bonding and which causes the PAs to assemble into high aspect ratio nanofibres (cylindrical or twisted), a hydrophobic region usually an alkyl chain, a region of charged amino acids to facilitate water solubility and pH or salt – induced self-assembly (optional) and another region which may be used for the display of bioactive epitopes on the surface of the nanostructure (Webber et al. 2009). Thus, these PAs invariably incorporate the β-sheet forming peptide region and the active epitope as separate portions of the PA molecule.

More recently, work by Mazza and co – workers demonstrated the self-assembly of a PA comprising only of a β- sheet forming peptide region and an alkyl chain, the β-sheet forming peptide region also being the active epitope. Their work demonstrated that the PA, palmitoyl dalargin (pDal), a novel analogue of the hexapeptide dalargin, an opioid receptor agonist was transported into the brain. Their data showed that dalargin was not detected in tissue samples (plasma, liver or brain) following intravenous administration of either dalargin or pDal, and what could be detected in plasma was the main metabolite of dalargin ($_{D}$- Ala^{2} –Leu^{5}- enkephalin). On the contrary, pDal was detected in all the tissue samples and most importantly in the brain up to 4 hours following intravenous administration of pDal nanofibres (Mazza et al. 2013). Thus, PAs combining the β- sheet forming peptide and the active epitope into one region may be used to facilitate the transport and delivery of active peptides as therapeutics for treatment of CNS pathologies. PAs designed in this manner are expected to yield the active peptide following cleavage of the ester bond linking the peptide to the alkyl chain by endogenous esterases as reported by Lalatsa and co – workers for a similarly modified peptide (palmitoyl $leucine^{5}$-enkephalin; TPLENK) which was shown to yield the active peptide, $leucine^{5}$-enkephalin following administration of TPLENK (Lalatsa et al. 2012a).

The molecular design of these PA nanofibers is essentially like that of pro drugs which dissociate to release the active moiety at the desired site of action. These PA nanofibers consist of a peptide molecule covalently linked to the alkyl chain (palmitic acid tail) through an ester bond. Following transport and localisation at the site of action, the ester linkage between the alkyl chain and peptide would be cleaved by endogenous carboxylesterases. These enzymes catalyze the hydrolysis of a variety of ester containing xenobiotics and endogenous compounds to yield the free acids. They therefore limit distribution of potentially toxic substances and facilitate their elimination by converting them into polar molecules. This process of bioconversion is exploited in the design of pro drugs for the release of the active drug at the desired site of action (Sogorb and Vilanova 2002; Satoh and Hosokawa 1998).

For the synthesized PAs therefore, hydrolysis of the ester bond by the carboxylesterase will lead to dissociation of the nanofibers yielding free palmitic acid and the peptide molecule as separate entities.

From the foregoing, the PAs synthesized in this present study may be employed in the delivery of non-BBB penetrating drugs to the brain by aiding their transport across the BBB. Thus, O-Palm-Y-G-G-L-R-F and G-G-Y- (O-Palm) - F-R-L could be employed in the transport and delivery of therapeutics to the brain for the treatment of glioblastoma and other intracranial tumours.

On the other hand, this PA design will enable the transport of methionine^{5}-enkephalin to the brain using the self-assembling PA analogue, O-Palm-Y-G-G-F-M. Methionine^{5}-enkephalin has been reported in previous studies to possess inhibitory activities against different cancers including neuroblastoma (Zagon and McLaughlin 1989), pancreatic cancer (Zagon et al. 1997); ovarian cancer (Donahue et al. 2011) and human squamous cell carcinoma of the head and neck (McLaughlin et al. 2003).

Thus, the synthesized analogue (O-Palm-Y-G-G-F-M) would facilitate the transport and delivery of methionine^5- enkephalin to the brain for the treatment of intracranial tumours as shown for dalargin (Mazza et al. 2013).

Furthermore, the present study has shown that a PA possessing a mid-chain located acyl chain rather than the conventional terminal acyl chain is also able to self-assemble into nanofibres. This "T"-PA [G-G-Y- (O-Palm) - F-R-L] showed the formation of extensive nanofibre networks at low aqueous PA concentration (0.1 % $^{w}/_{v}$) after a short sonication time of 5 minutes as revealed in TEM and SEM micrographs (Figure 4-22; Figure 4-25). Such extensive network was not observed in the linear PA (O-Palm-Y-G-G-L-R-F) comprising the same amino acids but possessing the conventional terminally located acyl chain (Figure 4-21; Figure 4-24). Also, CG MD modelling data further supported the tendency for the "T"-PA (Figure 4-29) to self-assemble into nanofibre networks. The MD modeling data revealed that the "T"-PA had a greater tendency to form multiple inter-chain contacts in the assembled fibres. This is in agreement with the formation of fibre networks observed in TEM and SEM micrographs for this the "T"-PA (Figure 4-22; Figure 4-25). The linear PA on the other hand showed less tendency for inter-chain contacts in the MD modelling (Figure 4-30; Appendix XII) and this also correlated with the formation of individual (not joined) fibres revealed in the TEM and SEM micrographs (Figure 4-21; Figure 4-24). This suggests that the unique molecular architecture of the "T"-PA may provide additional advantages for the application of similarly designed PAs in drug delivery as they may provide more drug loading efficiency than the conventional PAs comprising terminally located acyl substituents.

Therefore, the data reported in this present study indicates that in the PAs synthesised, the hydrophobic interactions of the alkyl chains, the intermolecular hydrogen bonding of the peptide segments as well as stacking of the aromatic side chains (of phenylalanine and tyrosine residues) by $\pi - \pi$ interactions necessary for formation of fibres (Reches and Gazit 2003; Paramonov et al. 2006; Yan et al. 2008) were not disrupted by changing the position of the acyl chain as in the case of G-G-Y-(O-Palm)-F-R-L ("T"-PA) which possessed a mid-chain acyl substituent.

Thus, this current work has demonstrated the ability of a PA possessing a mid-chain acyl substituent ("T"-PA) to self-assemble into nanofibres which has not been previously reported in literature. PAs possessing such molecular architecture could represent a unique drug delivery construct for delivery of therapeutics to the brain. The position (mid-chain location) of the acyl chain may confer an added advantage for the formation of slightly different supramolecular structure from what would be obtained from the conventional linear (terminal acyl chain) PAs. Moreover, there is indication that PAs possessing mid-chain located acyl substituents may be more hydrophobic and they form more extensive networks than their linear counterparts. This may also be advantageous in the delivery of hydrophobic drugs which may be better solubilised using PAs with this unique ("T") architecture.

Chapter 5 Conclusion and Future work

5.1 Conclusion

Glioblastoma still remains a largely incurable disease in spite of tremendous research and resultant advances in the treatment strategies employed in the management of the disease (Stupp et al. 2009; Chamberlain 2010; Grossman et al. 2010). This calls for urgent development of novel strategies for the effective management of the disease to yield better treatment outcomes (Chamberlain 2010; Raizer 2011; Malmström et al. 2012).

Chemotherapy induced dose-limiting myelosuppression is a major limitation in the successful management of glioblastoma using clinically employed cytotoxic agents (Newlands et al. 1992; Peters et al. 1993; Carey 2003; Stupp et al. 2005; Chamberlain 2010). This imposes a limitation on the extent of potentially beneficial dose intensification (Boesen et al. 1994; Tolcher et al. 2003; Crawford et al. 2004; Su et al. 2005; Tosoni et al. 2006; Gerber et al. 2007) with currently used therapeutic agents. The incidence of myelosuppression frequently necessitates dose delays or reductions and in some cases the need for outright disruption of drug treatment. This compromises the effectiveness of the therapeutic agents as there are indications that continuous exposure of tumour cells to cytotoxic therapy may improve treatment outcomes by improving chemosensitivity of tumour cells (Dolan et al. 1990; Brandes et al. 2006; Wick et al. 2007). Moreover, dose interruptions have been shown to compromise tumour response to therapy (Hitron 2011).

In this study, lomustine an alkylating nitrosourea that has been clinically employed in glioblastoma chemotherapy was selected as the model drug. Lomustine like other nitrosoureas produces dose limiting myelosuppression manifesting as neutropenia and thrombocytopenia. This necessitates the observance of “treatment holidays” in clinical practice.

Thus, patients receive an initial dose of lomustine (100 – 130 mg m^{-2}) with a rest period of 6 – 8 weeks and repeat doses are administered only if haematologic parameters are recovered at the end of this rest period (Cianfriglia et al. 1980; van den Bent et al. 1998; van den Bent et al. 2006; Jakacki et al. 1998).

Lomustine is soluble in organic solvents but practically insoluble in water (Ph Eur 2014). This solubility profile of lomustine poses a challenge in the aqueous formulation of the drug. The self-assembling amphiphilic GCPQ nanoparticles employed in this study had been previously shown to facilitate the encapsulation of the hydrophobic intravenous anaesthetic, propofol at a higher level than is obtained with triblock copolymers. The polymer formulation increased the brain activity of propofol by producing sleep times that were up to 10 times those obtained with commercial formulations of the drug. This demonstrates the efficiency of GCPQ nanoparticles in aqueous formulation of hydrophobic drugs (Qu et al. 2006).

In this study, formulation of lomustine using the GCPQ nanoparticles enabled the administration of a higher dose (10 times; 13 mg kg^{-1}) of the drug, while the ethanolic formulation of the drug could only be administered at a dose of 1.2 mg kg^{-1} due to the limited aqueous solubility of the drug. Evaluation of the antitumour activities of the nanoparticle based formulation of lomustine in tumour bearing mice demonstrated significantly ($p < 0.05$) increased survival outcomes compared to the low dose ethanolic formulation. Mice that were treated with the high dose nanomedicine (Q-LOM) formulation had a mean survival time of 33.2 days, the mice treated with the low dose ethanolic formulation had a mean survival time of 22.5 days and untreated control mice had a mean survival time of 21.3 days. Also, weight measurements of treated and untreated mice did not show any difference in the weight of mice treated with the Q-LOM formulation compared to mice that received the low dose ethanolic formulation and untreated controls.

Thus, administration of the Q-LOM formulation did not lead to additional gross toxic effects in the mice that received this formulation as this would have been reflected as weight loss in the treated mice (van den Bent et al. 2003; Hofland et al. 2005). Therefore, the GCPQ nanoparticle based formulation permitted the administration of a high dose of lomustine in a dose intense manner by intravenous administration once daily for 10 consecutive days. This resulted in markedly improved survival outcome in Q-LOM treated mice which had a survival time 1.5 times longer than mice treated with the low dose ethanolic formulation without leading to additional toxicity.

Furthermore, assessment of the toxicity of the Q-LOM formulation on haematologic parameters revealed that there was no effect of this formulation as well as the low dose ethanolic formulation on the white blood cells of treated animals compared to the untreated controls. This indicates that the Q-LOM formulation did not produce neutropenia in the treated animals after the 10 consecutive daily doses administered. However, there was a transient drop in the red blood cell counts of the Q-LOM treated mice with recovery by Day 7. Also, there was a drop in the platelet counts for both groups of treated animals at Day 7 following completion of the dosing regimen. Although the Q-LOM treatment group had a lower nadir value than the low dose ethanolic formulation treatment group, there was no significant difference between the platelet counts for both groups. The platelet counts for the low dose ethanolic formulation treatment group were recovered by day 14, while for the Q-LOM group, the counts were recovered by day 21. This indicates that the occurrence of thrombocytopenia resulting from lomustine therapy (van den Bent et al. 2006; Intile et al. 2009) could still potentially occur with the nanoparticle based formulation. Nevertheless, there was no indication of delayed or cumulative myelosuppression with the Q-LOM formulation as weight measurements and blood counts of animals showed recovery from the effects of the drug with time after dosing had been completed.

Lomustine, like other nitrosoureas is known to produce delayed and cumulative myelosuppression (Jakacki et al. 1998; Smaaland et al. 2002). Therefore, the alteration in the pattern of myelosuppressive effects of lomustine produced by the Q-LOM formulation could be clinically important as this may result in quicker recovery of haematologic parameters with Q-LOM formulation. Moreover, flow cytometry analysis of blood samples showed that there was no effect of either formulation on leucocytes and erythrocytes of the both groups of treated mice, and a quicker recovery of platelet counts. The transient drop in platelet counts of both Q-LOM and the low dose formulation treated groups of animals which was observed on Day 1 was recovered by Day 7 after dosing had been completed for both groups of animals. Although there is therapeutic benefit derivable from the nanoparticle formulation, there is still the need for even safer therapies for the effective management of glioblastoma. Thus, the optimal strategy for effective treatment of glioblastoma still remains an enigma and the question still remains "is *ordo ad chaos*" possible at all (Olar and Aldape 2014).

Therefore, this study has shown that the nanoparticle based formulation of lomustine enabled the administration of a higher dose of the drug which resulted in significantly ($p < 0.05$) prolonged survival without commensurate toxicity.

Furthermore, three self-assembling PAs, O-Palm-Y-G-G-L-R-F, G-G-Y- (O-Palm) - F-R-L and O-Palm-Y-G-G-F-M, a novel analogue of the naturally occurring neuropeptide methionine^5- enkephalin were synthesised and characterised.

O-Palm-Y-G-G-L-R-F and G-G-Y- (O-Palm) - F-R-L were synthesised as potential carriers for the delivery of materials to the brain. The two PAs comprised essentially the same amino acid residues but differ in their molecular architecture. O-Palm-Y-G-G-L-R-F has the molecular architecture of conventional PAs, with a terminal acyl chain (linear PA), while G-G-Y- (O-Palm) - F-R-L on the other hand possessed a mid-chain located acyl chain, thus shaped into a "T" ("T"-PA).

Both PAs were shown to self-assemble into nanofibres in aqueous medium at relatively low concentration (0.1 % $^{w}/_{v}$). However, the resulting assemblies showed different morphologies as revealed by the electron micrographs for the aqueous dispersions of the PAs. The "T"-PA showed the formation of slightly curved nanofibres which are joined together to form extensive nanofibre networks after probe sonication for a short period of 5 minutes and this network formation was maintained with 15 minutes sonication time. The linear PA on the other hand showed formation of individual nanofibres with straight needle-like morphology after probe sonication for 5 minutes and 15 minutes. Previous reports in literature showed the self-assembly of PAs into nanofibres which further entangle into self-supporting gels at low PA concentration (0.25 – 0.5 % $^{w}/_{v}$). The self-assembly of these PAs are usually triggered by the addition of metal ions or lowering of pH of solution (Beniash et al. 2005; Stendahl et al. 2006). Also, CG MD data revealed that the "T"-PA had a tendency to aggregate faster and to a greater extent than the linear PA. The final assemblies for the "T"-PA showed branching and the formation of nanofibre networks through multiple inter-chain contacts. Aggregation of the linear PA appeared to proceed more slowly than the "T"-PA. Also, the formation of nanofibre network was less frequent in the linear PA and was observed in only one out of three simulation runs for the PA. This correlates to the morphologies revealed in the electron micrographs of the PAs.

Therefore, these data demonstrate that changing the position of the acyl chain from the terminal end of the molecule does not disrupt the molecular interactions required for self-assembly of the PAs into nanofibres. On the other hand, the "T"-PA demonstrated quicker self-assembly and the formation of nanofibre networks than the conventional linear PA. This suggests that the unique structure of the "T"-PA may be a platform for more efficient encapsulation and delivery of materials to the brain using this and similarly designed PAs.

Moreover, the "T"-PA appears to be more hydrophobic than the linear PA, suggesting that the "T"-PA might afford better solubilisation and loading of hydrophobic molecules. To the best of my knowledge, this is the first report of the synthesis, characterisation and demonstration of the self-assembly of PAs with this unique ("T" shape) molecular architecture.

The novel methionine^5- enkephalin analogue synthesised, O-Palm-Y-G-G-F-M also self-assembled into nanofibres at low PA concentration (0.1 $\%^{w}/_{v}$) in aqueous medium. The parent peptide methionine^5- enkephalin was modified by the attachment of a palmitoyl group to the OH side chain of the tyrosyl residue of the peptide. It has been previously shown that similarly designed PAs are delivered across the BBB to the brain (Lalatsa et al. 2012; Mazza et al. 2013). Methionine^5-enkephalin has been studied for its antiproliferative activities against a number of cancers (Zagon and McLaughlin 1989; Zagon et al. 1997; McLaughlin et al. 2003; McLaughlin et al. 2003 Donahue et al. 2011). Therefore, O-Palm-Y-G-G-F-M has the potential for application in the treatment of intracranial tumours as the attachment of the palmitoyl group would enhance brain transport and delivery of methionine^5-enkephalin to the tumours.

5.2 Future work

In order to derive maximal benefit from the nanoparticle based strategy for glioblastoma treatment, experiments need to be carried out to determine the optimal dose of the formulation required to yield the desired therapeutic benefit but with minimal side effects. This would involve variations in the actual dose of formulation administered, the duration of treatment (that is the number of doses given) and the frequency of administration of doses.

Also, studies should be carried out to measure the direct effect of the drug formulations on the tumours by assessing tumour volumes and biological changes in tumour characteristics due to the effect of the treatment. This study may lead to the generation of information that would inform the design of an optimal dosing regimen that would deliver maximum therapeutic outcomes of the drug treatment.

Also, evaluation of the toxic effects of the formulation on the blood parameters by flow cytometry analysis also needs to be optimised. Such analysis would inherently be more sensitive and specific than the clinical (human) haemocytometer since mouse (or the particular animal type) specific antibodies would be employed for flow cytometry analysis.

In addition, targeting ligands could be attached to the GCPQ nanoparticles for specific tumour targeting. The efficacy of such targeted delivery system in further improving the survival outcomes with the GCPQ nanoparticle based formulations would be assessed. Also, the capability of such targeted nanoparticle delivery system to lead to even better toxicity profiles, especially in reducing the effects of the drug formulation on the platelets would also be evaluated.

Furthermore, the potential for the use of the PAs synthesised for the brain delivery of therapeutic agents should be investigated. This would also reveal the potential advantages that may be derived from the increased hydrophobicity of the "T"-PA. The studies should include comparison between the two PAs [O-Palm-Y-G-G-L-R-F (linear PA) and G-G-Y- (O-Palm) - F-R-L ("T"-PA)] to determine whether there is an advantage in varying the molecular architecture in terms of drug encapsulation and stability of resulting composites. The studies would show whether the formation of nanofibre networks by the "T"-PA would afford higher loading efficiency and controllable release of loaded molecules.

Further studies should also be carried out to elucidate the observed differences in the self-assembly profile of the two PAs, with the aim to understand fully the molecular basis for the differences. This would help in understanding the molecular basis for the higher tendency for the formation of nanofibre networks by the "T"-PA. Such studies should also assess the formation and stability of higher order structures obtainable from the two PAs.

Also, other "T"-PAs should be studied and compared with their linear counterparts to determine if the differences observed between the two PAs in this study would be universally manifested.

Investigation of the in vitro and in vivo antiproliferative activities of the novel methionine^{5}- enkephalin (O-Palm-Y-G-G-F-M) analogue should be carried out. This would be a potential bio-therapeutic agent for application in the treatment of intracranial tumours. This is inherently advantageous because such a peptide-based therapeutic agent could provide a safer alternative to currently used cytotoxic agents which produce myelosuppressive effects.

References

1. Abbott, N.J. 2004. Evidence for bulk flow of brain interstitial fluid: significance for physiology and pathology. *Neurochem Int*. 45(4), pp 545–552.
2. Abbott, N.J. 2005. Dynamics of CNS barriers: evolution, differentiation, and modulation. *Cell Mol Neurobiol*. 25(1), pp 5–23.
3. Abbott, N.J. and Romero, I.A. 1996. Transporting therapeutics across the blood-brain barrier. *Mol Med Today*. (2)3, pp 106–113.
4. Abbott, N.J. et al., 2010. Structure and function of the blood–brain barrier. *Neurobiol Dis*. 37(1), pp 13–25.
5. Abbott, N.J., Rönnbäck L. and Hansson E. 2006. Astrocyte–endothelial interactions at the blood–brain barrier. *Nature Rev. Neurosci*. 7(1), 41–53.
6. Adler–Abramovich, L. et al., 2006. Thermal and chemical stability of diphenylalanine peptide nanotubes: implications for nanotechnological applications. *Langmuir* 22(3), pp 1313–1320.
7. Agarwal, S. et al., 2011a. Delivery of molecularly targeted therapy to malignant glioma, a disease of the whole brain. *Expert Rev Mol Med*. 13, e17.
8. Agarwal, S. et al., 2011b. Role of breast cancer resistance protein (ABCG2/BCRP) in the distribution of Sorafenib to the brain. *J Pharmacol Exp Ther*. 336(1), pp 223–233.
9. Agarwal, S.et al., 2013. Function of the blood–brain barrier and restriction of drug delivery to invasive glioma cells: Findings in an orthotopic rat xenograft model of glioma. *Drug Metab Dispos*. 41, pp 33–39.
10. Aguilar, M–I. 2004a. HPLC of Peptides and Proteins. Basic Theory and Methodology. In: *HPLC of peptides and proteins. Methods and protocols. Methods in Molecular Biology*™. New Jersey: Humana Press Inc., 2004, 251.
11. Aguilar, M–I. 2004b Reversed–Phase High–Performance Liquid Chromatography. In: In: *HPLC of peptides and proteins. Methods and protocols. Methods in Molecular Biology*™. New Jersey: Humana Press Inc., 2004, 251.
12. Aguilar, M–I. and Hearn, M.T.W. 1996. High–resolution reversed–phase high–performance liquid chromatography of peptides and proteins. In: Karger, B.L. and Hancock, W.S., eds., *High Resolution Separation and Analysis of Biological Macromolecules Part A: Fundamentals. Methods in enzymology*. 270. Academic Press Inc. 1996, pp 3–26.
13. Ahsan, F. et al., 2002. Targeting to macrophages: role of physicochemical properties of particulate carriers—liposomes and microspheres—on the phagocytosis by macrophages. J Control Release 79, pp 29–40.

14. Albericio, F. 2000. Orthogonal protecting groups for N–α –amino and C–terminal carboxyl functions in solid–phase peptide synthesis. *Biopolymers Peptide Science* (55), pp 123–139.
15. Allard, E., Passirani, C. and Benoit, J.P. 2009. Convection–enhanced delivery of nanocarriers for the treatment of brain tumors. *Biomaterials*. 30, pp 2302–2318.
16. Andersen, A.P. 1978. Postoperative irradiation of glioblastomas. Results in a randomized series. *Acta Radiol Oncol Radiat Phys Biol*. 17(6), pp 475-484.
17. Anderson, T., McMenamin, M.G. and Schein, P.S. 1975. Chlorozotocin, 2-(3-(2-chloroethyl)-3-nitrosoureido)-D-glucopyranose, an antitumor agent with modified bone marrow toxicity. *Cancer Res*. 35(3), pp 761–765.
18. Antosova, Z. et al., 2009. Therapeutic application of peptides and proteins: parenteral forever? *Trends Biotechnol*. 27(11), pp 628–635.
19. Ashmore, S.M., Thomas, D.G. and Darling, J.L. 1999. Does P–glycoprotein play a role in clinical resistance of malignant astrocytoma? *Anticancer Drugs*. 10(10), pp 861–872.
20. Atherton, E. et al., 1978. A mild procedure for solid phase peptide synthesis: use of fluorenylmethoxy–carbonylamino–acids. *J Chem Soc Chem Comm*. pp 537–539.
21. Attenello, F.J. et al., 2008. Use of Gliadel (BCNU) wafer in the surgical treatment of malignant glioma: a 10-year institutional experience. *Ann Surg Oncol*. 15(10), pp 2887–2893.
22. Audie, J. and Boyd, C. 2010. The synergistic use of computation, chemistry and biology to discover novel peptide–based drugs: the time is right. *Curr Pharm Des*. 16(5), pp 567–582.
23. Ayres, C.E. et al., 2010. Nanotechnology in the design of soft tissue scaffolds: innovations structure and function, Nanomed Nanobiotechnol. 2, pp 20–34.
24. Baklaushev, V.P., et al. 2012. New experimental model of brain tumors in brains of adult immunocompetent rats. *Br J Med Med Res*. 2(2), pp 206–215.
25. Balss, J. et al., 2008. Analysis of the IDH1 codon 132 mutation in brain tumors. *Acta Neuropathol*. 116(6), pp 597–602.
26. Barber, J., Cross, H.F. and Parkinson, J.A. 1993. High–Resolution NMR of DNA and drug–DNA interactions. In: Jones, C., Mulloy, B., and Thomas, A.H. eds., *Spectroscopic Methods and Analyses: NMR, Mass Spectrometry, and Metalloprotein Techniques. Methods in Molecular Biology* 17. New Jersey: Humana Press Inc. 1993, pp 87–113.
27. Basso D.M. et al., 1996. MASCIS evaluation of open field locomotor scores: effects of experience and teamwork on reliability. Multicenter animal spinal cord injury study. J Neurotrauma. 13, pp 343–359.

28. Bartlett, D.W. and Davis, M.E. 2007. Physicochemical and biological characterization of targeted, nucleic acid–containing nanoparticles. *Bioconjug Chem*. 18, pp 456–468.
29. Batchelor, T.T. et al., 2013. Phase III randomized trial comparing the efficacy of cediranib as monotherapy, and in combination with lomustine, versus lomustine alone in patients with recurrent glioblastoma. J Clin Oncol. 31(26), pp 3212–3218.
30. Baumann, M. et al., 1992. Response of xenografts of human malignant gliomas and squamous cell carcinomas to fractionated irradiation. *Int J Radiat Oncol Biol Phys*. 23(4), pp 803–809.
31. Baur, M. et al., 2010. Frequent MGMT (06–methylguanine–DNA methyltransferase) hypermethylation in long–term survivors of glioblastoma: a single institution experience. *Radiol Oncol*. 44(2), pp 113–120.
32. Baura, G.D. et al., 1993. Saturable transport of insulin from plasma into the central nervous system of dogs in vivo. A mechanism for regulated insulin delivery to the brain. *J Clin Invest*. 92(4), pp 1824–1830.
33. Begley, D.J. 2003. Understanding and circumventing the blood–brain barrier. *Acta Pædiatr Suppl*. 92(443), pp 83–91.
34. Begley, D.J. 2004. Delivery of therapeutic agents to the central nervous system: the problems and the possibilities. *Pharmacol Ther*. 104(1), pp 29–45.
35. Begley, D.J. The Blood-brain Barrier: Principles for Targeting Peptides and Drugs to the Central Nervous System. *J. Pharm. Pharmacol*. 48(2), pp 136–146.
36. Bello, L. et al., 2001. Alpha(v)beta3 and alpha(v)beta5 integrin expression in glioma periphery. *Neurosurgery*. 49(2), pp 380–9, discussion 390.
37. Beniash, E. et al., 2005. Self–assembling peptide amphiphile nanofibers matrices for cell entrapment. *Acta Biomaterialia*. 1, pp 387–397.
38. Berendsen, H.J.C. et al., 1984. Molecular dynamics with coupling to an external bath. J Chem Phys. 81(8), pp 3684–3690.
39. Bernacki, J. et al. 2008. Physiology and pharmacological role of the blood–brain barrier. *Pharmacol. Rep*. 60(5), pp 600–622.
40. Bernal, G.M. et al. 2014. Convection-enhanced delivery and in vivo imaging of polymeric nanoparticles for the treatment of malignant glioma. *Nanomedicine*. 10(1):149–157.
41. Bertossi, M. et al., 1997. Ultrastructural and morphometric investigation of human brain capillaries in normal and peritumoral tissues. *Ultrastruct Pathol*. 21(1), pp 41–49.

42. Bethune, C.R. et al., 2001. Lipid association improves the therapeutic index of lomustine [1-(2-chloroethyl)-3-cyclohexyl-1-nitrosourea] to suppress 36B-10 tumor growth in rats. *Cancer Res*. 61(9), pp 3669–3674.
43. Bhaskar, S. et al., 2010. Multifunctional nanocarriers for diagnostics, drug delivery and targeted treatment across blood–brain barrier: perspectives on tracking and neuroimaging. Part Fibre Toxicol. 7(3), pp 1– 25.
44. Biemann, K. 1990. In: McCloskey J.A. ed., *Mass Spectrometry. Methods in Enzymology*. 193, Academic Press Inc, 1990, pp 455–479.
45. Black, K.L. and Ningaraj, N.S 2004. Modulation of brain tumor capillaries for enhanced drug delivery selectively to brain tumor. *Cancer Control*. 11(3), pp 165–173.
46. Bleehen, N.M. and Stenning S.P 1991. A Medical Research Council trial of two radiotherapy doses in the treatment of grades 3 and 4 astrocytoma. The Medical Research Council Brain Tumour Working Party. *Br J Cancer*. 64(4), pp 769–774.
47. Bobo, R.H. et al., 1994. Convection-enhanced delivery of macromolecules in the brain. *Proc Natl Acad Sci USA*. 91(6), pp 2076–2080.
48. Bock, H.C. et al 2010. First–line treatment of malignant glioma with carmustine implants followed by concomitant radiochemotherapy: a multicenter experience. *Neurosurg Rev*. 33(4), pp 441–449.
49. Bodanszky, M. 1993. Solid Phase Peptide Synthesis. In: *Peptide Chemistry a practical textbook*. Germany: Springer – Verlag, 1993, 149–170.
50. Boesen, J.J.B. 1994. Circumvention of chemotherapy-induced myelosuppression by transfer of the mdrl gene. *Biotherapy*. 6, pp 291–302.
51. Bokstein, F. et al., 2008. A common sense approach to radiotherapy planning of Glioblastoma multiforme situated in the temporal lobe *Int J Radiat Oncol Biol Phys*. 72(3), pp 900–904.
52. Boockvar, J.A. et al., 2010. Safety and maximum tolerated dose of superselective intraarterial cerebral infusion of bevacizumab after osmotic blood–brain barrier disruption for recurrent malignant glioma. *J Neurosurg*. 114(3), pp 624–632.
53. Brada, M. et al., 2010. Temozolomide versus procarbazine, lomustine, and vincristine in recurrent high-grade glioma. J Clin Oncol. 28(30), pp 4601–4608.
54. Bradbury, M.W and Davson, H. 1965. The transport of potassium between blood, cerebrospinal fluid and brain. *J Physiol*. 181(1), pp 151–174.

55. Brandes, A.A. et al., 2006. Temozolomide 3 weeks on and 1 week off as first-line therapy for recurrent glioblastoma: phase II study from gruppo italiano cooperativo di neuro-oncologia (GICNO). *Br J Cancer*. 95(9), pp 1155–1160.
56. Brandes, A.A. et al., 2008. Glioblastoma in adults. *Crit Rev Oncol Hemat*. 67, pp 139–152.
57. Brandsma, D. et al., 2008. Clinical features, mechanisms, and management of pseudoprogression in malignant gliomas. Lancet Oncol. 9, pp 453–461.
58. Brem, S. Cotran, R. and Folkman, J. 1972. Tumor angiogenesis: a quantitative method for histologic grading. *J Natl Cancer Inst*. 48(2), pp 347–356.
59. Brightman M. W and Reese T. S. (1969) Junctions between intimately apposed cell membranes in the vertebrate brain. *J Cell Biol*. 40, pp 648–677.
60. Brightman, M.W. 1977. Morphology of blood-brain interfaces. *Exp. Eye Res*. 25 (Suppl.), pp 1–25.
61. Briscoe, W.T., Anderson, S.P. and May, H.E. 1990. Base sequence specificity of three 2-chloroethylnitrosoureas. *Biochem Pharmacol*. 40(6):1201–1209.
62. Brooks, B.R. et al., 1983. CHARMM: A program for macromolecular energy, minimization, and dynamics calculations. J Comput Chem. 4, pp 187–217.
63. Bruhn, H. et al., 1989. Noninvasive differentiation of tumors with use of localized 1H NMR spectroscopy in vivo: initial experience in patients with cerebral tumors. *Radiology* 172(2), pp 541–548.
64. Burger, A.M, Fiebig, H-H. 2002. Screening using animal systems. In: Bruce C. Baguley B. C.; Kerr D. J. eds., *Anticancer drug development*. Academic Press, pp 285–299.
65. Burger, P.C. and Green, S.B. 1987. Patient age, histologic features, and length of survival in patients with glioblastoma multiforme. *Cancer*. 59, pp 1617–1625.
66. Cairncross, G. et al., 1994. Chemotherapy for anaplastic oligodendroglioma. National Cancer Institute of Canada Clinical Trials Group. *J Clin Oncol*. 12(10), pp 2013–2021.
67. Calabria, A.R. and Shusta, E.V. 2006. Blood–brain barrier genomics and proteomics: elucidating phenotype, identifying disease targets and enabling brain drug delivery. *Drug Discov Today* 11(17-18), pp 792–799.
68. Carey, P.J. 2003. Drug-induced myelosuppression: diagnosis and management. *Drug Saf*. 26(10), pp 691–706.
69. Cavalli, F. 1982. VP-16-213 (Etoposide). A critical review of its activity. *Cancer Chemother Pharmacol*.7, pp 81–85.

70. Cavalli, S., Albericio, F. and Kros, A. 2010. Amphiphilic peptides and their cross–disciplinary role as building blocks for nanoscience. *Chem Soc Rev*. 39, pp 241–263.
71. Çetin, M. et al., 2000. The effect of medroxyprogesterone acetate on bone marrow and testis during cytotoxic chemotherapy. Cell Biol Toxicol. 16, pp 385–390.
72. Cha S. 2004. Perfusion MR imaging of brain tumors. Top Magn Reson Imaging. 15(5), pp 279–289.
73. Cha, S. et al. 2007. Differentiation of glioblastoma multiforme and single brain metastasis by peak height and percentage of signal intensity recovery derived from dynamic susceptibility–weighted contrast–enhanced perfusion MR imaging. AJNR Am J Neuroradiol. 28(6), pp 1078–1084
74. Chamberlain, M.C. 2010. Temozolomide: therapeutic limitations in the treatment of adult high–grade gliomas. *Expert Rev Neurother*. 10, pp 1537−1544.
75. Chamberlain, M.C. and Raizer, J. 2009. Extended exposure to alkylator chemotherapy: delayed appearance of myelodysplasia. *J Neurooncol*. 93(2), pp 229–232.
76. Chamberlain, M.C., Kormanik, P.A. and Barba, D. 1997. Complications associated with intraventricular chemotherapy in patients with leptomeningeal metastases. *J Neurosurg*. 87(5), pp 694–699.
77. Chang, C.H. et al., 1983. Comparison of postoperative radiotherapy and combined postoperative radiotherapy and chemotherapy in the mul tidisciplinary management of malignant gliomas. A joint radiation therapy oncology group and eastern cooperative oncology group study. *Cancer*. 52(6), pp 997–1007.
78. Chellata, F. et al., 2005. Therapeutic potential of nanoparticulate systems for macrophage targeting. *Biomaterials*. 26, pp 7260–7275.
79. Chen, P.C., Mwakwari, S.C. and Oyelere, A.K. 2008. Gold nanoparticles: from nanomedicine to nanosensing. *Nanotechnol Sci Appl*. 1, pp 45–65.
80. Chen, Y. et al., 2009. P–glycoprotein and breast cancer resistance protein influence brain distribution of dasatinib. *J Pharmacol Exp Ther*. 330(3), pp 956–963.
81. Cheng, C.J. et al., 1972. Interaction of 1-(2-Chloroethyl)-3-cyclohexyl-1-nitrosourea (NSC 79037) with nucleic acids and proteins in vivo and in vitro. *Cancer Res*. 32, pp 22–27.
82. Chow, A. et al. 2011. Bone marrow CD169+ macrophages promote the retention of hematopoietic stem and progenitor cells in the mesenchymal stem cell niche. *J Exp Med*. 208(2), pp 261–271.

83. Chow, A. et al., 2013. CD169+ macrophages provide a niche promoting erythropoiesis under homeostasis, myeloablation and in JAK2V617F-induced polycythemia vera. *Nat Med*. 19(4), pp 429–436.
84. Cianfriglia, F. et al., 1980. CCNU-chemotherapy of hemispheric supratentorial glioblastoma multiforme. *Cancer*. 45 (6), pp 1289–1299.
85. Cloughesy, T.F and Black, K.L. 1995. Pharmacological blood-brain barrier modification for selective drug delivery. *J Neurooncol*. 26(2), pp 125–132.
86. Colombo, G., Soto, P. and Gazit E. 2007. Peptide self– assembly at nanoscale: a challenging target for computational and experimental biotechnology. *TRENDS in Biotechnology*. 25(5), pp 211–218.
87. Combs, S.E. et al., 2008. Radiochemotherapy with temozolomide as re-irradiation using high precision fractionated stereotactic radiotherapy (FSRT) in patients with recurrent gliomas. J Neurooncol. 89(2), pp 205–210.
88. Corradin, G., Kajava, A.V. and Verdini, A. 2010. Long synthetic peptides for the production of vaccines and drugs: a technological platform coming of age. *Sci Transl Med*. 2(50), pp 50rv3.
89. Crawford, J., Dale, D.C. and Lyman, G.H. 2004. Chemotherapy-induced neutropenia: risks, consequences, and new directions for its management. *Cancer*. 100(2), pp 228–237.
90. Cui, H., Webber, M.J. and Stupp, S.I. 2010. Self-assembly of peptide amphiphiles from molecules to nanostructures to biomaterials. *Peptide Science*. 94(1), pp 1–18.
91. Curran W.J Jr. et al. 1993. Recursive partitioning analysis of prognostic factors in three Radiation Therapy Oncology Group malignant glioma trials. J *Natl Cancer Inst*. 85(9), pp 704–710.
92. Dale, D.C. 2002. Colony-stimulating factors for the management of neutropenia in cancer patients. *Drugs*. 62(Suppl.1), pp 1–15.
93. Dallas, S., Miller, D.S. and Bendayan, R. 2006. Multidrug resistance-associated proteins: expression and function in the central nervous system. *Pharmacol. Rev*. 58(2), pp 140–161.
94. Davis, M.E, Chen, Z(G). and Shin, D.M. 2008. Nanoparticle therapeutics: an emerging treatment modality for cancer. *Nat Rev Drug Discov*. 7, pp 771–782.
95. de Groot, J.F. et al., 2010. Tumor invasion after treatment of glioblastoma with bevacizumab: radiographic and pathologic correlation in humans and mice. *Neuro Oncol*. 12(3), pp 233–242.
96. de Hoffmann, E. and Stroobant, V. 2007. *Mass Spectrometry: Principles and Applications*. 3rd edition. England: Wiley, 2007.
97. DeAngelis, L.M. 2001. Brain Tumours. *N Engl J Med*. 344(2), pp 114–123.
98. DeAngelis, L.M. and Boutros, D. 2005. Leptomeningeal metastasis. *Cancer Invest*. 23(2), pp 145–154.

99. Declèves, X. et al., 2002. Molecular and functional MDR1–Pgp and MRPs expression in human glioblastoma multiforme cell lines. *Int J Cancer*. 98(2), pp 173–180.
100. Deeken, J.F and Wolfgang, L. 2007. The blood-brain barrier and cancer: Transporters, treatment, and Trojan horses. *Clin Cancer Res*. 13(6), pp 1663–1674.
101. Demeule, M. et al., 2001. Expression of multidrug-resistance P-glycoprotein (MDR1) in human brain tumors. *Int J Cancer*. 93(1), pp 62–66.
102. Derossi, D. et al., 1994. The third helix of the Antennapedia homeodomain translocates through biological membranes. *J Biol Chem*. 269(14), pp 10444–10450.
103. Desgrosellier, J.S. and Cheresh, D.A. 2010. Integrins in cancer: Biological implications and therapeutic opportunities. *Nat Rev Cancer*. 2010. 10(1), pp 9–22.
104. Dolan, M.E., Moschel, R.C. and Pegg, A.E. 1990. Depletion of mammalian O6- alkylguanine-DNA alkyltransferase activity by O6- benzylguanine provides a means to evaluate the role of this protein in protection against carcinogenic and therapeutic alkylating agents. *Proc Natl Acad Sci USA*. 87, 5368–5372.
105. Dolecek, T.A. et al., 2012. CBTRUS statistical report: primary brain and central nervous system tumors diagnosed in the United States in 2005–2009. *Neuro Oncol* 14, pp v1–v49.
106. Donahue, R.N., McLaughlin, P.J. and Zagon I.S. 2011. The opioid growth factor (OGF) and low dose naltrexone (LDN) suppress human ovarian cancer progression in mice. *Gynecol Oncol*. 122, pp 382–388.
107. Drin, G. et al. 2003. Studies on the internalization mechanism of cationic cell-penetrating peptides. *J Biol Chem*. 278(33), pp 31192–31201.
108. du Vigneaud, V. et al., 1954. The synthesis of oxytocin. *J Am Chem Soc*. 76, pp 3115–3121.
109. Duhamel, J. 2012. Internal Dynamics of Dendritic Molecules Probed by Pyrene Excimer Formation. *Polymers* 4, pp 211–239.
110. Dumenco, L.L. et al., 1989. Increase in nitrosourea resistance in mammalian cells by retrovirally mediated gene transfer of bacterial 06-alkylguanine-DNA alkyltransferase. Cancer Res 49, pp 6044–6051.
111. Elting, L.S. et al., 2001. Incidence, cost, and outcomes of bleeding and chemotherapy dose modification among solid tumor patients with chemotherapy-induced thrombocytopenia. J Clin Oncol. 19(4), pp 1137–1146.
112. European Pharmacopoiea 2014. Volume 2. Lomustine. Council of Europe. Strasborg. pp 2630–2631.

113. Ewig, R.A.G. and Kohn, K.W. 1977. DNA damage and repair in mouse leukemia L1210 cells treated with nitrogen mustard, 1,3-Bis(2-chloroethyl)-1-nitrosourea, and other nitrosoureas. *Cancer Res*. 37, pp 2114–2122.
114. Fallon, A., Booth, R.F.G. and Bell, L.D. 1987. High performance reversed phase chromatography. In: Burdon, R.H., and van Knippenberg, P.H. eds. *Applications of HPLC in biochemistry. Laboratory techniques in biochemistry and molecular biology*. 17. The Netherlands: Elsevier Science Publishers B. V. (Biomedical Division), 1987, pp 73–89.
115. Fattori, S. et al. 2007. Human brain tumors: multidrug–resistance P–glycoprotein expression in tumor cells and intratumoral capillary endothelial cells. *Virchows Arch*. 451(1), pp 81–87.
116. Felix, A.M. and Merrifield, R.B. 1970. Azide Solid–Phase Peptide Synthesis. *J Am Chem Soc*. 92, pp 1385–1391.
117. Fernando, L. P. et al., 2010. Mechanism of cellular uptake of highly fluorescent conjugated polymer nanoparticles. *Biomacromolecules*. 11(10), pp 2675–2682.
118. Filippini, G. et al. 2008. Prognostic factors for survival in 676 consecutive patients with newly diagnosed primary glioblastoma. *Neuro Oncol*. 10(1), pp 79–87.
119. Fillebeen, C. et al., 1999. Receptor–mediated transcytosis of lactoferrin through the blood–brain barrier. *J Biol Chem*. 274(11), pp 7011–7017.
120. Fine, H.A. 1994. The basis for current treatment recommendations for malignant gliomas. *J Neurooncol*. 20, pp 111–120.
121. Fine, H.A. et al., 1993. Meta-analysis of radiation therapy with and without adjuvant chemotherapy for malignant gliomas in adults. *Cancer*. 71(8), pp 2585–2597.
122. Fishman, J.B. et al., 1987. Receptor–mediated transcytosis of transferrin across the blood–brain barrier. *J Neurosci Res*. 18(2), pp 299–304.
123. Florio, T. and Barbieri, F. 2012. The status of the art of human malignant glioma management: the promising role of targeting tumor–initiating cells. *Drug Discov Today*. 17 (19/20), pp 1103–1110.
124. Franklin, C. I. 1992. Does the extent of surgery make a difference in high grade malignant astrocytoma. *Australas Radiol*. 36(1), pp 44–47.
125. Friedman, H.S. et al. 2009. Bevacizumab alone and in combination with irinotecan in recurrent glioblastoma. *J Clin Oncol*. 27(28), pp 4733–4740.
126. Fung, S.Y., Yang, H. Chen, P. 2008.) sequence effect of self-assembling peptides on the complexation and in vitro delivery of the hydrophobic anticancer drug ellipticine. PLoS ONE. 3(4), e1956.
127. Furnari, F. B. et al., 2007. Malignant astrocytic glioma: genetics, biology, and paths to treatment. *Genes Dev*. 21, pp 2683–2710.

128. Ganong, W.F. 2000. Circumventricular organs: definition and role in the regulation of endocrine and autonomic function. *Clin Exp Pharmacol Physiol*. 27(5-6), pp 422–427.
129. Gao, H. et al., 2014. Incorporation of lapatinib into core–shell nanoparticles improves both the solubility and anti–glioma effects of the drug. *Int J Pharm*. 461(1–2), pp 478–488.
130. Garrett, N.L. et al. 2012. Label–free imaging of polymeric nanomedicines using coherent anti–stokes Raman scattering microscopy. *J Raman Spectrosc* 43(5), pp 681–688.
131. Gerber, D.E. et al., 2007. The impact of thrombocytopenia from temozolomide and radiation in newly diagnosed adults with high-grade gliomas. *Neuro Oncol*. 9(1), pp 47–52.
132. Gerson, S.L. 2004. MGMT: Its role in cancer aetiology and cancer therapeutics. *Nat Rev Cancer*. 4(4), pp 296–307.
133. Gesellchen, P.D. and Santerre, R.F. 1991. Synthesis of peptides and proteins by chemical and biotechnological means. In: Lee V.H.L. ed., *Peptide and protein drug delivery*. New York: Marcel Dekker Inc., 1991, pp 57–135.
134. Gingrich, M.B. and Traynelis, S.F., 2000. Serine proteases and brain damage – is there a link? *Trends Neurosci*. 23(9), pp 399–407.
135. Gingrich, M.B. et al., 2000. Potentiation of NMDA receptor function by the serine protease thrombin. *J Neurosci*. 20(12), pp 4582–4595.
136. Glas, M. et al., 2009. Long-term survival of patients with glioblastoma treated with radiotherapy and lomustine plus temozolomide. *J Clin Oncol*. 2009 Mar 27(8), pp 1257–1261.
137. Go, K.G. et al. 1995. Localised proton spectroscopy and spectroscopic imaging in cerebral gliomas, with comparison to positron emission tomography. *Neuroradiology*. 37, pp 198–206.
138. Graff, C.P. and Wittrup, K.D. 2003. Theoretical analysis of antibody targeting of tumor spheroids: importance of dosage for penetration, and affinity for retention. *Cancer Res*. 63(6), pp 1288–1296.
139. Griffiths, I.W. 1997. J. J. Thomson – the centenary of his discovery of the electron and his invention of mass spectrometry. *Rapid Commun Mass Spectrom*. 11, pp 2–16.
140. Gross, M.L. 1990. Tandem Mass Spectrometry: Multisector magnetic instruments. In: McCloskey J.A. ed., *Mass Spectrometry. Methods in Enzymology*. Academic Press Inc, 1990, 193, pp 131–153.

141. Grossman, R. et al., 2014. Combination of anti-VEGF therapy and temozolomide in two experimental human glioma models. *J Neurooncol*. 116(1), pp 59–65.
142. Grossman, S.A. 2003. Arguments against the routine use of currently available adjuvant chemotherapy in high-grade gliomas. *Semin Oncol*. 30(suppl 19), pp 19–22.
143. Grossman, S.A. et al., 2010. Survival of Patients with Newly Diagnosed Glioblastoma Treated with Radiation and Temozolomide in Research Studies in the United States. *Clin Cancer Res*. 16(8), pp 2443–2449.
144. Guler, M.O., Claussen, R.C., Stupp, S.I. 2005. Encapsulation of pyrene within self-assembled peptide amphiphile nanofibers. *J Mater Chem*. 15, pp 4507–4512.
145. Gulyaev, A.E. et al. 1999. Significant transport of doxorubicin into the brain with polysorbate 80-coated nanoparticles. *Pharm Res*. 16(10), pp 1564–1569.
146. Gundersen, S., Lote, K. and Watne, K. 1998. A retrospective study of the value of chemotherapy as adjuvant therapy to surgery and radiotherapy in grade 3 and 4 gliomas. *Eur J Cancer*. 34(10), 1565–1569.
147. Günther, H. 1995. The physical basis of the nuclear magnetic resonance experiment. Part I. In: Günther H., translator, *NMR Spectroscopy: Basic principles, concepts, and applications in chemistry*. England: John Wiley & Sons, 1995.
148. Guo, W. et al. 2013. Transferrin modified PEG–PLA–resveratrol conjugates: in vitro and in vivo studies for glioma. Eur J Pharmacol. 718(1–3), pp 41–47.
149. Gutenberg A. et al., 2013. MGMT promoter methylation status and prognosis of patients with primary or recurrent glioblastoma treated with carmustine wafers. *Br J Neurosurg*. 27(6), pp 772–778.
150. Guthrie D.J.S. 1997. 1H nuclear magnetic resonance (NMR) in the elucidation of peptide structure. In: Irvine G.B. and Williams, C.H. eds., Neuropeptide protocols. *Methods in Molecular Biology™*. New Jersey: Humana Press Inc., 1997, 73, pp 163–184.
151. Gutin, P.H. et al. 2009. Safety and efficacy of bevacizumab with hypofractionated stereotactic irradiation for recurrent malignant gliomas. *Int J Radiat Oncol Biol Phys*. 75(1), pp 156–163.
152. Hainsworth, J.D. et al. 2010. Concurrent radiotherapy and temozolomide followed by temozolomide and sorafenib in the first-line treatment of patients with glioblastoma multiforme. *Cancer*. 116(15), pp 3663–3669.
153. Hall, W.A. et al., 2006. Osmotic blood-brain barrier disruption chemotherapy for diffuse pontine gliomas. *J Neurooncol*. 77(3), pp 279–284.

154. Halperin, E.C., Burger, P.C. and Bullard, D.E. 1988. The fallacy of the localized supratentorial malignant glioma. Int J Radiat Oncol Biol Phys. 15(2), pp 505–509.
155. Halperin, E.C. et al., 1989. Radiation therapy treatment planning in supratentorial glioblastoma multiforme: an analysis based on post mortem topographic anatomy with CT correlations. *Int J Radiat Oncol Biol Phys*. 17(6), pp 1347–1350.
156. Hammoud, M.A. et al., 1996. Prognostic significance of preoperative MRI scans in glioblastoma multiforme. *J Neurooncol*. 27(1), pp 65–73.
157. Hansen, A.J. 1985. Effect of anoxia on ion distribution in the brain. *Physiol* Rev. 65(1), pp 101–148.
158. Harada. K. et al. 1998. Intratumoral cytogenetic heterogeneity detected by comparative genomic hybridization and laser scanning cytometry in human gliomas. *Cancer Res*. 58(20), pp 4694–4700.
159. Harper, J.D. and Lansbury, P.T Jr. 1997. Models of amyloid seeding in Alzheimer's disease and scrapie: mechanistic truths and physiological consequences of the time-dependent solubility of amyloid proteins. *Annu Rev Biochem.* 66, 385–407.
160. Harrison, A.G. and Cotter, R.J. 1990. Methods of Ionization. In: McCloskey J. A. ed., *Mass Spectrometry. Methods in Enzymology*. Academic Press Inc, 1990, 193, pp 280–285.
161. Hartgerink, J.D., Beniash, E. and Stupp, S.I. 2001. Self-Assembly and Mineralization of Peptide-Amphiphile Nanofibers. Science. 294, 1684–1688.
162. Hartgerink, J.D., Beniash, E. and Stupp, S.I. Peptide-amphiphile nanofibers: A versatile scaffold for the preparation of self-assembling materials *Proc Natl Acad Sci USA*. 2002, 99, 5133–5138
163. Hattingen, E. et al. 2008. Prognostic value of choline and creatine in WHO grade II gliomas. *Neuroradiology*. 50(9), pp 759–767.
164. He, J. et al., 2001. Glioblastomas with an oligodendroglial component: a pathological and molecular study. *J Neuropathol Exp Neurol*. 60(9), pp 863–871.
165. Hegi, M.E. et al., 2004. Clinical trial substantiates the predictive value of O-6-methylguanine-DNA methyltransferase promoter methylation in glioblastoma patients treated with temozolomide. *Clin Cancer Res*. 10(6):1871–1874.
166. Hegi, M.E. et al., 2005. MGMT gene silencing and benefit from temozolomide in glioblastoma. *N Engl J Med*. 352(10), pp 997–1003.

167. Henkel, B., Zhang, L. and Bayer, E. 1997. Investigations on solid–phase peptide synthesis in N–to–C direction (inverse synthesis). *Liehigs Ann./Recueil*. 10, pp 2161–2168.
168. Henriksen, E.J. and Prasannarong, M. 2013. The role of the renin–angiotensin system in the development of insulin resistance in skeletal muscle. *Mol Cell Endocrinol*. 378(1–2), pp 15–22.
169. Herminghaus, S. et al. 2002. Increased choline levels coincide with enhanced proliferative activity of human neuroepithelial brain tumors. *NMR Biomed*. 15, pp 385–392.
170. Herrlinger, U. et al., Phase II trial of lomustine plus temozolomide chemotherapy in addition to radiotherapy in newly diagnosed glioblastoma: UKT-03 J *Nat Rev Drug Discov*. 24(27):4412–4417.
171. Hess K.R. 1999. Extent of resection as a prognostic variable in the treatment of gliomas. *J Neurooncol*. 42(3), pp 227–231.
172. Hillenkamp, F. and Karas M. 1990. Mass spectrometry of peptides and proteins by matrix–assisted ultraviolet laser desorption/ionization. In: McCloskey J.A. ed., *Mass Spectrometry. Methods in Enzymology*. Academic Press Inc, 1990, 193.
173. Hinds, M.G. and Norton, R.S. 1997. NMR spectroscopy of peptides and proteins: Practical considerations. *Molecular Biotechnology*. 7(3), pp 315–331.
174. Hitron, A. et al., 2011. Incidence and risk factors of clinically significant chemotherapy-induced thrombocytopenia in patients with solid tumors. *J Oncol Pharm Practice*. 17(4), pp 312–319.
175. Ho, C.S. et al., 2003. Electrospray Ionisation Mass Spectrometry: Principles and Clinical Applications. *Clin Biochem Rev*. 24, pp 3–12.
176. Hofland, K.F. et al. 2005. Dexrazoxane protects against myelosuppression from the DNA cleavage -enhancing drugs etoposide and daunorubicin but not doxorubicin. *Clin Cancer Res*. 11, pp 3915–3924.
177. Holm, B. Jensen, P.B. and Sehested, M. 1996. ICRF-187 rescue in etoposide treatment in vivo. A model targeting high-dose topoisomerase II poisons to CNS tumors. *Cancer Chemother Pharmacol*. 38, pp 203–209.
178. Home Office, 2012. Animals (scientific procedures) Act 1986 amendment regulations. United Kingdom: Crown copyright.
179. Homma, T. et al. 2006. Correlation among pathology, genotype, and patient outcomes in glioblastoma. *J Neuropathol Exp Neurol*. 65(9), pp 846–854.
180. Hong, B. et al., 2013. Multiple microsurgical resections for repeated recurrence of glioblastoma multiforme. *Am J Clin Oncol*. 36(3), pp 261–268.

181. Hong, S. et al. 2007. The binding avidity of a nanoparticle–based multivalent targeted drug delivery platform. *Chem Biol*. 14(1), pp 107–115.
182. Hoogstraten, B. et al., 1973. CCNU (1-[2-chloroethyl]-3-cyclohexyl-1-nitrosourea, NSC-79037) in the treatment of cancer Phase II study. *Cancer*. 32(1), pp 38–43.
183. Hoover, W.G. 1985. Canonical dynamics: Equilibrium phase-space distributions. *Phys Rev A*. 31(3), pp 1695–1697.
184. Huang, Z. et al., 2010. Biological synthesis of tooth enamel instructed by an artificial matrix. *Biomaterials*. 31(35), pp 9202–9211.
185. Hummel, G., Reineke, U. and Reimer, U. 2006. Translating peptides into small molecules. In: Bartlett, P. A. and Entzeroth, M. Eds., Exploiting Chemical Diversity for Drug Discovery. *Mol Biosyst*. Royal Society of Chemistry, 2(10), pp 499–508.
186. Hünenberger, P.H. 2005. Thermostat algorithms for molecular dynamics simulations. *Adv Polym Sci*. 173, pp 105–149.
187. Huse, J.T. et al. 2011. Molecular subclassification of diffuse gliomas: Seeing order in the chaos. *Glia*. 59:1190–1199.
188. Iadecola, C. 2004. Neurovascular regulation in the normal brain and in Alzheimer's disease. *Nat Rev Neurosci*. 5(5), pp 347–360.
189. Ichimura, K. et al. 2009. IDH1 mutations are present in the majority of common adult gliomas but rare in primary glioblastomas. *Neuro Oncol.* 11(4), pp 341–347.
190. Intile, J.L. et al., 2009. Evaluation of dexamethasone as a chemoprotectant for CCNU-induced bone marrow suppression in dogs. *Vet Comp Oncol*. 7(1), pp 69–77.
191. Jafri, N.F. et al. 2013. Relationship of glioblastoma multiforme to the subventricular zone is associated with survival. *Neuro Oncol*. 15(1), pp 91–96.
192. Jain, R.K. et al., 2007. Angiogenesis in brain tumours. *Nat Rev Neurosci*. 8(8):610–622.
193. Jakacki, R.I. et al., 1998. Dose-intensification of procarbazine, CCNU (Lomustine), vincristine (PCV) with peripheral blood stem cell support in young patients with gliomas. *Med Pediatr Oncol*. 31(6), pp 483–490.
194. Jakacki, R.I. et al., 2008. A Phase I Trial of Temozolomide and lomustine in newly diagnosed high-grade gliomas of childhood. *Neuro Oncol*. 10(4), pp 569–576.
195. James, C.D. et al. 1989. Mitotic recombination of chromosome 17 in astrocytomas. *Proc Natl Acad Sci USA*. 86, pp 2858–2862.

196. Jarzabek, M.A. et al., 2013. Molecular imaging in the development of a novel treatment paradigm for glioblastoma (GBM): an integrated multidisciplinary commentary. *Drug Discov Today*. 18(21-22), pp 1052–1066.
197. Jenkinson M.D. et al., 2007. Advanced MRI in the management of adult gliomas. *Br J Neurosurg*. 21(6), pp 550–561.
198. Jeong, S.M. et al. 2006. Changes in magnesium concentration in the serum and cerebrospinal fluid of neuropathic rats. *Acta Anaesthesiol. Scand*. 50, pp 211–216.
199. Johansson, A. et al., 2000. An improved procedure for N– to C–directed (inverse) solid–phase peptide synthesis. *J Comb Chem*. 2(5), pp 496–507.
200. Johnson–Léger, C. et al., 2006. Protein therapeutics − lessons learned and a view of the future. *Expert Opin Biol Ther*. 6(1), pp 1–7.
201. Jones, C. and Mulloy, B. 1993. Introduction to nuclear magnetic resonance. In: Jones, C., Mulloy, B. and Thomas, A.H. eds., *Spectroscopic methods and analyses: NMR, mass spectrometry, and metalloprotein techniques. Methods in Molecular Biology*™. New Jersey: Humana Press Inc., 1993, 17.
202. Jonsson, A.P. 2001. Mass spectrometry for protein and peptide characterisation. *Cell Mol Life Sci*. 58(7), pp 868–884.
203. Jorgensen, W.L. et al., 1983. Comparison of simple potential functions for simulating liquid water. *J Chem Phys*. 79(2), pp 926–935.
204. Joshi, M. and Fehlings, M.G 2002. Development and characterization of a novel, graded model of clip compressive spinal cord injury in the mouse: Part 1. Clip design, behavioral outcomes, and histopathology. *J Neurotrauma*. 19(1), pp 175–190.
205. Juillerat- Jeanneret L. 2008. The Targeted delivery of cancer drugs across the blood- brain barrier: chemical modifications of drugs or drug nanoparticles? *Drug Discov Today*. 13(23/24), pp.1099–1106.
206. Juratli, T.A., Schackert, G. and Krex, D. 2013. Current status of local therapy in malignant gliomas – A clinical review of three selected approaches. *Pharmacol Ther*. 139(3), pp 341–358.
207. Kann, Jr. H.E. 1978. Comparison of biochemical and biological effects of four nitrosoureas with differing carbamoylating activities. *Cancer Res*. 38, pp 2363–2366.
208. Kanugula, S. and Anthony E Pegg, A.E. 2003. Alkylation damage repair protein O6-alkylguanine-DNA alkyltransferase from the hyperthermophiles Aquifex aeolicus and Archaeoglobus fulgidus. *Biochem J*. 375(Pt 2), pp. 449–455.

209. Kappelle, A.C. et al., PCV chemotherapy for recurrent glioblastoma multiforme. *Neurology*. 56(1), pp 118–120.
210. Kebarle, P. 2000. A brief overview of the present status of the mechanisms involved in electrospray mass spectrometry. *J. Mass Spectrom*. 35, pp 804–817.
211. Keles, E.G., Anderson B. and Berger, M.S. 1999. The effect of extent of resection on time to tumor progression and survival in patients with glioblastoma multiforme of the cerebral hemisphere. *Surg Neurol*. 52(4), pp 371–379.
212. Keles, G.E. et al. 2004. Volume of residual disease as a predictor of outcome in adult patients with recurrent supratentorial glioblastomas multiforme who are undergoing chemotherapy. *J Neurosurg*. 100(1), pp 41–46.
213. Kent, S.B.H. 1988. Chemical synthesis of peptides and proteins *Ann. Rev. Biochem*. 57, pp 957–989.
214. Kesari, S. 2011. Understanding glioblastoma tumor biology: The Potential to improve current diagnosis and treatments. *Semin Oncol*. 38(6), Suppl 4, pp S2–S10.
215. Khasraw, M. and Lassman, A.B. 2010. Advances in the Treatment of Malignant Gliomas. *Curr Oncol Rep*. 12(1), pp 26–33.
216. Kim, J.A. et al., 2012. Role of cell cycle on the cellular uptake and dilution of nanoparticles in a cell population. *Nat Nanotechnol*. 7(1), pp 62–68.
217. Kleihues, P. and Ohgaki, H. 1999. Primary and secondary glioblastomas: From concept to clinical diagnosis. *Neuro Oncol*. 1(1), pp 44–51.
218. Kleihues, P. and Ohgaki, H. 2000. Phenotype vs genotype in the evolution of astrocytic brain tumors. *Toxicol Pathol*. 28(1):164-170.
219. Kniesel, U. and Wolburg, H. 2000. Tight junctions of the blood-brain barrier. *Cell Mol Neurobiol* 20, pp 57–76.
220. Kohn, K.W. 1977. Interstrand cross-linking of DNA by 1, 3-Bis (2-chloroethyl)-1-nitrosourea and other 1-(2-haloethyl)-1-nitrosoureas. *Cancer Res.* 37, pp 1450–1454.
221. Koolman J. and Roehm, K.H. 2005 Color Atlas of Biochemistry 2nd Edition. Stuttgart, NewYork: Thieme. http://faculty.ksu.edu.sa/ [Accessed 10 February 2014] .
222. Kreisl, T.N. et al., 2009. Phase II trial of single-agent bevacizumab followed by bevacizumab plus irinotecan at tumor progression in recurrent glioblastoma. J Clin Oncol. 27(5), pp 740–745.
223. Kreth F.W. et al., 2013. Gross total but not incomplete resection of glioblastoma prolongs survival in the era of radiochemotherapy. Ann Oncol. 24(12):3117–23.

224. Krex, D. et al., 2007. Long–term survival with glioblastoma multiforme. *Brain*. 130(Pt 10), pp 2596–2606.
225. Kriegler, A.B., Bernardo, D. and Verschoor, S.M. 1994. Protection of murine bone marrow by dexamethasone during cytotoxic chemotherapy. *Blood*. 83(1), pp 65–71.
226. Kroll, R.A. and Neuwelt, E.A. 1998. Outwitting the blood–brain barrier for therapeutic purposes: osmotic opening and other means. *Neurosurgery*. 42(5), pp 1083–1099; discussion 1099–1100.
227. Kunwar, S. et al. 2010. Phase III randomized trial of CED of IL13-PE38QQR vs gliadel wafers for recurrent glioblastoma. *Neuro Oncol*. 12(8), pp 871–881.
228. Lacroix, M. et al., 2001. A multivariate analysis of 416 patients with glioblastoma multiforme: prognosis, extent of resection, and survival. *J Neurosurg*. 95(2), pp 190–198.
229. Ladner, R. et al., 2004. Phage display–derived peptides as therapeutic alternatives to antibodies. *Drug Discov Today*. 9(12), pp 525–529.
230. Lagas, J.S. et al., 2009. Brain accumulation of dasatinib is restricted by P–glycoprotein (ABCB1) and breast cancer resistance protein (ABCG2) and can be enhanced by elacridar treatment. *Clin Cancer Res*. 15(7), pp 2344–2345.
231. Lalatsa A, et al. 2012a A Prodrug Nanoparticle Approach for the Oral Delivery of a Hydrophilic Peptide, Leucine5-enkephalin, to the Brain. *Mol Pharm*. 9:1665−1680.
232. Lalatsa, A. et al., 2012b. Delivery of peptides to the blood and brain after oral uptake of quaternary ammonium palmitoyl glycol chitosan nanoparticles. *Mol Pharm*. 9(6), pp 1764–1774.
233. Langham, A.A., Waring, A.J. and Kaznessis, Y.N. 2007. Comparison of interactions between beta–hairpin decapeptides and SDS/DPC micelles from experimental and simulation data. *BMC Biochem*. 8, pp 11.
234. Laperriere, N. et al. 2002. Radiotherapy for newly diagnosed malignant glioma in adults: a systematic review. *Radiother Oncol*. 64(3), pp 259–73.
235. Law, M. et al., 2002. High–grade gliomas and solitary metastases: differentiation by using perfusion and proton spectroscopic MR imaging. *Radiology*. 222(3), pp 715–721.
236. Laxton, R.C. et al., 2013. Primary glioblastoma with oligodendroglial differentiation has better clinical outcome but no difference in common biological markers compared with other types of glioblastoma. Neuro Oncol. 15(12), pp 1635–1643.

237. Lee, O.-S., Cho, V., Schatz, G.C. 2012. Modeling the self-assembly of peptide amphiphiles into fibers using coarse-grained molecular dynamics. *Nano Lett*. 12(9), pp 4907–4913.
238. Lee, V.H.L 1991. Changing needs in drug delivery in the era of peptide and protein drugs. In: Lee V.H.L. ed., *Peptide and protein drug delivery*. New York: Marcel Dekker Inc., 1991, pp 1–56.
239. Lee F, Weinmann R. 2008. Animal cancer models in anticancer drug discovery and development. In: S. Li (ed.) *Mouse models of human blood cancers*. Springer Science + Business Media, LLC. 2008, pp 245–258.
240. Lehn, J-M. 2002. Toward complex matter: Supramolecular chemistry and self-organization. *PNAS*. 99(8), pp 4763–4768.
241. Leon, S.P., Folkerth, R.D. and Black, P.M. 1996. Microvessel density is a prognostic indicator for patients with astroglial brain tumors. *Cancer*. 77(2), pp 362–72.
242. Leu, D. et al. 1984. Distribution and elimination of coated polymethyl [2-14C] methacrylate nanoparticles after intravenous injection in rats. *J Pharm Sci*. 73, pp 1433–1437.
243. Levin V. A. (1999) Chemotherapy for brain tumors of astrocytic and oligodendroglial lineage: The past decade and where we are heading. *Neuro Oncol*. 1: 69–80.
244. Levin, V.A. et al., 1970. The uptake, distribution and antitumor activity of 1-(2-chloroethyl)-3-cyclohexyl-l-nitrosourea in the murine glioma. *Cancer Res*. 30, pp 2451–2455.
245. Lidar, Z. et al., 2004. Convection-enhanced delivery of paclitaxel for the treatment of recurrent malignant glioma: a Phase I/II clinical study. *J Neurosurg*. 100(3), pp 472–479.
246. Liebner, S. et al., 2000. Claudin-1 and claudin-5 expression and tight junction morphology are altered in blood vessels of human glioblastoma multiforme. *Acta Neuropathol (Berl).* 100(3): 323–331.
247. Lima, F.R.S. et al. 2012. Glioblastoma: Therapeutic challenges, what lies ahead. *Biochimica et Biophysica Acta*. 1826, pp 338–349.
248. Lindner, H. and Helliger, W. 2004. Hydrophilic interaction chromatography. In: *HPLC of peptides and proteins. Methods and protocols. Methods in Molecular Biology™*. New Jersey: Humana Press Inc., 2004, 251.

249. Lloyd–Williams, P., Albericio, F. and Giralt, E. 1997. Chemical approaches to the synthesis of peptides and proteins. In: Rees C.W. series ed., *Chemical approaches to the synthesis of peptides and proteins*. New York: CRC Press, 1997, pp 1–93.
250. Loffet, A. 2002. Peptides as drugs: is there a market? *J Pept Sci*. 8(1), pp 1–7.
251. Lonardi, S., Tosoni, A., Brandes, A.A. 2005. Adjuvant chemotherapy in the treatment of high grade gliomas. *Cancer Treat Rev*. 31, pp 79–89.
252. Long, D.M. 1979. Capillary ultrastructure in human metastatic brain tumors. *J Neurosurg*. 51(1), pp 53–58.
253. Loo, J.A. 2000. Electrospray ionization mass spectrometry: a technology for studying noncovalent macromolecular complexes. *Int J Mass Spectrom*. 200, pp 175–186.
254. Louis, D.N. et al. 2007. *WHO Classification of Tumors of the Central Nervous System*. 4th edn. IARC: Lyon, France, 2007.
255. Lucchese G. et al. 2007. Peptidology: short amino acid modules in cell biology and immunology. *Amino Acids*. 33(4), pp703–707.
256. Lwin Z. et al. 2013. Glioblastoma management in the temozolomide era: have we improved outcome? *J Neurooncol*. 115(2), pp 303–310.
257. Lyman, G.H. et al., 1998. The economics of febrile neutropenia: implications for the use of colony-stimulating factors. *Eur J Cancer*. 34 (12), pp 1857–1864.
258. Lymann. G.H et al., 2013. The impact of the granulocyte colony-stimulating factor on chemotherapy dose intensity and cancer survival: a systematic review and meta-analysis of randomized controlled trials. *Ann Oncol*. 2013. 24(10), pp 2475–2484.
259. Malmström, A. et al., 2012. Temozolomide versus standard 6-week radiotherapy versus hypofractionated radiotherapy in patients older than 60 years with glioblastoma: The Nordic randomised phase 3 trial. *Lancet Oncol* 13(9), pp 916–926.
260. Mandl, E.S. 2008. Repeated surgery for glioblastoma multiforme: only in combination with other salvage therapy. *Surg Neurol*. 69(5), pp 506–509, discussion 509.
261. Mangiola, A. et al. 2010. Glioblastoma therapy: going beyond Hercules Columns. *Expert Rev. Neurother*. 10(4), pp 507–514.
262. Mant, C.T. and Hodges R.S. 1996. Analysis of Peptides by High–Performance Liquid Chromatography. *Methods Enzymol*. Academic Press Inc., 1996, 271, pp 3–50.
263. Mant, C.T. et al., 1997. Analysis of synthetic peptides by high–performance liquid chromatography. In: Fields, G.B. ed., *Solid phase peptide synthesis. Methods in Enzymol*. Academic Press Inc., 289, pp 426–69.

264. Mant, C.T. et al., 2007. HPLC Analysis and Purification of Peptides. In: Fields, G. ed., *Peptide characterization and application protocols. Methods in Molecular Biology*. New Jersey: Humana Press Inc.2007, 386, pp 3–55.
265. Manwani, D. and Bieker, J.J. 2008. The erythroblastic island. *Curr Top Dev Biol*. 82, pp 23–53.
266. Marrink, S.J. et al., 2007. The MARTINI force field: Coarse grained model for biomolecular simulations. *J Phys Chem B*. 111(27), pp 7812–7824.
267. Maxwell, M.B. and Maher, K.E. 1992. Chemotherapy-induced myelosuppression. *Semin Oncol Nurs*. 8(2), pp 113–123.
268. Mazza, M. et al., 2013. Nanofiber-Based Delivery of Therapeutic Peptides to the Brain. *ACS Nano*. 7 (2), pp 1016–1026.
269. McAllister, L.D. et al., 2000. Cognitive outcomes and long-term follow-up results after enhanced chemotherapy delivery for primary central nervous system lymphoma. *Neurosurgery*. 46(1), pp 51-60, discussion 60–61.
270. McGregor, D.P. 2008. Discovering and improving novel peptide therapeutics. *Curr Opin Pharmacol*. 8(5), pp 616–619.
271. McLaughlin, P.J., Levin, R.J. and Zagon I.S. 2003. Opioid growth factor (OGF) inhibits the progression of human squamous cell carcinoma of the head and neck transplanted into nude mice. *Cancer Letters*. 199, pp 209–217.
272. McMahon, B.J. and Kwaan, H.C. 2012. Thrombotic and bleeding complications associated with chemotherapy. *Semin Thromb Hemost*. 38, pp 808–817
273. McPhail, D. et al., 2000. Liposomes encapsulating polymeric chitosan based vesicles – a vesicle in vesicle system for drug delivery. *Int J Pharm*. 200:73–86.
274. Meienhofer, J. et al., 1979. Solid phase synthesis without repetitive acidolysis. Preparation of leucyl-alanyl-glycyl-valine using 9-fluorenylmethoxycarbonylamino acids. *Int J Pept Protein Res*. 13, pp 35–42.
275. Merrifield, R.B. 1963. Solid phase peptide synthesis. I. The synthesis of a tetrapeptide. *J. Am. Chem. Soc*. 85(14), pp 2149–2154.
276. Merrifield, R.B. 1986. Solid Phase Synthesis. *Science*. 232, pp 341–347.
277. Meyerand, M.E. et al. 1999. Classification of biopsy–confirmed brain tumors using single–voxel MR spectroscopy. *AJNR Am J Neuroradiol*. 20(1), pp 117–123.
278. Mineo, J.F. et al. 2007. Prognosis Factors of Survival Time in Patients with Glioblastoma Multiforme: A multivariate Analysis of 340 Patients. *Acta Neurochir (Wien)*. 149, pp 245–253.
279. Misra, A. et al., 2003. Drug delivery to the central nervous system: a review. *J Pharm Sci*. 6(2):252–273.

280. Missirlis, D. and Hubbell, J.A. 2010. In vitro uptake of amphiphilic, hydrogel nanoparticles by J774A.1 cells. J Biomed Mater Res A. 93(4), pp 1557–65.
281. Moghimi, S.M., Hunter, A.C. and Murray, J.C. 2001. Long-circulating and target-specific nanoparticles: Theory to Practice. *Pharmacol Rev*. 53, pp 283–318.
282. Möller-Hartmann, W. et al. 2002. Clinical application of proton magnetic resonance spectroscopy in the diagnosis of intracranial mass lesions. *Neuroradiology*. 44(5), pp 371–381.
283. Montgomery, J.A. et al., 1975. Decomposition of N-(2-Chloroethyl)-N-nitrosoureas in aqueous media. *J Med Chem*. 18(6), pp 568–571.
284. Monticelli, L. et al., 2008. The MARTINI coarse-grained force field: Extension to proteins. J Chem Theory Comput. 4(5), pp 819–834.
285. Mori, M. et al., 1990. Macrophage heterogeneity in bone marrow culture in vitro. *J Cell Sci*. 95(3), pp 481-485.
286. Morris, H.R. et al., 1997. A novel geometry mass spectrometer, the Q–TOF, for low–femtomole/attomole–range biopolymer sequencing. *J Protein Chem*. 16(5), pp 469–479.
287. Morstyn, G. et al., 1988. Effect of granulocyte colony stimulating factor on neutropenia induced by cytotoxic chemotherapy. *Lancet*. 1(8587), pp 667–672.
288. Nabors, M.W. et al., 1991. Multidrug resistance gene (MDR1) expression in human brain tumors. *J Neurosurg*. 75(6), 941–946.
289. Nadal, A., Fuentes, E., Pastor, J., McNaughton, P.A., 1995. Plasma albumin is a potent trigger of calcium signals and DNA synthesis in astrocytes. *Proc Natl Acad Sci. USA*. 92(5), pp 1426–1430.
290. Nagai, Y. et al., 2006. Slow release of molecules in self-assembling peptide nanofiber scaffold. *J control Release*. 115(1), pp 18–25.
291. Nakamura, H. et al., 2013. Can MRI-derived factors predict the survival in glioblastoma patients treated with postoperative chemoradiation therapy? *Acta Radiol*. 54(2), pp 214–220.
292. Nathan, D.G. 1987. Stem Cells and Hematopoiesis. In: Smaaland, R. et al., 2002. Rhythms in human bone marrow and blood cells. *Chronobiol Int*. 19(1), pp 101–127.
293. Neeland, I.J. et al., 2012. Dysfunctional adiposity and the risk of prediabetes and type 2 diabetes in obese adults. *JAMA*. 308(11), pp 1150–1159.
294. Newcomb, E.W. et al., 1998. Survival of patients with glioblastoma multiforme is not influenced by altered expression of P16, P53, EGFR, MDM2 or Bcl-2 Genes. *Brain Pathol*. 8(4), pp 655–667.

295. Newlands, E.S. et al., 1992. Phase I trial of temozolomide (CCRG 81045: M&B 39831: NSC 362856) *Br J Cancer*. 65(2), 287–291.
296. Newlands, E.S. et al., 1997. Temozolomide: a review of its discovery, chemical properties, pre-clinical development and clinical trials. *Cancer Treat Rev*. 23(1), pp 35–61.
297. Neyns, B. et al., 2011. Phase II study of sunitinib malate in patients with recurrent high-grade glioma. *J Neurooncol*. 103(3), pp 491–501.
298. Nieder, C., Adam, M. and Grosu, A.L. 2006. Combined modality treatment of glioblastoma multiforme: the role of temozolomide. *Rev Recent Clin Trials*. 1(1), pp 43–51.
299. Nischwitz, V., Berthele, A. and Michalke, B. 2008. Speciation analysis of selected metals and determination of their total contents in paired serum and cerebrospinal fluid samples: an approach to investigate the permeability of the human blood– cerebrospinal fluid-barrier. *Anal. Chim. Acta*. 627(2), pp 258–269.
300. Niyazi, M. et al., 2011. Therapeutic options for recurrent malignant gliomas. *Radiother Oncol*. 98(1):1–14.
301. Nobusawa, S. et al. 2009. IDH1 mutations as molecular signature and predictive factor of secondary glioblastomas. *Clin Cancer Res*. 15(19), pp 6002–6007.
302. Nomura, T., Inamura, T. and Black, K.L 1994. Intracarotid infusion of bradykinin selectively increases blood-tumor permeability in 9L and C6 brain tumors. *Brain Res*. 659(1-2), pp 62–66.
303. Norden, A.D. et al. 2008. Bevacizumab for recurrent malignant gliomas: efficacy, toxicity, and patterns of recurrence. *Neurology*. 70(10), pp 779–787.
304. Nose, S. and Klein, M.L. 1983. Constant pressure molecular dynamics for molecular systems. Mol Phys. 50(5), pp 1055–1076.
305. Nose, S.A. 1984. Molecular-dynamics method for simulations in the canonical ensemble. Mol Phys. 52(2), pp 255–268.
306. Ochs, K. and Kaina, B. 2000. Apoptosis induced by DNA damage O6-methylguanine is Bcl-2 and caspase-9/3 regulated and Fas/caspase-8 independent. *Cancer Res*. 60:5815–5824.
307. Ohgaki, H. and Kleihues P. 2007. Genetic pathways to primary and secondary glioblastoma. *Am J Pathol*. 170(5), pp 1445–1453.
308. Ohgaki, H. and Kleihues P. 2013. The definition of primary and secondary glioblastoma. *Clin Cancer Res*. 19(4):764–772.
309. Ohgaki, H. and Kleihues, P. 2005. Epidemiology and etiology of gliomas. *Acta Neuropathol*. 109(1), pp 93–108.

310. Ohgaki, H. et al. 2004. Genetic pathways to glioblastoma: a population–based study. *Cancer Res*. 64(19), pp 6892–6899.
311. Olar, A. and Aldape, K.D. 2014. Using the molecular classification of glioblastoma to inform personalized treatment. *J Pathol*. 232, pp 165–177.
312. Olar, A. et al. 2012. Absence of IDH1–R132H mutation predicts rapid progression of nonenhancing diffuse glioma in older adults. *Ann Diagn Pathol*. 16(3), pp 161–170.
313. Oliverio, V.T. et al., 1970. The absorption, distribution, excretion, and biotransformation of the carcinostatic 1-(2-Chloroethyl)-3-cyclohexyl-l-nitrosourea in animals. *Cancer Res*. 30, pp 1330–1337.
314. Ommaya, A.K. 1963. Subcutaneous reservoir and pump for sterile access to ventricular cerebrospinal fluid. *Lancet*. 2(7315), pp 983–984.
315. Ommaya, A.K. 1984. Implantable devices for chronic access and drug delivery to the central nervous system. *Cancer Drug Deliv*. 1(2), pp 169–179.
316. Owens, D.E. and Peppas, N.A. 2006. Opsonization, biodistribution, and pharmacokinetics of polymeric nanoparticles. *Int J Pharm*. 307, pp 93–102.
317. Palmer, L.C. 2007. Supramolecular self-assembly codes for functional structures. *Philos Transact A Math Phys Eng Sci*. 365, pp 1417–1433.
318. Palmer, L.C. and Stupp, S.I. 2008. Molecular self-assembly into one-dimensional nanostructures. *Acc Chem Res*. 41, pp 1674–1684.
319. Panasci, L.C. et al., 1977. A structure-activity analysis of chemical and biological parameters of chloroethylnitrosoureas in mice. *Cancer Res*. 37(8 Pt 1), pp 2615–2618.
320. Paramonov, S.E., Jun, H-W. and Hartgerink, J.D. 2006. Self assembly of Peptide- Amphiphile Nanofibres: The Roles of Hydrogen bonding and Amphiphilic Packing. *J Am Chem Soc*. 128(22), pp 7291–7298.
321. Pardridge, W.M. 1991. *Peptide Drug Delivery to the Brain*. New York: Raven Press.
322. Pardridge, W.M. 1995. Transport of small molecules through the blood-brain barrier: biology and methodology. *Adv Drug Deliv Rev*. 15(1-3), pp 5–36.
323. Pardridge, W.M. 2005. The blood–brain barrier: bottleneck in brain drug development. *NeuroRx.* 2(1), pp 3–14.
324. Pardridge, W.M. 2007. shRNA and siRNA delivery to the brain. *Adv Drug Deliv Rev*. 59(2–3), pp 141–152.

325. Pardridge, W.M. et al., 1990. Evaluation of cationized rat albumin as a potential blood–brain barrier drug transport vector. *J Pharmacol Exp Ther*. 255(2), pp 893–899.
326. Parrinello, M. and Rahman, A. 1981. Polymorphic transitions in single crystals: A new molecular dynamics method. J Appl Phys. 52(12), pp 7182–7190.
327. Parsons, D.W. et al. 2008. An integrated genomic analysis of human glioblastoma multiforme. *Science*. 321(5897):1807–1812.
328. Pegg, A.E. 1990. Mammalian O6-alkylguanine-DNA alkyltransferase: regulation and importance in response to alkylating carcinogenic and therapeutic agents. *Cancer Res*. 50(19), pp 6119–6129.
329. Peters, W. P. et al., 1993. Comparative effects of granulocyte-macrophage colony-stimulating factor (GM-CSF) and granulocyte colony-stimulating factor (G-CSF) on priming peripheral blood progenitor cells for use with autologous bone marrow after high-dose chemotherapy. *Blood*. 81(7), pp 1709–1719.
330. Petri, B. et al., 2007. Chemotherapy of brain tumour using doxorubicin bound to surfactant-coated poly (butyl cyano acrylate) nanoparticles: Revisiting the role of surfactants. *J Control Release*. 117(1), pp 51–58.
331. Phillips, H.S. et al., 2006. Molecular subclasses of high-grade glioma predict prognosis, delineate a pattern of disease progression, and resemble stages in neurogenesis. *Cancer Cell*. 9(3), pp 157–173.
332. Pollak, M.N. et al., 1989. Recombinant GM-CSF in myelosuppression of chemotherapy. In: Smaaland, R. et al., 2002. Rhythms in human bone marrow and blood cells. *Chronobiol Int*. 19(1), pp 101–127.
333. Pratt, W.B. et al., 1994. The anticancer drugs. In: Pratt, W.B. ed., *The anticancer drugs*. 2nd edition. New York: Oxford University Press, pp 128–133.
334. Qian, L. et al. 2013. Cationic core–shell nanoparticles with carmustine contained within O^6–benzylguanine shell for glioma therapy. *Biomaterials*. 34(35), pp 8968–8978.
335. Qu, X. et al., 2006. Carbohydrate-based micelle clusters which enhance hydrophobic drug bioavailability by up to 1 order of magnitude. *Biomacromolecules*. 7(12), pp 3452–3459.
336. Quinn, J.A. et al., 2009. Phase II trial of temozolomide plus o6-benzylguanine in adults with recurrent, temozolomide-resistant malignant glioma. *J Clin Oncol*. 27(8), pp 1262–1267.

337. Radhakrishnan, K. et al. 1995. The Trends in Incidence of Primary Brain Tumors in the Population of Rochester, Minnesota. *Ann Neurol*. 37(1), pp 67–73.
338. Rainov, N.G. et al., 1997. Prognosis factors in malignant glioma: Influence of the overexpression of oncogene and tumor–suppressor gene products on survival. *J Neurooncol*. 35(1), pp 13–28.
339. Raizer, J. 2011. Issues in Developing Drugs for Primary Brain Tumors: Barriers and Toxicities. *Toxicol Pathol*. 39(1), pp 152–157.
340. Rajagopal, K. and Schneider, J.P. 2004. Self–assembling peptides and proteins for nanotechnological applications. *Curr Opin Struct Biol*. 14, pp 480–486.
341. Ramos, P. et al., 2013. Macrophages support pathological erythropoiesis in polycythemia vera and β-thalassemia. *Nat Med*. 19(4):437–45.
342. Reches, M. and Gazit, E. 2003. Insights into the Self-Assembly of Phenylalanine Oligopeptides by Replica Exchange MD Simulations with the GBSW Implicit-Solvent Model. *Science*. 300, pp 625–662.
343. Reches, M., Porat, Y. and Gazit E. 2002. Amyloid fibril formation by pentapeptide and tetrapeptide fragments of human calcitonin. *J Biol Chem*. 277(38), pp 35475–35480.
344. Reed, D.J. et al. 1975. 2-Chloroethanol formation as evidence for a 2-chloroethyl alkylating intermediate during chemical degradation of 1-(2-chloroethyl)-3-cyclohexyl-1-nitrosourea and 1-(2-Chloroethyl)-3-(trans-4-methylcyclohexyl)-1-nitrosourea. *Cancer Res*. 35, pp 568–576.
345. Reifenberger, G. et al., 1993. Amplification and overexpression of the MDM2 gene in a subset of human malignant gliomas without p53 mutations. *Cancer Res*. 53(12), pp 2736–2739.
346. Reithmeier, T. et al., 2010. BCNU for recurrent glioblastoma multiforme: efficacy, toxicity and prognostic factors. *BMC Cancer*. 10:30.
347. Rosenthal, M.A., Ashley, D.L. and Cher, L. 2004. BCNU as second line therapy for recurrent high-grade glioma previously treated with Temozolomide. *J Clin Neurosci*. 11(4), pp 374–375.
348. Salmaggi, A. et al.2003. Intracavitary VEGF, bFGF, IL-8, IL-12 levels in primary and recurrent malignant glioma. *J Neurooncol*. 62(3), pp 297–303.
349. Sanai, N. and Berger, M.S. 2009. Operative Techniques for Gliomas and the Value of Extent of Resection. *Neurotherapeutics*. 6(3):478–486.
350. Sandberg, D.I. et al., 2000. Ommaya reservoirs for the treatment of leptomeningeal metastases. Neurosurgery. 47(1), pp 49–54, discussion 54–55.

351. Sarker, M.H., Hu, D.E. and Fraser, P.A. 2000. Acute effects of bradykinin on cerebral microvascular permeability in the anaesthetized rat. *J Physiol*. 528(1), pp 177—187.
352. Sasso, F.C. et al., 2004. Glucose metabolism and coronary heart disease in patients with normal glucose tolerance. *JAMA*. 291(15), pp 1857–1863.
353. Sato, A.K. et al., 2006. Therapeutic peptides: technological advances driving peptides into development. *Curr Opin Biotechnol*. 17(6), pp 638–642.
354. Satoh, T. and Hosokawa, M. 1998. The mammalian carboxylesterases: From molecules to functions. *Annu Rev Pharmacol Toxicol*. 38, pp 257–288.
355. Sauer, I. et al. 2005. An apolipoprotein E-derived peptide mediates uptake of sterically stabilized liposomes into brain capillary endothelial cells. *Biochemistry*. 44(6), pp 2021–2029.
356. Sausville, E.A, Burger, A.M. 2006. Contributions of human tumor xenografts to Anticancer Drug Development. *Cancer Res*. 66, pp 3351–3354.
357. Scherer, H.J. 1940. Cerebral astrocytomas and their derivatives. *Am J Cancer*. 40, pp 159–198.
358. Schlageter, K.E. et al., 1999. Microvessel organization and structure in experimental brain tumors: microvessel populations with distinctive structural and functional properties. *Microvasc. Res*. 58, pp 312– 328.
359. Schofield, R. 1986. Assessment of cytotoxic injury to bone marrow. *Br J Cancer*. 53(Suppl. VII), pp 115–125.
360. Schold, S.C. 1989. O6-alkylguanine-DNA alkyltransferase and sensitivity to procarbazine in human brain-tumor xenografts. *J Neurosurg*. 70(4), pp 573–577.
361. Scott, B.J. et al., Bevacizumab salvage therapy following progression in high-grade glioma patients treated with VEGF receptor tyrosine kinase inhibitors. *Neuro Oncol*. 12(6), pp 603–607.
362. Selek, L. et al. 2014. Imaging and histological characterization of a human brain xenograft in pig: the first induced glioma model in a large animal. *J Neurosci Methods*. 221, pp159–165.
363. Server, A. et al., 2010. Proton magnetic resonance spectroscopy in the distinction of high-grade cerebral gliomas from single metastatic brain tumors. *Acta Radiol*. 51(3), 316–325.
364. Service, R.F. 2005. How far can we push self- assembly? *Science*. 309(5731), pp 95.
365. Shapiro, W.R. 1971. Studies on the chemotherapy of experimental brain tumors: evaluation of 1-(2-chloroethyl)-3-cyclohexy-1-nitrosourea, vincristine and 5-fluorouracil. J Natl Cancer Inst. 46, pp 359–368.

366. Shaw, C. 1994. Peptide purification by reverse–phase HPLC. In: Walker, J.M. ed., *Basic protein and peptide protocols. Methods in Molecular Biology*. New Jersey: Humana Press Inc., 1994, 32.
367. Shweiki, D. et al., 1992. Vascular endothelial growth factor induced by hypoxia may mediate hypoxia-initiated angiogenesis. *Nature*. 359(6398), pp 843–845.
368. Siew, A. et al. 2012. Enhanced oral absorption of hydrophobic and hydrophilic drugs using quaternary ammonium palmitoyl glycol chitosan nanoparticles. *Mol Pharm*. 9(1), pp 14–28.
369. Simpson, J.R. et al., 1993. Influence of location and extent of surgical resection on survival of patients with glioblastoma multiforme: results of three consecutive Radiation Therapy Oncology Group (RTOG) clinical trials. *Int J Radiat Oncol Biol Phys*. 26(2), pp 239–244.
370. Singh, R. and Lillard, J.W. Jr. 2009. Nanoparticle–based targeted drug delivery. *Exp Mol Pathol*. 86(3), pp 215–223.
371. Smaaland, R. et al., 2002. Rhythms in human bone marrow and blood cells. *Chronobiol Int*. 19(1), pp 101–127.
372. Smart, S. et al., 1996. High–throughput purity estimation and characterisation of synthetic peptides by electrospray mass spectrometry. *Int J Pept Protein Res*. 47(1–2), pp 47–55.
373. Smith, D.D. and Hanly, A.M. 1997. Purification of Synthetic Peptides by High Performance Liquid Chromatography. In: Irvine, G.B. and Williams, C.H. eds., *Neuropeptide protocols. Methods in Molecular Biology*™. New Jersey: Humana Press Inc., 73, pp 75–87.
374. Smith, I.C. and Blandford, D.E. 1995. Nuclear magnetic resonance spectroscopy. *Anal Chem*. 67(12), pp 509R–518R.
375. Smith, R.D. et al., 1990. New developments in biochemical mass spectrometry: electrospray ionization. *Anal Chem*. 62(9), pp 882–899.
376. Sogorb, M.A. and Vilanova, E. 2002. Enzymes involved in the detoxification of organophosphorus, carbamate and pyrethroid insecticides through hydrolysis. *Toxicol Lett*. 128, pp 215–228.
377. Solouki, T. et al., 1995. Attomole biomolecule mass analysis by matrix–assisted laser desorption/ionization Fourier transform ion cyclotron resonance. *Anal Chem*. 67(22), pp 4139–4144.
378. Song, E. et al. 2005. Antibody mediated in vivo delivery of small interfering RNAs via cell–surface receptors. *Nat Biotechnol*. 23(6), pp 709–717.
379. Soppimath, K. S. et al., 2000. Biodegradable polymeric nanoparticles drug delivery devices. *J Control Release*. 70(1-2), pp 1–20

380. Spiegl–Kreinecker, S. et al., 2002. Expression and functional activity of the ABC–transporter proteins P–glycoprotein and multidrug–resistance protein 1 in human brain tumor cells and astrocytes. *J Neurooncol*. 57(1), pp 27–36.
381. Stamatovic, S.M., Keep, R.F. and Andjelkovic, A 2008. Brain Endothelial Cell-Cell Junctions: How to "Open" the Blood Brain Barrier Curr *Neuropharmacol*. 6(3), pp 179–192.
382. Stark, A.M. et al. 2005. Glioblastoma multiforme–report of 267 cases treated at a single institution. *Surg Neurol*. 63(2), pp 162– 169.
383. Steiniger, S.C. et al. 2004. Chemotherapy of glioblastoma in rats using doxorubicin-loaded nanoparticles. *Int J Cancer*. 109(5), pp 759–767.
384. Stendahl, J.C. et al., 2006. Intermolecular forces in the self–assembly of peptide amphiphile nanofibers. *Adv. Funct. Mater*. 16, pp 499–508.
385. Stepišnik, J. 2006. Spectroscopy: NMR down to earth. News and views. *Nature*. 439, pp 799–801.
386. Stewart, L.A. 2002. Chemotherapy in adult high–grade glioma: a systematic review and meta–analysis of individual patient data from 12 randomised trials. *Lancet*. 359(9311), pp 1011–1018.
387. Stummer, W. et al., 2006. Fluorescence–guided surgery with 5–aminolevulinic acid for resection of malignant glioma: a randomised controlled multicentre phase III trial. Lancet Oncol. 7(5), pp 392–401.
388. Stummer, W. et al. 2008. Extent of resection and survival in glioblastoma multiforme: identification of and adjustment for bias. *Neurosurgery*. 62(3), pp 564–576, discussion 564–76.
389. Stupp, R. et al., 2005. Radiotherapy plus Concomitant and Adjuvant Temozolomide for glioblastoma. N Engl J Med. 352:987–996.
390. Stupp, R. et al., 2009. Effects of radiotherapy with concomitant and adjuvant temozolomide versus radiotherapy alone on survival in glioblastoma in a randomised Phase III study: 5-year analysis of the EORTC-NCIC trial. *Lancet Oncol*. 10, pp 459–466.
391. Stupp, S.I. and Palmer, L.C. 2014. Supramolecular chemistry and self-assembly in organic materials design. *Chem Mater*. 26, pp 507−518.
392. Su, Y.W. et al., 2005. Treatment-related myelodysplastic syndrome after temozolomide for recurrent high-grade glioma. *J. Neurooncol*. 71(3), pp 315–318.
393. Suizdak, G. 1994. The emergence of mass spectrometry in biochemical research. *Proc Nat. Acad Sc. USA*. 91, pp 11290–11297.
394. Suizdak, G. 2006. *The expanding role of mass spectrometry in biotechnology*. 2nd edition. San Diego: MCC Press, pp 1–32.

395. Tamai, I. and Tsuji, A. 2000 Transporter-mediated permeation of drugs across the blood-brain barrier. *J Pharm Sci*. 89(11), pp 1371–1388.
396. Tamura, M., Mennel, H.D., Zülch, K.J. 1979. Brain tumour chemotherapy using a rat glioma model. *J Cancer Res Clin Oncol*. 94(1), pp 39–46.
397. Tang, B.C. et al., 2010. Enhanced efficacy of local etoposide delivery by poly(ether-anhydride) particles against small cell lung cancer in vivo. *Biomaterials*. 31(2), pp 339–44.
398. Tano, K. et al. 1990. Isolation and structural characterization of a cDNA clone encoding the human DNA repair protein for O6-alkylguanine. *Proc Natl Acad Sci. USA*. 87(2), pp 686–690.
399. Teicher, A.B. 2006. Tumor models for efficacy determination. *Mol Cancer Ther*. 5(10), pp 2435–2443.
400. Thomson, J.J. 1913. Rays of positive electricity and their applications to chemical analysis. 2nd edition. London: Longmans Green and Co. https://archive.org/details/rayspositiveele01thomgoog Accessed 15 March 2014.
401. Toedt, G. et al. 2011. Molecular signatures classify astrocytic gliomas by IDH1 mutation status. *Int J Cancer*. 128(5), pp 1095–1103.
402. Tohma, Y. et al. 1998. PTEN (MMAC1) mutations are frequent in primary glioblastomas (de novo) but not in secondary glioblastomas. *J Neuropathol Exp Neurol*. 57(7), pp 684–689.
403. Tolcher, A.W. et al., 2003. Marked inactivation of O6-alkylguanine-DNA alkyltransferase activity with protracted temozolomide schedules. *Br J Cancer*. 88(7), pp 1004–1011.
404. Tosoni, A. et al., 2006. Is protracted low-dose temozolomide feasible in glioma patients? *Neurology*. 66(3), pp 427–429.
405. Tóth, K., et al., 1996. MDR1 P-glycoprotein is expressed by endothelial cells of newly formed capillaries in human gliomas but is not expressed in the neovasculature of other primary tumors. *Am J Pathol*. 149(3), pp 853–858.
406. Tsonchev, S., Schatz, G.C. and Ratner, M.A. 2003. hydrophobically- driven self- assembly: A geometric packing analysis. *Nano Lett*. 3, pp 623–626.
407. Tsonchev, S., Schatz, G.C. and Ratner, M.A. 2004. electrostatically- directed self- assembly of cylindrical peptide amphiphile nanostructures. *J Phys Chem. B* 108, pp 8817–8822.
408. Tysseling-Mattiace, V. M. et al., 2008 Self-assembling nanofibers inhibit glial scar formation and promote axon elongation after spinal cord injury. *J Neurosci*. 28(14), pp 3814–3823.
409. Uchegbu, I.F. et al., 2001. Quaternary ammonium palmitoyl glycol chitosan—a new polysoap for drug delivery. *Int J Pharm*. 224(1–2), pp 185–199.

410. van den Bent, M.J. 1998. Response rate and prognostic factors of recurrent oligodendroglioma treated with procarbazine, CCNU and vincristine chemotherapy. *Neurology*. 51(4), pp 1140–1145.
411. van den Bent, M.J. et al. 2003. Phase II Study of first-line chemotherapy with temozolomide in recurrent oligodendroglial tumors: The European Organization for Research and Treatment of Cancer Brain Tumor Group Study 26971. *J Clin Oncol*. 21(13), pp 2525–2528.
412. van den Bent, M.J. et al., 2006. Adjuvant procarbazine, lomustine, and vincristine improves progression-free survival but not overall survival in newly diagnosed anaplastic oligodendrogliomas and oligoastrocytomas: a randomized European Organisation for Research and Treatment of Cancer Phase III trial. *J Clin Oncol*. 24(18), pp 2715–2722.
413. van der Walle, C.F. and Olejnik, O. 2011 An overview of the field of peptide and protein delivery. In: van der Walle C.F. ed., *Peptide and protein delivery*. London: Elsevier, pp 1–22.
414. van Nispen, J.W. 1987. Synthesis and analysis of (poly) peptides. *Pure & Appl. Chem*. 59(3), pp 331–344.
415. Vauthier. C. et al. 2003. Poly(alkylcyanoacrylates) as biodegradable materials for biomedical applications. *Adv Drug Deliv Rev*. 55, pp 519–548.
416. Velichko, Y.S., Stupp, S.I. and de la Cruz, M.O. 2008. Molecular simulation study of peptide amphiphile self-assembly. *J Phys Chem B.* 112, pp 2326–2334.
417. Verhaak, R.G. et al., 2010. Integrated genomic analysis identifies clinically relevant subtypes of glioblastoma characterized by abnormalities in PDGFRA, IDH1, EGFR, and NF1. *Cancer Cell*. 19(1), pp 98–110
418. Vlieghe, P. et al., 2010. Synthetic therapeutic peptides: science and market. *Drug Discov Today*. 15(1–2), pp 40–56.
419. von Deimling, A. et al., 1992. p53 mutations are associated with 17p allelic loss in grade II and grade III astrocytoma. *Cancer Res*. 52(10), pp 2987–2990.
420. von Deimling, A. et al., 1993. Subsets of glioblastoma multiforme defined by molecular genetic analysis. *Brain Pathol*. 3, pp 19–26.
421. Vredenburgh, J.J. et al., 2007. Bevacizumab plus irinotecan in recurrent glioblastoma multiforme. J Clin Oncol. 25(30), pp 4722–4729.
422. Wait, R. (1993) Introduction to Mass Spectrometry. In: Jones, C., Mulloy, B., and Thomas, A.H. eds., *Spectroscopic Methods and Analyses: NMR, Mass Spectrometry, and Metalloprotein Techniques. Methods in Molecular Biology 17*. New Jersey: Humana Press Inc. 1993.
423. Walker, C. et al. 2003. Phenotype versus genotype in gliomas displaying inter– or intratumoral histological heterogeneity. *Clin Cancer Res*. 9(13), pp 4841–4851.

424. Walker, M.D. et al., 1978. Evaluation of BCNU and/or radiotherapy in the treatment of anaplastic gliomas. *J Neurosurg*. 49(3), pp 333–343.
425. Walker, M.D., Strike, T.A. and Sheline, G.E 1979. An analysis of dose-effect relationship in the radiotherapy of malignant gliomas. *Int J Radiat Oncol Biol Phys*. 5(10), pp 1725–1731.
426. Walsh, G. 2006. Biopharmaceutical benchmarks 2006. *Nat Biotechnol*. 24, pp 769–776.
427. Wang, Y. et al. 2012. Glioblastoma with an oligodendroglioma component: distinct clinical behavior, genetic alterations, and outcome. *Neuro Oncol*. 14(4):518–25.
428. Watanabe, K. et al., 1996. Overexpression of the EGF receptor and p53 mutations are mutually exclusive in the evolution of primary and secondary glioblastomas. *Brain Pathol*. 6(3), pp 217–223; discussion 23–4.
429. Watson, J.T. and Sparkman, O.D. 2007. *Introduction to mass spectrometry: Instrumentation, Applications and Strategies for data interpretation*. 4th edition. England: Wiley.
430. Watt, P.M. 2006. Screening for peptide drugs from the natural repertoire of biodiverse protein folds. *Nat Biotechnol*. 24(2), pp 177–183.
431. Webber M.J. et al., 2011. Supramolecular nanostructures that mimic VEGF as a strategy for ischemic tissue repair *Proc Nat Acad Sci*. 108(33), pp 13438–13443.
432. Webber, M.J., Kessler, J.A. and Stupp S.I. 2009. Emerging peptide nanomedicine to regenerate tissues and organs. *J Intern Med*. 267, pp 71–88.
433. Weiler, M. et al., 2010. Chemoradiotherapy of newly diagnosed glioblastoma with intensified temozolomide. *Int J Radiat Oncol Biol Phys*. 77(3), pp 670–676.
434. Weiss R.B. and Issell, B.F. 1982. The nitrosoureas: carmustine (BCNU) and lomustine (CCNU). *Cancer Treat Rev*. 9, pp 313–330.
435. Weller, M. et al., Standards of care for treatment of recurrent glioblastoma - are we there yet? *Neuro Oncol*. 15(1), pp 4–27.
436. Wen, P.Y. and Kesari, S. 2008. Malignant Gliomas in Adults. *N Engl J Med*. 359, pp 492–507.
437. Westphal, M. et al. 2003. A phase 3 trial of local chemotherapy with biodegradable carmustine (BCNU) wafers (Gliadel wafers) in patients with primary malignant glioma. *Neuro Oncol*. 5(2), pp 79–88.
438. White, P.D. and Chan, W.C. 2000. Basic Principles. In: Chan, W.C. and White, P.D. eds., *Fmoc solid phase synthesis: A practical approach*. Oxford University Press, 2000, pp 9–40.

439. Whitesides, G.M and Grzybowski, B. 2002. Self- assembly at all scales. *Science*. 295(5564), pp 2418–2421.
440. Wick, A. et al., 2007. Efficacy and tolerability of temozolomide in an alternating weekly regimen in patients with recurrent glioma. *J Clin Oncol*. 25(22), pp 3357–3361.
441. Williams, D.H. and Fleming, I. 1996. *Spectroscopic methods in organic chemistry*. 5th edition. The McGraw–Hill Companies, pp 63–71.
442. Winkler, I.G. et al. 2010. Bone marrow macrophages maintain hematopoietic stem cell (HSC) niches and their depletion mobilizes HSCs. *Blood*. 116(23), pp 4815–4828.
443. Wong, E.T. et al., 1999. Outcomes and prognostic factors in recurrent glioma patients enrolled onto Phase II clinical trials. *J Clin Oncol*. 17(8), pp 2572–2578.
444. Wood, J.R, Green, S.B. and Shapiro, W.R 1988. The prognostic importance of tumor size in malignant gliomas: A computed tomographic scan study by the Brain Tumor Cooperative Group. *J Clin Oncol*. 6(2), pp 338–343.
445. Yamasaki, F. et al., 2010. Glioblastoma treated with postoperative radio-chemotherapy: prognostic value of apparent diffusion coefficient at MR imaging. *Eur J Radiol*. 73(3), pp 532–537.
446. Yan, et al., 2008. Organogels Based on Self-Assembly of Diphenylalanine Peptide and Their Application To Immobilize Quantum Dots. *Chem Mater*. 20 (4), pp 1522–1526.
447. Yan, H. et al., 2009. IDH1 and IDH2 mutations in gliomas. *N Engl J Med*. 360, pp 765–773.
448. Yang, F. et al., 2010. Sorafenib induces growth arrest and apoptosis of human glioblastoma cells through the dephosphorylation of signal transducers and activators of transcription 3. *Mol Cancer Ther*. 9(4):953–962.
449. Yi, N. et al., 2014. Combined delivery of BCNU and VEGF siRNA using amphiphilic peptides for glioblastoma. *J Drug Target*. 22(2), pp 156–164.
450. Young, G.S. 2007. Advanced MRI of adult brain tumors. *Neurol Clin*. 25(4), pp 947–973.
451. Yung, W.K. et al. 2000. A phase II study of temozolomide vs. procarbazine in patients with glioblastoma multiforme at first relapse. *Br J Cancer*. 83(5), pp 588–593.
452. Yust-Katz, S. et al. 2013. Phase 1/1b study of lonafarnib and temozolomide in patients with recurrent or temozolomide refractory glioblastoma. *Cancer*. 119 (15), pp 2747–2753.

453. Zagon I. S. et al., 1997. Opioid growth factor (OGF) inhibits human pancreatic cancer transplanted into nude mice. *Cancer Letters*. 112(2), pp 167–175.
454. Zagon I.S. and McLaughlin P.J. 1989. Endogenous opioid systems regulate growth of neural tumor cells in culture. Brain Research. 490, pp 14–25.
455. Zhang S. et al., 1993. Spontaneous assembly of a self-complementary oligopeptide to form a stable macroscopic membrane. *Proc Natl Acad Sci USA*. (90), pp 3334–3338.
456. Zhang, P. et al. 2012. Transferrin–modified c[RGDfK]–paclitaxel loaded hybrid micelle for sequential blood–brain barrier penetration and glioma targeting therapy. *Mol Pharm*. 9(6), pp 1590–1598.
457. Zhang, S. 2002. Emerging biological materials through molecular self–assembly. *Biotechn Adv*. 20, pp 321–339.
458. Zhang, S. and Altman, M. 1999. Peptide self–assembly in functional polymer science and engineering. *React Funct Polym*. 41, pp 91–102.
459. Zhang, S. Nat Biotechnol. 2003. 21, 1171–1178.
460. Zhou, Y.H. et al., 2003. The expression of PAX6, PTEN, vascular endothelial growth factor, and epidermal growth factor receptor in gliomas: relationship to tumor grade and survival. *Clin Cancer Res*. 9(9), pp 3369–3375.
461. Zylber-Katz, E. et al., 2000. Pharmacokinetics of methotrexate in cerebrospinal fluid and serum after osmotic blood-brain barrier disruption in patients with brain lymphoma. *Clin Pharmacol Ther*. 67(6), pp 631–641.

Appendices

Appendix I

A

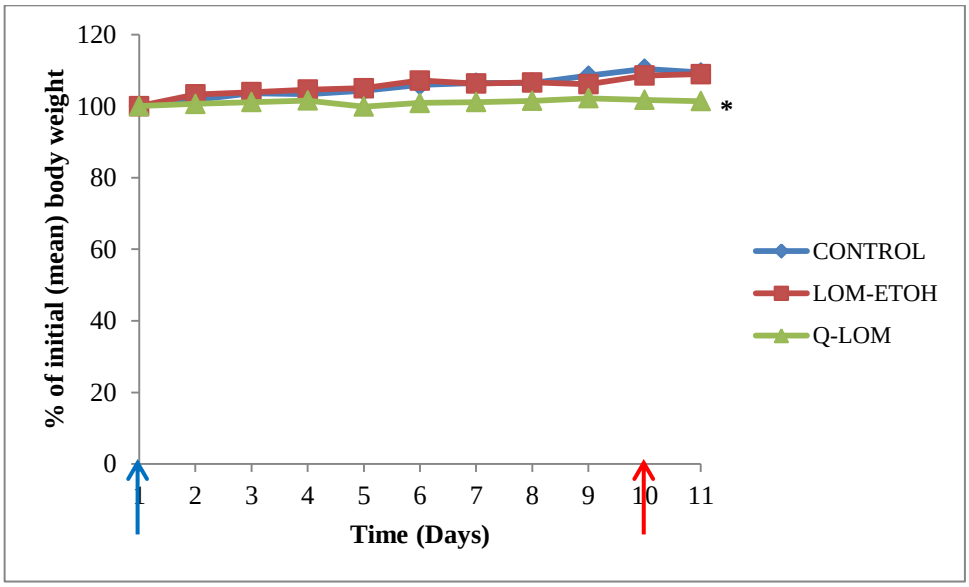

B

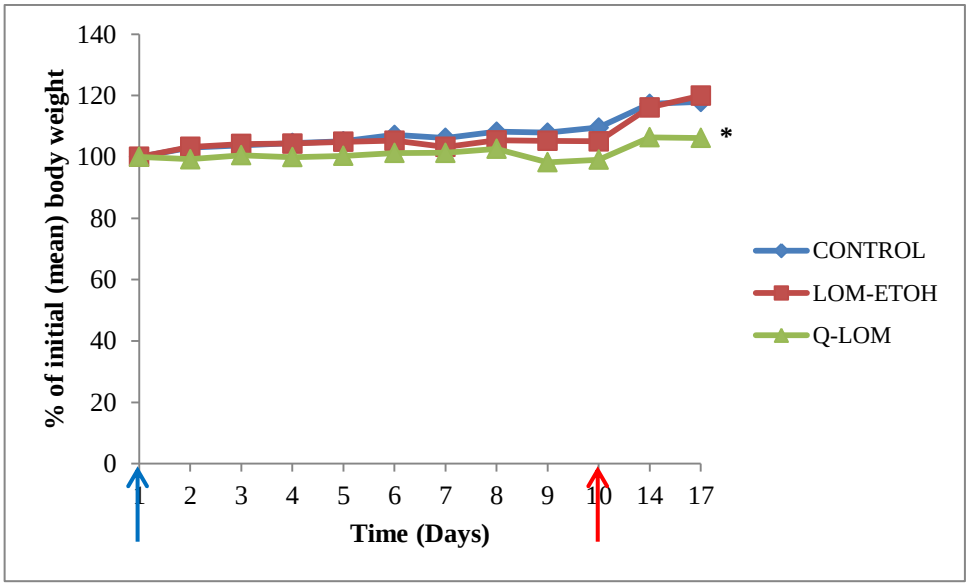

C

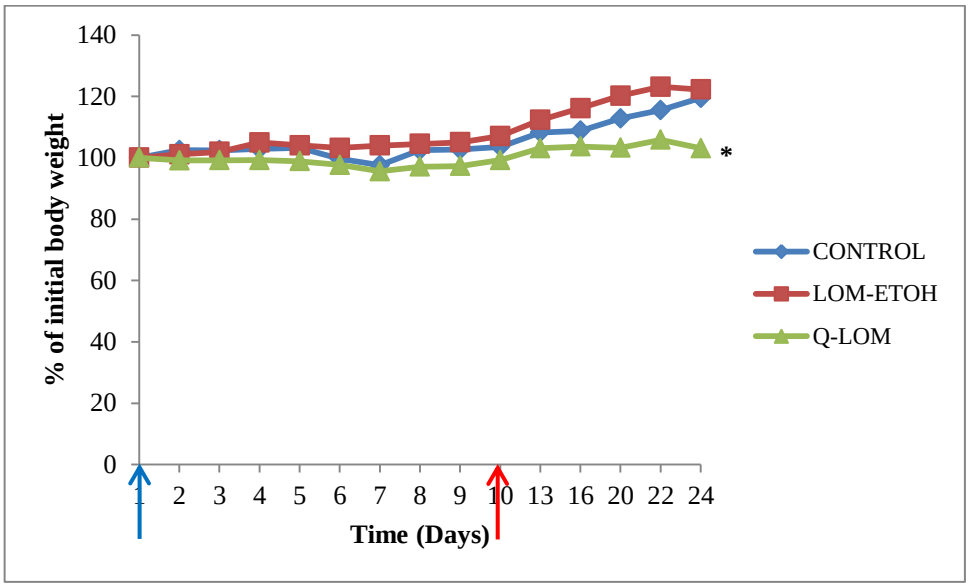
140
120
100
80
60
40
20
0
% of initial body weight
1 2 3 4 5 6 7 8 9 10 13 16 20 22 24
Time (Days)
*
CONTROL
LOM-ETOH
Q-LOM

D

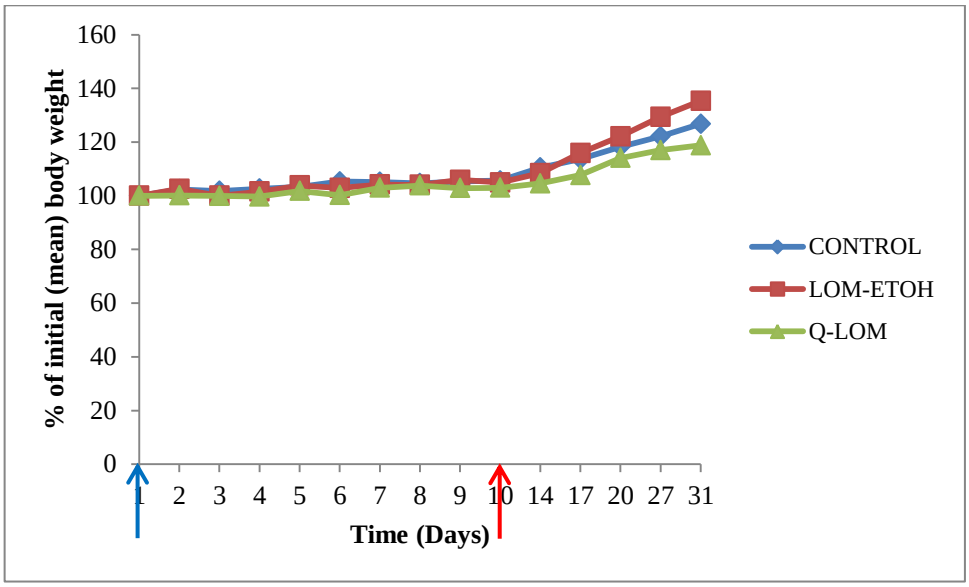
160
140
120
100
80
60
40
20
0
% of initial (mean) body weight
1 2 3 4 5 6 7 8 9 10 14 17 20 27 31
Time (Days)
CONTROL
LOM-ETOH
Q-LOM

E

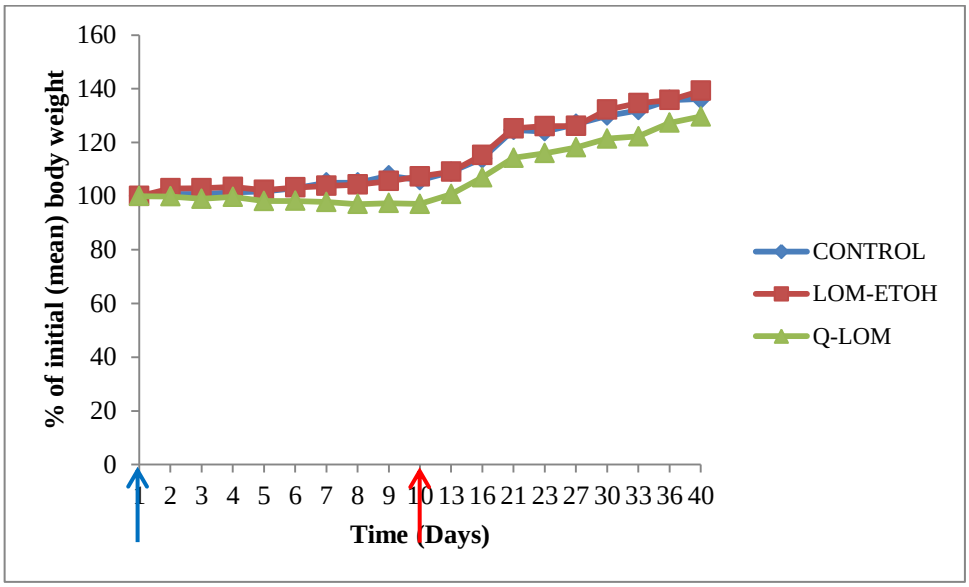

Weight measurement for animals culled for analysis of blood samples by percentage of their initial body weight, A: Day 1; B: Day 7; C: Day 14; D: Day 21 and E: Day 30 after completion of 10 consecutive daily doses of lomustine formulations

Key: Blue arrow: Treatment start date; Red Arrow: Treatment end date. Weights were recorded from commencement of dosing until mice were culled for collection of blood samples for analysis. Days 1, 7, 14, 21 and 30 correspond to number of days following completion of 10 consecutive daily doses of lomustine formulations

*: Significantly different ($p < 0.05$) from CONTROL and Lom-ETOH (One-way ANOVA with Tukey post hoc test)

Appendix II

A

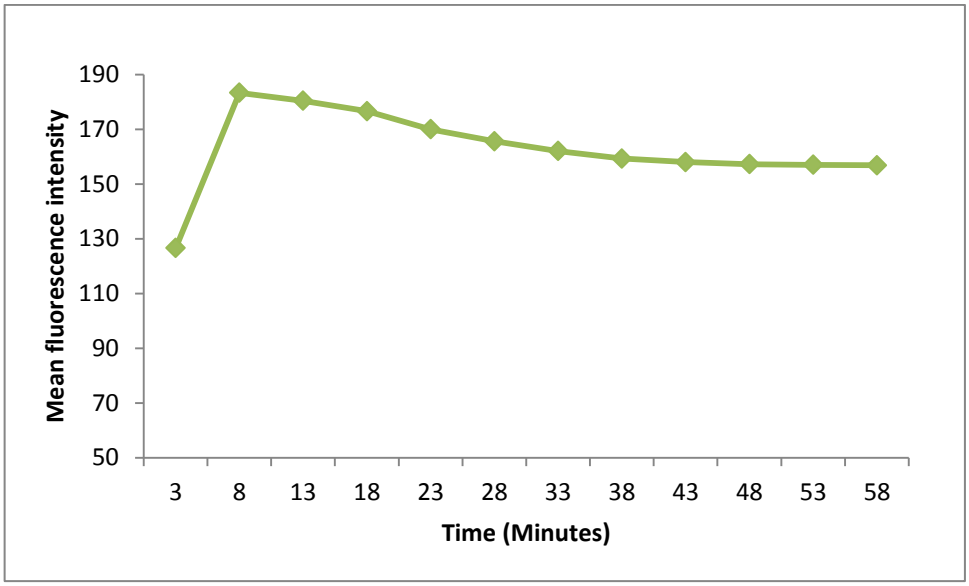

B

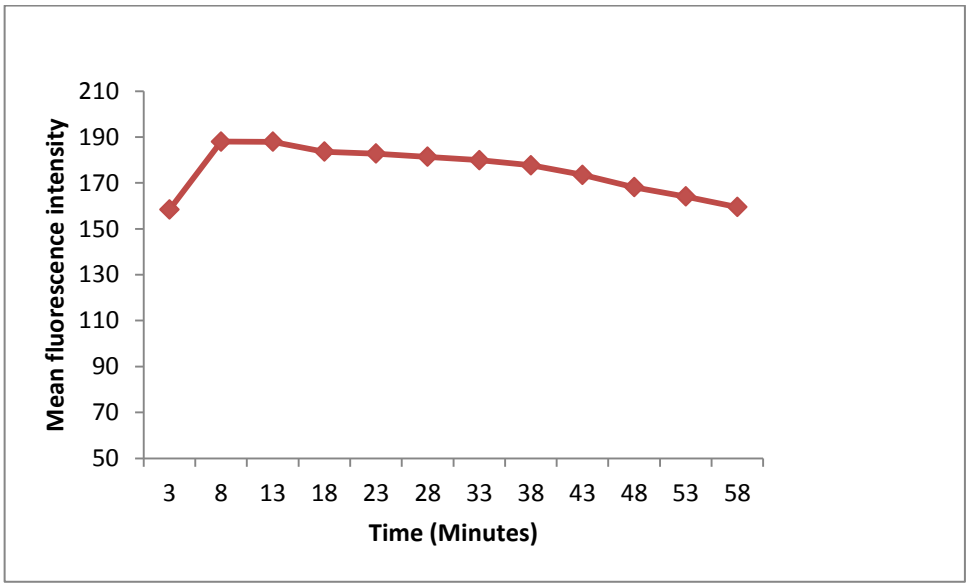

Semi-quantitative assessment of fluoresc ence intensity of confocal images for A: GCPQ NR and B: Liposome NR treated J774A.1 cells

Appendix III

A

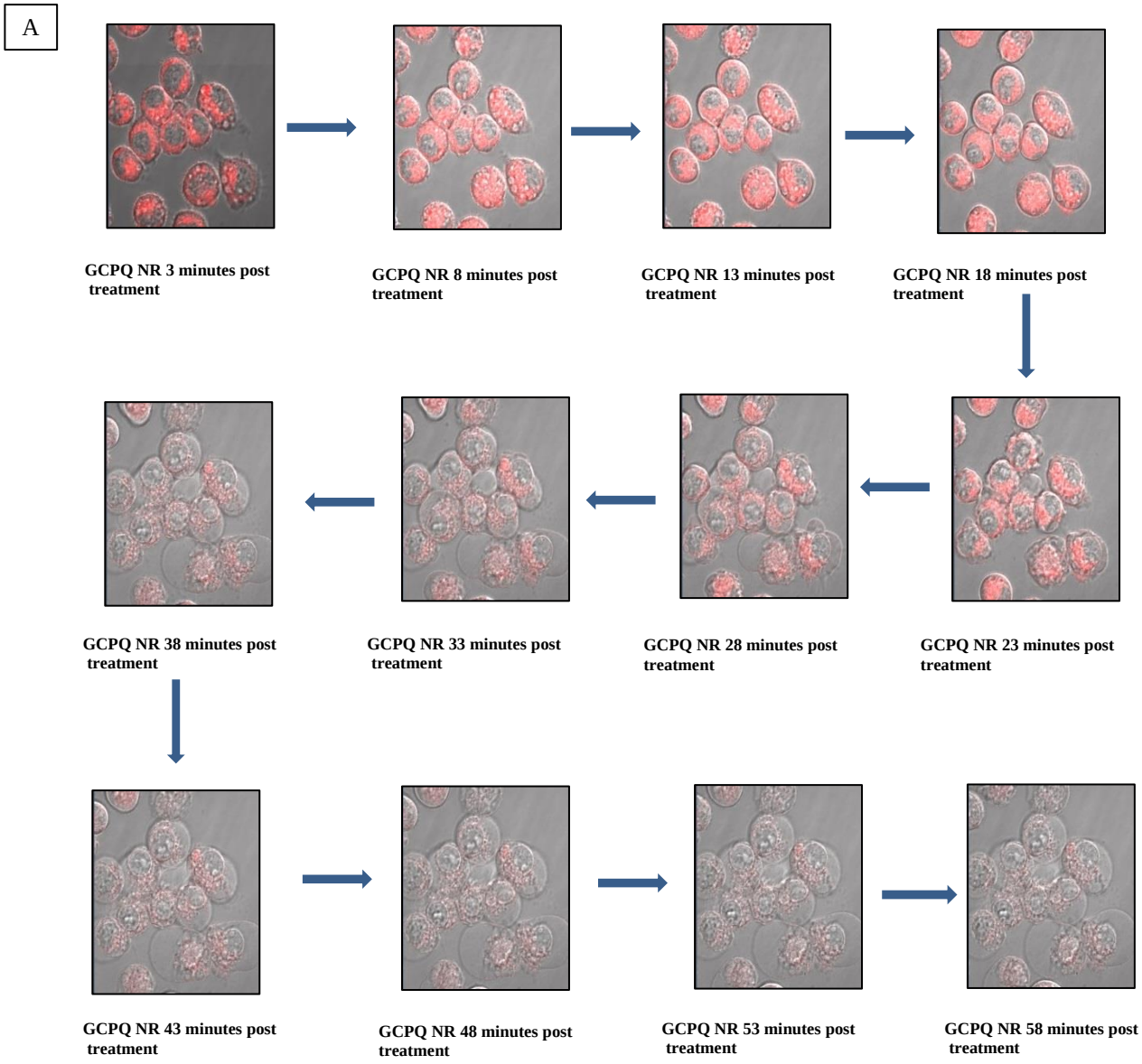

Confocal microcopy images showing uptake of GCPQ NR by J774A.1 over time (Time lapse experiment)

B

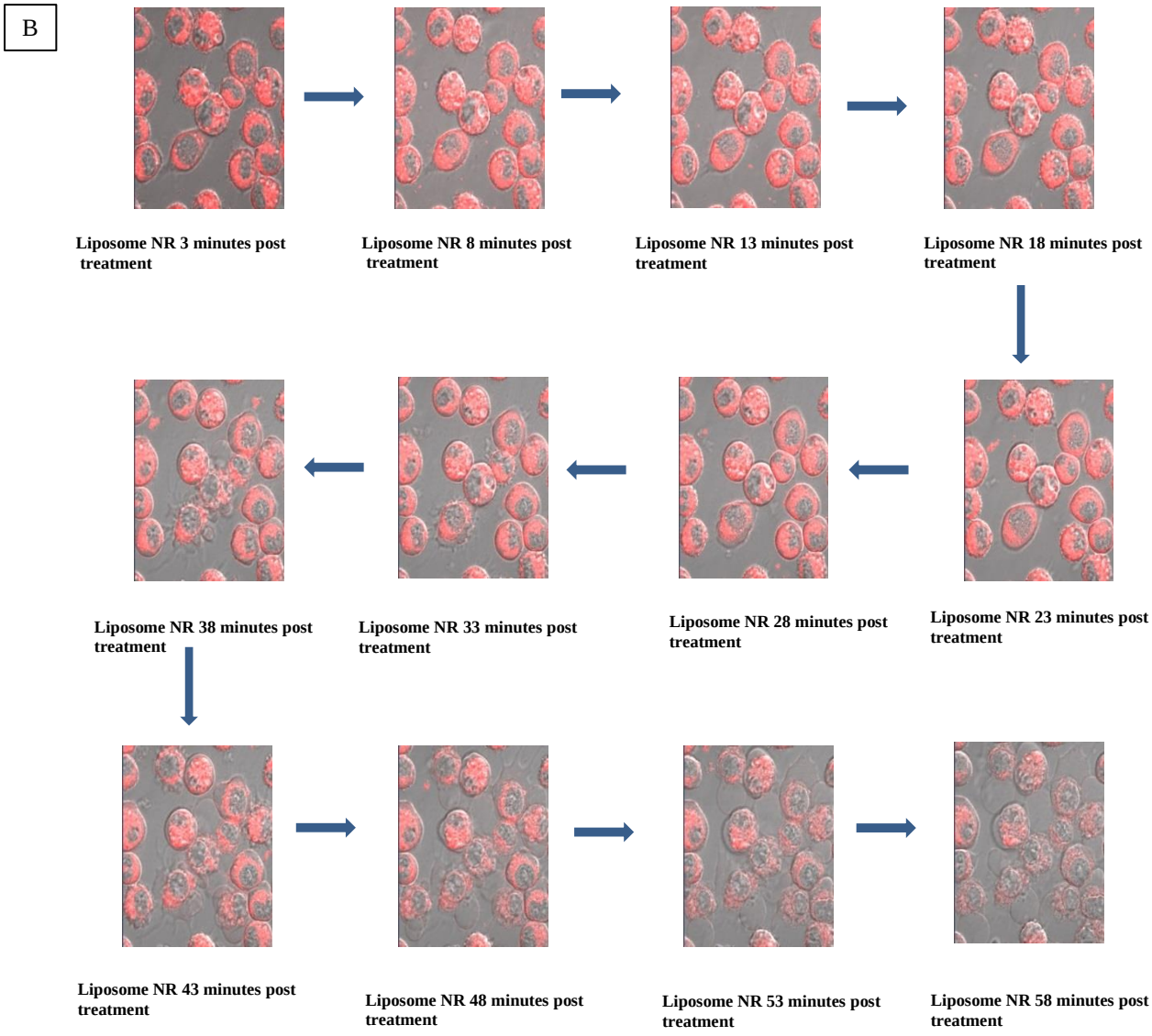

Confocal microcopy images showing uptake of Liposome NR by J774A.1 over time (Time lapse experiment)

Appendix IV

Time	**Flow rate** **(mL min^{-1})**	**% A** **0.02 % TFA/ H_2O**	**% B** **90 % MeCN/ 0.016 % TFA/ H_2O**
0	15	45	55
52	15	0	100
57	15	0	100
60	15	45	55
61	0	45	55

Gradient table for preparative RP HPLC purification of O-Palm-Y-G-G-L-R-F and G-G-Y- (O-Palm) - F-R-L

Appendix V

Time	**Flow rate** **(mL min^{-1})**	**% A** **0.02 % TFA/ H_2O**	**% B** **90 % MeCN/ 0.016 % TFA/ H_2O**
0	20.4	45	55
40	20.4	0	100
45	20.4	0	100
52	20.4	45	55

Gradient table for preparative RP HPLC purification of O-Palm-Y-G-G-F-M

Appendix VI

Time	**Flow rate** **(mL min^{-1})**	**% A** **0.02 % TFA/ H_2O**	**% B** **90 % MeCN/ 0.016 % TFA/ H_2O**
0	1.2	100	0
20	1.2	0	100
25	1.2	0	100
32	1.2	100	0

Gradient table for analytical RP HPLC determination of purity of synthesised PAs

Appendix VII

Extended					**T-shaped**				
i	*j*	*k*	θ_{eq}	k_θ /kJ mol^{-1} rad^{-2}	*i*	*j*	*k*	θ_{eq}	k_θ /kJ mol^{-1} rad^{-2}
1	10	11	132.00	50	1	2	3	129.00	200
10	11	12	137.00	50	2	3	12	125.00	100
11	12	14	134.00	100	3	12	16	118.00	200
12	14	17	150.00	200	12	16	19	149.00	200
10	1	2	97.00	50	2	3	4	100.00	50
11	12	13	101.00	50	3	12	13	92.00	100
12	14	15	106.00	50	12	16	17	97.00	100
14	17	18	82.00	200	16	19	20	91.00	100
1	2	3	114.00	100	3	4	5	117.00	200
1	2	4	140.00	200	3	4	6	140.00	200
14	15	16	143.00	100	12	13	14	145.00	200
17	18	19	140.00	200	12	13	15	120.00	200
17	18	20	122.00	100	16	17	18	144.00	100
3	5	6	144.00	50	5	7	8	143.00	100
4	5	6	143.00	50	6	7	8	138.00	100
5	6	7	140.00	25	7	8	9	120.00	100
6	7	8	180.00	25	8	9	10	180.00	100
7	8	9	180.00	25	9	10	11	180.00	50

Bond angle parameters for the linear and "T"-PAs

Key: i, j and k refer to atom indices following the numbering used for the CG mapping scheme, θeq is the equilibrium bond angle between particles i, j and k and kθ is the force constant.

Appendix VIII

Atom Number	**Extended**			**T-shaped**		
	Residue	MARTINI particle type	Charge	Residue	MARTINI particle type	Charge
1	palm-TYR	Qd	+1	GLY	Qd	+1
2	palm-TYR	SC4	0	GLY	Nda	0
3	palm-TYR	SC4	0	palm-TYR	Nda	0
4	palm-TYR	SC4	0	palm-TYR	SC4	0
5	palm-TYR	Na	0	palm-TYR	SC4	0
6	palm-TYR	C1	0	palm-TYR	SC4	0
7	palm-TYR	C1	0	palm-TYR	Na	0
8	palm-TYR	C1	0	palm-TYR	C1	0
9	palm-TYR	C1	0	palm-TYR	C1	0
10	GLY	Nda	0	palm-TYR	C1	0
11	GLY	Nda	0	palm-TYR	C1	0
12	LEU	Nda	0	PHE	Nda	0
13	LEU	AC1	0	PHE	SC4	0
14	ARG	Nda	0	PHE	SC4	0
15	ARG	N0	0	PHE	SC4	0
16	ARG	Qd	+1	ARG	Nda	0
17	PHE	Qa	-1	ARG	N0	0
18	PHE	SC4	0	ARG	Qd	+1
19	PHE	SC4	0	LEU	Qa	-1
20	PHE	SC4	0	LEU	AC1	0

MARTINI particle types chosen to model the linear and "T"-PAs. The atom number for each particle corresponds to that used for the CG mapping scheme

Appendix IX

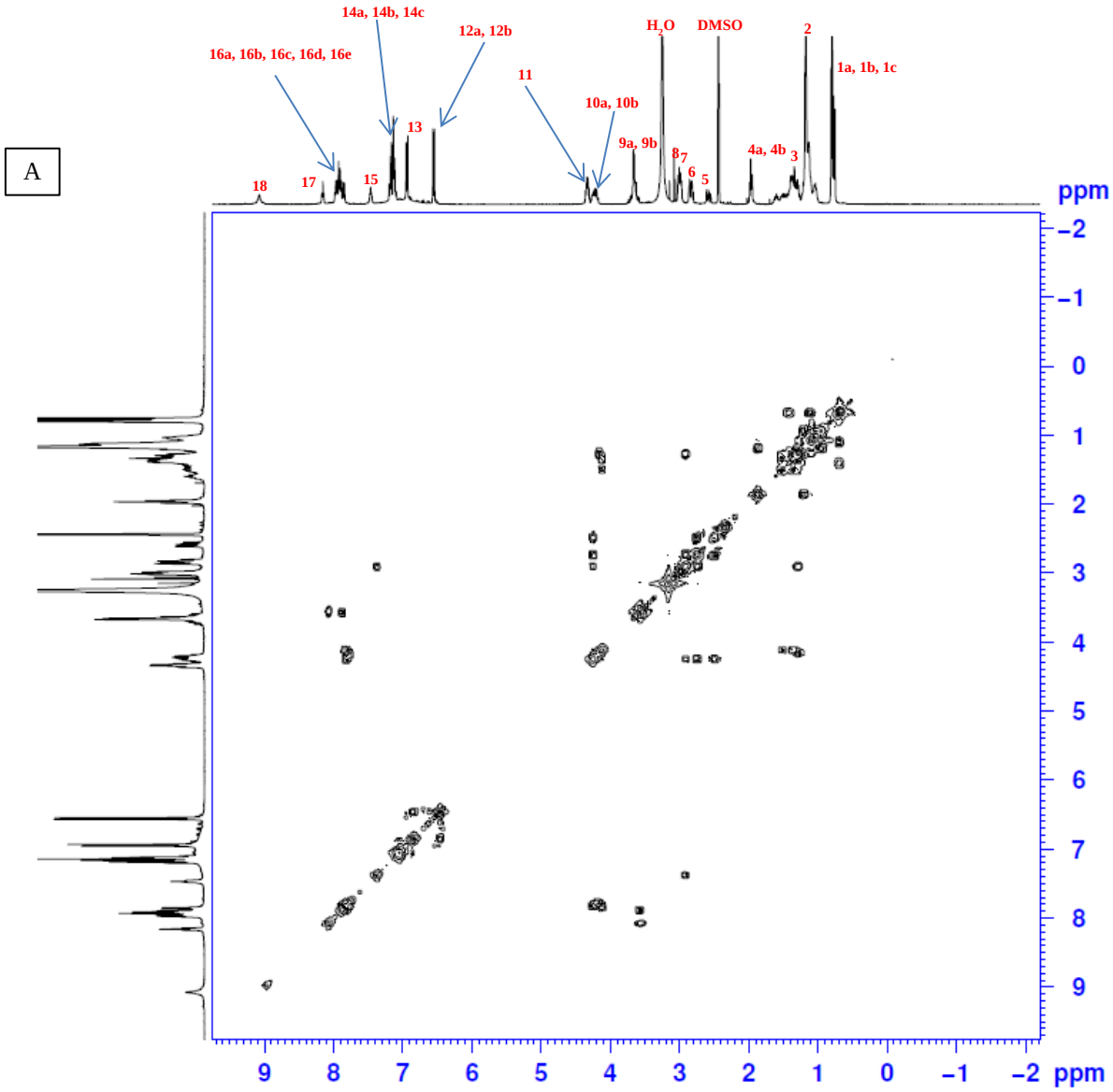

COSY (fixed) spectra for O-Palm-Y-G-G-L-R-F

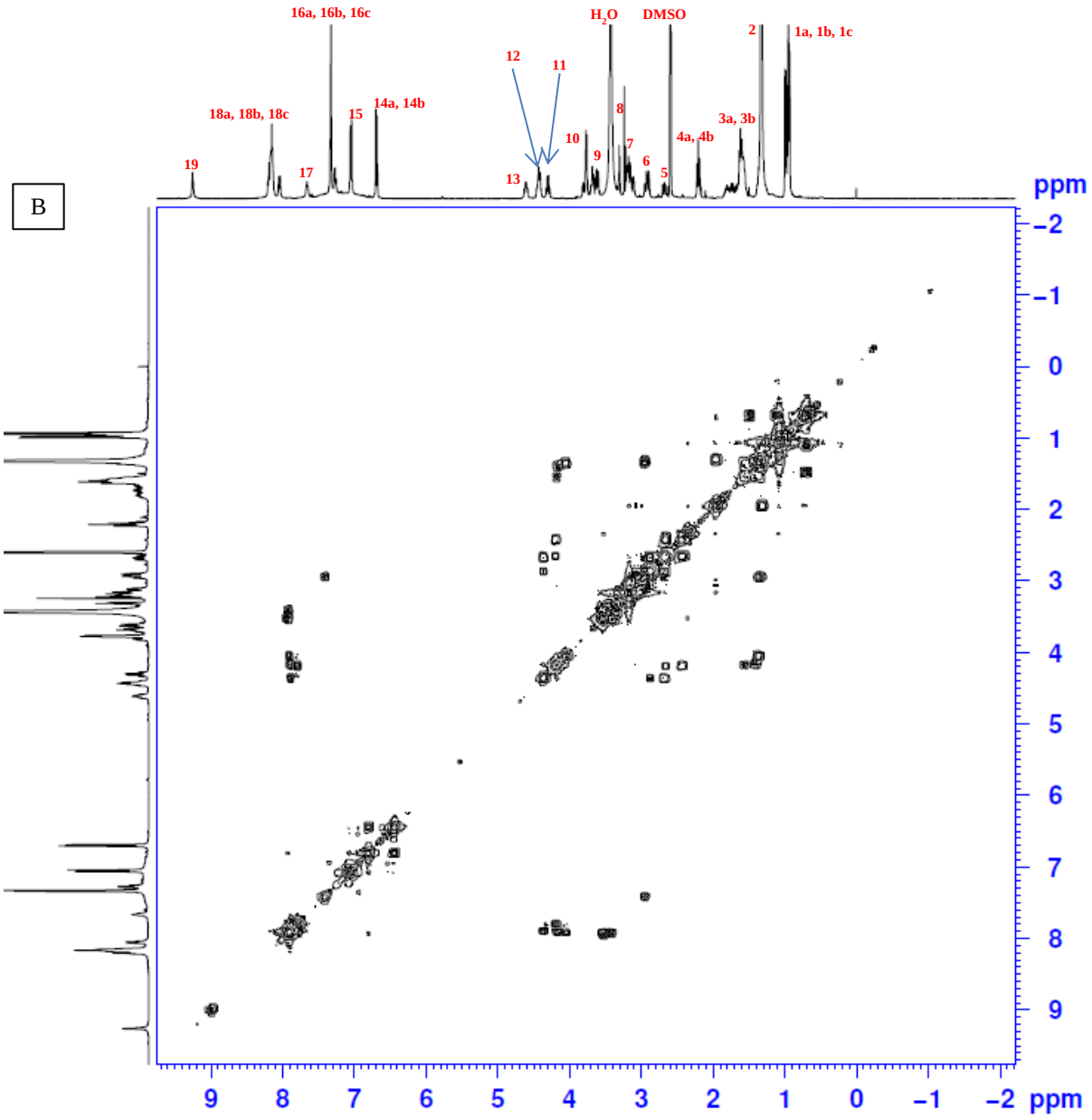

COSY (fixed) spectra for G-G-Y- (O-Palm)-F-R-L

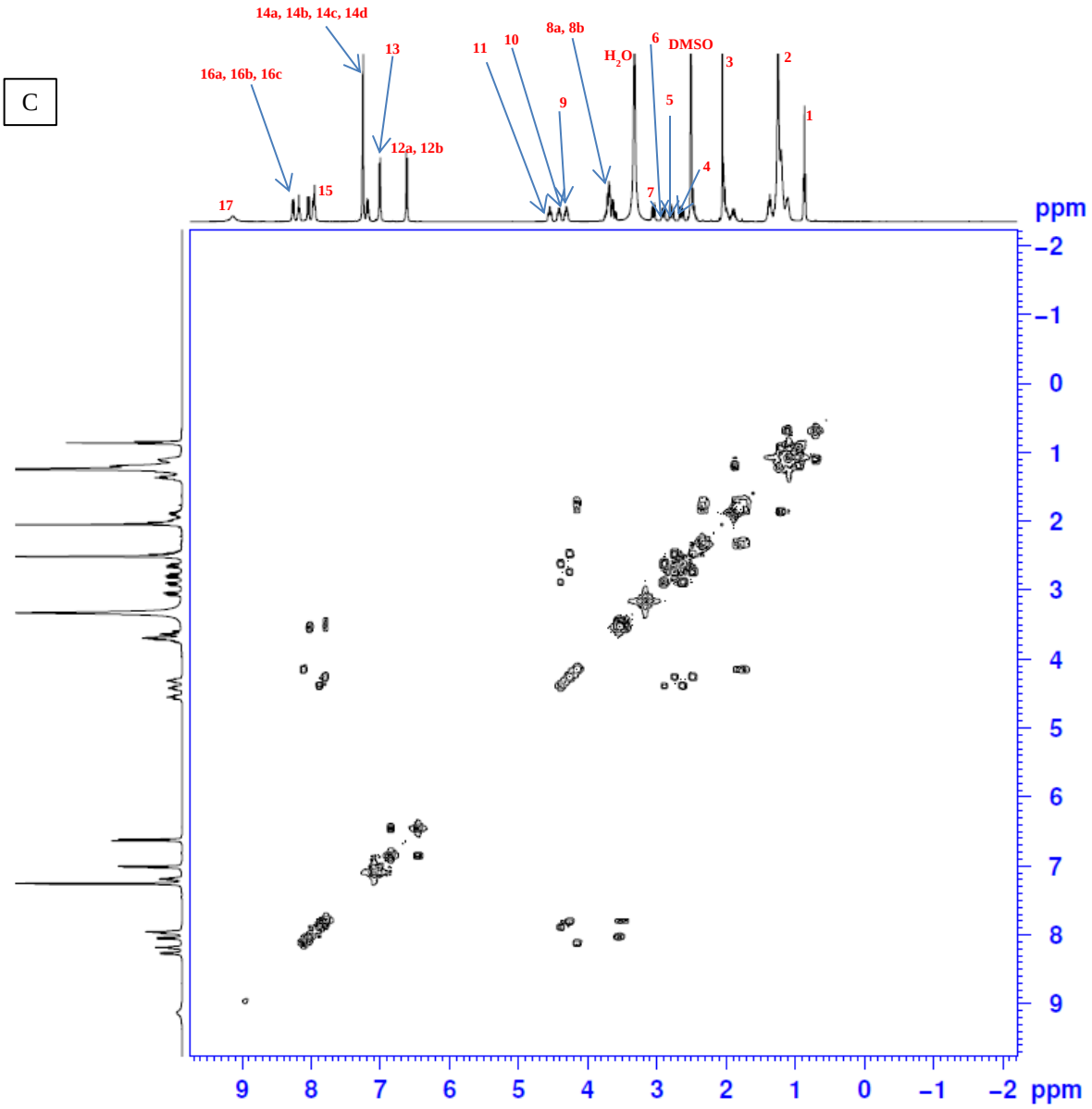

COSY (fixed) spectra for O-Palm-Y-G-G-F-M

Appendix X

A

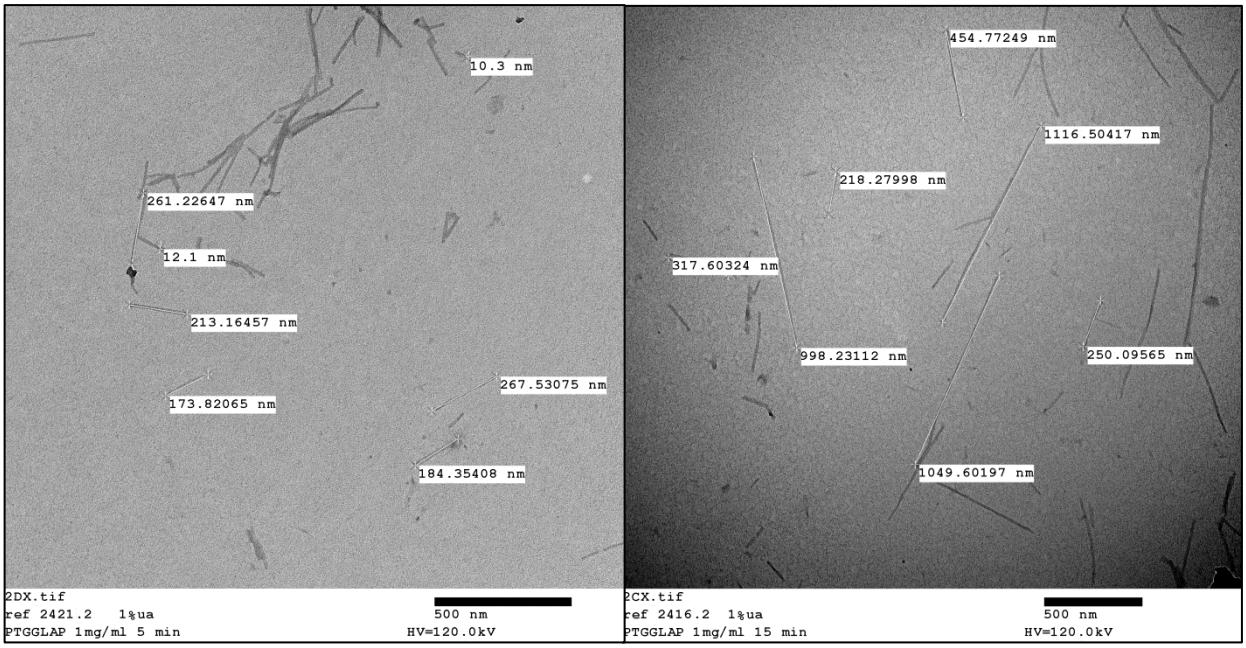

B

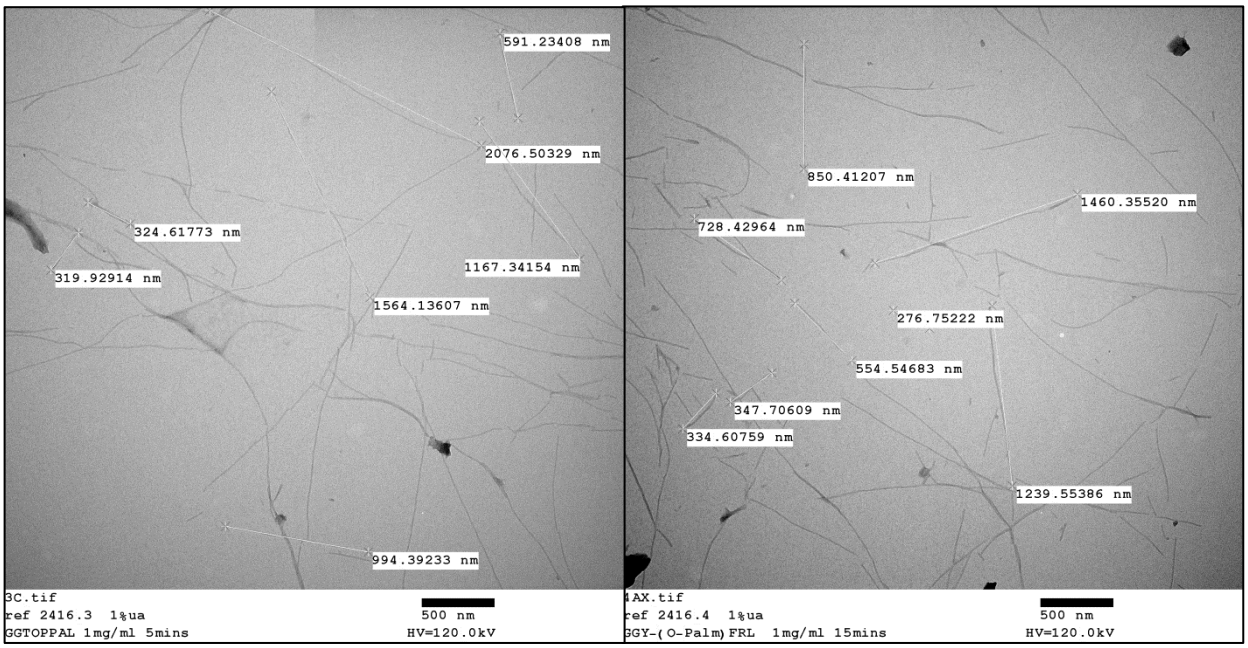

C

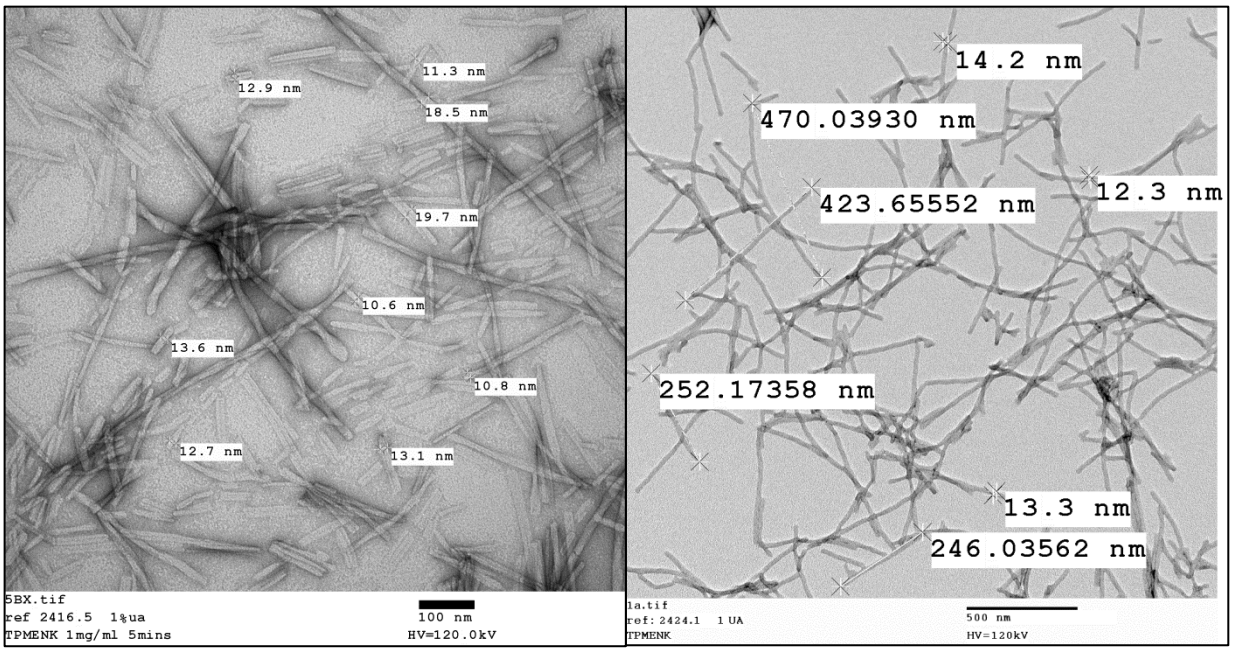

TEM micrographs for PAs with measurements: (A): O-Palm-Y-G-G-L-R-F; (B): G-G-Y- (O-Palm) - F-R-L; (C): O-Palm-Y-G-G-F-M. Measurements are as generated by the AMT digital camera software.

Appendix XI

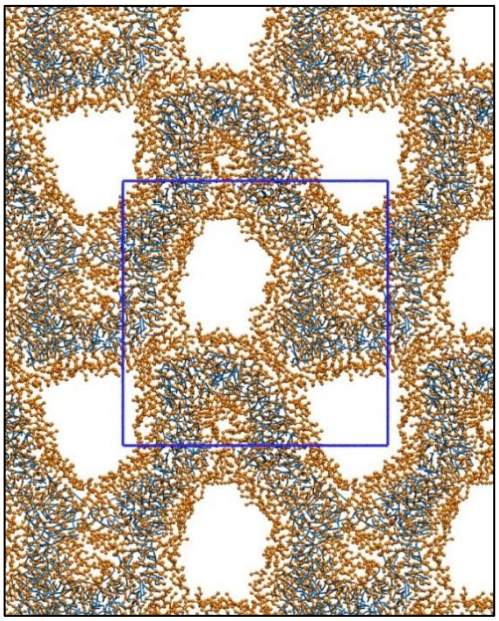

Run 1

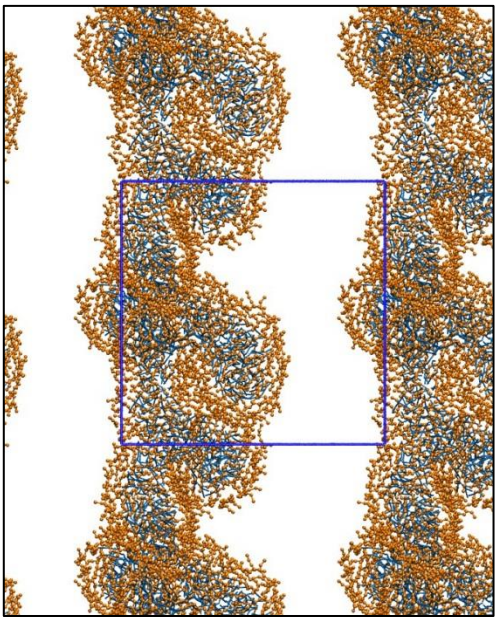

Run 2

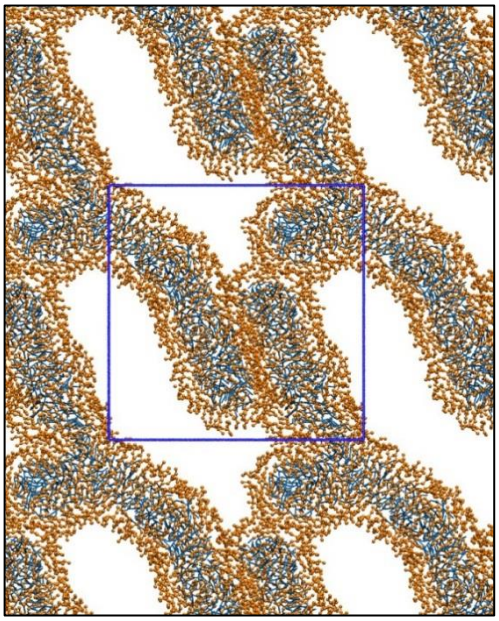

Run 3

Snapshots of the simulations of nanofibre formed through self-assembly of G-G-Y- (O-Palm) -F-R-L ("T"-PA)

Key: Orange spheres: Peptide backbone; blue lines: acyl chain. Side chain particles, water and ions are removed for clarity.

Appendix XII

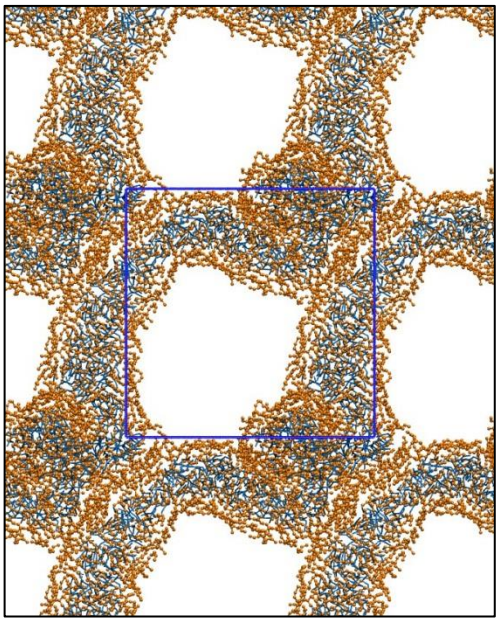

Run 1

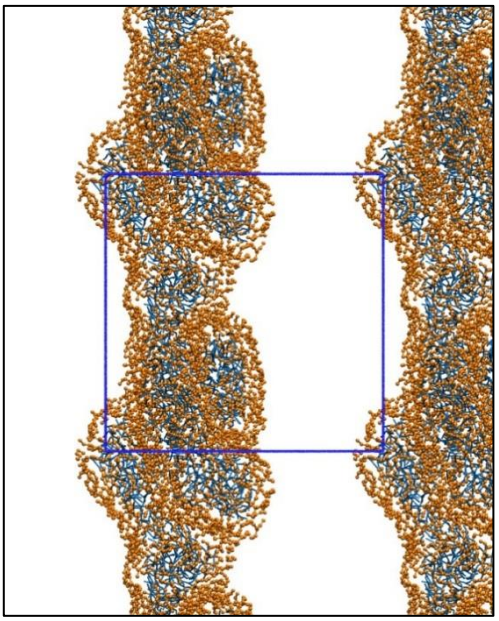

Run 2

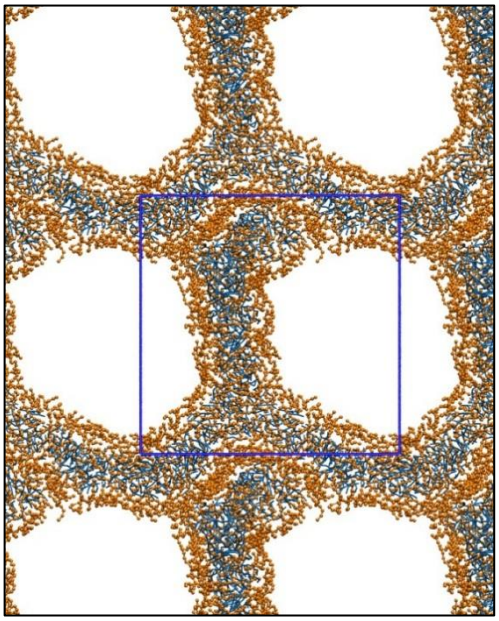

Run 3

Snapshots of the simulations of nanofibre formed through self-assembly of O-Palm-Y-G-G-L-R-F (Linear PA)

Key: Orange spheres: Peptide backbone; blue lines: acyl chain. Side chain particles, water and ions are removed for clarity.